IRON COORDINATION CHEMISTRY OF N_2, N_2H_2, N_2H_4, AND NH_3: INVESTIGATING THE MECHANISM OF N_2 REDUCTION TO AMMONIA

by

JUSTIN L. CROSSLAND

A DISSERTATION

Presented to the Department of Chemistry
and the Graduate School of the University of Oregon
in partial fulfillment of the requirements
for the degree of
Doctor of Philosophy

September 2009

University of Oregon Graduate School

Confirmation of Approval and Acceptance of Dissertation prepared by:

Justin Crossland

Title:

"Iron Coordination Chemistry of N2, N2H2, N2H4, and NH3: Investigating the Mechanism of N2 Reduction to Ammonia"

This dissertation has been accepted and approved in partial fulfillment of the requirements for the degree in the Department of Chemistry by:

Darren Johnson, Chairperson, Chemistry
David Tyler, Advisor, Chemistry
Michael Haley, Member, Chemistry
Kenneth Doxsee, Member, Chemistry
Scott Bridgham, Outside Member, Biology

and Richard Linton, Vice President for Research and Graduate Studies/Dean of the Graduate School for the University of Oregon.

September 5, 2009

Original approval signatures are on file with the Graduate School and the University of Oregon Libraries.

An Abstract of the Dissertation of

Justin Lee Crossland for the degree of Doctor of Philosophy

in the Department of Chemistry to be taken September 2009

Title: IRON COORDINATION CHEMISTRY OF N_2, N_2H_2, N_2H_4, and NH_3:

INVESTIGATING THE MECHANISM OF N_2 REDUCTION TO AMMONIA

Approved: _____

Dr. David R. Tyler

The coordination chemistry of iron with N_2 is becoming increasingly important as chemists try to find alternative routes to the production of ammonia. Current biological and industrial processes use iron to catalyze the formation of ammonia from N_2; however, huge amounts of energy are required for this conversion. Understanding how dinitrogen and other intermediates of dinitrogen reduction interact with iron could lead to energy efficient processes for the production of ammonia.

This dissertation explores the synthesis and reactivity of an iron dinitrogen complex that reacts with acid to produce ammonia at room temperature and pressure. This dissertation also explores the progress toward determining the mechanism of this reaction in hopes of improving the yields of ammonia.

Chapter I describes both the biological nitrogen fixation process and the industrial production of ammonia and provides an in-depth look at progress toward an alternative

route to ammonia using iron complexes described in the literature thus far.

Chapter II details the synthesis, characterization, and reactivity of dihydrogen and dinitrogen complexes of iron. These complexes are precursors to the active ammonia producing complex and are among a handful of dihydrogen and dinitrogen complexes that have been structurally characterized. Chapter III explores the synthesis and stability of $Fe(DMeOPrPE)_2N_2$. This complex produces ammonia and hydrazine upon protonation with a strong acid. Optimizing the yield of ammonia from this protonation is also described.

Chapter IV discusses the synthesis and reactivity of several complexes of iron containing intermediates relevant to dinitrogen reduction, including diazene (N_2H_2), hydrazine (N_2H_4), and ammonia. By studying these intermediates, a mechanism of ammonia formation from the protonation of $Fe(DMeOPrPE)_2N_2$ is proposed that may also provide insights into the mechanism of nitrogenase. Chapter V provides a summary of this research.

This dissertation includes previously published and unpublished co-authored material.

CURRICULUM VITAE

NAME OF AUTHOR: Justin Lee Crossland

PLACE OF BIRTH: Mt. Shasta, CA

DATE OF BIRTH: April 23, 1982

GRADUATE AND UNDERGRADUATE SCHOOLS ATTENDED:

University of Oregon, Eugene, OR
Pacific University, Forest Grove, OR

DEGREES AWARDED:

Doctor of Philosophy in Chemistry, 2009, University of Oregon
Master of Science in Chemistry, 2005, University of Oregon
Bachelor of Science in Chemistry, 2004, Pacific University

AREAS OF SPECIAL INTEREST:

Nitrogen Fixation
Coordination Chemistry
Small Molecule Activation
NMR Spectroscopy

PUBLICATIONS:

Crossland, J. L.; Young, D. M.; Zakharov, L. N.; Tyler, D. R. Precursors to dinitrogen reduction: Structures and reactivity of *trans*-$[Fe(DMeOPrPE)_2(H_2)H]^+$ and *trans*-$[Fe(DMeOPrPE)_2(N_2)H]^+$. *Dalton Trans.* **2009**, *submitted.*

Crossland, J. L.; Balesdent, C. G.; Tyler, D. R. Intermediates in the reduction of N_2 to NH_3: Synthesis of iron η^2 hydrazido(1-) and diazene complexes. *Dalton Trans.* **2009**, 4420-4422.

Szymczak, N. K.; Braden, D. A.; Crossland, J. L.; Turov, Y.; Zakharov, L. N.; Tyler, D. R. Aqueous coordination chemistry of H_2. Why is coordinated H_2 inert to substitution by water in *trans*-$Ru(P_2)_2(H_2)H^+$-type complexes? *Inorg. Chem.* **2009**, *48*, 2976-2984.

Yelle, R. B.; Crossland, J. L.; Szymczak, N. K.; Tyler, D. R. Theoretical Studies of N_2 Reduction to Ammonia in $Fe(dmpe)_2N_2$. *Inorg. Chem.* **2009**, *48,* 861-871.

Crossland, J. L.; Zakharov, L. N.; Tyler, D. R. (Ethane-1,2-diyl)bis[bis(3-methoxypropyl)methylphosphonium] bis(tetraphenylborate) diethyl ether solvate. *Acta Cryst.* **2008,** *E64,* o1111.

Crossland, J. L.; Zakharov, L. N.; Tyler, D. R. Synthesis and characterization of an iron(II) η^2-hydrazine complex. *Inorg. Chem.* **2007,** *46,* 10476-10478.

Crossland, J. L.; Zakharov, L. N.; Tyler, D. R. Hexakis(pyridine *N*-oxide-κO)iron(II) tetraphenylborate. *Acta Cryst.* **2007,** *E63,* m1196-m1197.

Gilberston, J. D.; Szymczak, N. K.; Crossland, J. L.; Miller, W. K.; Lyon, D. K.; Foxman, B. M.; Davis, J.; Tyler, D. R. Coordination chemistry of H_2 and N_2 in aqueous solution. Reactivity and mechanistic studies using trans-$FeII(P_2)_2X_2$-type complexes (P_2 = a chelating, water-solubilizing phosphine). *Inorg. Chem.* **2007,** *46,* 1205-1214.

Perchellet, E. M.; Wang, Y.; Weber, R. L.; Sperfslage, B. J.; Lou, K. Crossland, J. Hua, D. H.; Perchellet, J. P. Synthetic 1,4-anthracenedione analogs induce cytochrome *c* release, caspase-9, -3, and -8 activities, poly(ADP-ribose) polymerase-1 cleavage and internucleosomal DNA fragmentation in HL-60 cells by a mechanism which involves caspase-2 activation but not Fas signaling. *Biochem. Pharmacol.* **2004,** *67,* 523-537.

ACKNOWLEDGMENTS

I would first like to thank my advisor, Professor David Tyler, for his guidance these past years. He has provided me the freedom to pursue my science in numerous directions and his commitment to excellence has pushed me to where I am today.

I need to thank the people who have contributed to this project, particularly John Gilbertson and Nathaniel Szymczak, who established the foundation upon which most of this dissertation was based. Robert Yelle is acknowledged for theoretical contributions to this work aimed at determining the mechanism of ammonia formation. Lev Zakharov is acknowledged for all crystal structure determinations presented in this thesis. I also would like to thank Mike Strain for his assistance over the years with the NMR spectrometers. Numerous rotation students have contributed to the work presented here including: Eric Abbey, Adam Glass, Rick Glover, Doug Young, and Chantal Balesdent. I was also fortunate to have an excellent undergraduate research student, Dan Regan, working along side me.

Big thanks are given to past and present members of the Tyler lab who have provided support, constructive criticism, and friendship throughout my graduate career. Adam Marwitz and Timothy Carter have been great friends through the years and are acknowledged for their assistance in many extracurricular activities.

Finally I must thank my family for always supporting me and providing me with the opportunity to pursue this degree. Particularly, I am forever indebted to my beautiful wife Dr. Nicole Crossland for putting up with me and supporting me during this endeavor.

TABLE OF CONTENTS

LIST OF FIGURES

LIST OF TABLES

LIST OF SCHEMES

Scheme Page

CHAPTER IV

CHAPTER I

IRON DINITROGEN COORDINATION CHEMISTRY: RELEVANCE TO NITROGEN FIXATION

1.1 Introduction

All life on Earth depends on nitrogen fixation; the process by which atmospheric dinitrogen is reduced to ammonia. Organisms cannot directly incorporate dinitrogen into molecules such as proteins and nuclei acids; instead reduced forms of dinitrogen are needed for biomolecule synthesis. While having a source of reduced N_2 is crucial for life to exist, the process of reducing N_2 is very energy intensive.

The inertness of the dinitrogen molecule is partly due to its triple bond, having a dissociation energy of 944 kJ/mol. However, this factor is not solely responsible for the inertness of N_2 as other triply bonded small molecules, notably CO, readily undergo a wide variety of chemical transformations. Rather, the inertness of N_2 arises from the large gap between the HOMO and LUMO (22.9 eV), causing the molecule to be resistant to electron transfer and Lewis acid reactivity.[1]

In spite of this inertness, both biological and industrial processes exist that reduce dinitrogen to ammonia, with each process accounting for roughly 50% of the global NH_3 supply.[2] Because of the high energy requirements for the current industrial production of ammonia a low-energy alternative is desirable. Since the discovery of the first

dinitrogen complex in 1965 by Allen and Senoff,[3] chemists have sought an alternative means to achieve this reduction using homogeneous catalysis. One feature common to both the biological and industrial routes to ammonia is the use of iron as the active metal. Coordination chemists have taken this inspiration and made significant advancements in the coordination chemistry of iron with dinitrogen, as well as the reduction of dinitrogen using homogeneous iron complexes.

This chapter will briefly cover the biological and industrial production of ammonia and then delve into the coordination chemistry of homogeneous iron complexes with dinitrogen and reduced dinitrogen intermediates (i.e. N_2H_2, N_2H_4, and NH_3). The transformations of coordinated N_2 will be explored including protonation reactions. This chapter will focus on mono and binuclear iron complexes, the chemistry of iron clusters as related to nitrogen fixation will not be covered here.[4,5] The chemistry of simple iron salts and their ability to catalyze N_2 reduction in the presence of a strong reducing agent will also not be covered here.[1,6-10]

1.2 The Haber-Bosch Process

Industrial production of ammonia is achieved via the Haber-Bosch process.[11,12] In the Haber-Bosch process, hydrogen gas is first produced, typically by steam reformation of natural gas or partial oxidation of hydrocarbons, and then reacted with dinitrogen over a promoted iron catalyst (other metals, such as ruthenium are also commonly used) at high temperature (>200°C) and pressure (>400 atm) (eq. 1).

$$N_2 + H_2 \xrightarrow[\substack{>200\ ^\circ C \\ >400\ atm}]{Fe} 2NH_3 \quad (1)$$

The overall reaction in converting N_2 to NH_3 is actually exothermic (-46 kJ/mol), but due to the significant activation barrier, high temperatures are needed to increase the rate of ammonia formation. The intense pressure is needed to shift the equilibrium in favor of ammonia, as increasing the temperature also causes the equilibrium to shift toward the reactant gases. Although this process requires huge amounts of energy it is actually quite energy efficient, with state of the art Haber-Bosch plant efficiencies approaching the theoretical limit.[12]

1.3 Biological Nitrogen Fixation

Nature uses nitrogenase enzymes to convert atmospheric N_2 to NH_3.[13-16] These enzymes, which are limited to certain bacterial species (100-200 species), are responsible for all biologically fixed nitrogen.[2] Nitrogenase enzymes catalyze the reduction of dinitrogen to ammonia, and although the breaking of the dinitrogen bond is extremely energy intensive as shown above, these enzymes are able to perform the conversion at biological temperatures and atmospheric pressures (eq. 2).

$$N_2 + 8H^+ + 8e^- + 16\ MgATP \longrightarrow 2NH_3 + H_2 + 16MgADP + 16P_i \quad (2)$$

There are three types of nitrogenase enzymes varied by their metal composition in the active site; iron and molybdenum, iron and vanadium, and iron only.[17] The three

nitrogenases all have similar structures and reactivity, with the latter two types synthesized only under molybdenum deficient conditions.[18] The structure of the iron-molybdenum nitrogenase enzyme, which is the most efficient and commonly studied type, consists of two separate protein clusters: dinitrogenase reductase (iron containing dimer) which supplies electrons for the reduction and dinitrogenase (iron and molybdenum containing tetramer) where dinitrogen binding and reduction occur.[18] The FeMo cofactor is contained within the dinitrogenase protein.

The FeMo cofactor consists of seven Fe atoms bridged by nine S atoms with one Mo atom. A homocitrate ligand is coordinated to the Mo atom. The FeMo cofactor is attached to the protein backbone through a cysteine residue and a histidine residue. Refined crystal structure data of the FeMo cofactor at 1.16Å resolution revealed the existence of a central atom within the iron-sulfur cluster (Fig. 1).[19] The identity of this central atom is still highly debated, but from the electron density it is expected to be either C, N, or O.[20-29]

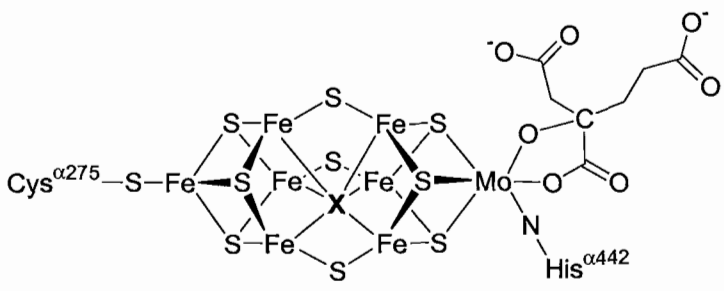

Figure 1. Structure of FeMo cofactor of nitrogenase enzyme.[19] The identity of X is unknown, but thought to be either C, N, or O.

The FeMo cofactor is accepted to be the site of N_2 binding and reduction based on a wide variety of evidence.[13] In fact recent site-directed mutagenesis studies have

suggested that two of the "belt" iron atoms of the FeMo cofactor are the site of N_2 binding and reduction.[30-33] These results are consistent with the fact that iron is the only metal common to all the types of nitrogenase enzymes.

The exact mechanism of N_2 reduction mediated by nitrogenase remains unknown, however growing evidence supports a mechanism that proceeds through diazene and hydrazine intermediates in route to ammonia formation (Fig. 2, bottom pathway).[34-38] This proposed mechanism is in contrast to the mechanisms detailed by Chatt[39] and Schrock[40] for Mo and W systems (Fig. 2, top pathway).

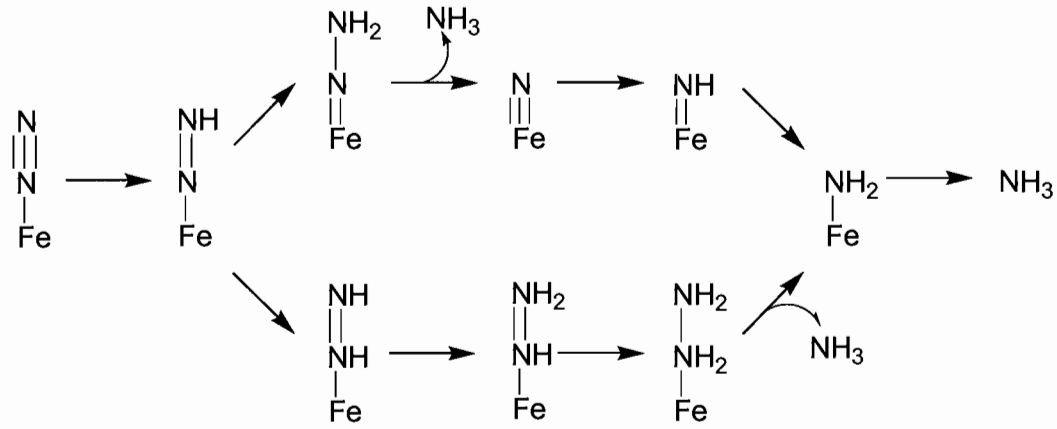

Figure 2. Proposed pathways for N_2 reduction in nitrogenase[34] (bottom pathway) and synthetic Mo and W systems[39,40] (top pathway).

Because of the growing biochemical evidence suggesting that iron is responsible for the reduction of N_2 to ammonia in nitrogenase, understanding the coordination chemistry of iron with dinitrogen and reduced dinitrogen species, such as diazene, hydrazine, and ammonia, is becoming increasingly important.

1.4 Coordination of N_2 to Iron

The coordination of dinitrogen to a transition metal can be described by the Dewar-Chatt-Duncanson bonding model. In end-on bonded dinitrogen complexes, the filled dinitrogen σ orbital ($3\sigma_g$) donates electron density to the empty metal d_{z^2} or $d_{x^2-y^2}$ orbitals forming a σ bond, while back-donation occurs from a filled metal orbital (d_{xz}, d_{yz}, d_{xy}) to the unfilled antibonding π orbital ($1\pi_g$) of the dinitrogen ligand (Fig. 3).[1,41] As the metal becomes more electron rich, more back donation occurs and the N-N bond is activated (elongated).

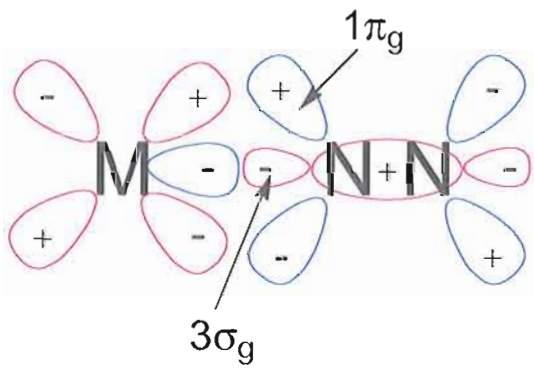

Figure 3. Dewar-Chatt-Duncanson model for the coordination of N_2 to a transition metal center. Red orbitals are filled, blue orbitals are unfilled.

Dinitrogen is both a poor σ donor and a poor π acceptor, making it a poor ligand in general; however, numerous iron dinitrogen complexes have been synthesized with a variety of ancillary ligands (Tables 1 & 2). All iron dinitrogen complexes display an η^1, or end-on, binding geometry. The majority of Fe-N_2 complexes contain a terminally bonded N_2 ligand (Table 1); however, there are a growing number of bridging dinitrogen complexes (Table 2). Nearly all of these complexes contain tertiary phosphines as coligands. Iron dinitrogen complexes are typically prepared by displacement of a

weakly bound ligand (such as H_2), abstraction of a halide or other loosely bound ligand, addition of N_2 to a coordinatively unsaturated precursor, or reduction of a precursor complex under a N_2 atmosphere.

The extent of activation of the coordinated N_2 ligand in these complexes is measured by the N-N bond length, where crystal structures have been obtained, and by IR or Raman spectroscopy to determine the N-N stretching frequency. Tables 1 and 2 list the N-N bond lengths and/or N-N stretching frequencies for all the Fe-N_2 complexes synthesized to date. As can be seen from the N-N bond lengths and N-N stretching frequencies, most of the iron dinitrogen complexes exhibit minimal activation of the N_2 ligand as compared with dinitrogen complexes of other metals.[42-44] It is important to note however that the term activation refers only to the lengthening of the N-N bond and the decrease in the N-N stretching frequency as compared with uncoordinated N_2; strong activation is not necessarily a requirement to observe reactivity of the coordinated N_2 molecule as will be seen in the following section.

Nearly all iron dinitrogen complexes contain phosphine ligands. An electron rich metal center is needed to coordinate N_2, thus electron donating ligands such as phosphines are needed. The oxidation state of the iron affects the degree of N_2 activation, with iron(0) N_2 complexes being among the most activated. Coordination number also has a large effect of the activation of N_2 with lower coordination numbers often showing increased activation of the N_2 molecule. The most activated N_2 complexes have a coordination number of only four.

Table 1. Terminal Dinitrogen Iron Complexes.

Complex	ν_{NN} (cm^{-1})	N-N bond length (Å)	Ref.
$[Fe(\eta^5\text{-}C_5H_5)(DIPPE)(N_2)][BPh_4]$	2112	1.13	45
$Fe(PEtPh_2)_3(N_2)(H)_2$	2055	–	46
$Fe(PBuPh_2)_3(N_2)(H)_2$	2060	–	46
$Fe(PEtPh_2)_2(N_2)(H)_2$	1989	–	46
$Fe(PPh_3)_3(N_2)(H)_2$	2074	–	47
$Fe(PMePh_2)_3(N_2)(H)_2$	2058	–	48
$[Fe(P(EtPPh_2)_3)(N_2)H][BPh_4]$	2100	–	49
$[Fe(N(EtPPh_2)_3)(N_2)H][BPh_4]$	2090	1.102	49,50
$Fe(N(EtPPh_2)_3)(N_2)$	1967	–	49,50
$[Fe(DPPE)_2(N_2)H][BPh_4]$	2130	–	51
$[Fe(DPPE)_2(N_2)]$	2068	–	52
$Fe(PhBP^iPr_3)(N_2)(MgCl\text{-}(THF)_2)$	1830	–	53
$[Fe(PhBP^iPr_3)(N_2)][Mg(18\text{-}C\text{-}6)]$	1884	–	53
$[Fe(N(EtP^iPr_2)_3)(N_2)(H)][PF_6]$	2090	1.113	54
$[Fe(DMeOPrPE)_2(N_2)H][BPh_4]$	2088	1.112	55
$[Fe(DMeOPrPE)_2(N_2)Cl][Cl]$	2094	–	56
$Fe(DMeOPrPE)_2(N_2)$	1966	–	57
$[Fe(DHBuPE)_2(N_2)H][Cl]$	2095	–	56
$[Fe(DMPE)_2(N_2)H]$	2094	1.13	58
$[Fe(DMPE)_2(N_2)]$	1975	–	59
$[Fe(DEPE)_2(N_2)H]$	2090	1.070	60,61
$[Fe(DEPE)_2(N_2)]$	1955	1.139	62
$[Fe(DEPE)_2(N_2)Cl][BPh_4]$	2088	1.073	63
$[Fe(DEPE)_2(N_2)Br][BPh_4]$	2091	–	63
$[Fe(DMPE)_2(N_2)Cl][BPh_4]$	2105	–	58
$[Fe(Ph_2PEtPPhEtPPhEtPh_2)(N_2)H][Br]$	2130	1.076	64
$[Fe(P(EtPMe_2)_3)(N_2)H][BPh_4]$	2117	–	65
$[Fe(P(EtP^iPr_2)_3)(N_2)][BPh_4]$	1985	1.1279	66
$[Fe(P(EtP^iPr_2)_3)(N_2)H][BF_4]$	2095	–	66
$[Fe(Si(o\text{-}C_6H_4PPh_2)_3)(N_2)]$	2041	1.106	67,68
$[Fe(Si(o\text{-}C_6H_4PPh_2)_3)(N_2)][Na([12]c\text{-}4)_2]$	1961	–	67
$[Fe(Si(o\text{-}C_6H_4P^iPr_2)_3)(N_2)]$	2008	1.065	67,68
$Fe(((2,6\text{-}HMe_2)_2C_6H_3N{=}CMe)_2C_5H_3N)_3(N_2)_2$	2124, 2053	1.090, 1.104	69
$Fe(((2,6\text{-}HMe_2)_2C_6H_3N{=}CPh)_2C_5H_3N)_3(N_2)_2$	2130, 2074	1.106, 1.107	70
$Fe(((2,6\text{-}HMe_2)_2C_6H_3N{=}CPh)_2C_5H_3N)_3(N_2)$	2061	–	70

$Fe(2,6\text{-}^{i}Pr_2PCH_2)_2C_5H_3N)(N_2)(SiH_2Ph)H$	2032	1.120	[71]
$Fe(2,6\text{-}^{i}Pr_2PCH_2)_2C_5H_3N)(N_2)H_2$	2016	–	[71]
$Fe(NHC)(N_2)_2$	2109, 2031	1.115	[72]
$Fe(NHC)(N_2)(C_2H_4)$	2056	–	[72]
$Fe(NHC)(N_2)(PMe_3)$	2032	–	[72]
$Fe(PEt_3)_2(CO)_2(N_2)$	2097	1.078	[73]
$Fe(PO^{i}Pr_3)_2(CO)_2(N_2)$	2141	–	[73]

NHC = 2,6-bis((2,6-diisopropylbenzene)imidazol-2-ylidene)pyridine

Table 2. Bridging Dinitrogen Iron Complexes

Complex	ν_{NN} (cm^{-1})	N-N bond length (Å)	Ref.
$[\{Fe(\eta^5\text{-}C_5H_5)(DPPE)\}_2(N_2)]^{2+}$	2040	–	[74]
$[\{Fe(\eta^5\text{-}C_5H_5)(DMPE)\}_2(N_2)]^{2+}$	2054	–	[75]
$[Fe(PPh_3)_2Et(\mu\text{-}N_2)]_2[Mg(THF)_4]$	1830	–	[76]
$\{Fe(PhBP^{i}Pr_3)\}_2(\mu\text{-}N_2)$	–	1.138	[53,77]
$[\{Fe(PhBP^{i}Pr_3)\}_2(\mu\text{-}N_2)][Na(THF)_6]$	–	1.171	[53]
$[\{FeCl(DEPE)_2\}_2(N_2)][BPh_4]_2$	2081	–	[78]
$\{Fe(PEt_3)_2(CO)_2\}_2(\mu\text{-}N_2)$	–	1.134	[73]
$\{Fe(POMe_3)_2(CO)_2\}_2(\mu\text{-}N_2)$	–	1.13	[79]
$\{Fe(MesNC^{t}BuCHC^{t}BuNMes)\}_2(\mu\text{-}N_2)$	1778	1.182	[80]
$[\{Fe(MesNC^{t}BuCHC^{t}BuNMes)\}_2(\mu\text{-}N_2)][K]_2$	1589, 1123	1.233	[80]
$\{Fe(MesNCMeCHCMeNMes)\}_2(\mu\text{-}N_2)$	1810	1.186	[81]
$[\{Fe(MesNCMeCHCMeNMes)\}_2(\mu\text{-}N_2)][K]_2$	1625, 1437	1.215	[81]
$\{Fe(MesNC^{t}BuCHC^{t}BuNMes)(^{t}BuC_5H_4N)\}_2(\mu\text{-}N_2)$	–	1.161	[81]
$\{Fe(MesNCMeCHCMeNMes)(^{t}BuC_5H_4N)\}_2(\mu\text{-}N_2)$	1770	1.151	[81]

1.5 Reactivity of N_2 Coordinated to Iron

Now that the coordination of dinitrogen to iron has been explored, we will now focus on the reactivity of this coordinated dinitrogen ligand. The reactivity of Fe-N_2 complexes will be separated into three categories: displacement of N_2, protonation of N_2, and elongation of the N-N bond.

1.5.1 Displacement of N_2

The displacement of the dinitrogen ligand is a commonly observed reaction pathway since the N_2 ligand is typically weakly coordinated to the iron center. The ancillary ligands often dictate the binding strength of the N_2 ligand, with increased electron donating ability increasing back-donation and stabilizing the coordinated N_2.

Dinitrogen ligands of iron complexes are typically substituted by CO and nitriles, such as MeCN and PhCN.[51,55,57,59,82,83] Some N_2 ligands can also be displaced by organic solvents. In *trans*-[Fe(DPPE)$_2$(N_2)H][BPh_4] the N_2 ligand can be displaced by pyridine, acetone, or THF.[51] Acetone has also be shown to displace the N_2 ligand of [Fe(η^5-C_5H_5)(DPPE)(N_2)][PF_6].[74] Although organic solvents have been shown to displace N_2, one of the few water-soluble N_2 complexes, *trans*-[Fe(DMeOPrPE)$_2$(N_2)H]$^+$ is inert to substitution by H_2O.[82]

The substitution reactivity of N_2 in the five coordinate complex Fe(DEPE)$_2N_2$ complex has been extensively studied and can be displaced by a wide variety of ligands including CO, CS_2, H_2, CO_2, and HCl.[84,85] The Fe(DEPE)$_2N_2$ complex was also shown to cleave C-S, C-H, and N-H bonds of various heterocycles, however this resulted in loss of the dinitrogen ligand without functionalization.[86]

1.5.2 Protonation of Fe-N_2 Complexes

The most common type of reactivity studied for iron dinitrogen complexes has been the reactivity of the coordinated N_2 toward protonation.[87] This mode of reactivity is aimed at mimicking biological nitrogen fixation by using a proton source and the electrons of the iron complex to reduce the coordinated dinitrogen to ammonia.

Leigh and coworkers were the first to observe such reactivity in 1991. Using DMPE as the ancillary ligands, the dinitrogen hydride complex, *trans*-$[Fe(dmpe)_2(N_2)H]^+$ (Scheme 1), was synthesized by N_2 substitution of H_2 in *trans*-$[Fe(dmpe)_2(H_2)H]^+$.[59,88,89]

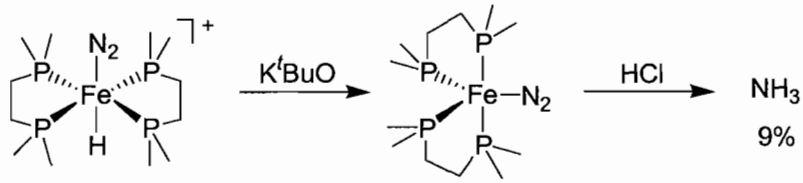

Scheme 1. Synthesis of $Fe(DMPE)_2N_2$ and protonation to yield ammonia.

The dinitrogen ligand in *trans*-$[Fe(DMPE)_2(N_2)H]^+$ is minimally activated with a N-N bond length of 1.13Å and ν_{NN} = 2094 cm^{-1}. The complex produced trace amounts of ammonia (<4%) upon protonation with H_2SO_4 and no NH_3 upon exposure to HCl.[88] However, by deprotonating the hydride ligand to form $Fe(DMPE)_2N_2$, which results in the formal reduction of the iron center from 2+ to 0, the activation of the dinitrogen ligand can be sufficiently increased (ν_{NN} = 1975 cm^{-1}) to allow reaction with a strong acid (Scheme 1). Optimized yields of ammonia produced from this five coordinate Fe-N_2 complex reached 20% using HCl at low temperatures.[89] Using HCl they also showed that the iron dichloride starting material, *trans*-$Fe(DMPE)_2Cl_2$, was regenerated.[88]

The iron(0) N_2 complex, $Fe(DMPE)_2N_2$ was never isolated and the assignment of this complex as the active ammonia producing species was thrown into question by work done on the analogous DEPE system.

In contrast to the reactivity observed by Leigh, Komiya and coworkers were unable to detect any ammonia formation during the protonation of $Fe(DEPE)_2N_2$ (Scheme 2).[62,84] Access to this complex was achieved by a different route than that described for the DMPE system. $Fe(DEPE)_2N_2$ was directly generated from *trans*-$Fe(DEPE)_2Cl_2$ and sodium metal under an atmosphere of dinitrogen. This species was isolated and the crystal structure was obtained, confirming the proposed structure.

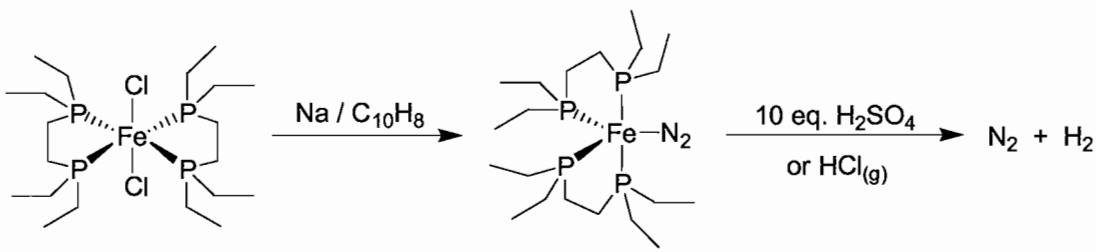

Scheme 2. Synthesis of $Fe(DEPE)_2N_2$ and protonation to yield N_2 and H_2.

Upon protonation with HCl or H_2SO_4, no NH_3 or N_2H_4 were produced, only N_2 and H_2 were observed (Scheme 2). This result is puzzling as both the DMPE and DEPE iron(0) N_2 complexes display similar activation of the coordinated dinitrogen, ν_{NN} = 1975 cm^{-1} and ν_{NN} = 1955 cm^{-1} respectively. Because $Fe(DEPE)_2N_2$ was isolated in pure form it threw into doubt that the $Fe(DMPE)_2N_2$ complex was in fact responsible for ammonia formation. However, continued work on the protonation of iron N_2 phosphine complexes showed that production of ammonia observed in the protonation of $Fe(DMPE)_2N_2$ was not unique.

Using a mixed nitrogen phosphine tripodal ligand, $N(CH_2CH_2PPh_2)_3$, and following a similar synthetic strategy as that used by Leigh, George and coworkers were able to produce hydrazine and ammonia from an iron dinitrogen complex (Scheme 3).[50] Starting from $[Fe(N(CH_2CH_2PPh_2)_3)(N_2)H][BPh_4]$, which had previously been synthesized by Sacconi, they were able to deprotonate the hydride ligand using *n*-BuLi to form the iron(0) complex $Fe(N(CH_2CH_2PPh_2)_3)N_2$ (Scheme 3). This complex displayed similar activation of the N_2 as the other iron(0) complexes, with a $\nu_{NN} = 1967$ cm^{-1}. Upon exposure to HBr, hydrazine (11%) and ammonia (3%) were produced.

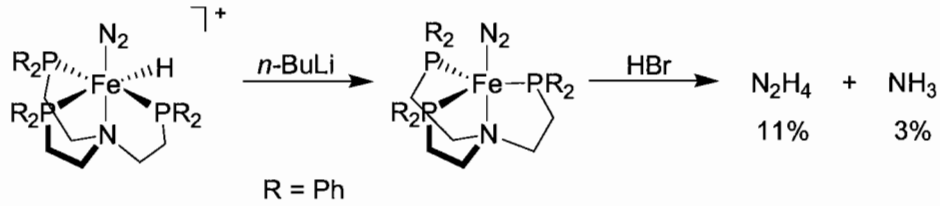

Scheme 3. Synthesis of $Fe(N(CH_2CH_2PPh_2)_3)N_2$ and protonation to yield N_2H_4 and NH_3.

Following the work of Leigh our group was also able to observe ammonia upon protonation of an iron(0) N_2 complex (Scheme 4).[57] The dinitrogen hydride complex, *trans*-$Fe(DMeOPrPE)_2(N_2)H]^+$, was again synthesized by substitution of N_2 for H_2 in *trans*-$[Fe(DMeOPrPE)_2(H_2)H]^+$. Of particular note is that this dihydrogen complex was generated directly from H_2 and *trans*-$Fe(DMeOPrPE)_2Cl_2$, instead of sodium borohydride, thus H_2 was the ultimate source of electrons for the reduction of N_2 to NH_3. Again the N_2 ligand in the six-coordinate hydride species is minimally activated, N-N = 1.112Å and $\nu_{NN} = 2088$ cm^{-1}, and is unreactive toward protonation.[55] By deprotonating the hydride ligand to form $Fe(DMeOPrPE)_2N_2$ the activation of the N_2 is increased (ν_{NN}

= 1966 cm^{-1}) and protonation of the complex with 1M triflic acid produces 15% NH_3 and 2% N_2H_4 (Scheme 4).[57]

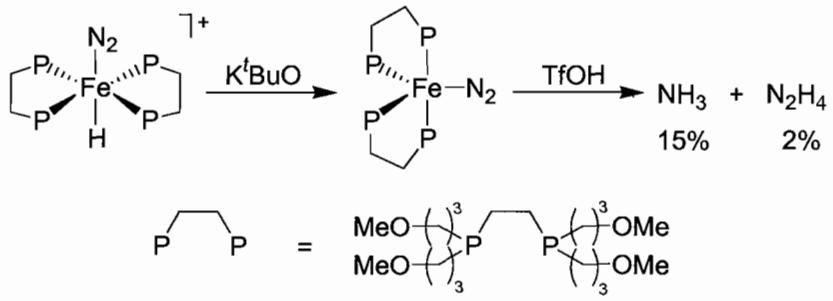

Scheme 4. Synthesis of $Fe(DMeOPrPE)_2N_2$ (DMeOPrPE = 1,2-(bis(dimethoxypropyl)phosphino)ethane) and protonation to yield NH_3 and N_2H_4.

Recently protonation of an iron N_2 complex utilizing a tripodal ligand system has been revisited. Using a unique tripodal ligand, $Si(1,2\text{-}C_6H_4PPh_2)_3$, Peters and coworkers were able to synthesize an iron(I) N_2 complex that could generate hydrazine on exposure to a strong acid (Scheme 5).[67] The N_2 ligand seems to be minimally activated (ν_{NN} = 2041 cm^{-1}), however this complex produces 17% hydrazine upon reaction with HBF_4. The yield of hydrazine was increased to 47% by addition of a one-electron reducing agent ($CrCl_2$). Interestingly, further reduction of the iron(I) dinitrogen complex to the iron(0) N_2 complex results in increased activation of the N_2 (ν_{NN} = 1967 cm^{-1}), yet no reduction of N_2 is observed under the same reaction conditions. The authors hypothesize that the increased reducing ability of the iron(0) N_2 complex favors H^+ reduction over N_2 reduction.

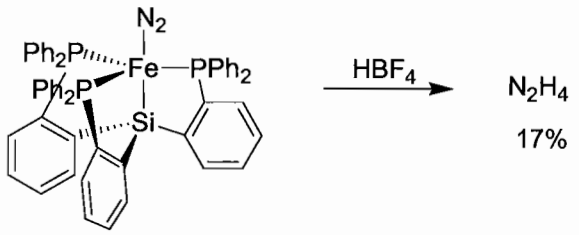

Scheme 5. Protonation of $Fe(Si(1,2\text{-}C_6H_4PPh_2)_3)N_2$ to yield N_2H_4 and NH_3.

Field and coworkers have also recently utilized a tripodal ligand. $Fe(P(CH_2CH_2P^iPr_2)_3)N_2$ was synthesized by reducing the chloride precursor under a N_2 atmosphere (Scheme 6).[66] Exposure of this complex to a weak acid, lutidinium tetrafluoroborate, results in protonation of the iron center to yield $[Fe(P(CH_2CH_2P^iPr_2)_3)(N_2)H)]^+$ (Scheme 6). No ammonia or hydrazine was observed, although the protonation of this complex with strong acids has not yet been reported.

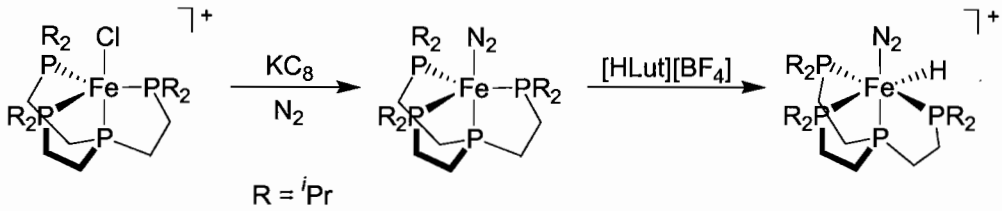

Scheme 6. Synthesis of $Fe(P(CH_2CH_2P^iPr_2)_3)N_2$ and protonation to yield $[Fe(P(CH_2CH_2P^iPr_2)_3)(N_2)H]^+$.

As demonstrated above, the protonation of iron N_2 complexes is very inefficient, producing limited yields of ammonia and/or hydrazine. From the results of these protonation experiments we can draw some conclusions. The first is that increasing the activation of the coordinated N_2 ligand does not necessarily lead to increased yields of N_2 reduction. This arises due to two factors: increasing the reducing ability of the iron center favors H^+ reduction, and increasing the electron density of the iron center favors

protonation of the metal center rather than the dinitrogen ligand. Theoretical calculations have shown that for the reaction of $Fe(DMPE)_2N_2$ with acid, protonation of the electron rich iron center is favored over protonation of the terminal nitrogen by 40 kcal/mol.[90] Attempts have been made to address this problem by increasing the steric bulk around the iron center, thus favoring protonation of the N_2, without success.

Another factor limiting the yields of N_2 reduction in these systems is that the only source of electrons is the iron center. Since these iron centers are likely donating only two electrons ($Fe^0 \rightarrow Fe^{II}$), 3 separate iron complexes must be used to fully reduce N_2 to NH_3 (a six electron process), thus limiting the theoretical yields. Peters has shown that by addition of an external reducing reagent the yields of N_2 reduction can be significantly increased.[67]

It is interesting to note that systems using tripodal ligands favor the formation of hydrazine while systems using bidentate ligands favor the formation of ammonia. This difference provides information about the mechanism of N_2 reduction in these systems. One mechanistic consideration is that tripodal ligands may not be able to accommodate η^2 ligand binding modes. Such an η^2 ligand binding mode is possible with bidentate ligand systems as was shown recently in the syntheses and structural characterizations of *cis*-$[Fe(P_2)_2(\eta^2\text{-}N_2H_4)]^{2+}$, where P_2 = DMPE or DMeOPrPE.[91,92] In fact one of these η^2-N_2H_4 complexes has been shown to produce ammonia and hydrazine upon protonation via a disproportionation mechanism.[91]

Another key difference between the two ligand geometries is that protonation of the iron center results in a *trans* hydride with bidentate ligands and a *cis* hydride with

tripodal ligands. The strong *trans* influence of the hydride ligand in the bidentate systems could affect the stability of a coordinated N_2H_4 molecule favoring cleavage of the N_2H_4 to NH_3.

1.5.3 Elongation of the N-N Bond

Complete cleavage of dinitrogen in the absence of H^+ has been observed for some group 5 and 6 metals,[93-96] however no such reaction has yet been observed for iron dinitrogen complexes. Toward this goal recent progress has been made in elongating the N-N bond using unique ligand sets.

Peters and coworkers have synthesized three Fe-N_2 complexes that show atypical activation of the coordinated N_2 ligand.[53] Reduction of a tris(phosphino)borate iron chloride complex with Mg^0 under a dinitrogen atmosphere results in formation of a terminally bonded N_2 complex (Scheme 7).

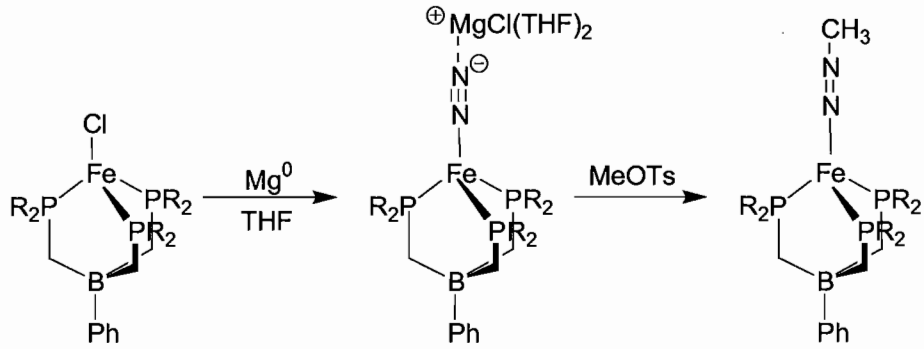

Scheme 7. Synthesis and reactivity of a terminal N_2 iron complex stabilized by tris(phosphino)borate ligands, where R = ^{i}Pr.

The complex shows a relatively low energy stretching frequency of 1830 cm^{-1}. This activated N_2 molecule can then be functionalized by reaction with an electrophile (MeOTs) (Scheme 7). While this type of reactivity had been previously observed for Mo and W systems,[97] this represents the first and only example of the direct conversion

of an iron coordinated N_2 molecule to a diazenido (N_2R^-) complex by addition of an electrophile.

If the iron halide precursor is reduced using Na/Hg amalgam, a bridged dinitrogen complex is obtained (Scheme 8). This dinuclear Fe^I N_2 bridged complex has a N-N bond length of 1.138Å. Further exposure of this complex to Na/Hg amalgam results in a one electron reduction to the mixed valence Fe^IFe^0 N_2 complex, which elongates the N-N bond to 1.171Å.

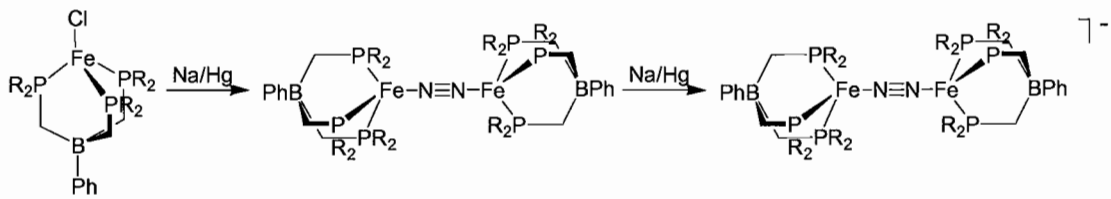

Scheme 8. Synthesis of bridged N_2 iron complexes stabilized by tris(phosphino)borate ligands, where R = ^{i}Pr.

Holland and coworkers have been able to achieve significant elongation of the N-N bond using low-coordinate iron complexes stabilized by bulky β-diketiminate ligands (Fig. 4).[80,81] By reducing the chloride precursor with sodium naphthalenide or potassium/graphite they were able to synthesize bridged dinitrogen complexes with N-N bond lengths of 1.18Å (Scheme 9).

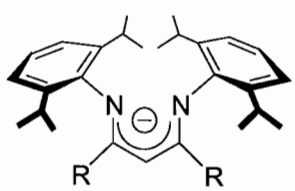

Figure 4. β-Diketiminate ligands used by Holland and coworkers, where R = CH_3 or ^{t}Bu.

The stability of these complexes was explored in the presence of a variety of ligands (CO, PPh_3, C_6H_6), with reactivity resulting in loss of N_2 and coordination of the ligand. The steric bulk of the ligand affects the stability, with the ^{t}Bu complex being more stable than the Me complex. Further reduction of these complexes results in even more activation of the N-N bond, with the N-N bond lengths reaching over 1.2Å (Scheme 9). These N-N bond distances are the longest observed for any iron dinitrogen complex. Even though the N_2 ligands in these complexes are quite activated, reaction of the Me complex with various electrophiles gave no evidence for transformation of the N_2 molecule.

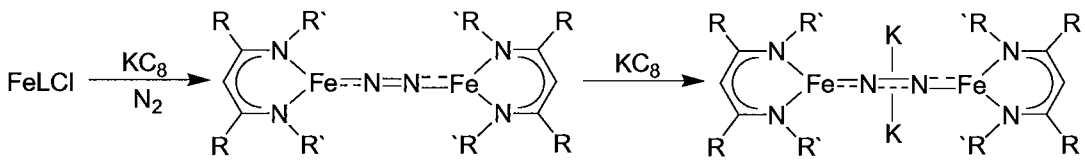

Scheme 9. Synthesis of bridged dinitrogen iron complexes stabilized by β-diketiminate ligands, where R = CH_3 or ^{t}Bu.

1.6 Coordination Chemistry of Reduced Dinitrogen Species with Iron

The coordination chemistry of reduced dinitrogen species with iron is becoming increasingly important. Currently the mechanism of N_2 fixation, both in synthetic and biological systems, is unknown. However, recent biochemical evidence for dinitrogen reduction in nitrogenase suggests a mechanism that proceeds through diazene and hydrazine intermediates on the way to ammonia. Thus the study of iron coordination complexes of these ligands is important in helping to interpret these biochemical results and to confirm the proposed mechanism. The following section will describe the

coordination chemistry of N_2H_2, N_2H_4, NH_3, nitride to iron as these species represent potential intermediates in nitrogen fixation. The coordination chemistry of aryl and alkyl substituted N_2 species (i.e. N_2R_2, N_2R_4, etc.) will not be discussed here.

1.6.1 Iron Diazene (N_2H_2) Complexes

Diazene (N_2H_2), which represents the addition of two electrons and two protons to dinitrogen, is one of the first intermediates along the pathway from N_2 to ammonia. Diazene is known to be an intermediate in nitrogenase,[37] therefore the coordination chemistry of diazene with iron is important. Unfortunately, coordination complexes of diazene (N_2H_2) are rare,[98,99] especially those containing iron. The lack of diazene complexes likely arises from the reactive nature of the diazene molecule. Diazene is very unstable and readily decomposes (eq. 3) and/or disproportionates (eq. 4) on the order of seconds.[100,101] However, by coordination of diazene to a transition metal center the diazene molecule can be stabilized. Diazene complexes are primarily synthesized by oxidation of a hydrazine complex, typically with $Pb(OAc)_4$, although other oxidizing reagents such as O_2 and $[FeCp]^+$ have been used successfully. This method of preparation circumvents the problem of having uncoordinated diazene in solution which would quickly disproportionate, although as will be discussed below, there are examples where diazene has been generated in solution and coordinated to an iron center.

$$N_2H_2 \longrightarrow N_2 + H_2 \quad (3)$$

$$2N_2H_2 \longrightarrow N_2H_4 + N_2 \quad (4)$$

Using a variety of iron sulfur scaffolds Sellmann and coworkers were able to successfully synthesize a handful of bridging η^1 diazene complexes. Using the NHS_4

ligand they were able to oxidize the terminal η^1 N_2H_4 complex to a bridging diazene complex (eq. 5).[102] The coordinated diazene has a *trans* geometry with a N-N bond distance of 1.30Å.

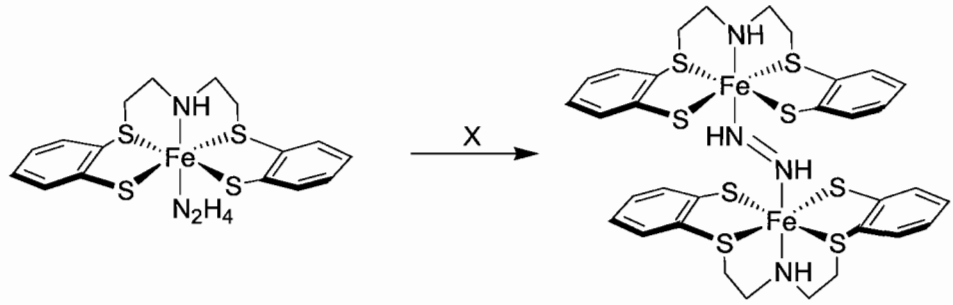

(5)

A related complex using an all sulfur ligand was later synthesized by Sellmann's group. The bridging η^1 diazene complex could be prepared by oxidation of the corresponding hydrazine complex (Scheme 10)[103] or by trapping diazene gas generated in situ (Scheme 10).[104] The diazene ligand was again found to coordinate in a *trans* geometry with a N-N bond distance of 1.288Å.

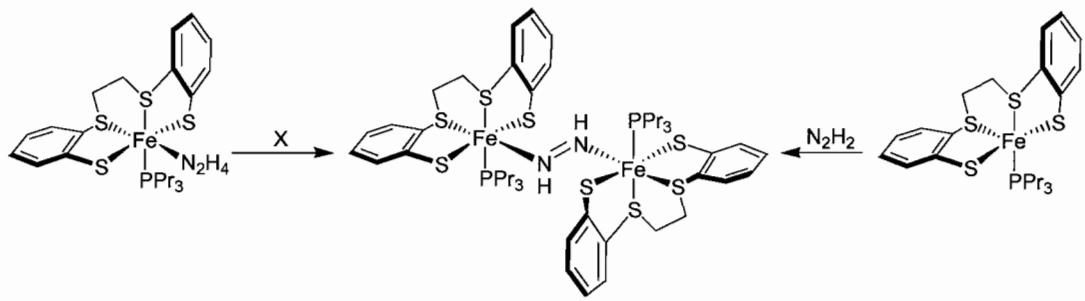

Scheme 10. Synthesis of a bridged diazene iron complex.

A third example synthesized by Sellmann and coworkers utilized yet another tetradentate sulfur ligand (eq. 6).[105] Using this ligand they were able to crystallographically characterize both diastereomers (the diastereomers arise due to the

chirality of the iron center) and study the isomerization reaction. The diazene ligand in these complexes is stabilized by steric shielding, strong π-bonds between the iron d-orbitals and the π system of diazene, and bifurcated hydrogen bonding between the diazene protons and the thiolate ligands.

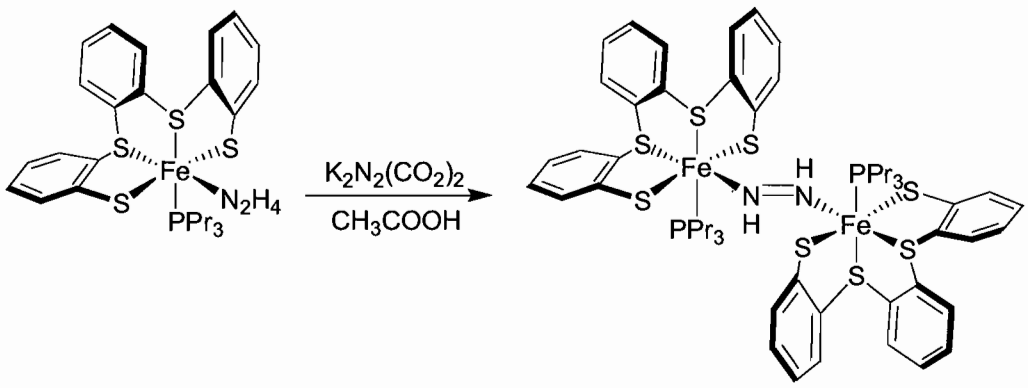

(6)

Iron phosphine scaffolds have also recently been used to stabilize diazene. Reaction of $Fe(P_2)_2N_2$ (where P_2 = DMPE or DMeOPrPE) with hydrazine results in the formation of an iron(0) diazene complex and formation of H_2 (Scheme 11).[107,108] The crystal structure of *cis*-$Fe(DMPE)_2(N_2H_2)$ was obtained and showed *trans*-diazene coordinated in an η^2 geometry. These iron(0) diazene complexes can also be synthesized by an alternative route. Deprotonation of the η^2-N_2H_4 complex with K^{t}BuO results in deprotonation of the coordinated hydrazine to form diazene (Scheme 11).[92,107] The complex can be represented by two resonance forms; an iron(0) diazene complex or an iron(II) hydrazido(2-) complex, however calculations favor the iron(0) diazene resonance form.[92] It was also observed that further reaction of *cis*-$Fe(DMPE)_2(N_2H_2)$ with a mixture of K^{t}BuO and ^{t}BuLi (Schlosser base) resulted in formation of $Fe(DMPE)_2N_2$.

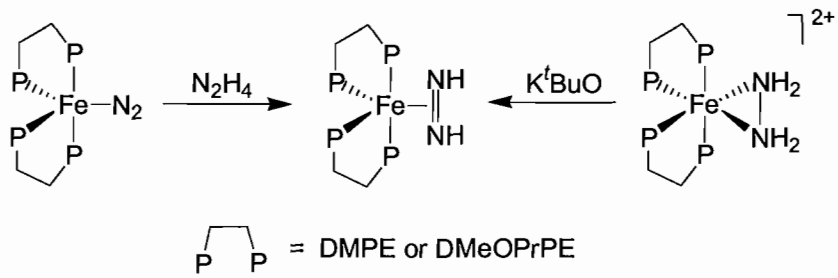

Scheme 11. Synthesis of η^2 diazene complexes stabilized by bidentate phosphine ligands.

1.6.2 Iron Hydrazine (N_2H_4) Complexes

Hydrazine represents the addition of four electrons and four protons to dinitrogen. Hydrazine is also considered a likely intermediate of nitrogen fixation and can be reduced by nitrogenase to ammonia. As with diazene, there are relatively few examples of hydrazine coordinating to an iron center. Nearly all iron N_2H_4 complexes contain hydrazine bonded in a terminal[109-120] η^1 geometry or a bridging[116,121] η^1 geometry. Recently an η^2 coordination mode has been observed using iron phosphine scaffolds.[91,92] A few of these iron hydrazine complexes will be highlighted here.

Sellmann and coworkers have synthesized several iron hydrazine complexes using biologically relevant thiolate ligands. Most significantly, one particular iron thiolate system was shown to stabilize N_2H_2, N_2H_4, and NH_3 ligands. Unfortunately the final ligand in the series, N_2, did not coordinate to the complex.[112]

While most iron hydrazine complexes contain only a single hydrazine ligand there are a few examples of an iron scaffold accommodating multiple hydrazine ligands. Albertin and coworkers have synthesized a bis η^1 hydrazine complex.[114] Oxidation of the hydrazine ligands using $Pb(OAc)_4$ to yield the bis diazene complex was

unsuccessful. Lee and coworkers have also been able to synthesize an iron complex that accommodates multiple hydrazine ligands. By reacting a iron(II) thiolate dimer with hydrazine an iron dimer containing two bridging hydrazine ligands and four terminal hydrazine ligands was obtained.[116]

Our group has recently synthesized a novel η^2 N_2H_4 complex and explored its acid base reactivity.[91,107] Addition of a strong acid (1M TfOH) to a solution of *cis*-$[Fe(DMeOPrPE)_2(N_2H_4)]^{2+}$ results in the formation ammonia (21%) via a disproportionation reaction. This reaction suggests that the hydrazine complex could be an intermediate in the reduction of N_2 in iron phosphine systems. As described in the previous section, the η^2 N_2H_4 complex can also be deprotonated to yield η^2 diazene (N_2H_2) and hydrazido(1-) (N_2H_3) complexes.

Holland's group has shown that an η^1 N_2H_4 complex undergoes N-N bond cleavage at elevated temperatures (60 °C) to yield a bridged $-NH_2$ complex (eq. 7).[120] This represents a very rare example of N-N bond cleavage among iron systems and demonstrates the utility of low-coordinate iron complexes in the discovery of novel reactivity pathways.

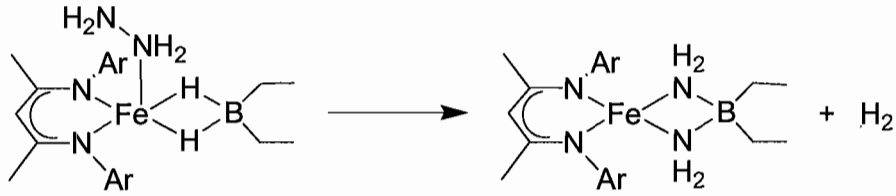

(7)

1.6.3 Iron Ammonia (NH_3) Complexes

Iron complexes containing ammonia ligands are more common than diazene or hydrazine complexes, however only a handful of these complexes will be highlighted here. Sellmann and coworkers have synthesized ammonia complexes containing thiolate ligands. These complexes are important due to the use of biologically relevant ligands and the fact that other reduced dinitrogen intermediates (i.e. N_2H_4, N_2H_4) have been synthesized using the same scaffold.[112]

Holland has observed the addition of two equivalents of ammonia to a low-coordinate sulfido bridged iron dimer.[122] Chirik has also recently discovered a low-coordinate iron ammonia complex synthesized by the addition of a NH transfer reagent to an iron bis dinitrogen complex (eq. 8). The source of the ammonia ligand is the NH transfer reagent, the dinitrogen ligands are simply displaced.[123] These complexes prove that the low-coordinate iron centers in nitrogenase should be able to stabilize ammonia ligands.

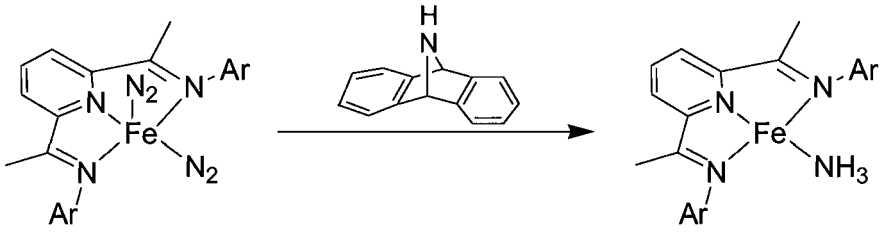

(8)

An ammonia complex supported by bidentate phosphine ligands, *trans*-$[Fe(DMPE)_2(NH_3)H]^+$, has been synthesized by Bergman's group. Because this same scaffold has been shown to reduce N_2 to ammonia under acidic conditions this complex

may represent the last intermediate complex in the mechanism of ammonia production from N_2.[124]

1.6.4 Iron Nitride Complexes

Nitrogenase is proposed to proceed through a mechanism proceeding through diazene and hydrazine intermediates, where the N-N bond is cleaved toward the end of the overall reaction. Conversely, it has been shown that for Mo and W systems cleavage of the N-N bond is achieved relatively early, releasing one equivalent of NH_3 and forming a metal nitride intermediate. The nitride complex is then further reduced and protonated to produce a second equivalent of ammonia. Therefore, if iron containing systems were to follow a similar mechanism as that observed for Mo and W systems, iron nitride complexes could be potentially important intermediates.

Several bridging and terminal nitrido complexes of iron have been synthesized in a variety of oxidation states.[53,77,125-130] In keeping with the theme of this review only those iron nitrido complexes that exhibit reactivity related to nitrogen fixation will be highlighted here. It is important to highlight that no iron nitride complex has yet been generated directly from dinitrogen; instead these iron nitride complexes are typically generated by loss of N_2 from an iron azide precursor.

Smith and coworkers have recently synthesized an iron nitride complex using the phenyltris(1-mesitylimidazol-2-ylidene)borate ligand (Scheme 12).[131] Reaction of the chloride precursor with sodium azide followed by irradiation and loss of N_2 generates the four-coordinate iron nitrido complex. Unlike other terminal nitrido species, the complex was able to be isolated and the solid-state structure was obtained.

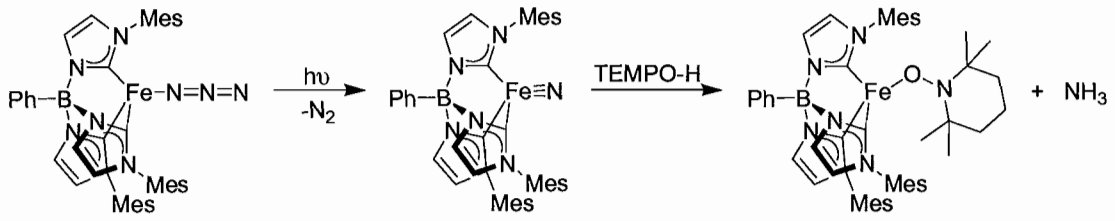

Scheme 12. Synthesis of an iron nitride complex and reaction with a hydrogen atom source to yield ammonia.

Reaction of the nitride complex with TEMPO-H (TEMPO-H = 1-hydroxy-2,2,6,6-tetramethylpiperidine) results in up to 74% ammonia (Scheme 12). It is thought the initial N-H bond forming step occurs through a hydrogen atom transfer. Metal hydrides can also act as hydrogen atom sources, although with significantly lower yields of ammonia. This reaction is unique among iron ammonia producing reactions in that the protons and electrons are coming from the same source. However, the ammonia is not coming directly from dinitrogen.

Peters and coworkers have shown the utility of tris(phosphino)borate ligands in stabilizing many potential intermediates of nitrogen fixation.[132] Using this ligand they have been able to generate a low-oxidation state bridging nitride species.[130] The nitride complex is generated using sodium azide followed by reduction with sodium mercury amalgam (Scheme 13).

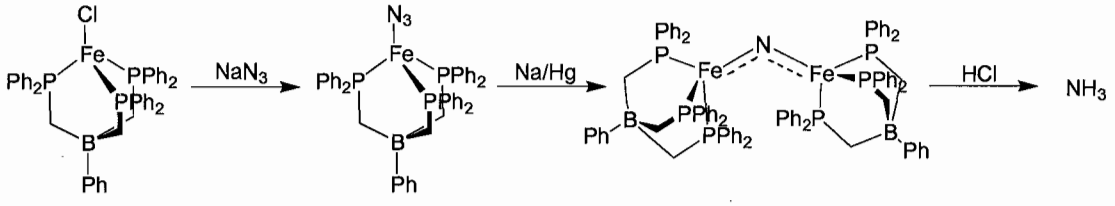

Scheme 13. Synthesis of a bridged iron nitride complex and reaction with acid to produce ammonia.

This nitride can be converted to ammonia in good yield (80-95%) upon exposure to 3 equivalents of HCl. Again however the ammonia is not directly generated from dinitrogen. In an analogous system where the phenyl groups on the phosphines have been replaced by isopropyl groups, they were able to show the generation of a terminal nitride species that underwent a coupling reaction to produce the bridging dinitrogen complex.[53,77] This nitride coupling reaction represents the microscopic reverse of the dinitrogen cleavage reaction, however with this system they were unable to achieve this cleavage reaction.

1.7 Summary

As more and more biochemical evidence implicates iron as the active metal in biological nitrogen fixation understanding how dinitrogen and reduced dinitrogen species interact with iron is becoming increasingly important. There are now numerous synthetic iron dinitrogen coordination complexes, all of which contain an end-on (η^1) bonded N_2. While iron dinitrogen complexes are predominantly terminally bound, there are increasing numbers of bridged dinitrogen complexes. The activation of the coordinated N_2 is governed by the electronics of the ancillary ligands, with increased electron donation increasing activation. Coordination number and iron oxidation state also greatly influence the activation of dinitrogen. As both coordination number and oxidation decrease, the extent of N-N bond activation increases. It is important to note however that increased activation does not necessarily lead to increased reactivity of the coordinated dinitrogen.

The reactivity of iron dinitrogen complexes can be separated into three categories: displacement, protonation, and elongation. Because dinitrogen is often weakly bound a commonly observed reaction pathway is the displacement of the N_2 ligand. Numerous ligands have been shown to displace N_2 including H_2, CO, MeCN, acetone, etc. Five-coordinate iron dinitrogen complexes using a variety of phosphine ligands have shown that dinitrogen can be successfully reduced to ammonia and/or hydrazine by addition of a strong acid. While these complexes do not contain biologically relevant ancillary ligands, this class of compounds represents one of the few functional mimics of nitrogenase. Recently, progress has been made toward the goal of cleaving the N-N bond of dinitrogen, with low-coordinate iron dinitrogen complexes showing the largest degree of N-N bond elongation.

The iron coordination chemistry of diazene, hydrazine, and ammonia is growing more important as biochemical evidence suggests that these species are present during the mechanism of nitrogen fixation in nitrogenase enzymes. The study of these complexes is crucial in providing spectroscopic and reactivity benchmarks for comparison with data obtained on nitrogenase enzymes.

1.8 Bridge

This chapter reviewed the literature on iron dinitrogen coordination chemistry as well as reduced dinitrogen intermediates including diazene, hydrazine, ammonia, and nitride complexes. Chapter II will describe the synthesis, characterization, and reactivity of dihydrogen and dinitrogen complexes containing a water-soluble bidentate phosphine

ligand. Chapter II contains previously published co-authored material. These dinitrogen and dihydrogen complexes are precursors to the active ammonia producing complex that will be described in Chapter III. Chapter III contains previously published co-authored material. Chapter IV will then discuss investigations into the mechanism of ammonia formation through the synthesis of iron coordination complexes containing N_2 reduction intermediates. Chapter IV contains previously published co-authored material. Finally, Chapter V will provide a summary of this dissertation. Appendix B also contains previously published co-authored material.

CHAPTER II

PRECURSORS TO DINITROGEN REDUCTION: STRUCTURES AND REACTIVITY OF *trans*-$[Fe(DMeOPrPE)_2(\eta^2\text{-}H_2)H]^+$ AND *trans*-$[Fe(DMeOPrPE)_2(N_2)H]^+$

Some of this work has been previously published and is reproduced with permission from:
Crossland, J. L.; Zakharov, L. N.; Tyler, D. R. *Acta Cryst.* **2007**, *E63*, m1196-1197.
Crossland, J. L.; Zakharov, L. N.; Tyler, D. R. *Acta Cryst.* **2008**, *E64*, o1111.
Crossland, J. L.; Young, D. M.; Zakharov, L. N; Tyler, D. R. *Dalton Trans.* **2009**, *manuscript submitted.*

2.1 Introduction

Since the discovery of the first dinitrogen complex by Allen and Senoff in 1965,[1] extensive research has focused on creating a homogeneous catalyst capable of reducing dinitrogen to ammonia at room temperature and pressure.[2-4] Many remarkable advances have been made toward this goal,[5-7] including the achievement of a catalytic cycle.[8] The chemistry of iron dinitrogen complexes represents a growing subset of this field,[9,10] largely due to the fact that increasing evidence implicates an iron reaction site in the mechanism of nitrogenase enzymes.[11-13] Several groups, including our own, have found that addition of acid to five-coordinate iron dinitrogen phosphine species yields varying amounts of ammonia and/or hydrazine.[14-18] Of particular interest to our group was a cycle pioneered by Leigh (Scheme 1).[19] In the Leigh cycle, a *trans*-$[Fe(P_2)_2(H_2)H]^+$

complex (P_2 = a bidentate phosphine) is generated from *trans*-$[Fe(P_2)_2Cl_2]^+$, a hydride source, and an acid. Following exchange of N_2 for H_2, the hydride ligand can be "reductively" deprotonated to yield the five-coordinate iron(0) dinitrogen complex. Protonation of this complex results in moderate yields of ammonia and/or hydrazine.

This chapter describes our modifications of the Leigh cycle (Scheme 1) and the synthesis, characterization, and substitution reactivity of the precursor dihydrogen and dinitrogen complexes leading to the formation of $Fe(DMeOPrPE)_2N_2$ (DMeOPrPE = 1,2-bis(dimethoxypropylphosphino)ethane), the active ammonia producing complex.[20,21]

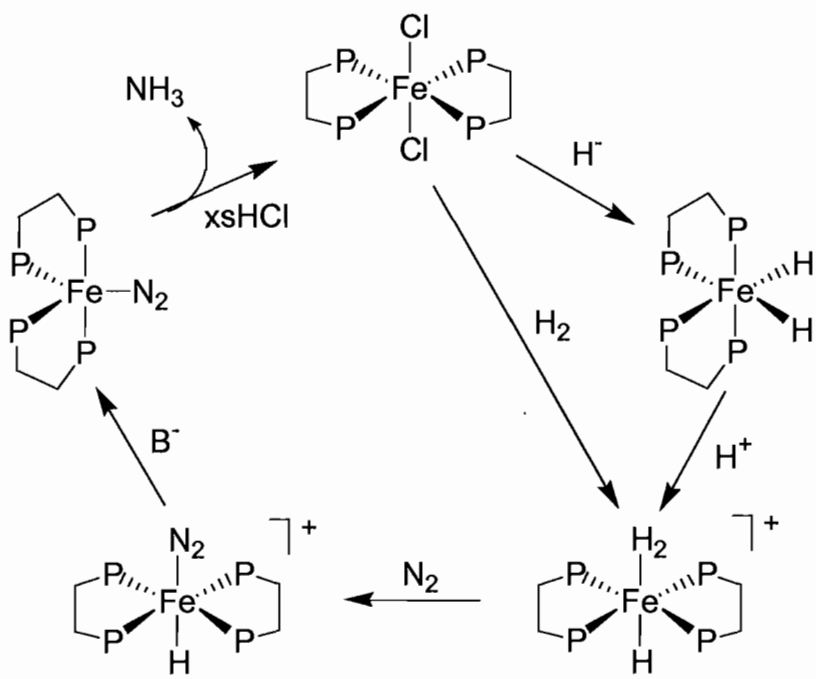

Scheme 1. Leigh cycle for the reduction of N_2 to NH_3 in $Fe(P_2)_2N_2$ systems. The direct reaction of the *trans*-$[Fe(P_2)_2Cl_2]^+$ with dihydrogen represents our modification of the Leigh cycle.

2.2 Experimental

2.2.1 Materials and Reagents

All manipulations were carried out in either a Vacuum Atmospheres Co. glove box (argon- or N_2-filled) or on a Schlenk line using argon or nitrogen. HPLC grade THF, hexane, and diethyl ether (Burdick and Jackson) were dried and deoxygenated by passing them through commercial columns of CuO, followed by alumina under an argon atmosphere. Toluene (Aldrich) was distilled under N_2 from CaH_2 and degassed via three freeze-pump-thaw cycles. Commercially available reagents were used as received. *trans*-Fe(DMeOPrPE)$_2$Cl$_2$[22] and *trans*-[Fe(DMeOPrPE)$_2$(CH$_3$CN)H]$^{+}$[21] were synthesized as previously reported. Deuterated solvents were purchased from Cambridge Isotope Laboratories and used as received.

2.2.2 Instrumentation

$^{31}P\{^1H\}$ and ^1H NMR spectra were recorded on either a Varian Unity/Inova 300 spectrometer at an operating frequency of 299.94 (^1H) and 121.42 (^{31}P) MHz or a Varian Unity/Inova 500 spectrometer at an operating frequency of 500.62 (^1H) and 202.45 (^{31}P) MHz. The ^1H and ^{31}P chemical shifts were referenced to the solvent peak and to an external standard of 1% H_3PO_4 in D_2O, respectively. NMR samples were sealed under argon or dinitrogen in 7 mm J. Young tubes. Note that the ^1H NMR data for the methyl and methylene regions in complexes containing the DMeOPrPE ligand were generally broad and uninformative and therefore are not reported in the synthetic descriptions below. Elemental analyses were performed by Robertson Microlit Laboratories. Mass spectra were obtained using an Agilent 1100 LC/MS Mass Spectrometer. The samples

were dissolved in Et_2O and introduced into the ionization head (ESI) using the infusion method.

2.2.3 X-Ray Crystallography

X-ray diffraction data were collected at 100K (*trans*-[Fe(DMeOPrPE)$_2$(H_2)H][BPh_4]) and 173K ([Fe(DMeOPrPE)$_2$Cl][BPh_4] and *trans*-[Fe(DMeOPrPE)$_2$(N_2)H][BPh_4]) on a Bruker Apex CCD diffractometer with MoKα-radiation (λ=0.71073 Å). Absorption corrections were applied by SADABS.[23] The structures were found by direct methods and calculations of difference Fourier maps. All non-hydrogen atoms were refined with anisotropic thermal parameters. Some of the C and O atoms in the -$(CH_2)_3$OMe groups of [Fe(DMeOPrPE)$_2$Cl][BPh_4] and *trans*-[Fe(DMeOPrPE)$_2$(N_2)H][BPh_4] are disordered over two positions and were refined with restrictions; the standard C-C and C-O distances were used in the refinements as targets for corresponding bond distances. H atoms in such groups were treated in calculated positions and refined in a rigid group model. All H atoms in *trans*-[Fe(DMeOPrPE)$_2$(H_2)H][BPh_4] were found on the difference F-map and refined with isotropic thermal parameters. It was found that the Fe atom in *trans*-[Fe(DMeOPrPE)$_2$(H_2)H][BPh_4] was disordered over two positions (in a 85:15 ratio) related to two opposite orientations of the HFe(H_2) fragment. The Fe1 and Fe1a positions are out from the average plane of the four P atoms bonded to the Fe atom on 0.14 and 0.22 Å, respectively. Positions of the H atoms corresponding to the second orientation of this fragment were not found and the H atoms were refined in the positions

with highest occupation only, but with occupation factors of 1.0. All calculations were performed by Bruker SHELXTL 6.10 package.

Crystal data for *trans*-[Fe(DMeOPrPE)$_2$(H$_2$)H][BPh$_4$] (I). $C_{60}H_{103}BFeO_8P_4$, M = 1142.96, triclinic, space group P-1, a = 10.8357(10), b = 16.9005(16), c = 18.2311(17) Å, α = 90.013(2), β = 105.896(1), γ = 103.852(2)°, V = 3109.8(5) Å^3, D_c = 1.221 g cm^{-3}, μ = 0.396 mm^{-1}, Z = 2, λ = 0.71073 Å, T = 100 K, 24706 reflections collected, 13266 independent (R_{int} =0.0130), R_1 [$I > 2\sigma(I)$] = 0.0310, wR_2 [$I > 2\sigma(I)$] = 0.0810, R_1 (all data) = 0.0346, wR_2 (all data) = 0.0841.

Crystal data for *trans*-[Fe(DMeOPrPE)$_2$Cl][BPh$_4$] (II). $C_{60}H_{100}BClFeO_8P_4$, M = 1175.39, triclinic, space group P-1, a = 13.5949(11), b = 15.4389(13), c = 16.0182(13) Å, α = 97.9400(10), β = 94.0320(10), γ = 103.9340(10)°, V = 3213.0(5) Å^3, D_c = 1.215 g cm^{-3}, μ = 0.425 mm^{-1}, Z = 2, λ = 0.71073 Å, T = 173 K, 30038 reflections collected, 13652 independent (R_{int} =0.0450), R_1 [$I > 2\sigma(I)$] = 0.0625, wR_2 [$I > 2\sigma(I)$] = 0.1304, R_1 (all data) = 0.0933, wR_2 (all data) = 0.1504.

Crystal data for *trans*-[Fe(DMeOPrPE)$_2$(N$_2$)H][BPh$_4$] (III). $C_{60}H_{101}BFeN_2O_8P_4$, M = 1168.97, triclinic, space group P-1, a = 13.466(2), b = 15.443(3), c = 16.219(3) Å, α = 97.2619(3), β = 94.169(3), γ = 104.408(3)°, V = 3221.5(10) Å^3, D_c = 1.205 g cm^{-3}, μ = 0.384 mm^{-1}, Z = 2, λ = 0.71073 Å, T = 173 K, 36541 reflections collected, 14419 independent (R_{int} =0.0194), R_1 [$I > 2\sigma(I)$] = 0.0451, wR_2 [$I > 2\sigma(I)$] = 0.1264, R_1 (all data) = 0.0561, wR_2 (all data) = 0.1367.

2.2.4 Methods

Synthesis of *trans*-[Fe(DMeOPrPE)$_2$(H$_2$)H][BPh$_4$] (I). *trans*-Fe(DMeOPrPE)$_2$Cl$_2$ (1.86 g, 2.086 mmol), NaBPh$_4$ (1.43 g, 4.172 mmol), and Proton Sponge (0.45 g, 2.086 mmol) were combined as solids in a 120 mL Fischer-Porter tube. THF (15 mL) and Et$_2$O (15 mL) were then added, and the resulting solution was immediately charged with 1 atm of H$_2$. The solution turned from green to orange to a faint yellow with the production of a white precipitate (NaCl) over the course of several hours. The reaction was allowed to stir for 48 hrs to ensure completion. The solution was then filtered through Celite under an argon atmosphere. The complex was precipitated as an oil by addition of hexane. The oil was redissolved in toluene, filtered through Celite, and again precipitated with hexane. The remaining oil was triturated with hexane to yield 2.32 g (97% yield) of a tan colored powder. X-ray quality crystals were grown by slow evaporation of a THF solution. Anal. Calcd. for $C_{60}H_{103}BFeO_8P_4$: C, 63.02; H, 9.09. Found: C, 62.98; H, 9.30. $^{31}P\{^1H\}$ NMR (toluene-d_8): δ 85.0 (s). ^{31}P NMR (toluene-d_8): δ 85.0 (d, $^2J_{P\text{-}H}$ = 47 Hz). ^1H NMR (toluene-d_8) of the hydride region: δ -11.1 (s, br) and δ -15.1 (quintet, $^2J_{H\text{-}P}$ = 49 Hz).

Synthesis of [Fe(DMeOPrPE)$_2$Cl][BPh$_4$] (II). NaBPh$_4$ (0.384 g, 1.12 mmol) was added to a Et$_2$O solution of *trans*-Fe(DMeOPrPE)$_2$Cl$_2$ (0.1 g, 0.112 mmol) under argon. After stirring for 1 hr the solvent was evaporated. The yellow residue was extracted into toluene and the solution was filtered through Celite. The complex was precipitated as a yellow solid by addition of hexane. The yellow powder was washed with hexane followed by diethyl ether (0.097 g, 74% yield). Crystals suitable for X-ray

diffraction were grown from a saturated diethyl ether solution. $^{31}P\{^{1}H\}$ NMR (toluene-d_8) at 193 K: δ 55.9 (s). ^{31}P NMR (toluene-d_8) at 193 K: δ 55.9 (s). No ^{31}P resonances were observed at room temperature. Anal. Calcd. for $C_{60}H_{100}BClFeO_8P_4$: C, 61.31; H, 8.58. Found: C, 60.98; H, 8.39. ESI (Et_2O, +ve): 855.4 $[Fe(DMeOPrPE)_2Cl]^+$.

Synthesis of *trans*-[Fe(DMeOPrPE)$_2$(N$_2$)H][BPh$_4$] (III). A THF/Et_2O solution of **I** prepared by the method above was charged with 2 atm of N_2 in a Fischer-Porter tube and stirred for 48 hrs. The Fischer-Porter tube was vented and refilled with N_2 several times over the course of the reaction to remove free H_2. The solution color changed from light yellow to light brown over the course of the reaction. The solvent was evaporated under an N_2 atmosphere and the resulting brown oil was triturated with hexanes to yield 2.28g of a tan solid (94% yield). X-ray quality crystals were grown by hexane diffusion into a THF solution. Anal. Calcd. for $C_{60}H_{101}BFeN_2O_8P_4$: C, 61.62; H, 8.71; N, 2.40. Found: C, 61.94; H, 8.97; N, 2.25. IR(KBr): (ν_{NN}) 2088 cm^{-1}. $^{31}P\{^{1}H\}$ NMR (toluene-d_8): δ 75.8 (s). ^{31}P NMR (toluene-d_8): δ 75.8 (d, $^{2}J_{P\text{-}H}$ = 49 Hz). ^{1}H NMR (solvent) of the hydride region: δ -18.6 (quintet, $^{2}J_{H\text{-}P}$ = 49 Hz).

Synthesis of *trans*-[Fe(DMeOEtPE)$_2$(H$_2$)H][BPh$_4$]. This complex was synthesized following the procedure described above for **I** using *trans*-$Fe(DMeOEtPE)_2Cl_2$. $^{31}P\{^{1}H\}$ NMR (toluene-d_8): δ 82.9 (s). ^{31}P NMR (toluene-d_8): δ 82.9 (d, $^{2}J_{P\text{-}H}$ = 48 Hz). ^{1}H NMR (toluene-d_8) of the hydride region: δ -10.9 (s, br) and δ -15.9 (quintet, $^{2}J_{H\text{-}P}$ = 48 Hz).

Substitution Kinetic Experiments. In a NMR tube fitted with a septum *trans*-$[Fe(DMeOPrPE)_2(H_2)H]BPh_4$ (**I**) (0.3 mL of a 0.00746 M solution in d_8-toluene,

0.00224 mmol), a solvent (0.3 mL of either toluene, acetone, tetrahydrofuran, dimethylformamide, dimethylacetamide, hexamethylphosphoramide), and acetonitrile (12 μL, 0.230 mmol) were sequentially added under Ar. Immediately after addition of the acetonitrile, the reaction was monitored by $^{31}P\{^{1}H\}$ NMR spectroscopy. For the first 25 minutes a spectrum was taken every 5 minutes. In the following 30 minutes a spectrum was collected at 10 minute intervals. For the remaining 6 hours the interval was increased to 30 minutes. The concentration of *trans*-$[Fe(DMeOPrPE)_2H(H_2)]BPh_4$ was determined by $^{31}P\{^{1}H\}$ peak integrations. The rate constants were then obtained by fitting the data (concentration versus time) with a single parameter exponential decay function using SigmaPlot software. The kinetic data for the reaction of acetonitrile with *trans*-$[Fe(DMeOPrPE)_2(N_2)H]BPh_4$ (**III**) was acquired in the same manner (identical concentration and solvents), except the following time intervals were used. For the first 3 minutes a spectrum was taken every 30 seconds. In the following 6 minutes a spectrum was collected at 1 minute intervals. In the following 12 minutes a spectrum was collected at 2 minute intervals. For the remaining 30 minutes the interval was increased to 5 minutes.

Test for Hydrogen Bonding in *trans*-$[Fe(DMeOPrPE)_2(H_2)H][BPh_4]$. A solution of **I** in toluene-d_8 (0.00746 M, 0.3 mL) was placed in an NMR tube fitted with a septum. The tube was then placed into the NMR magnet and allowed to equilibrate at -40°C for 15 minutes. After this equilibration period the ^{1}H spectrum was acquired and referenced to the toluene resonances. The sample was then ejected, 10 μL (60 equivalents) of acetone-d_6 was added, and the sample placed back into the magnet. The

procedure was repeated until 1000 equivalents of acetone had been added. The H_2 resonance shifted ~0.04 ppm downfield upon addition of the acetone, however other resonances of **I** also underwent shifts of similar magnitudes, both downfield and upfield in direction.

Synthesis of *trans*-[Fe(DMeOPrPE)$_2$(N_2H_4)H][BPh$_4$]. A N_2H_4/THF solution (1.7 mL, 0.072 M) was added to a stirring THF solution of **III** (0.14 g, 0.120 mmol) under argon. The reaction was stirred for 12 hrs. during which time the solution color changed from brown to bright yellow. The solvent was allowed to evaporate yielding a orange-yellow oil. The ^{15}N isotopologue was synthesized in the same manner using $^{15}N_2H_4$. $^{31}P\{^1H\}$ NMR (THF-d_8): δ 81.3 (s). ^{31}P NMR (THF-d_8): δ 81.3 (d, $^2J_{P\text{-}H}$ = 49 Hz). ^1H NMR (THF-d_8): δ -29.3 (quintet, $^2J_{H\text{-}P}$ = 49 Hz). $^{15}N\{^1H\}$ NMR (THF-d_8): δ -317 (s), -383 (s). ^{15}N NMR (THF-d_8): δ -317 (t, $^1J_{N\text{-}H}$ = 63 Hz), -383 (t, $^1J_{N\text{-}H}$ = 69 Hz). ^1H-^{15}N HMQC (THF-d_8): δ 2.4 (d, $^1J_{H\text{-}N}$ = 63 Hz), 0.5 (d, $^1J_{H\text{-}N}$ = 63 Hz).

Synthesis of *trans*-[Fe(DMeOPrPE)$_2$(NH_3)H][BPh$_4$]. THF saturated with NH_3 (2 mL) was added to a stirring THF solution of **III** (0.049 g, 0.042 mmol) under argon. The solution was stirred for two days over which time the solution color changed from pale brown to bright yellow. The solvent was allowed to evaporate leaving a bright orange-yellow oil. $^{31}P\{^1H\}$ NMR (C_6D_6): δ 82.0 (s). ^{31}P NMR (C_6D_6): δ 82.0 (d, $^2J_{P\text{-}H}$ = 48 Hz). ^1H NMR (C_6D_6) of the hydride region: δ -0.86 (s, br) and δ -29.6 (quintet, $^2J_{H\text{-}P}$ = 48 Hz). $^{15}N\{^1H\}$ NMR (THF-d_8): δ -441 (s). ^{15}N NMR (THF-d_8): δ -441 (quartet, $^1J_{NH}$ = 64 Hz). The ^{15}N isotopologue was prepared by degradation of *trans*-[Fe(DMeOPrPE)$_2$($^{15}N_2H_4$)H] prepared by the reaction of $^{15}N_2H_4$ with **III**.

Synthesis of *trans*-Fe(DMeOPrPE)$_2$HCl. An excess of tetraethylammonium chloride was added to a stirring THF solution of **III** under argon. The reaction was stirred for two hours then the solvent was allowed to evaporate yielding a bright orange oil. The product was extracted from the excess tetraethylammonium chloride using pentane. The product contained uncoordinated DMeOPrPE as an impurity. The free ligand was removed by running the pentane solution through a column of basic alumina and washing with pentane several times. The product, still bound to the alumina, was then isolated by washing the column with diethyl ether. The product was readily soluble in most organic solvents and thus could not be obtained as a solid by recrystallization. $^{31}P\{^1H\}$ NMR (C_6D_6): δ 83.0 (s). ^{31}P NMR (C_6D_6): δ 83.0 (d, $^2J_{PH}$ = 49 Hz). ^1H NMR (C_6D_6) of the hydride region: δ -32.5 (quintet, $^2J_{HP}$ = 49 Hz).

Reaction of *trans*-Fe(DMeOPrPE)$_2$HCl with $^{15}N_2H_4$. $TlPF_6$ was added to a THF-d_8 solution of *trans*-Fe(DMeOPrPE)$_2$HCl under argon and the solution was filtered through Celite directly into a J. Young NMR tube. To this NMR tube a 10-fold excess of $^{15}N_2H_4$ was added. The initial $^{31}P\{^1H\}$ NMR spectrum showed a mixture of *trans*-$[Fe(DMeOPrPE)_2(N_2H_4)H]^+$ and *trans*-$[Fe(DMeOPrPE)_2(NH_3)H]^+$. Due to addition of excess hydrazine a clean ^1H NMR spectrum could not be obtained. The tube was allowed to sit overnight. Hexane and pentane were then used to precipitate the products and the resulting oil was washed twice with pentane. The oil was then redissolved in toluene-d_8 and filtered through Celite into another J. Young NMR tube. The $^{31}P\{^1H\}$ NMR spectrum showed seven different iron phosphine species. By comparison of integrations in the $^{31}P\{^1H\}$ and ^1H NMR spectra, five of the species could be assigned as

they had been previously synthesized. The two other species were assigned as *trans*-$[Fe(DMeOPrPE)_2(N_2H_2)]^+$ and *trans*-$Fe(DMeOPrPE)_2(N_2H)$ (see discussion section). Only the NMR data for these two species is listed here. *trans*-$[Fe(DMeOPrPE)_2(N_2H_2)]^+$ $^{31}P\{^1H\}$ NMR (toluene-d_8): δ 79.6 (s). ^{31}P NMR (toluene-d_8): δ 79.6 (d, $^2J_{PH}$ = 49 Hz). ^1H NMR (toluene-d_8) : δ 14.985 (dd, $^1J_{HN}$ = 60 Hz, $^3J_{HH}$ = 24 Hz), δ 14.062 (ddt, $^1J_{HN}$ = 48 Hz, $^3J_{HH}$ = 24 Hz, $^4J_{HP}$ = 5 Hz), δ -17.8 (quintet, $^2J_{HP}$ = 49 Hz). *trans*-$Fe(DMeOPrPE)_2(N_2H)$ $^{31}P\{^1H\}$ NMR (toluene-d_8): δ 80.8 (s). ^{31}P NMR (toluene-d_8): δ 80.8 (d, $^2J_{PH}$ = 49 Hz). ^1H NMR (toluene-d_8) : δ 13.8 (d, $^1J_{HN}$ = 58 Hz), -19.2 (quintet, $^2J_{HP}$ = 49 Hz).

2.3 Results and Discussion

2.3.1 Synthesis of Dihydrogen and Dinitrogen Complexes

The iron dihydrogen complex, *trans*-$[Fe(DMeOPrPE)_2(\eta^2\text{-}H_2)H]^+$, was previously synthesized as the PF_6^- salt; however, attempts to isolate this complex as a solid were unsuccessful.[16,21] Following the same synthetic procedure, but using $NaBPh_4$ instead of $TlPF_6$, an isolable solid (**I**) was obtained (eq 1).

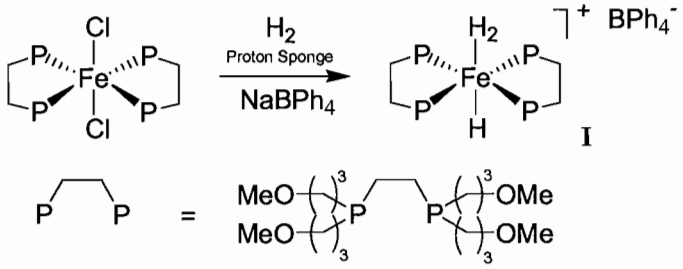

(1)

The solution characterization of **I** by NMR spectroscopy matched the previously reported data for the *trans*-$[Fe(DMeOPrPE)_2(\eta^2\text{-}H_2)H][PF_6]$ complex,[21] with a single

resonance observed in the $^{31}P\{^{1}H\}$ spectrum (85.0 ppm) and a broad singlet (-11.1 ppm) and quintet (-15.1 ppm, $^{2}J_{HP}$ = 49 Hz) observed in the low temperature (-40°C) ^{1}H spectrum. X-ray quality crystals of **I** were grown by slow evaporation of a THF solution (Fig.1). All hydrogen atoms were located, allowing visualization of the intact η^2 dihydrogen ligand. The structure closely matches the previously published X-ray structures of *trans*-$[Fe(DPPE)_2(H_2)H]^+$ and *trans*-$[Fe(DMPE)_2(H_2)H]^+$ (DPPE = 1,2-bis(diphenylphosphino)ethane; DMPE = 1,2-bis(dimethylphosphino)ethane).[24,25] Although the dihydrogen ligand was clearly found, X-ray methods are unreliable in accurately measuring the H-H bond distance, as evidenced by the fact that the measured H-H bond length (0.707 Å) is shorter than that of free dihydrogen (0.74 Å) and significantly shorter than the bond length determined by NMR methods.

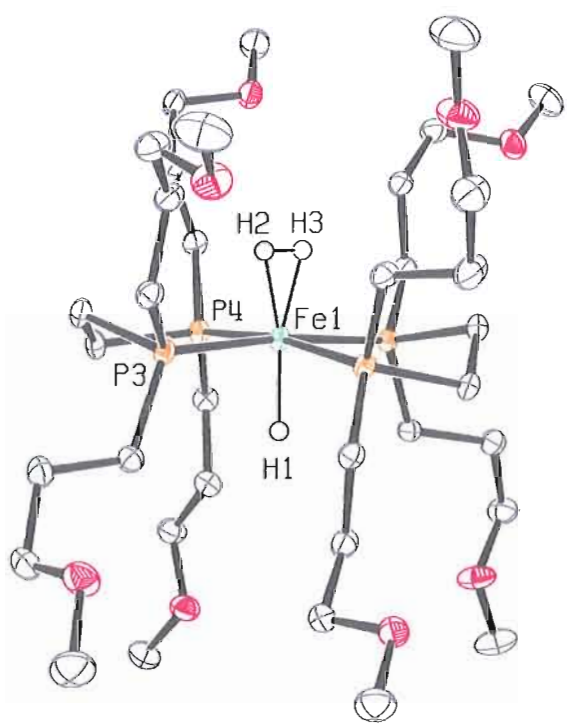

Figure 1. Molecular structure of *trans*-$[Fe(DMeOPrPE)_2(\eta^2\text{-}H_2)H][BPh_4]$ (**I**). The tetraphenylborate anion and hydrogen atoms of the phosphine ligands have been omitted for clarity.

Previous work showed that the reaction of *trans*-Fe(DMeOPrPE)$_2$Cl$_2$ with H_2 proceeds through a stepwise mechanism (Scheme 2); displacement of one chloride ligand with H_2 occurs first, followed by heterolysis of the coordinated H_2 to form the hydride ligand, and finally displacement of the second chloride with another equivalent of H_2.[21]

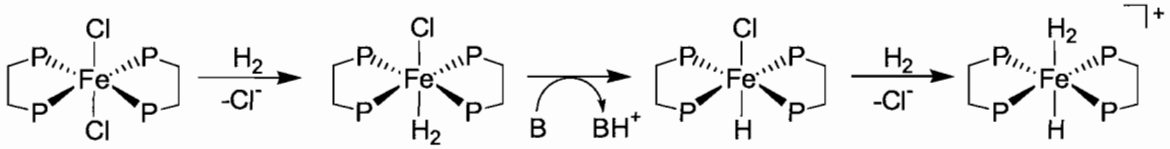

Scheme 2. Mechanism of the reaction of *trans*-Fe(DMeOPrPE)$_2$Cl$_2$ with H_2.

Substitution of the first chloride with H_2 likely proceeds through a dissociative mechanism because this reaction does not proceed in organic solvents without the addition of a chloride abstracting reagent. In support of this hypothesis, [Fe(DMeOPrPE)$_2$Cl]$^+$ (**II**) was synthesized by reacting *trans*-Fe(DMeOPrPE)$_2$Cl$_2$ with $NaBPh_4$ in diethyl ether in the absence of H_2.[26] The product was isolated as a yellow powder and X-ray quality crystals were grown from a saturated diethyl ether solution (Fig. 2). The five-coordinate structure is best described as having a distorted square-pyramidal geometry, with the chloride ligand occupying the apical position and the P-Fe-Cl angles ranging from 92.69° to 98.93°. The Fe-Cl bond length (2.3505 Å) of **II** is nearly unchanged from that of the dichloride starting material (2.354 Å), while the Fe-P bonds (2.2792-2.3175 Å) are slightly lengthened.[22] The five-coordinate complex **II**

readily binds H_2 in solution to form *trans*-$[Fe(DMeOPrPE)_2(H_2)Cl]^+$, as evidenced by ^{31}P and ^1H NMR spectroscopy, consistent with the mechanism in Scheme 2.[22]

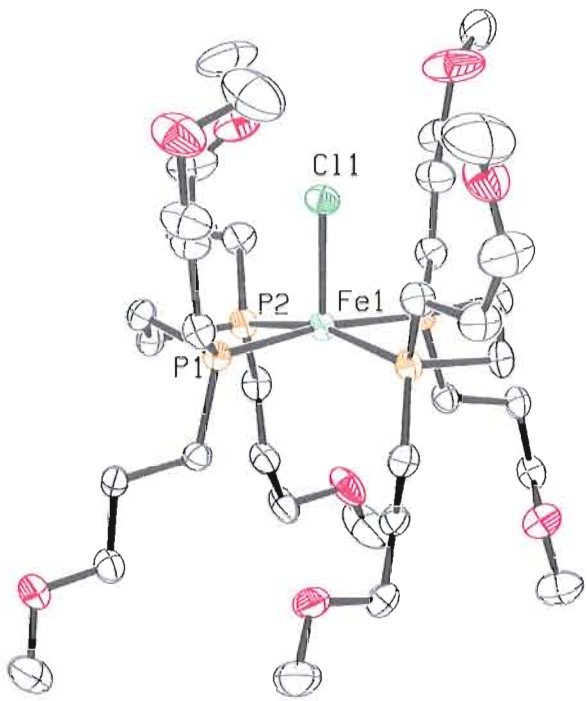

Figure 2. Molecular structure of $[Fe(DMeOPrPE)_2Cl]^+$ (**II**). The tetraphenylborate anion and hydrogen atoms have been omitted for clarity.

The dihydrogen complex **I** is a convenient starting material for the generation of *trans*-$[Fe(DMeOPrPE)_2(N_2)H]^+$. Complex **III**, *trans*-$[Fe(DMeOPrPE)_2(N_2)H][BPh_4]$, was synthesized from **I** by a ligand substitution reaction with N_2 (eq 2) at 1 atm. Because **I** is slightly more stable than **III,** the reaction vessel must be purged with N_2 several times, to remove any residual H_2, to achieve complete conversion.

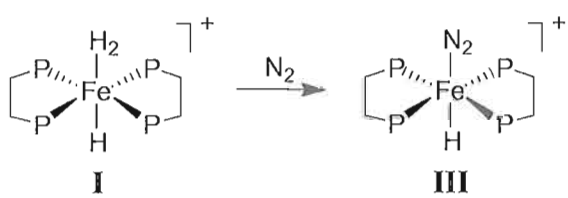

I **III** (2)

As with the *trans*-$[Fe(DMeOPrPE)_2(H_2)H]^+$ complex, previous attempts to isolate the *trans*-$[Fe(DMeOPrPE)_2(N_2)H]^+$ complex as the PF_6^- salt were unsuccessful.[21] Using the BPh_4^- counterion, complex **III** was isolated as a tan solid. Again, the NMR characterization of **III** matched with the previously reported data,[21] with a singlet at 75.8 ppm in the $^{31}P\{^1H\}$ spectrum and a hydride resonance at -18.6 ppm ($^2J_{HP}$ = 49 Hz) in the ^1H spectrum. Crystals of **III** were grown by layering a THF solution with hexanes and allowing the solution to stand under an N_2 atmosphere for ~1 week. The structure of **III** shows the end-on bonded dinitrogen ligand *trans* to the hydride ligand (Fig. 3). The iron-phosphorus bond lengths in **III** range from 2.2302—2.2379 Å; these bond lengths closely match the DMPE[27] and DEPE[28] analogs. The N-N bond length of 1.112 Å shows slight elongation compared with free dinitrogen (1.0975 Å), with the N-N bond length falling in between the DMPE (1.13 Å)[27] and DEPE (1.070 Å)[28] complexes.

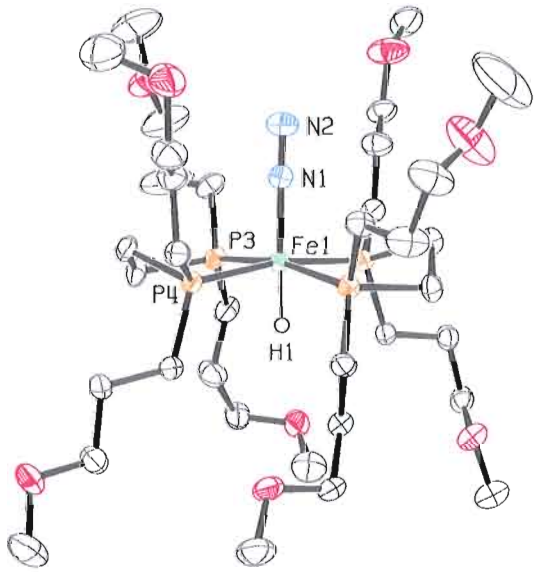

Figure 3. ORTEP representation of *trans*-$[Fe(DMeOPrPE)_2(N_2)H]^+$ (**III**). Ellipsoids are drawn at 50% probability. The tetraphenylborate counter-ion and hydrogen atoms of the phosphine ligands have been omitted for clarity.

2.3.2 Effect of Solvent on the Rate of H_2 and N_2 Substitution

The substitution of H_2 and N_2 by various small molecules is a commonly observed reaction because these ligands are typically weakly bonded. Both **I** and **III** are important species in the Leigh-type dinitrogen reduction cycle and their substitution reactivity was studied to gain insights into how to improve the yields of ammonia. It was previously shown with the *trans*-$[Ru(DMeOPrPE)_2(H_2)H]^+$ complex that a coordinated dihydrogen molecule can act as a hydrogen bond donor to a neutral acceptor molecule in solution, an interaction termed dihydrogen hydrogen bonding (DHHB).[29] If the coordinated H_2 in **I** were capable of donating a hydrogen bond to the bulk solvent, we wanted to explore how this would affect the reactivity. The substitution reactions of H_2 and N_2 in **I** and **III** by acetonitrile were chosen for study because these reactions have been studied in great detail in analogous systems[30-32] and the product of the reaction, *trans*-$[Fe(DMeOPrPE)_2(MeCN)H]^+$, has previously been characterized.[21]

Attempts to grow crystals of *trans*-$[Fe(DMeOPrPE)_2(MeCN)H]^+$ resulted in an unexpected transformation of the diphosphine ligand to a phosphonium dication (Fig. 4). At this point, the mechanism by which this diphosphonium is formed is unclear. We postulate that oxygen atom coordination of a methoxypropyl arm of the DMeOPrPE ligand to the iron center could activate the terminal methyl group for nucleophilic attack by another DMeOPrPE ligand; however, we currently have no evidence for such a mechanism. Alternatively, coordination of acetonitrile to the metal center could activate the methyl group toward nucleophilic attack by the phosphine ligand. Whatever the mechanism, the process occurs slowly and on a relatively small scale (<10% yield)

because these crystals were isolated after ~2 months and inspection of the mother liquor revealed two major resonances attributable to *trans*-$[Fe(DMeOPrPE)_2(MeCN)H]^+$ (80.9 ppm) and *trans*-$[Fe(DMeOPrPE)_2(MeCN)_2]^{2+}$ (63.7 ppm) as well as a minor resonance (38.7 ppm) assigned to the phosphonium cation.

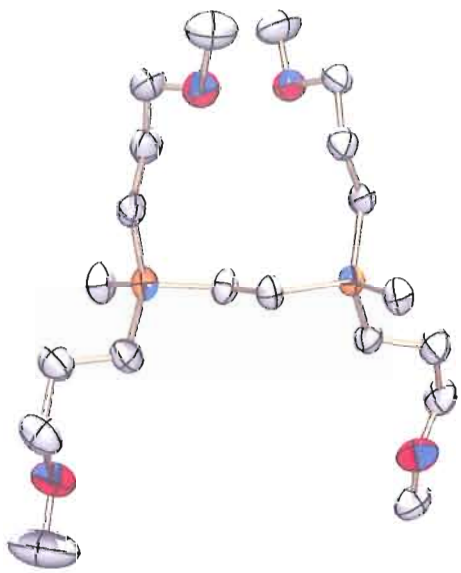

Figure 4. ORTEP representation of the phosphonium dication. Hydrogen atoms and tetraphenylborate anions have been omitted for clarity.

To probe the effect of solvent on the rate of substitution, the following solvents were used: toluene, acetone, tetrahydrofuran (THF), dimethylformamide (DMF), dimethylacetamide (DMA), and hexamethylphosphoramide (HMPA). These solvents were chosen because both **I** and **III** were stable in them and they represent a spectrum of hydrogen-bond accepting strengths without having any hydrogen-bond donating ability. A stock solution (0.00746 M) of **I** or **III** in toluene-d_8 (0.3 mL) was mixed with an equal volume of one the solvents listed above and to that solution a 100-fold excess of acetonitrile was added to ensure pseudo first-order kinetics. The rate of substitution was

then determined by monitoring the disappearance of **I** or **III** in the $^{31}P\{^{1}H\}$ NMR spectrum (Fig. 5). The hydrogen bond accepting strengths of the solvents were quantified using the β parameter.[33] Because these complexes are charged and the substitution is expected to proceed by a dissociative mechanism, solvent polarity could also affect the observed rates. Consequently, the solvent polarity was quantified using the $E_T(30)$ parameter.[33] The data are summarized in Table 1.

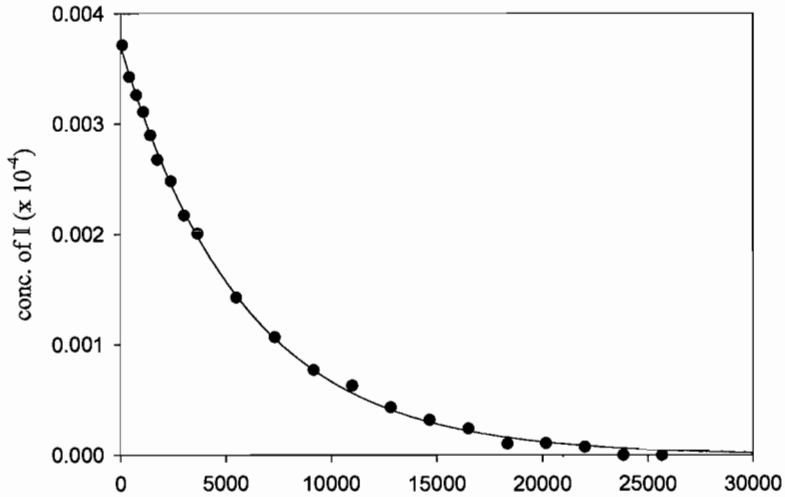

Figure 5. Sample kinetic trace of the concentration of **I** as a function of time in a toluene:DMF (50:50) solvent mixture.

Table 1. Summary of rate constants for **I** and **III** in various solvents, as well as solvent hydrogen-bond accepting strengths (β) and solvent polarity ($E_T(30)$) parameters.[33]

Solvent	**I** k_{obs} (x 10^{-4})	**III** k_{obs} (x 10^{-4})	β	$E_T(30)$
Toluene	1.70 ± 0.03	11.22 ± 0.16	0.11	33.9
Acetone	2.16 ± 0.06	13.10 ± 0.26	0.43	42.2
THF	1.71 ± 0.04	11.36 ± 0.21	0.55	37.4
DMF	1.71 ± 0.02	8.40 ± 0.13	0.69	43.8
DMA	1.58 ± 0.04	8.40 ± 0.14	0.76	43.7
HMPA	1.57 ± 0.02	8.12 ± 0.18	1.05	40.9

As can be seen in Table 1, the rate of N_2 substitution with acetonitrile occurs ~6 times faster than H_2 substitution. Surprisingly, the solvent has little effect on the rates of substitution. Upon changing from a non-polar solvent like toluene to a polar solvent like HMPA, the rate constants change by less than a factor of 2 for both **I** and **III**. The rate constants for both **I** and **III** do not trend with hydrogen bond accepting strength (β) or with solvent polarity ($E_T(30)$). This result suggests that either hydrogen bonding to the coordinated dihydrogen in **I** is very weak and does not affect the lability of the H_2 molecule, or that hydrogen bonding to coordinated H_2 is not occurring in this system. Unfortunately, two of the three tests previously used to determine the hydrogen bonding ability of H_2 in the *trans*-$[Ru(DMeOPrPE)_2(H_2)H]^+$ complex could not be used for **I** because the pyridine-*N*-oxide probe molecule used in the Ru study readily displaced the H_2 molecule (vide infra). The third test for hydrogen bonding, titrating **I** with a hydrogen bond accepting solvent and monitoring the chemical shift of the H_2 resonance, yielded no shift in the H_2 resonance attributable to hydrogen bonding. This result, combined with the kinetic data in Table 1, suggests that the H_2 molecule in **I** is either unable to donate a hydrogen bond, in contrast to the Ru analog, or that if DHHB is occurring then it is too weak to have any effect on the substitution reactivity.

2.3.3 Exploring DHHB in the Solid State

Further evidence for dihydrogen hydrogen bonding (DHHB) was sought by co-crystallizing a neutral hydrogen-bond acceptor molecule with *trans*-$[Fe(DMeOPrPE)_2(H_2)H][BPh_4]$. Pyridine-*N*-oxide was chosen as the hydrogen-bond acceptor molecule as it is a very potent hydrogen-bond acceptor and crystallizes readily.

However, addition of excess pyridine-*N*-oxide resulted in the complete substitution of all ligands, forming a homoleptic pyridine-*N*-oxide iron(II) complex, $[Fe(C_5H_5NO)_6][BPh_4]_2$ (Fig. 6). Addition of only 1 equivalent of pyridine-*N*-oxide resulted in substitution of the coordinated H_2 molecule, as evidenced by $^{31}P\{^1H\}$ NMR spectroscopy. Although this attempt at observing DHHB in the solid-state was unsuccessful, using a different hydrogen-bond acceptor molecule that does not have such a high affinity for iron(II) could perhaps be productive. Instead of pursuing this approach further, a different approach for identifying DHHB in the solid-state was undertaken by varying the identity of the phosphine ligand.

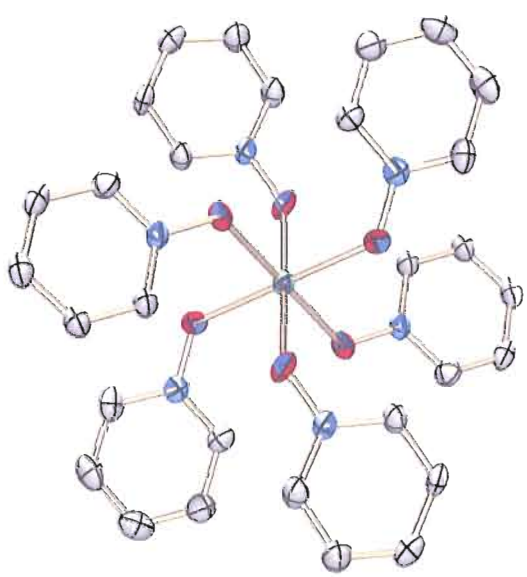

Figure 6. ORTEP representation of $[Fe(C_5H_5NO)_6][BPh_4]_2$. Hydrogen atoms and tetraphenylborate anions have been omitted for clarity.

Inspection of the crystal structure of *trans*-$[Fe(DMeOPrPE)_2(H_2)H]^+$ (Fig. 1) revealed that by perhaps using shorter methoxy phosphine arms, an intramolecular hydrogen bond could occur between the coordinated H_2 molecule and the ether group of

the phosphine ligand arm. The DMeOEtPE (DMeOEtPE = 1,2-bis(dimethoxyethylphosphino)ethane) ligand was chosen, as the resulting intramolecular hydrogen bond would result in a six-membered ring, hopefully further stabilizing the interaction (Fig. 7). The DMeOEtPE was also an excellent candidate as the dichloride starting material was already available in our lab.

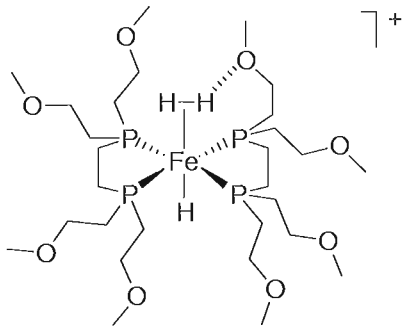

Figure 7. Proposed interaction of DMeOEtPE with coordinated H_2.

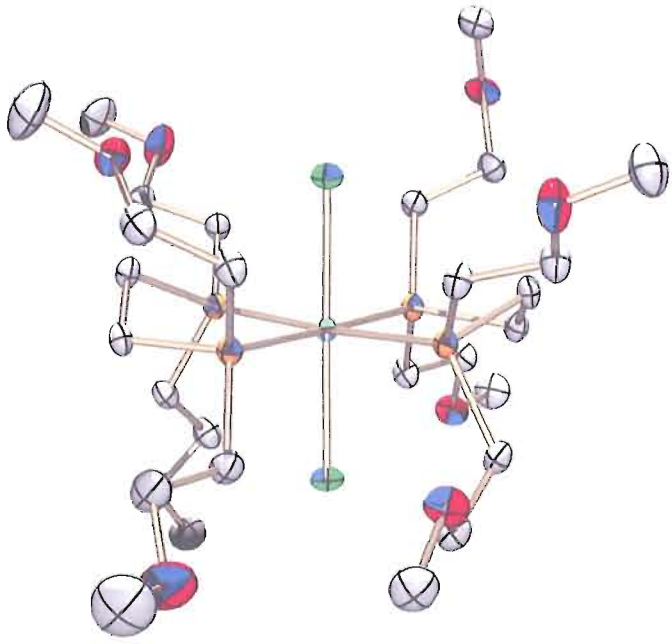

Figure 8. ORTEP representation of *trans*-Fe(DMeOEtPE)$_2$Cl$_2$. Hydrogen atoms have been omitted for clarity.

The dichloride starting material, *trans*-Fe(DMeOEtPE)$_2$Cl$_2$, was first purified by recrystalization and X-ray quality crystals were obtained, confirming the coordination geometry and ligand identity (Fig. 8). The same procedure was used to synthesize the dihydrogen complex, *trans*-[Fe(DMeOEtPE)$_2$(H$_2$)H]$^+$. One atmosphere of dihydrogen was added to a THF solution of *trans*-Fe(DMeOEtPE)$_2$Cl$_2$, NaBPh$_4$, and Proton Sponge. The reaction was allowed to stir for two days after which time the solution was bright orange in color. The complex was characterized in solution by NMR spectroscopy. The ^{31}P{^{1}H} NMR spectrum showed a single resonance at 82.9 ppm and the ^{1}H NMR spectrum showed the characteristic resonances at -10.9 and -15.9 ppm. Unlike the dihydrogen complex of DMeOPrPE, the DMeOEtPE complex was not stable in the absence of a dihydrogen atmosphere. Over the course of 24 hrs the solution color changed from bright orange to purple. It is unclear what this change in color represents, but one hypothesis is that the shortened phosphine arms allow the ether group to coordinate to the iron center and displace the H$_2$ molecule. This hypothesis is supported by the fact that *trans*-[Fe(DMeOPrPE)$_2$(H$_2$O)H]$^+$ is also purple in color[21] and that a crystal structure was later obtained showing the ether groups of DMeOEtPE coordinating to iron (vide infra).

Unfortunately, attempts to grow crystals of *trans*-[Fe(DMeOEtPE)$_2$(H$_2$)H]$^+$ even under a dihydrogen atmosphere were unsuccessful. However, from one of these attempted crystallizations, the phosphine oxide complex shown in Fig. 9 was obtained. This complex was presumably formed from O$_2$ leakage into the crystal growth setup.

Interestingly, the methoxyethyl arms of the phosphine oxide ligand are shown to coordinate to the iron center. The fate of the hydride ligand remains unclear.

Neither of the approaches presented here were successful in providing evidence for the phenomenon of dihydrogen hydrogen bonding (DHHB) in the solid state. While this result would be a significant achievement, as there are currently no crystals structures showing coordinated H_2 interacting with a neutral hydrogen bond acceptor molecule, it was not the primary focus of this dissertation and was abandoned.

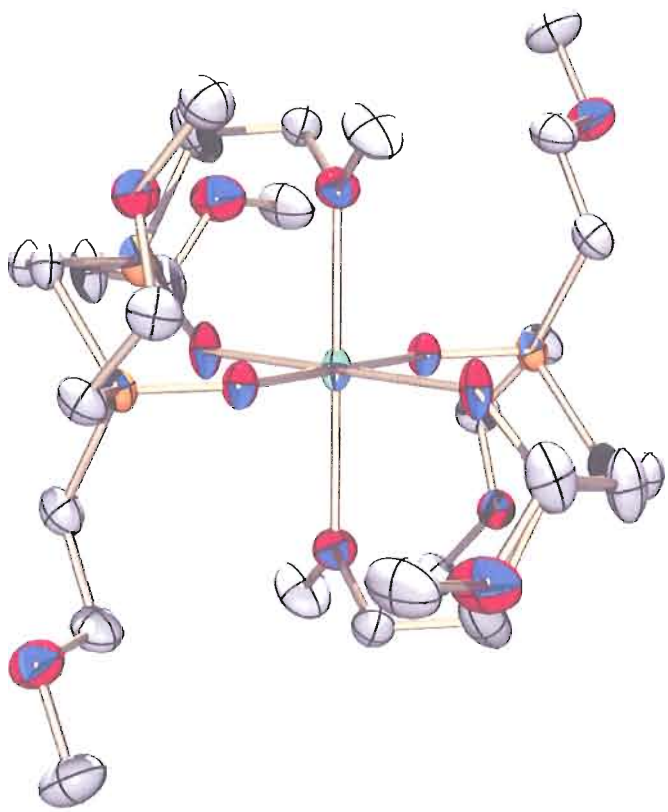

Figure 9. ORTEP representation of *trans*-$[Fe(DMeOEtP(O)E)_2]^{2+}$. Hydrogen atoms and tetraphenylborate anions have been omitted for clarity.

2.3.4 Hydride Complexes of N_2 Reduction Intermediates

The coordination chemistry of N_2 reduction intermediates, i.e. N_2H_2, N_2H_4, and NH_3, with iron is becoming increasingly important as growing biochemical data suggest that these species are likely formed during nitrogenase turnover.[34-36] The N_2 molecule in *trans*-$[Fe(DMeOPrPE)_2(N_2)H]^+$ is quite labile and should provide a convenient entry into coordination complexes of N_2H_2, N_2H_4, and NH_3.

The reaction of *trans*-$[Fe(DMeOPrPE)_2(N_2)H]^+$ with ammonia was first explored (eq. 3). Reaction of the dinitrogen complex with NH_3 in THF resulted in a color change from pale brown to bright yellow and the appearance of a new resonance at 82.0 ppm in the $^{31}P\{^1H\}$ NMR spectrum. This resonance splits into a doublet in the proton-coupled ^{31}P spectrum ($^1J_{PH}$ = 48 Hz) confirming that the hydride ligand is intact (Fig. 10). In order for the reaction to go to completion the reaction needs to be performed under an Ar atmosphere and excess ammonia bubbled through the solution to remove any residual dinitrogen.

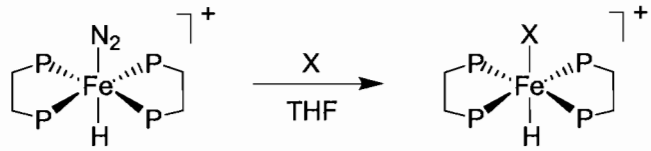

$X = N_2H_4$ or NH_3 (3)

The ^1H NMR spectrum shows a hydride resonance at -29.6 ppm and a broad singlet at -0.8 ppm, which is assigned to the coordinated ammonia (Fig. 10). This NMR data is characteristic of a six-coordinate complex with the ammonia bound *trans* to the hydride ligand as previously seen in the analogous DMPE complex, which was also characterized by X-ray diffraction.[37] The ^{15}N (-441 ppm, quartet, $^1J_{NH}$ = 64 Hz) and

$^{15}N\{^1H\}$ (-441 ppm, singlet) NMR data for this complex also confirmed the coordination of ammonia to iron.

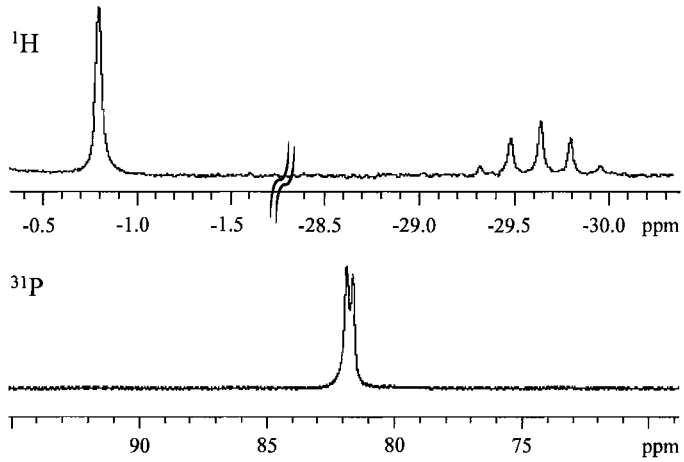

Figure 10. ^1H (top) and ^{31}P (bottom) NMR spectra for *trans*-$[Fe(DMeOPrPE)_2(NH_3)H]^+$.

The hydrazine complex, *trans*-$[Fe(DMeOPrPE)_2(N_2H_4)H]^+$, was also synthesized by substitution of the dinitrogen ligand (eq. 3). The bright yellow hydrazine complex shows a single resonance in the $^{31}P\{^1H\}$ NMR spectrum at 81.3 ppm, again splitting into a doublet when the proton decoupler is turned off (Fig. 11). Similar to the reaction with ammonia, the N_2 ligand seems to be more stable than the hydrazine complex and the N_2 must be removed to allow the reaction to proceed to completion. The ^1H NMR spectrum of the hydrazine complex shows a similar hydride resonance at -29.2 ppm (Fig. 11). The ^{31}P and ^1H NMR characterization suggest that the hydrazine is coordinated to the iron center, however to confirm the binding geometry of the hydrazine ligand the ^{15}N isotopologue was synthesized. The $^{15}N\{^1H\}$ NMR spectrum shows two singlet resonances at -317 and -383 ppm, suggesting an η^1 geometry. In the ^{15}N NMR spectrum

both of these resonances are observed as triplets ($^1J_{N\text{-}H}$ = 63, 69 Hz) (Fig. 11). The hydrazine protons could now also be definitively assigned due to ^{15}N coupling, with two broad doublets being observed at 3.68 (d, $^1J_{NH}$ = 68 Hz) and 2.87 (d, $^1J_{NH}$ = 59 Hz) ppm in the ^1H NMR spectrum. This assignment was also confirmed using a ^1H-^{15}N HMQC experiment.

Attempts were made to isolate the hydrazine complex however the complex was found to decompose over the course of several hours. The hydrazine complex was observed to decompose into a mixture of *trans*-$[Fe(DMeOPrPE)_2(NH_3)H]^+$, *trans*-$[Fe(DMeOPrPE)_2(N_2)H]^+$, *trans*-$[Fe(DMeOPrPE)_2(H_2)H]^+$. This was confirmed by $^{31}P\{^1H\}$ and ^1H NMR spectroscopy. These products likely arise from disproportionation of the coordinated hydrazine, which is a common reaction for hydrazine in the presence of transition metals,[38-41] however this has yet to be confirmed.

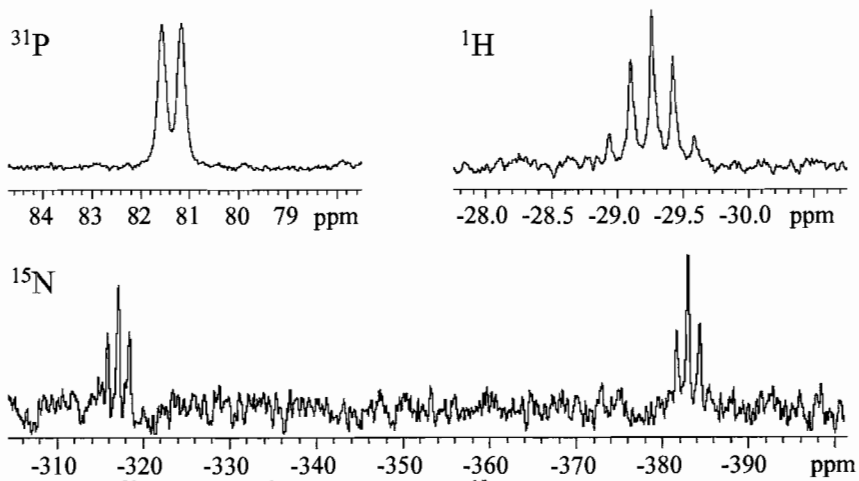

Figure 11. ^{31}P (top left), ^1H (top right), and ^{15}N (bottom) NMR spectra for *trans*-$[Fe(DMeOPrPE)_2(N_2H_4)H]^+$.

An alternative starting material for the generation of the ammonia and hydrazine complexes was sought because obtaining these complexes in pure form using the N_2 complex as the starting material proved to be difficult. If the *trans*-Fe(DMeOPrPE)$_2$HCl complex could be formed cleanly, then reaction of this complex with a chloride abstractor and the desired ligand (N_2H_4 or NH_3) should provide clean conversion to these complexes. *trans*-Fe(DMeOPrPE)$_2$HCl has been previously synthesized by reacting *trans*-Fe(DMeOPrPE)$_2$Cl$_2$ with a hydride source, however by this route the complex was never generated cleanly.[21] As *trans*-[Fe(DMeOPrPE)$_2$(N_2)H]$^+$ can be synthesized as an analytically pure solid the reaction of this complex with a chloride source should provide a clean synthesis of *trans*-Fe(DMeOPrPE)$_2$HCl. Indeed this reaction proceeds smoothly in THF using tetraethylammonium chloride as the organic soluble chloride source. The hydrido chloride complex was isolated as a bright orange oil and characterized in solution by NMR spectroscopy. This route provides a much cleaner synthesis of *trans*-Fe(DMeOPrPE)$_2$HCl with the only impurity being uncoordinated DMeOPrPE, which can be removed using chromatography. Unfortunately, *trans*-Fe(DMeOPrPE)$_2$HCl was soluble in all organic solvents, even hexane and pentane, thus isolation of the complex as a solid could not be achieved.

Reaction of *trans*-Fe(DMeOPrPE)$_2$HCl with excess $^{15}N_2H_4$ in the presence of $TlPF_6$ resulted in the generation of myriad species. Inspection of the $^{31}P\{^1H\}$ NMR spectrum showed seven different products (Fig. 12). By comparing the peak heights in the $^{31}P\{^1H\}$ and ^1H NMR spectra, most of the products could be assigned because they had been previously synthesized using alternative routes. The mixture contained *trans*-

$[Fe(DMeOPrPE)_2(H_2)H]^+$ (87.5 ppm), *trans*-$[Fe(DMeOPrPE)_2(NH_3)H]^+$ (81.3 ppm), *trans*-$[Fe(DMeOPrPE)_2(N_2H_4)H]^+$ (79.9 ppm), *trans*-$[Fe(DMeOPrPE)_2(N_2)H]^+$ (76.2 ppm), *cis*-$[Fe(DMeOPrPE)_2(N_2H_4)]^{2+}$ (74.4 and 61.5 ppm), as well as two peaks at 79.6 and 80.8 ppm that had not been previously observed. From the $^{31}P\{^1H\}$ and ^{31}P NMR data both of these unassigned resonances represented *trans* hydride complexes, i.e. *trans*-$Fe(DMeOPrPE)_2(X)H$. The ^1H NMR data proved crucial in determining the structures of these two unknown complexes.

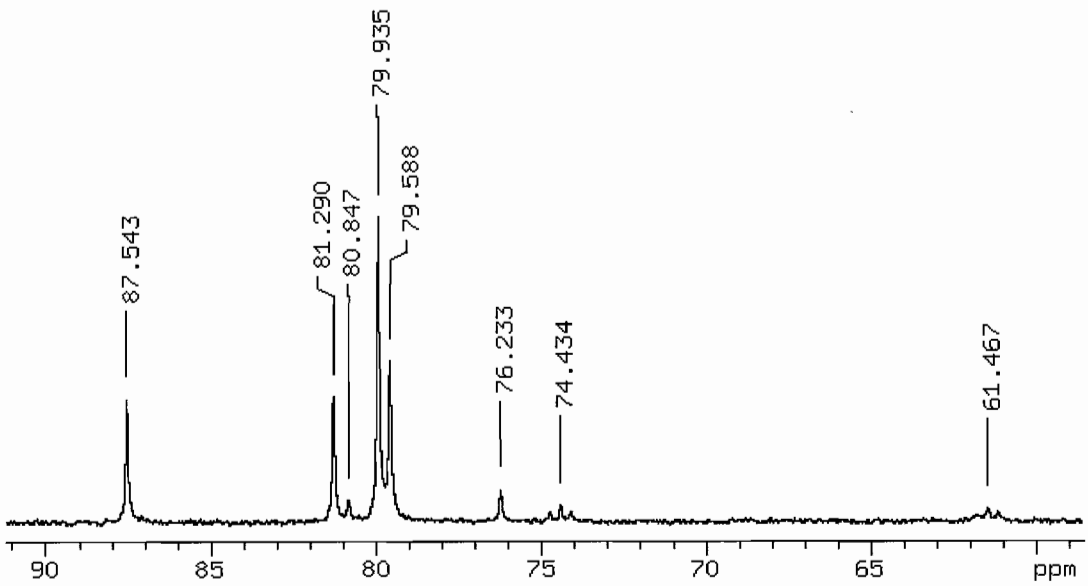

Figure 12. $^{31}P\{^1H\}$ NMR spectrum of the reaction of *trans*-$Fe(DMeOPrPE)_2HCl$ with excess $^{15}N_2H_4$.

These two mystery species both exhibited a multiplet in the downfield region (13-15 ppm) of the ^1H NMR spectrum (Fig. 13). From comparison with previously reported complexes,[42,43] these multiplets were tentatively assigned as *trans*-$[Fe(DMeOPrPE)_2(^{15}N_2H_2)H]^+$ and *trans*-$Fe(DMeOPrPE)_2(^{15}N_2H)$ (Fig. 14). The two major multiplets centered at 15 and 14.1 ppm are assigned to the diazene complex,

trans-[Fe(DMeOPrPE)$_2$($^{15}N_2H_2$)H]$^+$. The resonance at 15 ppm represents the proton attached to the terminal nitrogen atom of the coordinated diazene, with coupling to ^{15}N and the other diazene proton causing the observed doublet of doublets splitting pattern. Similar coupling is observed for the proton attached to the diazene nitrogen atom coordinated to the iron, with added coupling to phosphorus resulting in a doublet of doublet of triplets. The resonance at 13.8 ppm represents the lone proton on the terminal nitrogen of a coordinated deprotonated diazene. A doublet is observed due to coupling with ^{15}N.

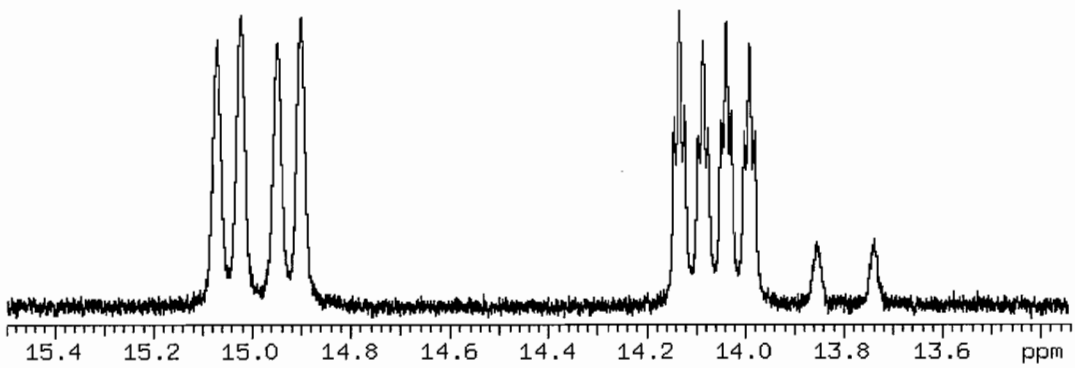

Figure 13. Downfield ^1H NMR spectrum of the reaction of *trans*-Fe(DMeOPrPE)$_2$HCl with excess $^{15}N_2H_4$.

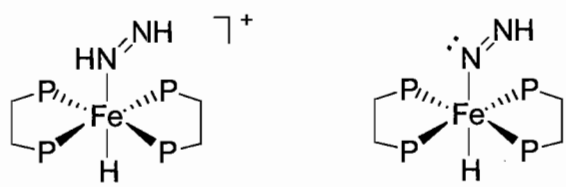

Figure 14. Proposed structures of *trans*-[Fe(DMeOPrPE)$_2$(N_2H_2)H]$^+$ (left) and *trans*-Fe(DMeOPrPE)$_2$(N_2H) (right).

At present the mechanism of the formation of *trans*-[Fe(DMeOPrPE)$_2$(N_2H_2)H]$^+$ is unclear. Hydrazine is known to produce diazene upon oxidation,[44,45] thus this

complex could have been formed by the oxidation of *trans*-$[Fe(DMeOPrPE)_2(N_2H_4)H]^+$, presumably by adventitious O_2. More likely however is that the diazene is formed by the disproportionation of hydrazine. As all other intermediates of hydrazine disproportionation are observed in this reaction this seems to be the most reasonable hypothesis, however the exact mechanism of this transformation is unclear. The deprotonated diazene complex, *trans*-$Fe(DMeOPrPE)_2(N_2H)$, likely arises from the deprotonation of *trans*-$[Fe(DMeOPrPE)_2(N_2H_2)H]^+$ by the excess hydrazine present in solution. It has previously been shown that the protons of diazene coordinated to a metal are quite acidic and can be easily deprotonated to form the diazenido complex.[46,47]

This is the first time that coordination complexes of N_2, N_2H_2, N_2H_4, and NH_3 complexes have been synthesized and characterized using the same iron scaffold. These complexes could provide useful data for comparison with trapped intermediates in nitrogenase turnover.[34-36] These complexes also provide an alternative mechanism (Scheme 3) to ammonia formation in the protonation $Fe(DMeOPrPE)_2N_2$ than the one that will be presented in chapter IV. Protonation of $Fe(DMeOPrPE)_2N_2$ results primarily in the formation *trans*-$[Fe(DMeOPrPE)_2(N_2)H]^+$. *trans*-$[Fe(DMeOPrPE)_2(N_2)H]^+$ could be reduced by remaining $Fe(DMeOPrPE)_2N_2$ and protonated to yield *trans*-$Fe(DMeOPrPE)_2(N_2H)$. This complex would then be readily protonated to form *trans*-$[Fe(DMeOPrPE)_2(N_2H_2)H]^+$. The diazene complex could then be further reduced by a second equivalent of $Fe(DMeOPrPE)_2N_2$ (if any remains) or the diazene complex may simply disproportionate into hydrazine and ammonia.

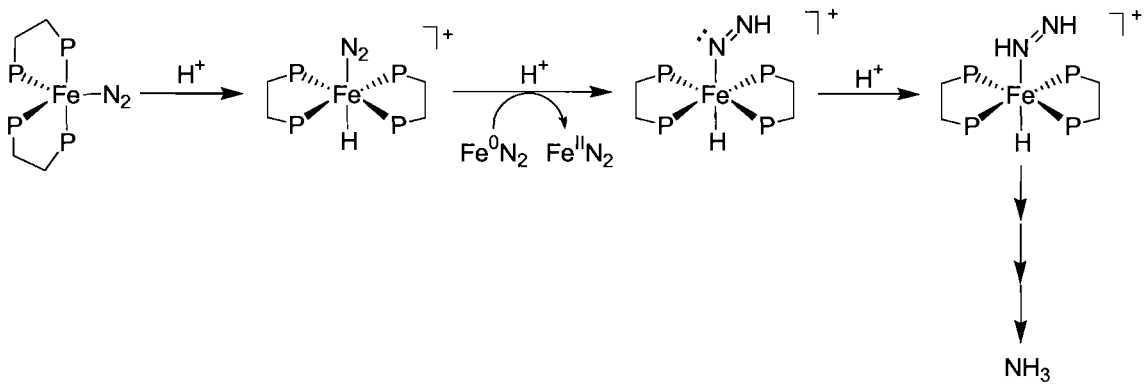

Scheme 3. Potential pathway of N_2 reduction to NH_3 from a dinitrogen hydride complex.

2.4 Conclusion

This chapter described the synthesis of *trans*-$[Fe(DMeOPrPE)_2(H_2)H]^+$ and *trans*-$[Fe(DMeOPrPE)_2(N_2)H]^+$ and the characterization of these complexes by solution and solid-state techniques. Both complexes are important species in a Leigh-type dinitrogen reduction cycle and their substitution reactivity was studied to gain insights into how to improve the yields of ammonia. The five coordinate complex $[Fe(DMeOPrPE)_2Cl]^+$ was also isolated and characterized by XRD and lends further support to the mechanism proposed for the formation of *trans*-$[Fe(DMeOPrPE)_2(H_2)H]^+$.[21]

The coordinated H_2 and N_2 molecules in these complexes are weakly bonded to iron and can be displaced by a wide variety of small molecules. The substitution rates with acetonitrile were monitored to determine the relative substitution rates of H_2 versus N_2. It was determined that the rate of N_2 substitution occurred ~6 times quicker than H_2 substitution, but neither complex showed any rate dependence on the solvent. The inability of solvent to impact the substitution of the H_2 complex was of particular interest

because our recent work suggested that coordinated H_2 can participate in hydrogen bonding in the analogous Ru complex.[29] However, preliminary ^1H NMR experiments suggest that the H_2 ligand of *trans*-$[Fe(DMeOPrPE)_2(H_2)H]^+$ does not participate in hydrogen bonding. Consequently, this is why the solvent has no influence on the rate of H_2 substitution in the Fe complex.

Finally, this chapter described the synthesis of iron hydride complexes of the type *trans*-$[Fe(DMeOPrPE)_2(X)H]^+$, where X = N_2H_2, N_2H_4, and NH_3. Iron coordination complexes of dinitrogen reduction intermediates are becoming increasingly important as more and more evidence points toward iron as the active metal in nitrogenase enzymes. These complexes represent the first series of iron complexes containing all of the important dinitrogen reduction intermediates and could represent an alternative N_2 reduction pathway in the protonation of $Fe(DMeOPrPE)_2N_2$ to the mechanism that will be presented in Chapter IV.

2.5 Bridge

Chapter II described the synthesis and reactivity of dihydrogen and dinitrogen complexes which are precursors to $Fe(DMeOPrPE)_2N_2$, the active ammonia producing complex. Chapter III will examine anion effects in the formation of $Fe(DMeOPrPE)_2N_2$, the stability of $Fe(DMeOPrPE)_2N_2$, and the protonation of $Fe(DMeOPrPE)_2N_2$ to produce ammonia. Chapter III also describes initial attempts at optimizing the protonation reaction and the determination of the reducing equivalents available for N_2 reduction.

CHAPTER III

REDUCTION OF DINITROGEN TO AMMONIA USING $Fe(DMeOPrPE)_2N_2$

Some of this work has been previously published and is reproduced with permission from: Crossland, J. L.; Young, D. M.; Zakharov, L. N; Tyler, D. R. *Dalton Trans.* **2009**, *manuscript submitted.*

3.1 Introduction

An estimated 40% of the world's population is sustained by industrially produced fertilizer, with ammonia being the primary component of these fertilizers.[1] Ammonia is industrially produced using the Haber-Bosch process. In this process N_2 and H_2 gases are heated and compressed over a heterogeneous iron catalyst to produce ammonia (eq. 1).[2] Due to the high temperatures and pressures this process requires a huge amount of energy, estimated to account for 1-2% of the world's annual energy consumption.[3]

$$N_2 + H_2 \xrightarrow[\substack{>200\ ^\circ C \\ >400\ atm}]{Fe} 2NH_3 \qquad (1)$$

Because of these high energy demands, and spurred on by recent biochemical studies that suggest iron is responsible for ammonia production in biological systems,[4-6] homogeneous iron complexes have found renewed interest as possible catalysts for a low-energy alternative to ammonia production. Iron dinitrogen complexes supported by

a variety of bidentate and tripodal phosphine ligands have shown the ability to reduce N_2 to NH_3 under acidic conditions (eqs. 2 and 3).[7-10]

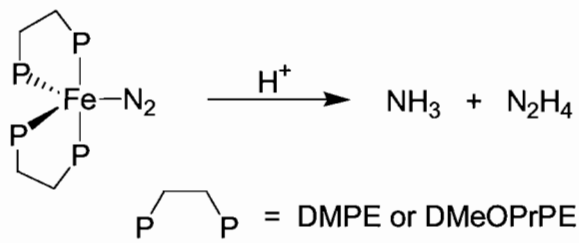

(2)

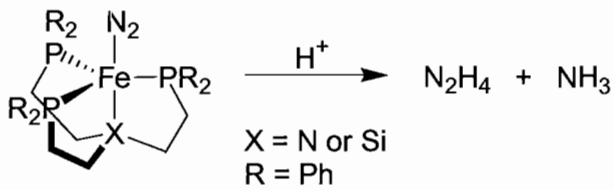

(3)

As discussed in the previous chapter, a scheme following the work of Leigh can be envisioned that could result in catalytic ammonia production (see Scheme 1, pg. 32). Our major modification to the system involves generating the dihydrogen hydride complex, *trans*-$[Fe(DMeOPrPE)_2(H_2)H]^+$ directly from *trans*-$Fe(DMeOPrPE)_2Cl_2$ and dihydrogen. This allows ammonia to be produced directly from dinitrogen, dihydrogen, and a proton source. This system is unique among other homogeneous iron systems that produce ammonia in that the electrons used for the reduction of dinitrogen come directly from dihydrogen and not from a hydride source or strong reducing agent, such as sodium metal.

This chapter will investigate details of the deprotonation of *trans*-$[Fe(DMeOPrPE)_2(N_2)H]^+$ to yield $Fe(DMeOPrPE)_2N_2$. The stability of the $Fe(DMeOPrPE)_2N_2$ complex will be explored as well as the reaction of this complex

with acid to produce ammonia and hydrazine. Initial work into the optimization of this protonation reaction will also be discussed.

3.2 Experimental

3.2.1 Materials and Reagents

All manipulations were carried out in either a Vacuum Atmospheres Co. glove box (argon or N_2 filled) or on a Schlenk line using argon or nitrogen. HPLC grade THF, hexane, and diethyl ether (Burdick and Jackson) were dried and deoxygenated by passing them through commercial columns of CuO, followed by alumina under an argon atmosphere. Toluene (Aldrich) was distilled under N_2 from CaH_2 and degassed via three freeze-pump-thaw cycles. Commercially available reagents were used as received. $TlBAr_F$[11] and $TlBF_4$[12] were synthesized by literature procedures. *trans*-$[Fe(DMeOPrPE)_2(N_2)H][BPh_4]$ was synthesized using the procedure presented in Chapter II. Deuterated solvents were purchased from Cambridge Isotope Laboratories and used as received.

3.2.2 Instrumentation

$^{31}P\{^1H\}$ and ^1H NMR spectra were recorded on either a Varian Unity/Inova 300 spectrometer at an operating frequency of 299.94 (^1H) and 121.42 (^{31}P) MHz or a Varian Unity/Inova 500 spectrometer at an operating frequency of 500.62 (^1H) and 202.45 (^{31}P) MHz. The ^1H and ^{31}P chemical shifts were referenced to the solvent peak and to an external standard of 1% H_3PO_4 in D_2O, respectively. NMR samples were sealed under argon or dinitrogen in 7 mm J. Young tubes. Note that the ^1H NMR data for the methyl

and methylene regions in complexes containing the DMeOPrPE ligand were generally broad and uninformative and therefore are not reported in the synthetic descriptions below.

3.2.3 Methods

Generation of *trans*-[Fe(DMeOPrPE)$_2$(H$_2$)H]X (X=BF$_4$, OTf, PF$_6$, BArF). These compounds were prepared analogously to *trans*-[Fe(DMeOPrPE)$_2$(H$_2$)H][BPh$_4$] (see Chapter II) using the appropriate counter-ion source; TlBF$_4$, TlOTf, TlPF$_6$, or TlBArF. The NMR characterization of these complexes matched that reported for the BPh$_4$ complex. These complexes were not isolated.

Generation of *trans*-[Fe(DMeOPrPE)$_2$(N$_2$)H]X (X=BF$_4$, OTf, PF$_6$, BAr$_F$). These compounds were prepared analogously to *trans*-[Fe(DMeOPrPE)$_2$(N$_2$)H][BPh$_4$] (see Chapter II) using the appropriate *trans*-[Fe(DMeOPrPE)$_2$(H$_2$)H]X starting material. These complexes were not isolated. $^{31}P\{^1H\}$ NMR (toluene-d_8): δ 75.5—76.9 (s). ^{31}P NMR (toluene-d_8): δ 75.5—76.9 (d, $^2J_{P\text{-}H}$ = 49 Hz). ^1H NMR (toluene-d_8) of the hydride region: BF$_4$, δ -18.35 (quintet, $^2J_{P\text{-}H}$ = 49 Hz); OTf, δ -18.4 (quintet, $^2J_{P\text{-}H}$ = 49 Hz); BPh$_4$, δ -18.6 (quintet, $^2J_{P\text{-}H}$ = 49 Hz); BAr$_F$, δ -18.8 (quintet, $^2J_{P\text{-}H}$ = 49 Hz).

Generation of Fe(DMeOPrPE)$_2$N$_2$. Solid ^{t}BuOK (2 eq.) was added to a stirring solution of *trans*-[Fe(DMeOPrPE)$_2$(N$_2$)H]$^+$ in toluene or Et2O/THF (2:1) in a dinitrogen filled glove box. The reaction was stirred for 13 hrs. after which time the solution was bright orange in color with a white precipitate. The solution was filtered through Celite and immediately used in the protonation reaction. $^{31}P\{^1H\}$ NMR (toluene-d_8): δ 79.9 (s). ^{31}P NMR (toluene-d_8): δ 79.9 (s).

Synthesis of $Fe(DMeOPrPE)_2(H)_2$. A solution of $Fe(DMeOPrPE)_2(N_2)$ in THF was charged with 1 atm of H_2 in a 50 mL Fisher-Porter tube and vigorously stirred for 6 hrs. The yellow oil was isolated by removing the solvent *in vacuo*. $^{31}P\{^1H\}$ NMR (DMSO-d_6) at 253K: 98.9 (t, $^2J_{P\text{-}P} = 20$ Hz), δ 84.8 (t, $^2J_{P\text{-}P} = 20$ Hz). ^1H NMR (DMSO-d_6) of the hydride region: -14.5 (quintet, $^2J_{P\text{-}H} = 36$ Hz), -14.7 (ddt, $^2J_{P\text{-}H} = 37$ Hz, $^2J_{P\text{-}H} = 14$ Hz, $^2J_{P\text{-}H} = 58$ Hz). Both *trans* and *cis* isomers are seen at various temperatures by ^1H and ^{31}P NMR spectroscopy, which has previously been observed in analogous iron dihydride complexes.[13]

Alternative synthesis of $Fe(DMeOPrPE)_2(H)_2$. To a stirring solution of *trans*-$[Fe(DMeOPrPE)_2H(H_2)]PF_6$ (50 mg, 0.056 mmol) in THF, solid ^{t}BuOK (13 mg, 0.112 mmol) was added. The mixture was stirred for 2 hours and then filtered through Celite. The yellow oil was isolated by removing the solvent *in vacuo*. The NMR spectra of the product synthesized by this route were identical to those described above.

Protonation of $Fe(DMeOPrPE)_2N_2$ and Determination of NH_3 and N_2H_4 yields. A solution of $Fe(DMeOPrPE)_2N_2$ prepared by the method above was immediately protonated with the appropriate acid (HCl, HBF_4, or HOTf) in a septum sealed 2-neck round bottom flask, and allowed to stir for 2 hrs after acid addition was complete in a dinitrogen filled glovebox. The flask was then removed from the glove box and the volatiles were vacuum-transferred onto a frozen HCl solution (1M HCl in Et_2O). A THF solution of ^{t}BuOK was then added to the remaining reaction mixture and stirred for 30 minutes. The volatiles were again vacuum-transferred into the same frozen HCl flask. Additional 1M HCl in ether was then added to the frozen HCl flask. The

mixture was allowed to thaw and then the solvents were removed *in vacuo*. The remaining residue was dissolved in water and analyzed for ammonia and hydrazine using the indophenol[14] and *p*-(dimethylamino)benzaldehyde[15] methods respectively. Yields of ammonia and hydrazine are reported relative to the amount of the *trans*-[$Fe(DMeOPrPE)_2H(N_2)$][BPh_4] starting material used.

Colorimetric Determination of Iron. Iron determinations were performed in a glovebox under a dinitrogen atmosphere and sealed in air-tight cuvettes before being analyzed on the UV-Vis spectrometer. A 1 mM stock solution of iron(II) chloride was prepared, along with a 0.05M 1,10-phenantholine stock solution. A standard curve was obtained by mixing 1.0 mL of the 1,10-phenanthroline solution and 0.2-1.0 mL of the iron(II) chloride stock solution, diluting to 10 mL total volume, and allowing to stand for 30 min before the absorption reading was taken. The concentration of iron(II) in the starting complex, *trans*-[$Fe(DMeOPrPE)_2(N_2)H$][BPh_4], was measured by diluting the complex to an appropriate concentration (within the measured standard curve), then adding 1.0 mL of the 1,10-phenanthroline solution, diluting to 10 mL total volume, and allowing to stand for 30 min. The reductive deprotonation and subsequent protonation reactions were then performed. An aliquot of the resulting reaction mixture was diluted to the appropriate volume, mixed with 1.0 mL of the 1,10-phenanthroline solution, diluted to 10 mL and allowed to stand for 30 min. All of the above procedures were performed in both H_2O and THF. The H2O was found to react with $Fe(DMeOPrPE)_2N_2$, thus anhydrous THF was used for the oxidation state determinations.

3.3 Results and Discussion

3.3.1 Anion Effects in the Deprotonation of trans-[Fe(DMeOPrPE)$_2$(N$_2$)H]$^+$

The deprotonation of the *trans*-[Fe(DMeOPrPE)$_2$(N$_2$)H]$^+$ complex is a key step in the Leigh cycle for producing ammonia (Scheme 1). In order to determine if there was an anion effect on the deprotonation reaction, the *trans*-[Fe(DMeOPrPE)$_2$(N$_2$)H]$^+$ complex was synthesized with various anions. The complexes with various counterions were synthesized analogously to *trans*-[Fe(DMeOPrPE)$_2$(H$_2$)H][BPh$_4$] and *trans*-[Fe(DMeOPrPE)$_2$(N$_2$)H][BPh$_4$] described in Chapter II using the appropriate chloride abstractor and anion source (Scheme 2). Spectroscopic characterization by NMR (^{31}P and ^{1}H) showed the resulting metal complexes to be identical to the BPh$_4$ complexes.

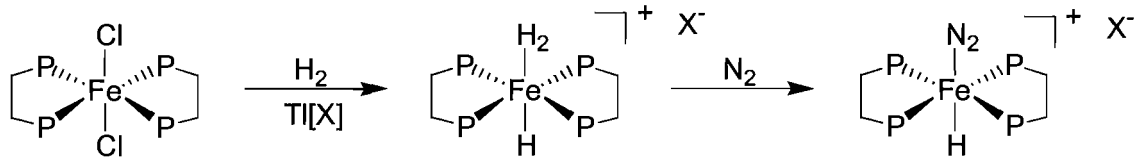

X= BAr_F^-, OTf^-, BF_4^-, PF_6^-

Scheme 1. Synthetic scheme for *trans*-[Fe(DMeOPrPE)$_2$(N$_2$)H][X] complexes.

Deprotonation of the *trans*-[Fe(DMeOPrPE)$_2$(N$_2$)H][X] complexes in toluene was then performed using 2 equivalents of ^{t}BuOK (eq. 4), and completion of the reaction was determined by a shift in the ^{31}P{^{1}H} resonance (~3 ppm downfield), the loss of hydride coupling in the ^{31}P spectrum, and the disappearance of the hydride peak in the ^{1}H NMR spectrum (Table 1). All of the complexes, with the exception of the BAr_F^-

complex (BAr_F^- = tetrakis(3,5-bis(trifluoromethyl)phenyl)borate), were shown to undergo deprotonation to yield $Fe(DMeOPrPE)_2N_2$ within 16 hrs (Table 1).

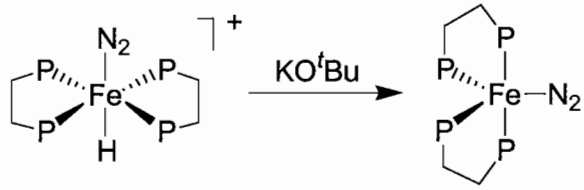

(4)

Table 1. NMR data of *trans*-$[Fe(DMeOPrPE)_2(N_2)H][X]$ complexes.

Anion	Initial ^{31}P • (ppm)	^{31}P • w/Base (ppm)	Hydride • (ppm)
BF_4^-	76.9	79.5	-18.35
PF_6^-	75.8	79.8	-18.4
OTf$^-$	76.0	79.3	-18.4
BPh_4^-	75.7	79.6	-18.6
BAr_F^-	75.5	75.5	-18.8

Closer inspection of the ^1H NMR spectra (Table 1) reveals that the hydride resonance shifts downfield as the size of the anion decreases, with the largest anion (BAr_F^-) being the only complex that was not deprotonated. This could be explained by an ion-pairing phenomenon where the anion is closely associated with the hydride ligand and assists in the deprotonation reaction.[16-18] It is proposed that the interaction of the anion with the hydride ligand decreases the electron density of the hydride, causing the ^1H resonance to shift downfield and the hydride to become slightly more acidic. This slight increase in acidity allows the ^{t}BuOK to deprotonate the hydride ligand. As the anions become larger, the approach to the hydride ligand becomes more hindered due to steric interactions with the phosphine ligands, and the ion-pairing interaction is

diminished. Thus, the BAr_F^- anion is too large to approach the hydride ligand, and the hydride ligand is not activated toward deprotonation. This hypothesis is intriguing because it suggests that by manipulation of the counter-ion size and phosphine ligand sterics the pK_a of the hydride ligand can be altered. Because the phosphine ligands impart water-solubility to the complexes, being able to lower the pK_a of the hydride could allow the deprotonation to occur in aqueous solution.

3.3.2 Synthesis and Stability of $Fe(DMeOPrPE)_2(N_2)$

Because the *trans*-$[Fe(DMeOPrPE)_2(N_2)H][BPh_4]$ complex can be isolated as an analytically pure solid, this particular complex was used for all the proceeding experiments. The iron(0) complex, $Fe(DMeOPrPE)_2N_2$, is generated cleanly by the addition of 2 equivalents of K^{t}BuO to a solution of *trans*-$[Fe(DMeOPrPE)_2(N_2)H][BPh_4]$ (eq. 5).

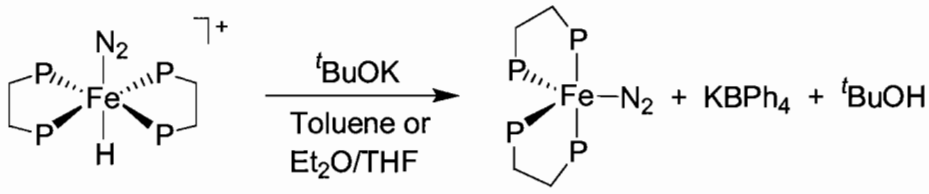

(5)

The reaction is allowed to stir for 13 hrs and is then filtered through Celite (removing $KBPh_4$) to yield a bright orange solution. The $Fe(DMeOPrPE)_2N_2$ complex displays a singlet resonance in the $^{31}P\{^1H\}$ NMR spectrum (Fig. 1). This resonance is also a singlet in the proton-coupled ^{31}P NMR spectrum indicating that the hydride ligand has been successfully removed. The reaction can also be monitored by ^1H NMR spectroscopy by watching the disappearance of the hydride ligand of *trans*-$[Fe(DMeOPrPE)_2(N_2)H]^+$. This "reductive" deprotonation proceeds most cleanly in

toluene, but has also successfully been run in a Et_2O/THF (2:1) solvent system. Two equivalents of base are typically used to ensure complete conversion, however one equivalent of KO^{t}Bu has been shown to work.

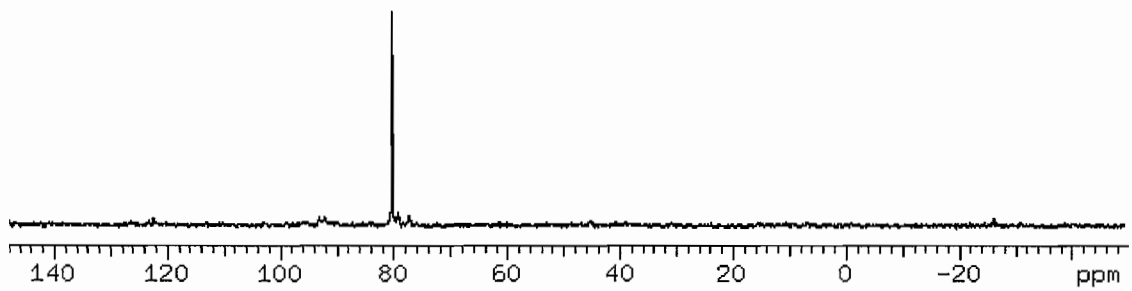

Figure 1. $^{31}P\{^1H\}$ NMR spectrum of $Fe(DMeOPrPE)_2N_2$ in toluene.

Attempts to isolate $Fe(DMeOPrPE)_2N_2$ as a solid have been unsuccessful due to the solubility imparted by the DMeOPrPE ligand and the instability of the complex. The $Fe(DMeOPrPE)_2N_2$ complex is not only unstable towards vacuum, but degrades upon standing in solution under an N_2 atmosphere. A common degradation product is uncoordinated phosphine (DMeOPrPE). Formation of free ligand is always observed when this particular iron-phosphine scaffold is reacted in the presence of a strong base. The formation of $Fe(DMeOPrPE)_2N_2$ is also highly sensitive to oxygen and water. Reaction of water with the five-coordinate complex results in degradation by two pathways. The first route is reprotonation of the iron center. The iron(0) center of $Fe(DMeOPrPE)_2N_2$ is very electron rich and can be protonated by water reforming the *trans*-$[Fe(DMeOPrPE)_2(N_2)H]^+$ complex. This is the reason the five-coordinate

complex can not be generated in water, the pK_a of the hydride ligand is too high to be deprotonated by hydroxide.

Exposure of $Fe(DMeOPrPE)_2N_2$ to water was also shown to result in another impurity, a species with two broad resonances at 98 and 89 ppm in the $^{31}P\{^1H\}$ NMR spectrum. This product was found to be *cis*-$Fe(DMeOPrPE)_2(H)_2$ by NMR spectroscopy. The $^{31}P\{^1H\}$ spectrum at -20°C consists of two resonances; δ 98 (t, $^2J_{P\text{-}P}$ = 17 Hz) and δ 84 ppm (t, $^2J_{P\text{-}P}$ = 17 Hz), representative of a *cis* arrangement of the bidentate phosphine ligands (Fig. 3). The hydride region of the ^1H spectrum at -40°C shows a quintet and a doublet of doublet of triplets with chemical shifts of -14.9 and -15.3 respectively (Fig. 2). Upon heating the sample to 80°C, the quintet is the only resonance seen (Fig. 2). These observations can be explained by an equilibrium between *cis*-$Fe(DMeOPrPE)_2(H)_2$ and *trans*-$Fe(DMeOPrPE)_2(H)_2$ (eq. 6).[13] The coupling constants correlate well to those seen in other iron-phosphine systems.

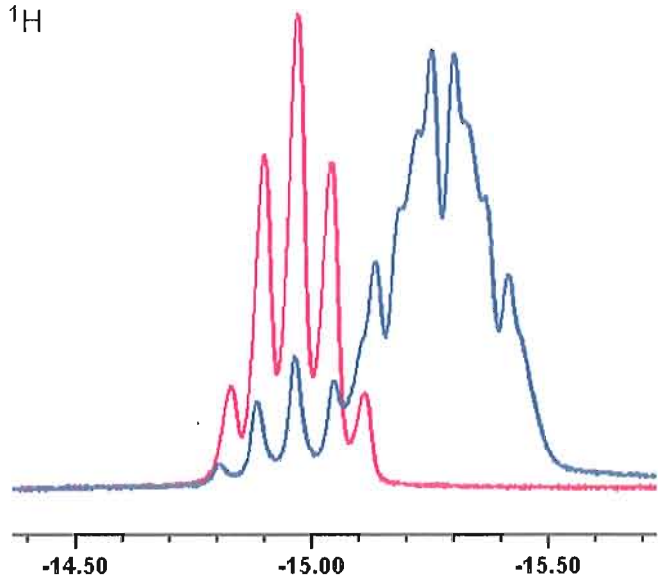

Figure 2. Variable temperature ^1H spectra of the hydride region of $Fe(DMeOPrPE)_2(H)_2$. The red trace is the spectrum at 80°C, the blue trace is the spectrum at -40°C

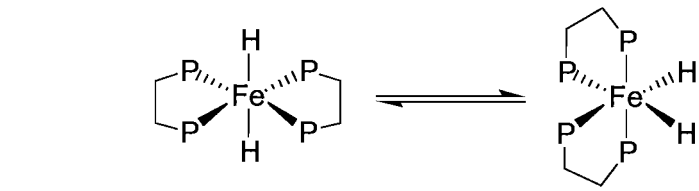

(6)

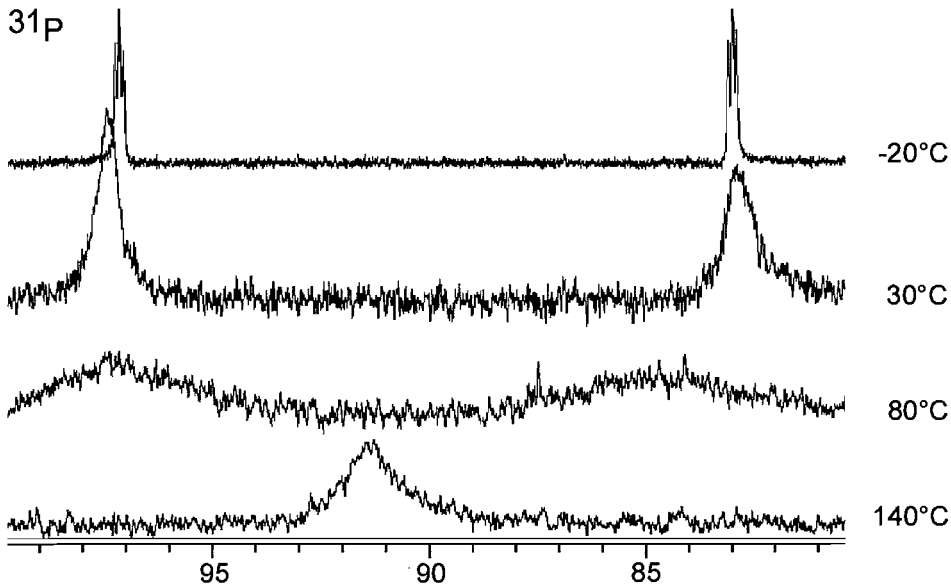

Figure 3. Variable temperature $^{31}P\{^{1}H\}$ NMR spectra of $Fe(DMeOPrPE)_2(H)_2$.

The $^{31}P\{^{1}H\}$ spectrum also shows the conversion to *trans*-$Fe(DMeOPrPE)(H)_2$ upon heating to 140°C (Fig. 3). The identity of the species was confirmed by two alternative synthetic routes: the oxidative addition of H_2 to $Fe(DMeOPrPE)_2N_2$ and the deprotonation of *trans*-$[Fe(DMeOPrPE)_2(H_2)H]^+$ (Scheme 3).

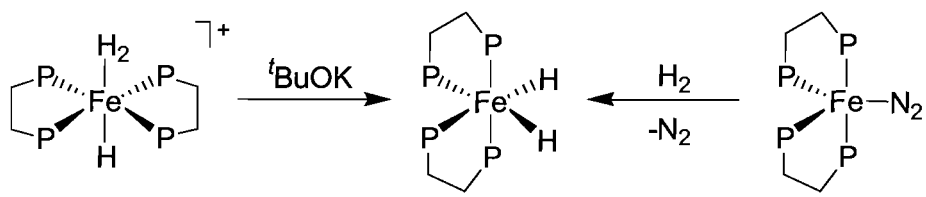

Scheme 2. Alternative syntheses for *cis*-$Fe(DMeOPrPE)_2(H)_2$.

The oxidative addition of H_2 to the iron(0) center is likely the reaction pathway that results in formation of *cis*-Fe(DMeOPrPE)$_2$(H)$_2$ from reaction of Fe(DMeOPrPE)$_2$N$_2$ with water. The highly reducing iron(0) complex likely reduces water to H_2, which can then further react with a second equivalent of iron(0) complex to form *cis*-Fe(DMeOPrPE)$_2$(H)$_2$. Because Fe(DMeOPrPE)$_2$N$_2$ is quite unstable it is typically generated and then immediately used in the protonation reaction.

3.3.3 Optimization of the Protonation of Fe(DMeOPrPE)$_2$(N$_2$)

Once the Fe(DMeOPrPE)$_2$N$_2$ complex is generated it can be protonated with a strong acid to yield a mixture of ammonia and hydrazine. After the initial report[7] very little was known about what reaction conditions favor ammonia formation, thus several variables were tested in order to optimize the yields of ammonia and hydrazine obtained from the protonation of Fe(DMeOPrPE)$_2$N$_2$. An undergraduate student working in our lab, Dan Regan, made significant contributions to this work.

A series of strong acids was selected to test whether the anion of the acid affected the yields of ammonia. The hypothesis was that as the coordinating ability of the anion increased the yields of ammonia would decrease. Triflic acid (TFOH), tetrafluoroboric acid (HBF_4) and hydrochloric acid (HCl) as 1M diethyl ether solutions were used to protonate Fe(DMeOPrPE)$_2$N$_2$. It was found that TfOH gave the highest yields of ammonia (17%), followed by HBF_4 (7 %) and finally HCl (4%). This trend agrees with the hypothesis that the coordinating ability of the anion decreases the yield of ammonia. Interestingly these acids each produced a uniquely colored solution that disappeared within seconds after acid addition. Addition of TFOH results in a dark purple

intermediate, HBF_4 results in a dark blue intermediate, and HCl results in a pale pink intermediate. It is unclear what these colors arise from, although it may be attributable to an electron transfer process. The identity of the reaction solvent also seems to have an effect on the observed yields of ammonia, with higher yields observed when the reaction is run in a THF/Et_2O solvent system instead of toluene. The affect of the addition rate of the acid was also examined using a syringe pump. The addition rate was varied from 0.15 mL/min to 3 mL/min with no difference seen in the yields of ammonia.

In the course of these optimization studies it was discovered that the presence of iron significantly altered the measured yields of ammonia. Iron was shown to have a positive interference on the yields of ammonia, affecting the measured yields by as much as 50%. Thus the actual yields of ammonia produced during these reactions were actually much lower than what had been measured. Once this interference was discovered a new analysis procedure was used to separate the ammonia and hydrazine from all the other reaction components. Using a base distillation technique the ammonia and hydrazine could be isolated and accurately analyzed using established analytical methods (see Experimental section). While the previous method gives an inaccurate measurement of the amount of ammonia present, the trends observed from this data should still be valid.

It should also be noted that addition of acid to *trans*-$[Fe(DMeOPrPE)_2(N_2)H]^+$ results in a trace amount (<2%) of ammonia. However, the yield of ammonia from this reaction is always much less than the yield of ammonia obtained from the protonation of $Fe(DMeOPrPE)_2N_2$ under identical reaction condition.

Now that an acceptable method for accurately determining the yields of ammonia has been established, other variables need to be investigated. These include performing the protonation reaction in a more polar solvent such as acetone, varying the identity of the base used to deprotonate *trans*-$[Fe(DMeOPrPE)_2(N_2)H]^+$, lowering the temperature of the reaction, and trying a sterically hindered weak base ($[HLut][BPh_4]$, Lut = lutidine) to favor protonation of the terminal nitrogen.

3.3.4 Determining the Oxidation State of Iron After the Protonation of $Fe(DMeOPrPE)_2(N_2)$

With hopes of improving the yields of ammonia even further we set out to study the mechanism of the protonation reaction. Because there are no added reducing agents present in the protonation reaction, the $Fe(DMeOPrPE)_2N_2$ complex must be the source of all the electron equivalents required for the reduction of N_2 to ammonia. The first step in determining the mechanism of ammonia formation was to determine how many electrons each iron center was donating to the overall reduction of N_2. The reduction of N_2 to ammonia is a six electron process. All six electrons likely do not come from a single iron center so to determine how many electrons each iron center donates a spectrophotometric determination of the iron(II) concentration was preformed. The concentration of iron(II) was determined at various stages of the protonation reaction: the *trans*-$[Fe(DMeOPrPE)_2(N_2)H]^+$ starting material, the $Fe(DMeOPrPE)_2(N_2)$ complex prior to protonation, and the reaction mixture after protonation (Table 2). The determination had to be done under anhydrous conditions because $Fe(DMeOPrPE)_2N_2$ degrades in water. A standard curve using phenanthroline in THF was prepared and

from this standard curve the concentration of iron(II) could be determined at the various stages of the reaction.

Table 2. Summary of the iron(II) spectrophotometric analysis.

Complex	Conc. Iron(II)
FeN_2H	1.65E-05 M
FeN_2	0
$FeN_2 + H^+$	1.75E-05 M

The concentration of iron(II) present in the starting material, *trans*-$[Fe(DMeOPrPE)_2(N_2)H]^+$, was first measured. This complex was then deprotonated, and the spectrophotometric determination showed no iron(II) as expected because the iron center is now in the zero oxidation state. After the protonation reaction was complete, the concentration of iron(II) returned to the level present in the *trans*-$[Fe(DMeOPrPE)_2(N_2)H]^+$ starting material, confirming that each iron center only donates two electrons to the reduction of N_2. Based on this information, the number of potential reaction mechanisms is reduced. These mechanisms will be discussed in more detail in Chapter IV.

3.4 Conclusions

The generation of $Fe(DMeOPrPE)_2N_2$ was described and effect of the anion on this reaction was determined. All anions used (BPh_4, PF_6, BF_4, BAr_F, OTf) were found to readily deprotonation in the presence of K^{t}BuO with the exception of the BAr_F anion.

The results suggest that an ion-pairing interaction of the anion with the hydride ligand removes electron density from the hydride ligand and thereby facilitates the deprotonation reaction. Once $Fe(DMeOPrPE)_2N_2$ is generated it is quite unstable and readily decomposes in the presence of trace water through both protonation and oxidation pathways. Reaction of $Fe(DMeOPrPE)_2N_2$ with a strong acid results in the formation of NH_3 and N_2H_4. Preliminary attempts at optimizing the protonation reaction were undertaken with solvent and acid identity having the largest effects on the observed yields. Finally this chapter determined that each $Fe(DMeOPrPE)_2N_2$ complex donates only two electrons toward the overall six electron reduction of N_2 to NH_3. This is one contributing factor to the relatively low yields of ammonia observed.

3.5 Bridge

Chapter III has described the synthesis of the active ammonia producing complex, $Fe(DMeOPrPE)_2N_2$ and the protonation of this complex to produce ammonia. Chapter IV will describe the investigation of the mechanism of ammonia formation through the synthesis and study of potential N_2 reduction intermediate complexes, such as diazene (N_2H_2), hydrazine (N_2H_4), and ammonia (NH_3).

CHAPTER IV

INVESTIGATION OF THE MECHANISM OF NH_3 FORMATION FROM THE PROTONATION OF $Fe(DMeOPrPE)_2N_2$

Some of this work has been previously published and is reproduced with permission from:
Crossland, J. L.; Balesdent, C. G.; Tyler, D. R. *Dalton Trans.* **2009**, 4420-4422.
Crossland, J. L.; Zakharov, L. N.; Tyler, D. R. *Inorg. Chem.* **2007**, *46*, 10476-10478.

4.1 Introduction

Iron is common to both the industrial (Haber-Bosch) and biological (nitrogenase) production of ammonia.[1,2] Research has accordingly focused on studying the chemistry of iron with dinitrogen and other dinitrogen derivatives.[3-9] As discussed in chapter III, some synthetic iron dinitrogen complexes including $Fe(DMeOPrPE)_2N_2$ have shown the ability to produce ammonia and/or hydrazine in the presence of acid.[10-13] Whereas the mechanism of ammonia production in these synthetic systems is currently unknown, growing data for nitrogenase supports a mechanism that proceeds through diazene and hydrazine intermediates in route to ammonia formation.[14,15] Therefore studying iron complexes of hydrazine and diazene could provide insights in the mechanism of biological nitrogen fixation as well as the mechanism of ammonia formation from the protonation of synthetic iron phosphine complexes.

This chapter will begin by describing the synthesis and characterization of a novel iron(II) hydrazine complex that shows unusual η^2-hydrazine coordination. The acid base reactivity of the hydrazine complex is explored, with deprotonation of the hydrazine complex yielding an η^2-hydrazido(1-) complex *cis*-$[Fe(DMeOPrPE)_2(N_2H_3)]^+$ and an iron(0) diazene complex *cis*-$Fe(DMeOPrPE)_2(N_2H_2)$. Attempts to synthesize an iron(II) diazene complex are also described. From the study of these potential intermediates a mechanism of N_2 reduction from the protonation of $Fe(DMeOPrPE)_2N_2$ is proposed. The iron coordination complexes described here may also provide insights into the mechanism of nitrogenase.

4.2 Experimental

4.2.1 Materials and Reagents

All manipulations were carried out in either a Vacuum Atmospheres Co. glove box (nitrogen or argon filled) or on a Schlenk line under argon or nitrogen. HPLC grade THF, diethyl ether, and hexane (Burdick and Jackson) were dried and deoxygenated by passing them through commercial columns of activated alumina under an argon atmosphere. All reagents, unless otherwise noted, were used as received. $FeCl_2(DMeOPrPE)_2$ was prepared by literature procedure.[16] Potassium azodiformate was prepared by hydrolysis of azodicarbonamide with KOH in EtOH.[17] Ferrocenium hexafluorophosphate,[18] and anthracene-9,10-biimine[19] were prepared using literature procedures. Azopropane was synthesized using the procedure described in Organic Syntheses, Coll. Vol. 6, p.78. [HDBU][OTf] was prepared by reacting DBU with 1M

TfOH in diethyl ether and removing the solvent *in vacuo*. Anhydrous $^{15}N_2H_4$ was extracted from $[^{15}N_2H_6][SO_4]$ using $NH_{3(l)}$ followed by evaporation of the ammonia. Reagent grade solvents were dried according to published procedures and deoxygenated with either an argon purge or three freeze-pump thaw cycles prior to use. Deuterated solvents were purchased from Cambridge Isotope Laboratories in 1g ampoules and dried over 3Å molecular sieves prior to use.

4.2.2 Instrumentation and Procedures

$^{31}P\{^1H\}$, ^{15}N, and ^1H NMR spectra were recorded on a Varian Unity/Inova 500 spectrometer at an operating frequency of 202.45 (^{31}P), 50.69 (^{15}N), and 500.62 (^1H) MHz. The ^1H and ^{31}P chemical shifts were referenced to the solvent peak and to an external standard of 1% H_3PO_4 in D_2O, respectively. The ^{15}N chemical shifts were referenced to an external standard of formamide/DMSO-d_6 (90:10), set to -267.8 ppm relative to nitromethane (0 ppm). When required, the samples were sealed under argon in 7 mm tubes fitted with Teflon valves. Note that the ^1H NMR data for the methyl and methylene regions in complexes containing the DMeOPrPE ligand were generally broad and uninformative and therefore are not reported in the synthetic descriptions below. Infrared spectra were recorded on a Nicolet Magna 550 FT-IR with OMNIC software. Samples were prepared as KBr pellets or as neat oils on NaCl plates. A Balzers ThermoStar GSD 300T quadrupole mass spectrometer, running Balzers Quadstar 422 software, was used for N_2 detection experiments. Mass spectra were obtained using an Agilent 1100 LC/MS Mass Spectrometer. The samples were dissolved in THF or Et_2O and introduced into the ionization head (ESI) using the infusion method.

4.2.3 X-ray Crystallography

Single crystals suitable for diffraction were grown as stated in the experimental procedure. The crystals were mounted on a glass fiber under Paratone N oil, and diffraction data were collected on a Bruker-AXS SMART APEX/CCD diffractometer using MoKα radiation (λ = 0.71073 Å) at 173 K. The crystallographic data and summary of the data collection and structure refinement are given in Appendix E. Absorption correction was applied by SADABS.[20] The structure was solved using direct methods and completed by subsequent difference Fourier syntheses and refined by full matrix least-squares procedures on reflection intensities (F^2). All non-hydrogen atoms were refined with anisotropic displacement coefficients. Terminal $-CH_2OCH_3$ groups in the structure are flexible and there are elongations for thermal ellipsoids of some atoms. These groups were refined with restrictions; the average value of C–O distances was used as a target for corresponding C–O bond lengths. The H atoms were placed at calculated positions and were refined as riding atoms. All software and sources scattering factors are contained in the SHELXTL (5.10) program package.

4.2.4 Syntheses

Synthesis of *cis*-[Fe(DMeOPrPE)$_2$(η^2-N$_2$H$_4$)][BPh$_4$]$_2$ (I). To a stirring solution of *trans*-Fe(DMeOPrPE)$_2$Cl$_2$ (0.22 g, 0.247 mmol) in THF, solid NaBPh$_4$ (0.169 g, 0.49 mmol) was added. Immediately a solution of N_2H_4 in THF (0.65 M, 0.5 mL) was added. The mixture was stirred for 1 hr after which it was filtered through Celite. The solvent was removed *in vacuo*. The red orange oil was redissolved in THF, filtered through Celite a second time, and again the solvent was removed *in vacuo*. The resulting red

orange oil was triturated with diethyl ether to yield a pale orange powder (0.27g, 96%). X-ray quality crystals were grown by layering a THF solution with hexane and allowing to stand at room temperature for 1 week. Anal. Calcd. for $C_{86}H_{130}B_2FeN_2O_8P_4$: C, 67.90; H, 8.61; N, 1.84. Found: C, 67.38; H, 8.17; N, 1.69. $^{31}P\{^1H\}$ NMR (CD_2Cl_2): δ 75.9 (t, $^2J_{P\text{-}P}$ = 36.5 Hz), δ 62.5 (t, $^2J_{P\text{-}P}$ = 36.4 Hz). ^1H NMR (CD_2Cl_2): δ 4.85 (s, br), δ 3.82 (s, br). IR(KBr): (ν_{NH}) 3291 cm^{-1}, 3271 cm^{-1}, 3243 cm^{-1}, 3197 cm^{-1}, (δ_{NH2}) 1616 cm^{-1}, 1580 cm^{-1}.

Synthesis of *cis*-[Fe(DMeOPrPE)$_2$(η^2-$^{15}N_2H_4$)][PF$_6$]$_2$. The synthesis of this complex was identical to that described above except that $TlPF_6$ was used in place of $NaBPh_4$ and $^{15}N_2H_4$ in place of N_2H_4. This complex could only be isolated as an oil. ^{15}N NMR (CD_2Cl_2): δ 140.7 (t, $^1J_{N\text{-}H}$ = 77 Hz). $^{15}N\{^1H\}$ NMR (CD_2Cl_2): δ 140.7 (s). $^{31}P\{^1H\}$ NMR (CD_2Cl_2): δ 75.8 (t, $^2J_{P\text{-}P}$ = 36.5 Hz), δ 62.4 (t, $^2J_{P\text{-}P}$ = 36.4 Hz). ^1H NMR (CD_2Cl_2): δ 4.85 (d, $^1J_{N\text{-}H}$ = 78 Hz), δ 3.82 (d, $^1J_{N\text{-}H}$ = 78 Hz).

Protonation of *cis*-[Fe(DMeOPrPE)$_2$(η^2-N$_2$H$_4$)][BPh$_4$]$_2$ (I). To a stirring solution of **I** (15 mg, 0.010 mmol) in a THF/Et_2O (1:1) solution, 0.5 ml of 1M TfOH in diethyl ether was added dropwise over the course of a couple minutes. The color of the solution went from orange to pale yellow to colorless upon addition of the acid. The solution was allowed to stir for 1 hr after which time the solvent was removed *in vacuo*. The remaining residue was dissolved in deionized water and analyzed for hydrazine and ammonia.[21,22] Yields of NH_3 for 7 trials were 21% ± 6% and yields of N_2H_4 for 9 trials were 64% ± 9%. These yields are reported as per mole of iron of **I**. To monitor

dinitrogen formation, a mass spectrometer was directly attached via a capillary to a sealed reaction flask inside an argon filled glovebox.

Synthesis of *cis*-Fe(DMeOPrPE)$_2$(N$_2$H$_2$). To a stirring solution of *cis*-[Fe(DMeOPrPE)$_2$(N$_2$H$_4$)][BPh$_4$]$_2$ (50 mg, 0.0335 mmol) in THF (3 mL), solid ^{t}BuOK (13 mg, 0.117 mmol) was added. The solution immediately changed color from bright red-orange to yellow with formation of a white precipitate. The solution was stirred for 15 min and then filtered through Celite. The solvent was removed *in vacuo* and the product was extracted with hexane. The hexane was then removed and the product was isolated as a yellow oil in 96% yield. The product contained uncoordinated DMeOPrPE ligand (~16% by ^{31}P{^{1}H} NMR). ^{31}P{^{1}H} NMR (THF-d_8): δ 75.8 (t, $^2J_{P\text{-}P}$ = 38 Hz), δ 71.2 (t, $^2J_{P\text{-}P}$ = 38 Hz). ESI+: *m/z* calcd for Fe(DMeOPrPE)$_2$(N$_2$H$_2$), 850.44. Found: [M+H$^+$]$^+$, 851.4. The ^{15}N isotopologue was synthesized in the same manner using *cis*-[Fe(DMeOPrPE)$_2$(^{15}N$_2$H$_4$)][BPh$_4$]$_2$ as the starting material. ^{31}P{^{1}H} NMR (THF-d_8): δ 75.8 (t, $^2J_{P\text{-}P}$ = 38 Hz), δ 71.2 (t, $^2J_{P\text{-}P}$ = 38 Hz). HMQC ^{1}H NMR (THF-d_8): δ 2.1 (br, s). ^{15}N{^{1}H} NMR (THF-d_8): -315.2 (s). ^{15}N NMR (THF-d_8): δ -315.2 (d, $^1J_{N\text{-}H}$ = 51 Hz).

Protonation of *cis*-Fe(DMeOPrPE)$_2$(N$_2$H$_2$). To a J. Young NMR tube containing *cis*-Fe(DMeOPrPE)$_2$(N$_2$H$_2$) (0.04 mmol, 35 mg) in Et$_2$O (0.6 mL) was added 83 μL of 1M TfOH in Et$_2$O. The solution changed in color from yellow to orange. The NMR data (^{31}P{^{1}H} and ^{15}N) showed quantitative conversion to *cis*-[Fe(DMeOPrPE)$_2$(N$_2$H$_4$)]$^{2+}$. The product was not isolated from this route.

Stepwise protonation of *cis*-Fe(DMeOPrPE)$_2$(N$_2$H$_2$). To a J. Young NMR tube containing *cis*-Fe(DMeOPrPE)$_2$(N$_2$H$_2$) (0.036 mmol, 31 mg) in THF (0.6 mL) was

added 16 mg of [HDBU][OTf] in THF. The NMR data ($^{31}P\{^{1}H\}$ and ^{15}N) showed quantitative conversion to *cis*-$[Fe(DMeOPrPE)_2(N_2H_3)]^+$. Then one equivalent of 1M TfOH was added and quantitative conversion to *cis*-$[Fe(DMeOPrPE)_2(N_2H_4)]^{2+}$ was observed by $^{31}P\{^{1}H\}$ and ^{15}N NMR spectroscopy. The products were not isolated during this procedure.

Alternative synthesis of *cis*-Fe(DMeOPrPE)$_2$(N_2H_2). Anhydrous hydrazine was added to a stirring THF/Et_2O solution of $Fe(DMeOPrPE)_2(N_2)$. The solution was stirred for 2 hours. The product was not isolated from this procedure. The $^{31}P\{^{1}H\}$ NMR spectrum showed a mixture of $Fe(DMeOPrPE)_2N_2$, *cis*-$Fe(DMeOPrPE)_2(N_2H_2)$, *cis*-$Fe(DMeOPrPE)_2(H)_2$, and uncoordinated DMeOPrPE (see Fig. S22).

Synthesis of *cis*-[Fe(DMeOPrPE)$_2$(N_2H_3)][BPh_4]. To a stirring solution of *cis*-$[Fe(DMeOPrPE)_2(N_2H_4)][BPh_4]_2$ (55 mg, 0.037 mmol) in THF, DBU (12 mg, 0.079 mmol) was added. The solution color immediately changed from red-orange to yellow. The solution was stirred for 15 min and then the solvent was removed *in vacuo*. The yellow product was extracted with toluene and precipitated by addition of hexane yielding a yellow oil in 93% yield. The product contained uncoordinated DMeOPrPE ligand (~13% by $^{31}P\{^{1}H\}$ NMR). $^{31}P\{^{1}H\}$ NMR (THF-d_8) at 298K: δ 77.1 (br, s), 72.8 (br, s), 68.8 (d, $^{1}J_{PP}$ = 129 Hz), 66.4 (d, $^{1}J_{PP}$ = 129 Hz). ESI+: *m/z* calcd. for *cis*-$[Fe(DMeOPrPE)_2(N_2H_3)]^+$, 851.44. Found: $[M]^+$, 851.4. The ^{15}N isotopologue was synthesized in the same manner using *cis*-$[Fe(DMeOPrPE)_2(^{15}N_2H_4)][BPh_4]_2$ as the starting material. $^{31}P\{^{1}H\}$ NMR (THF-d_8) at 193K: δ 77.9 (s), 73.7 (s), 72.2 (s), 70.7 (s), 69.2 (d, $^{1}J_{PP}$ = 130 Hz), 68.7 (d, $^{1}J_{PP}$ = 45 Hz), 65.9 (d, $^{1}J_{PP}$ = 45 Hz), 65.7 (d, $^{1}J_{PP}$ = 130

Hz). HMQC $^{1}H\{^{15}N\}$ NMR (THF-d_8) at 193K: δ 4.23 (s), 4.14 (s), 3.66 (s), 3.44 (s), 1.05 (s), 0.65 (s). HMQC ^{1}H NMR (THF-d_8) at 193K: δ 4.23 (d, $^{1}J_{NH}$ = 80 Hz), 4.14 (d, $^{1}J_{NH}$ = 75 Hz), 3.66 (d, $^{1}J_{NH}$ = 90 Hz), 3.44 (d, $^{1}J_{NH}$ = 92 Hz), 1.05 (d, $^{1}J_{NH}$ = 30 Hz), 0.65 (d, $^{1}J_{NH}$ = 30 Hz). $^{15}N\{^{1}H\}$ NMR (THF-d_8) at 193K: -367.6 (s), -369.9 (s), -377.4 (s). ^{15}N NMR (THF-d_8) at 193K: -367.6 (d, $^{1}J_{NH}$ = 50 Hz), -369.9 (d, $^{1}J_{NH}$ = 51 Hz), -377.4 (d, $^{1}J_{NH}$ = 80 Hz).

Protonation of *cis*-[Fe(DMeOPrPE)$_2$(N$_2$H$_3$)]$^+$. To a J. Young NMR tube containing *cis*-[Fe(DMeOPrPE)$_2$(N$_2$H$_3$)]$^+$ (0.036 mmol, 42 mg) in THF (0.6 mL) was added 36 μL of 1M TfOH in Et_2O. The solution changed in color from yellow to orange. The NMR data ($^{31}P\{^{1}H\}$ and ^{15}N) showed quantitative conversion to *cis*-[Fe(DMeOPrPE)$_2$(N$_2$H$_4$)]$^{2+}$. The product was not isolated from this route.

Synthesis of *cis*-Fe(DMeOPrPE)$_2$(CO$_3$). Solid $NaBPh_4$ (2 eq.) was added to a stirring solution of *trans*-Fe(DMeOPrPE)$_2$Cl$_2$ in THF. Immediately an excess of lithium carbonate was added. The reaction was allowed to stir for 24 hrs after which time the solution was bright red in color. The solution was filtered through Celite and the solvent was removed in vacuo. The product was isolated as a red powder by triturating with hexane. $^{31}P\{^{1}H\}$ NMR (acetone-d_6): δ 77.9 (t, $^{2}J_{P\text{-}P}$ = 38 Hz), δ 67.8 (t, $^{2}J_{P\text{-}P}$ = 38 Hz). $^{13}C\{^{1}H\}$ NMR (acetone-d_6): δ 158.4 (s).

Synthesis of *cis*-[Fe(DMeOPrPE)$_2$(O$_2$CCH$_3$)][BPh$_4$]. Solid $NaBPh_4$ (2 eq.) was added to a stirring solution of *trans*-Fe(DMeOPrPE)$_2$Cl$_2$ in THF. Immediately lithium acetate was added. The reaction was allowed to stir for 24 hrs after which time the solution was bright purple in color. The solution was filtered through Celite and the

solvent was removed in vacuo. The product was isolated as a purple powder by triturating with hexane. $^{31}P\{^{1}H\}$ NMR (acetone-d_6): δ 77.4 (t, $^{2}J_{P\text{-}P}$ = 38 Hz), δ 69.0 (t, $^{2}J_{P\text{-}P}$ = 38 Hz). $^{13}C\{^{1}H\}$ NMR (acetone-d_6): δ 183.9 (s).

Synthesis of *cis*-[Fe(DMeOPrPE)$_2$(C$_4$H$_4$N$_2$)][2BPh$_4$]. A THF solution of pyridazine (1 eq) was added to a stirring solution of *trans*-Fe(DMeOPrPE)$_2$Cl$_2$ and NaBPh$_4$. An immediate red color was observed. The solution was stirred for 2 hrs. and the product was precipitated as a red powder by addition of hexane. $^{31}P\{^{1}H\}$ NMR (acetone-d_6): δ 77.4 (t, $^{2}J_{P\text{-}P}$ = 38 Hz), δ 66.2 (t, $^{2}J_{P\text{-}P}$ = 38 Hz). ^{1}H NMR (acetone-d_6): δ 9.2 (t, $^{1}J_{H\text{-}H}$ = 3 Hz), δ 7.7 (t, $^{1}J_{H\text{-}H}$ = 3 Hz).

4.3 Results and Discussion

4.3.1 Synthesis of cis-[Fe(DMeOPrPE)$_2$(η^2-N$_2$H$_4$)]$^{2+}$

Several hydrazine complexes containing various transition metals have previously been synthesized,[23] yet there are relatively few examples containing iron, with all of these examples displaying an end-on (η^1) hydrazine coordination mode.[24-32] Here we describe the discovery of a new coordination mode of hydrazine to iron.

The synthesis of *cis*-[Fe(DMeOPrPE)$_2$(η^2-N$_2$H$_4$)][2BPh$_4$] (**I**) proceeded smoothly from the reaction of *trans*-FeCl$_2$(DMeOPrPE)$_2$ with 1 equivalent of hydrazine in the presence of a chloride abstractor (eq. 1). The complex was isolated by removal of the solvent *in vacuo* and trituration of the resulting oil with diethyl ether to yield **I** as an orange powder.

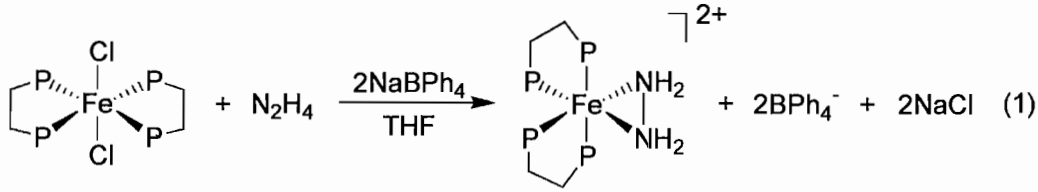

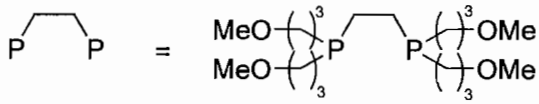

As shown in Figure 1, the room temperature $^{31}P\{^{1}H\}$ NMR spectrum of **I** exhibits two triplets at 75.9 and 62.5 ppm, with $^{2}J_{P\text{-}P} = 36$ Hz. These data are indicative of a *cis* arrangement of the bidentate phosphine ligands. The ^{1}H NMR spectrum reveals the presence of two broad singlets at 4.8 and 3.8 ppm, which are assigned to the hydrazine protons (Fig. 1). There are two proton resonances due to the idealized C_2 symmetry of the molecule imparted by the bidentate phosphine ligands.

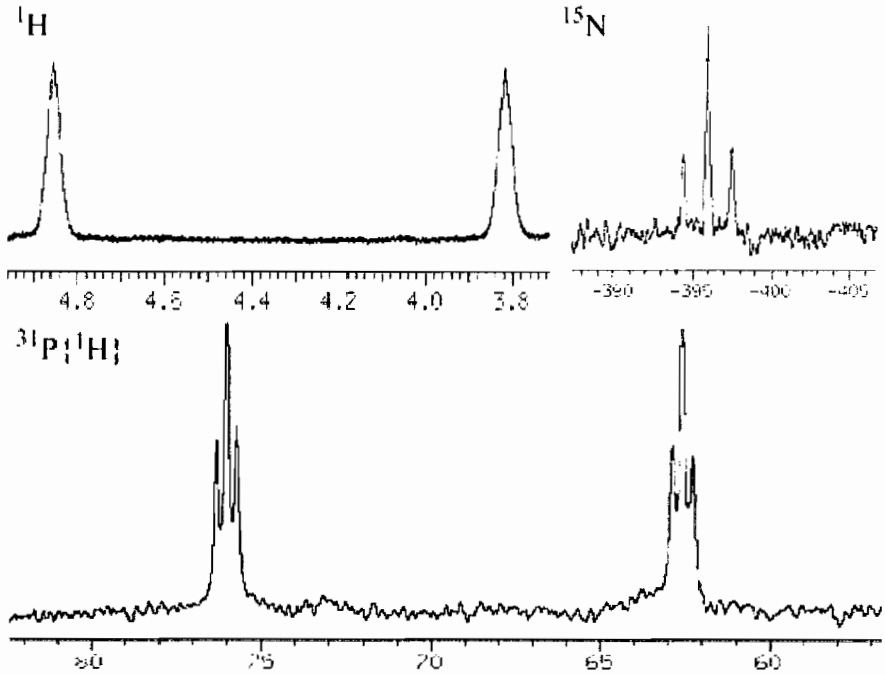

Figure 1. NMR spectra of *cis*-$[Fe(DMeOPrPE)_2(\eta^2\text{-}N_2H_4)]^{2+}$ (**I**). ^{1}H (top left), ^{15}N (top right), $^{31}P\{^{1}H\}$ (bottom).

To confirm the η^2 coordination geometry of the hydrazine the ^{15}N isotopolog of **I** was synthesized. The ^{15}N NMR spectrum showed a single triplet resonance at -395.5 ppm ($^1J_{N\text{-}H}$ = 77 Hz); turning on the ^1H decoupler caused the resonance to become a singlet, confirming equivalent nitrogen atoms each bound to two protons (Figure 1).[33-34] IR spectroscopy showed the presence of N-H stretches at 3313, 3227, 3117, and 2932 cm^{-1} (see Appendix E).

To investigate the solid-state structure, red-orange crystals of **I** were grown by layering a THF solution with hexane and analyzed by X-ray diffraction. The molecular structure of **I** (Fig. 2) shows the η^2 coordination geometry of hydrazine to the iron center.[35-37] The N-N bond distance of 1.442 Å agrees with previous η^2 hydrazine complexes and is consistent with an N-N single bond.[38]

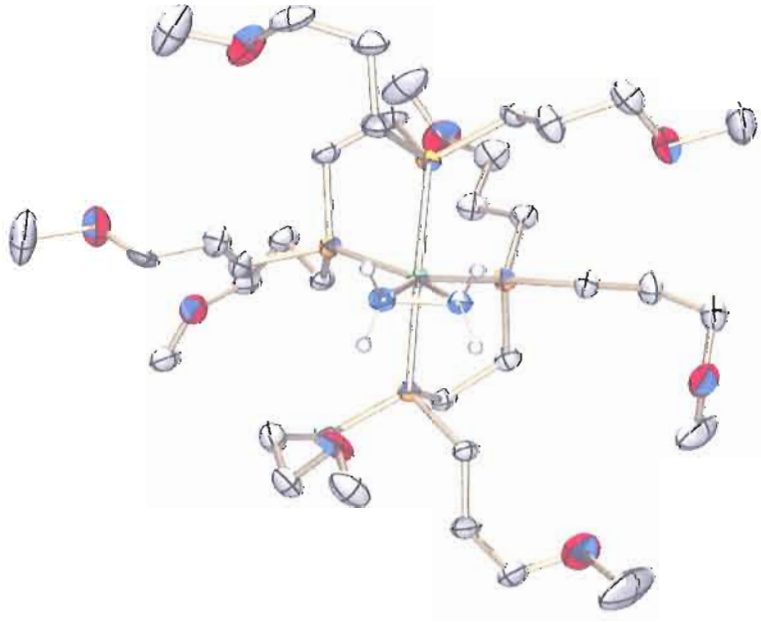

Figure 2. Molecular structure of *cis*-[Fe(DMeOPrPE)$_2$(η^2-N_2H_4)][BPh_4]$_2$ (**I**). The tetraphenylborate anions and hydrogen atoms of the phosphine ligands have been omitted for clarity. Selected bond distances (Å) and angles (°): N1-N2 1.442(3), Fe-N1 1.993(2), Fe-N2 2.006(2), Fe-P1 2.2315(8), Fe-P2 2.2716(8), Fe-P3 2.2769(8), Fe-P4 2.2324(8), N1-N2-Fe 68.37(14), N2-N1-Fe 69.36(14), N1-Fe-N2 42.28(10), N1-Fe-P4 109.49(8), N2-Fe-P1 105.23(7).

This particular coordination geometry of hydrazine may have significance for the mechanism of nitrogenase. Previously described iron hydrazine complexes have all shown terminal or bridging end-on (η^1) coordination modes; to our knowledge **I** is the first example of η^2 hydrazine coordination to iron. As previously mentioned, a hydrazine intermediate was recently trapped during nitrogenase turnover. ^{15}N ENDOR spectroscopy of this intermediate revealed the presence of a single type of ^{15}N nucleus, which is consistent with a symmetric coordination mode of the hydrazine.[39,40] This symmetric coordination mode could either be a bridging species (μ) or a mononuclear bidentate species (η^2).

While there are examples of hydrazine bridging two iron centers, until now there has been no evidence for η^2 hydrazine coordination to iron. Complex **I** suggests that the trapped hydrazine intermediate in nitrogenase could have an η^2 coordination mode. Therefore, both binuclear and mononuclear mechanisms of nitrogen fixation should be considered when formulating the mechanism of N_2 reduction in nitrogenase enzymes. After this novel iron hydrazine complex had been synthesized and fully characterized the acid base reactivity of the complex was explored.

4.3.2 Protonation of cis-[Fe(DMeOPrPE)$_2$(η^2-N$_2$H$_4$)]$^{2+}$

Initial reactivity studies were undertaken to examine the competence of **I** in producing hydrazine and/or ammonia (eq. 2). The addition of excess 1M triflic acid to a Et_2O/THF solution of **I** resulted in the formation of 21% NH_4^+ and 64% $N_2H_5^+$ (per mole Fe).[31-32]

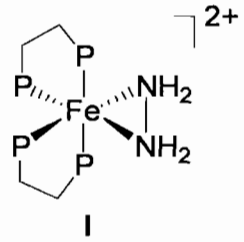

I

$$\xrightarrow[THF/Et_2O]{\text{xs TfOH}} \quad NH_4^+ + N_2H_5^+ \qquad (2)$$

Because no electron equivalents are present, the formation of ammonia must be the result of the disproportionation of hydrazine (eq 3) (N_2 gas was detected by mass spectrometry). The disproportionation of hydrazine in the presence of transition metals has been previously observed.[41-43]

$$3N_2H_4 \longrightarrow 4NH_3 + N_2 \qquad (3)$$

Because addition of acid to complex **I** results in the formation of ammonia, the η^2 hydrazine complex could potentially be an intermediate during the protonation reaction of $Fe(DMeOPrPE)_2N_2$ to produce ammonia as described in chapter III. Complex **I** could result from addition of $2e^-$ and $2H^+$ to an iron(II) diazene species.

4.3.3 Deprotonation of cis-[Fe(DMeOPrPE)$_2$(η^2-N$_2$H$_4$)]$^{2+}$

The deprotonation of *cis*-$[Fe(DMeOPrPE)_2(N_2H_4)]^{2+}$ was next explored. Synthesis of *cis*-$Fe(DMeOPrPE)_2(N_2H_2)$ (**III**) was achieved by the addition of three equivalents of K^{t}BuO to a THF solution of *cis*-$[Fe(DMeOPrPE)_2(N_2H_4)]^{2+}$ (**I**) (Scheme 1). The reaction was complete within minutes as evidenced by NMR spectroscopy and a color change from orange to yellow. An analogous complex with DMPE ligands has also recently been synthesized.[44]

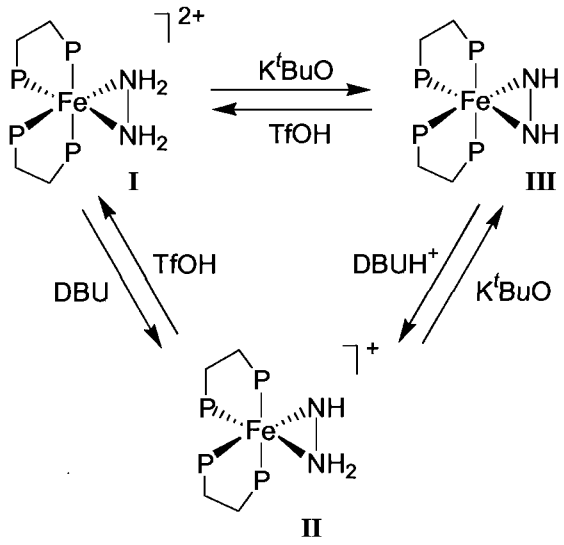

Scheme 1. Synthetic interconversion of iron hydrazine, hydrazido(1-), and diazene complexes.

The $^{31}P\{^{1}H\}$ NMR spectrum of **III** shows two triplet resonances at 75.8 and 71.2 ppm ($^{2}J_{PP}$ = 38 Hz) (Fig. 3). The two triplets are characteristic of two bidentate phosphine ligands and two equivalent *cis* ligands, suggesting an η^2 coordination mode of the diazene ligand.[10,45] The N-H protons of **III** were obscured by the DMeOPrPE resonances in the ^{1}H NMR spectrum, but were assigned as a broad singlet at 2.1 ppm using a $^{1}H-^{15}N$ HMQC experiment. In order to confirm the coordination geometry of the diazene moiety, the ^{15}N isotopologue was synthesized. The $^{15}N\{^{1}H\}$ NMR spectrum revealed a single resonance at -315.2 ppm, consistent with a symmetric coordination mode (Fig. 3). Upon turning the proton decoupler off, the ^{15}N resonance split into a doublet ($^{1}J_{N-H}$ = 52 Hz), confirming a single proton bound to each nitrogen atom. The ^{15}N resonance of **III** is ~80 ppm upfield from the resonance in the corresponding hydrazine complex (**I**).

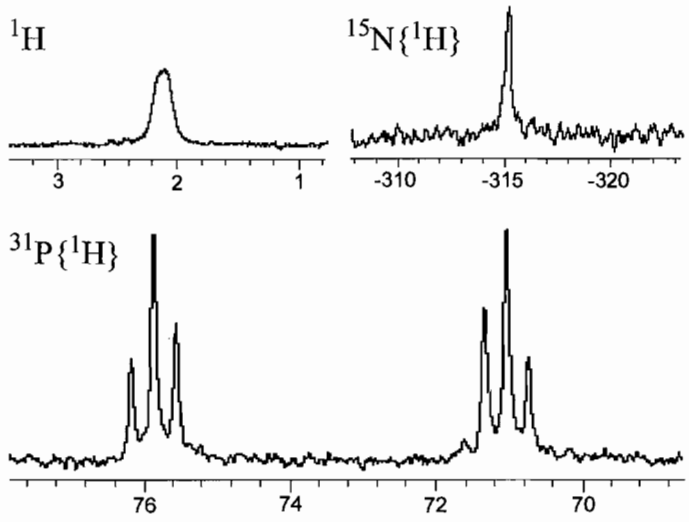

Figure 3. NMR spectra in THF-d_8 at 298K for *cis*-Fe(DMeOPrPE)$_2$(N_2H_2).

The deprotonation reaction **I** → **III** represents the microscopic reverse of the actual reaction that is proposed to take place in the reduction of N_2 to NH_3 (Scheme 2, pg. 103). The protonation of **III** to regenerate **I** was therefore investigated. The reprotonation could be achieved by addition of 2 equivalents of 1M trifluoromethanesulfonic acid (TfOH), as indicated by a color change from yellow to orange and by $^{31}P\{^{1}H\}$ and ^{15}N NMR spectroscopy.

Complex **III** can also be generated via an alternative route (eq. 4). Addition of N_2H_4 to a THF/Et_2O solution of Fe(DMeOPrPE)$_2N_2$ resulted in the formation of **III** and *cis*-Fe(DMeOPrPE)$_2$($H)_2$. Similar reactivity was also observed with the analogous Fe(DMPE)$_2$ scaffold.[46] The mechanism of this transformation is unclear; however, it likely involves substitution of hydrazine for dinitrogen followed by dehydrogenation of the hydrazine to form **III** and H_2. The H_2 then reacts with remaining Fe(DMeOPrPE)$_2N_2$ to form *cis*-Fe(DMeOPrPE)$_2$($H)_2$ (see Chapter III for details).

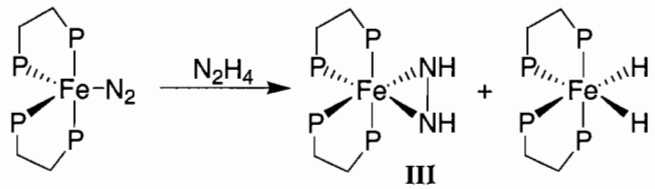

III (4)

The iron(II) hydrazido(1-) complex *cis*-$[Fe(DMeOPrPE)_2(N_2H_3)]^+$ (**II**), which is the intermediate species between complexes **I** and **III**, could also be synthesized from **I** via a deprotonation reaction using a slightly weaker base (Scheme 1). Thus, addition of two equivalents of DBU (DBU = 1,8-diazabicyclo{5.4.0}undec-7-ene) to **I** resulted in the disappearance of the two resonances of **I** and the appearance of four broad resonances in the $^{31}P\{^1H\}$ NMR spectrum. The broadness of the spectrum was not surprising as the hydrazido protons of **II** are likely undergoing rapid intramolecular exchange. Upon cooling to 193K, two overlapping ABMX splitting patterns are observed in the $^{31}P\{^1H\}$ spectrum (Fig. 4). The four-spin system is consistent with two inequivalent cis ligands. The two sets of ABMX patterns arise from two isomers frozen out at low temperatures, where the lone pair on the deprotonated nitrogen atom is either pointing parallel or perpendicular to the ethane bridges of the DMeOPrPE ligands (Fig. 5).

The ^{15}N isotopologue was generated to confirm the coordination mode and protonation state of the N_2H_3 moiety. The $^{15}N\{^1H\}$ NMR spectrum of complex **II** at room temperature shows a single broad resonance centered at -375 ppm. Upon cooling the sample to 193K, the $^{15}N\{^1H\}$ spectrum showed three resonances (Fig. 4). The resonances at -367.6 and -369.9 ppm are assigned as the two isomers of the deprotonated

nitrogen atom (N_α). The -NH_2 nitrogen atoms (N_β) of the two isomers overlap and are observed as a single resonance at -377.4 ppm. The ^{15}N NMR spectrum shows that the -NH (N_α) resonances are split into doublets ($^1J_{NH}$ = 50 Hz) and the -NH_2 (N_β) resonance is split into a triplet ($^1J_{NH}$ = 80 Hz), confirming the η^2 coordination geometry of the hydrazido(1-) ligand.

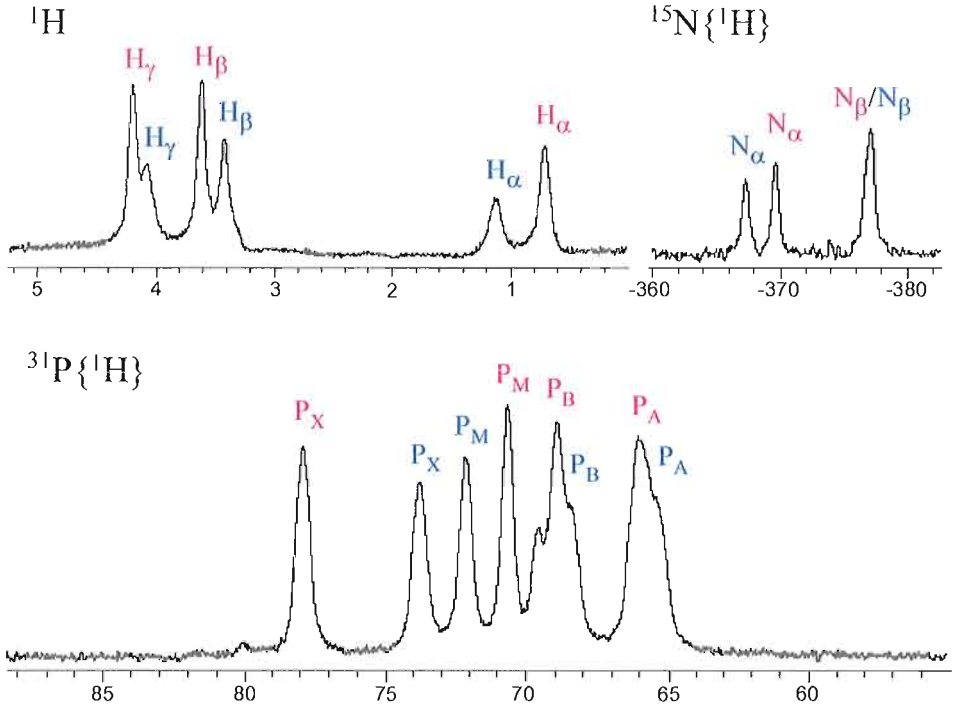

Figure 4. NMR spectra in THF-d_8 at 193K for *cis*-[Fe(DMeOPrPE)$_2$(N_2H_3)][BPh_4]. The peak labels correspond to the atomic labels given in Fig. 3. The spectrum labelled ^1H represents the ^1H-^{15}N HMQC (^{15}N decoupled) experiment. The red and blue labels distinguish between the two isomers.

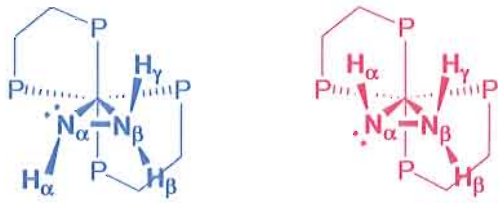

Figure 5. Isomers present at 193K for *cis*-[Fe(DMeOPrPE)$_2$(N_2H_3)][BPh_4]. The methoxypropyl groups have been omitted for clarity.

The assignment of the hydrazido protons of **II** in the ^{1}H NMR spectrum was ambiguous, as the resonances were obscured by the DMeOPrPE resonances. However, a ^{1}H-^{15}N HMQC experiment was able to locate the hydrazido protons. The ^{1}H HMQC (^{15}N decoupled) spectrum revealed six resonances (Fig. 4). Again this is explained as two isomers with three inequivalent protons each (Fig. 5). The hydrazido proton (H_{α}) resonance is upfield from the hydrazine proton (H_{β} & $H\gamma$) resonances as expected and the three proton resonances for each isomer are present in a 1:1:1 ratio. Although complex **II** could not be isolated, the combination of ^{31}P, ^{15}N, and ^{1}H-^{15}N HMQC NMR data strongly suggests that complex **II** contains an η^2-hydrazido(1-) ligand.

To probe the ability of these three species to interconvert, a series of acid/base experiments was performed and monitored by $^{31}P\{^{1}H\}$ and ^{15}N NMR spectroscopy. As with complex **III**, complex **II** was reprotonated with 1M TfOH to yield **I**. Complex **II** was also further deprotonated by addition of K^{t}BuO, yielding complex **III**. The last reaction to complete Scheme 1 involves reprotonating complex **III** in a stepwise manner, first to complex **II**, then to complex **I**. This was achieved in a two-step reaction, as monitored by $^{31}P\{^{1}H\}$ NMR spectroscopy. First, [HDBU][OTf] was used as the acid to convert **III** to **II**. Then, as before, complex **II** could be converted back to complex **I** by addition of 1M triflic acid.

4.3.4 Importance of an Iron(II) Diazene Complex

From these complexes we began to formulate a mechanism that is shown in Scheme 2. Four of the six species shown in Scheme 2 have now been synthesized and fully characterized, and protonation of the *cis*-N_2H_4 complex results in ammonia

formation. The last key intermediate that has yet to be synthesized is the iron(II) diazene complex (top right, Scheme 2). As shown in chapter III, each iron center donates only two electrons to the reduction process, thus the addition of two protons to $Fe(DMeOPrPE)_2N_2$ to produce the iron(II) diazene complex likely represents the first step in the mechanism. From the iron(II) diazene complex a couple of reaction pathways can be envisioned that could lead to ammonia formation.

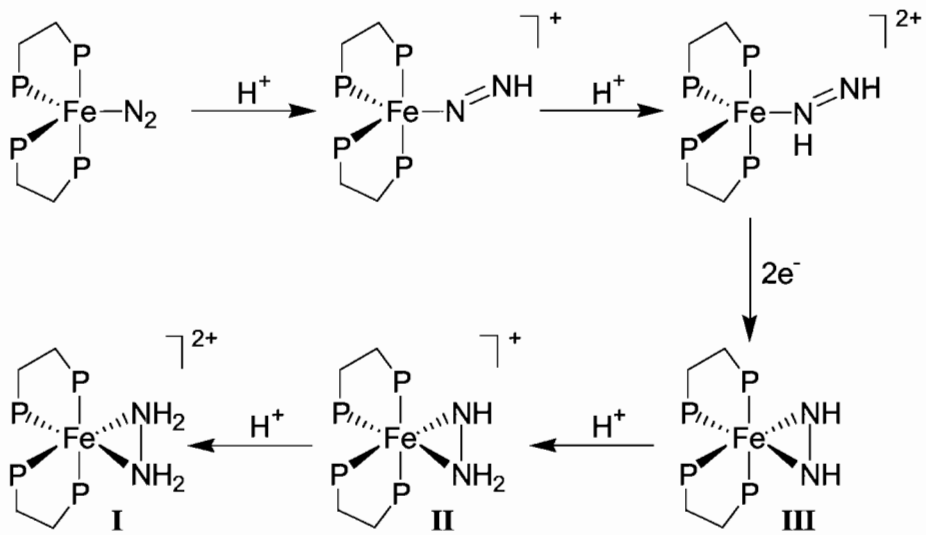

Scheme 2. Proposed mechanism of N_2 reduction following the protonation of $Fe(DMeOPrPE)_2N_2$.

The first pathway, as presented in the proposed mechanism above (Scheme 2), involves the outer-sphere reduction of the iron(II) diazene complex by a second equivalent of $Fe(DMeOPrPE)_2N_2$. According to DFT calculations this pathway seems favorable (see Appendix B) however it is unclear how much of the reducing agent, $Fe(DMeOPrPE)_2N_2$, remains intact at this point in the mechanism although it is likely to be quite small as protonation of $Fe(DMeOPrPE)_2N_2$ at the iron center to produce *trans*-$[Fe(DMeOPrPE)_2(N_2)H]^+$ is calculated to be favorable by over 60 kcal/mol.

An alternative reaction pathway from the iron(II) diazene complex could involve dissociation of the diazene molecule followed by disproportionation of diazene into ammonia and hydrazine. Diazene is a very reactive molecule and quickly decomposes and disproportionates in solution (eqs. 5 and 6).[47,48] The disproportionation of diazene could account for the observed yields of ammonia and hydrazine (ammonia would have to result from the further disproportionation of hydrazine). This pathway was tested by attempting to trap any uncoordinated diazene in solution during the protonation reaction and will be discussed in section 4.3.7.

$$N_2H_2 \longrightarrow N_2 + H_2 \quad (5)$$

$$2\,N_2H_2 \longrightarrow N_2H_4 + N_2 \quad (6)$$

As the above discussion demonstrates, synthesis and characterization of an iron(II) diazene complex is crucial in understanding the mechanism of ammonia formation. In order for ammonia to be produced the coordinated dinitrogen molecule must at least be reduced and protonated to form diazene. Once diazene is formed the ammonia and hydrazine can be formed through a series of disproportionation reactions or by further reduction by a second equivalent of $Fe(DMeOPrPE)_2N_2$. The synthesis of an iron(II) diazene complex was attempted by two separate routes: oxidation of **I** or **III**, and the direct coordination of generated diazene gas.

4.3.5 Attempted Synthesis of an Iron(II) Diazene Complex via Oxidation

Iron complexes containing coordinated diazene are very rare, with the iron(0) diazene complex, *cis*-$Fe(DMeOPrPE)_2(N_2H_2)$, being one of the few examples in the literature. The primary synthetic route to diazene complexes is oxidation of the

corresponding hydrazine complex using lead tetraacetate.[49,50] This synthetic route was attempted using one equivalent of $Pb(OAc)_4$ added to a THF solution of *cis*-$[Fe(DMeOPrPE)_2(N_2H_4)]^{2+}$ (eq. 7). The solution immediately changed color from orange to purple. The resulting purple solution showed the presence of two triplets at 78.4 and 69.8 ppm in the ^{31}P NMR spectrum (eq. 8). Unfortunately, control experiments using other acetate sources and the *cis*-N_2H_4 complex revealed that this purple *cis* product was not a diazene complex but rather a *cis* acetate complex (eq. 9). Because the acetate anions of the $Pb(OAc)_4$ were shown to displace N_2H_4, and no other Pb(IV) sources are commercially available, an alternative oxidizing reagent was sought.

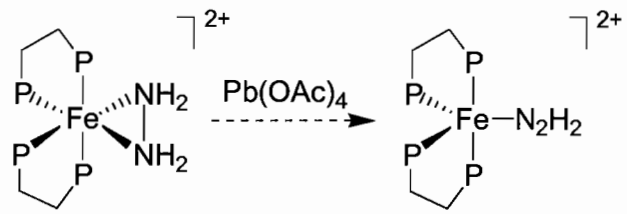

(7)

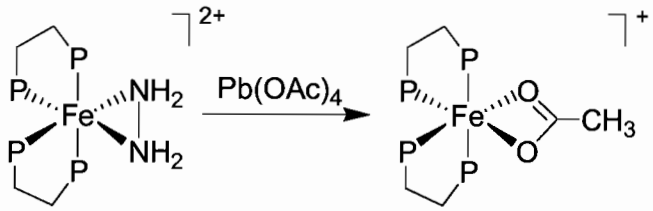

(8)

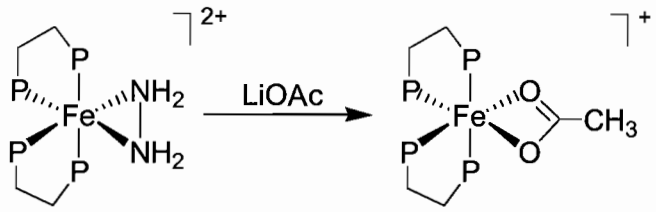

(9)

In research by Collman and coworkers a diazene complex was generated by addition of either *tert*-butyl hydroperoxide or ferrocenium hexafluorophosphate.[51] Two equivalents of ferrocenium hexafluorophosphate were added to a solution of the iron(0) diazene complex *cis*-Fe(DMeOPrPE)$_2$(N_2H_2). After ten minutes the $^{31}P\{^1H\}$ NMR spectrum showed the disappearance of the starting material resonances and the appearance of a new singlet resonance at 76.8 ppm (Fig. 6). This provides encouraging initial results, but the identity of this new resonance has yet to be determined. Further experiments need to be done with both of these reagents to determine if they do indeed selectively oxidize the hydrazine to diazene.

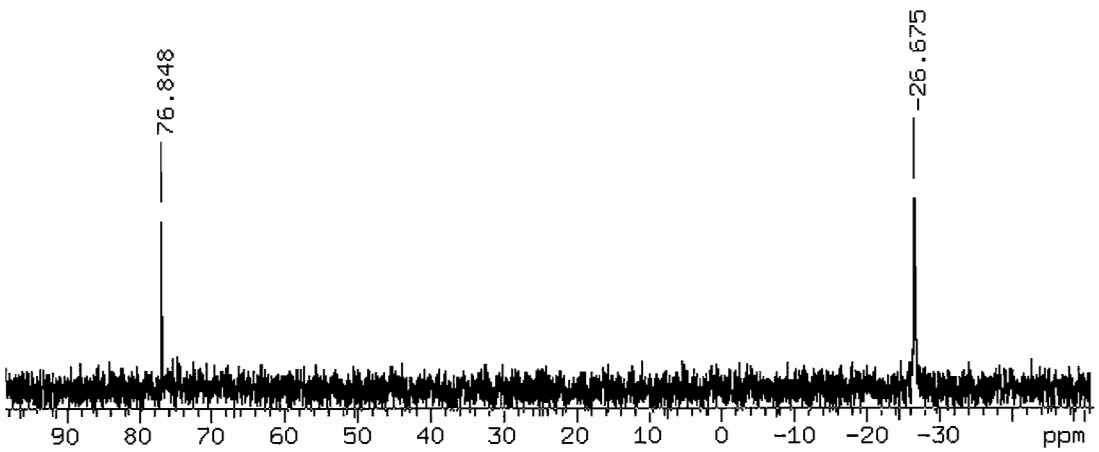

Figure 6. $^{31}P\{^1H\}$ NMR spectrum of the reaction of *cis*-Fe(DMeOPrPE)$_2$(N_2H_2) with [$FeCp_2$][PF_6]. The resonance at -26.7 represents uncoordinated DMeOPrPE.

4.3.6 Attempted Synthesis of an Iron(II) Diazene Complex via Direct Coordination

The oxidation of coordinated hydrazine is the primary route to diazene complexes, however Sellman and coworkers were able to show that diazene gas could be

generated in situ and trapped via coordination to iron.[52] Several reagents are known to generate diazene gas and a few of these reagents were tried.

Potassium azodicarboxylate was synthesized by hydrolysis of azodicarbonamide. This reagents decomposes under acidic aqueous conditions yielding diazene and carbon dioxide gases (eq. 10).[48] As was shown in the previous section, this iron phosphine scaffold readily reacts with acetate anions thus this reagent could not be used in situ. Instead the diazene gas was generated under acidic conditions in one flask and then immediately transferred into the flask containing the iron phosphine complex with an argon purge. An unsaturated iron phosphine complex was generated in the second flask by reaction of *trans*-$Fe(DMeOPrPE)_2Cl_2$ with $TlPF_6$ (eq. 11). After several minutes of purging, the solution changed from a dark brown color to a bright red solution and inspection of the $^{31}P\{^1H\}$ NMR spectrum revealed two triplet resonances at 77.9 and 67.8 ppm. However, it was shown by control reactions that this red *cis* species represented the iron carbonate complex (eq. 12). The source of carbonate in the diazene reaction is likely carbon dioxide reacting with trace amounts of water present in the THF. Because of the numerous sources of potential ligands in this reagent, potassium azodicarboxylate was abandoned as a diazene source.

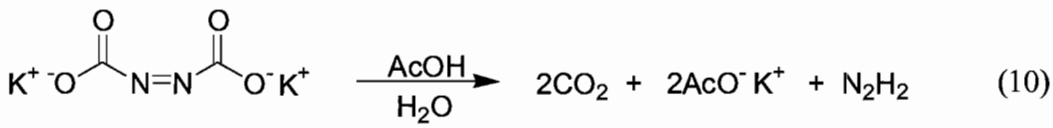

(10)

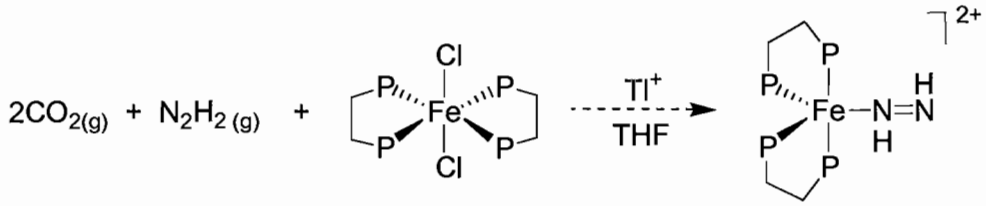

(11)

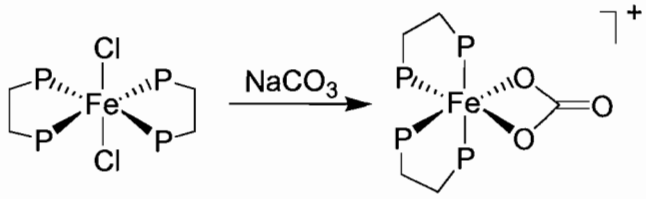

(12)

The next reagent used as a diazene source was benzenesulfonyl hydrazide. This reagent undergoes thermolysis at 115 °C to release diazene gas (eq. 13).[48] Because of the high temperatures needed, this reagent was again used in a separate flask and the evolved diazene gas was transferred to the iron phosphine solution by an argon purge. This transfer method was found to be quite inefficient and the only complex observed was *cis*-$[Fe(DMeOPrPE)_2(N_2H_4)]^{2+}$, which likely formed from the disproportionation of diazene to hydrazine as it traveled between the two flasks.

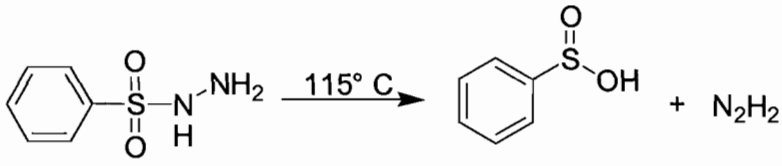

(13)

Based on the failed attempts described above another reagent was sought that could be used in situ and that did not produce any side products that could coordinate to the iron. Surveying the literature revealed a promising reagent synthesized by Corey.[53,54] The reagent is an adduct of diazene and anthracene that evolves diazene at

relatively mild temperatures (40-80°C) (eq. 14). This reagent was prepared by reacting diethylazodicarboxylate with anthracene followed by hydrolysis to give the diazene anthracene adduct as a white powder.

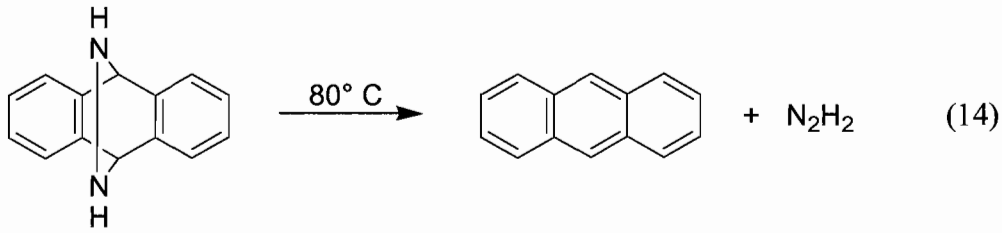

(14)

An excess of this reagent was added to a THF solution of *trans*-$Fe(DMeOPrPE)_2Cl_2$ and $TlPF_6$ in a J. Young NMR tube. The NMR tube was then warmed using a water bath and the reaction was monitored by ^{31}P NMR spectroscopy (Fig. 7). The $^{31}P\{^1H\}$ NMR spectrum revealed a mixture of products, with the primary product being the *cis*-N_2H_4 complex, *cis*-$[Fe(DMeOPrPE)_2(N_2H_4)]^{2+}$. It is encouraging to see the *cis*-N_2H_4 complex in the ^{31}P NMR spectrum as this means that the reagent is successfully generating diazene gas, which then disproportionates into hydrazine and forms the very stable *cis*-N_2H_4 complex. The resonance at 76.9 ppm closely matches the resonance observed in the reaction of the *cis*-N_2H_4 complex with $[FeCp_2][PF_6]$ and may represent the desired iron(II) diazene complex. However further characterization of this species is necessary before any conclusions can be drawn. One observation that can be made however is that because diazene is so unstable and because the hydrazine complex is quite stable it is unlikely that this route will ever be successful in synthesizing the iron(II) diazene complex in pure form. Because of this reason the oxidation of the

hydrazine complex is likely the best route to successfully synthesize an iron(II) diazene complex and should be the focus of further studies.

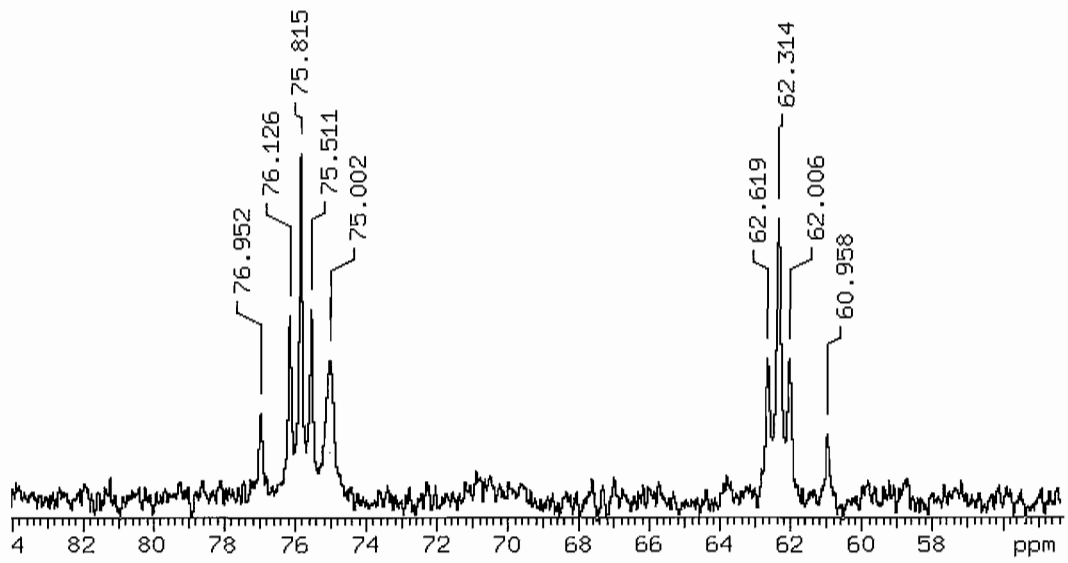

Figure 7. $^{31}P\{^{1}H\}$ NMR spectrum of the reaction of $Fe(DMeOPrPE)_2Cl_2$ with $TlPF_6$ in the presence of the anthracene-diazene adduct.

4.3.7 Protonation of $Fe(DMeOPrPE)_2N_2$ in the Presence of a Diazene Trap

The above studies suggest that an iron(II) diazene complex may not be stable and if such a complex were formed during the mechanism the complex could quickly dissociate. Once free in solution the diazene could disproportionate into ammonia and hydrazine. To test this hypothesis we set out to trap any uncoordinated diazene that was present in solution before it had a chance to disproportionate (Scheme 3).

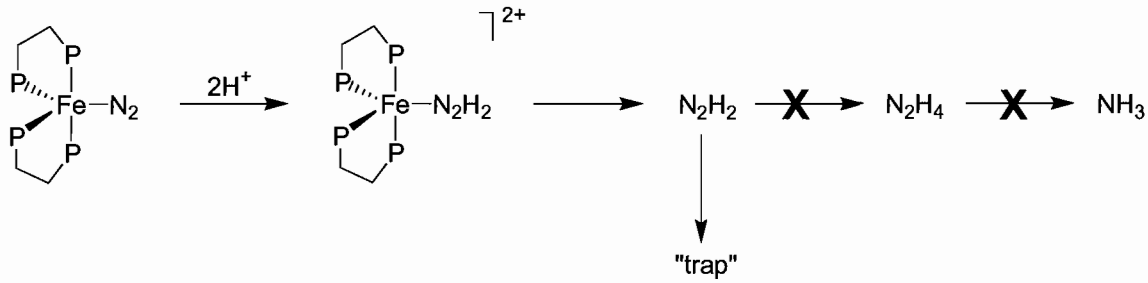

Scheme 3. Trapping of diazene produced from the dissociation of an iron(II) diazene complex produced from the protonation of $Fe(DMeOPrPE)_2N_2$.

If a diazene trapping reagent was present during the protonation reaction and the yields of ammonia and hydrazine were unchanged then the possibility of uncoordinated diazene disproportionation could be ruled out as the ammonia producing pathway. Because diazene is a well known hydrogenating reagent for carbon-carbon double and triple bonds[47,48] norbornene and diphenylacetylene were selected as diazene trapping reagents (eq. 15). These diazene traps were chosen as they were shown to be unreactive toward the iron(0) starting material.

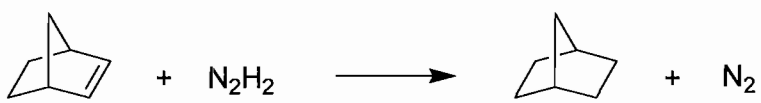

(15)

The protonation of $Fe(DMeOPrPE)_2N_2$ was performed in the presence of a 50-fold excess of the diazene trapping reagent in order to quickly trap the diazene before it could disproportionate. Control protonation reactions without the diazene traps present were also run in parallel. The ammonia yields were then determined using standard techniques and the results of these experiments are summarized in Table 1.

Table 1. Yields of NH_3 obtained from the protonation of $Fe(DMeOPrPE)_2N_2$ with or without a diazene trapping reagent present.

Control		Ph—≡—Ph
14	16	16

*values are % NH_3 based on Fe

From this preliminary data it can be seen that the diazene traps have no effect on the yields of ammonia, suggesting that diazene disproportionation is not responsible for ammonia production. Even if a 50-fold excess of the diazene trap is not enough to completely prevent the rapid disproportionation of diazene, some decrease in the yields of ammonia would be expected. One potential issue with these results that needs to be addressed is whether or not the strong acid (TfOH) used for the protonation is reacting with the alkene or alkyne and making them unreactive toward diazene.

4.3.8 Synthesis of Substituted Diazene (N_2R_2) Complexes

Because the synthesis of an iron diazene (N_2H_2) complex was not successful, coordination of a more stable diazene derivative was investigated. Azopropane was chosen because it is stable and can be synthesized using an established procedure. The first step in the synthesis of azopropane involved reacting propylamine with sulfuryl chloride to form *N,N*-dipropylsulfamide. The *N,N*-dipropylsulfamide was then reacted with sodium hydroxide and sodium hypochlorite to produce azopropane. Attempts to coordinate azopropane to iron by reacting azopropane with the *trans*-$Fe(DMeOPrPE)_2Cl_2$ in the presence of a chloride abstractor were unsuccessful. The reaction was monitored by ^{31}P NMR, however no evidence supporting coordination of

azopropane to iron was observed. One reason for the lack of reactivity could be that the propyl substituents provide enough steric bulk to prevent coordination to the iron center.

An alternative substituted diazene, pyridazine, was then selected as this molecule is slightly less sterically bulky and is also commercially available. Reaction of pyridazine with *trans*-$Fe(DMeOPrPE)_2Cl_2$ and a chloride abstractor resulted in an immediate red color (eq. 16).

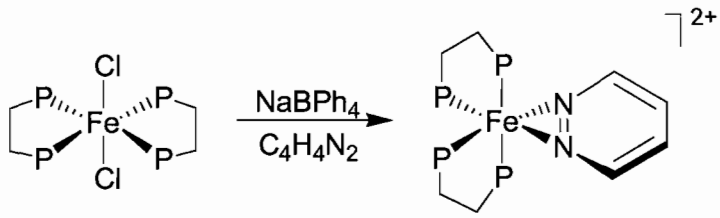

(16)

The ^{31}P NMR spectrum of the red solution showed clean conversion to a new *cis* species with triplets present at 77.4 ppm and 66.2 ppm (Fig. 8). This data suggests that the pyridazine is coordinated to the iron center in an η^2 geometry. The ^{1}H NMR spectrum was also obtained and clearly shows the presence of pyridazine protons, confirming that the pyridazine is coordinated to iron. This experiment proves that this particular iron phosphine scaffold can accommodate diazene ligands, at least in an η^2 geometry. One significant difference between pyridazine and the parent diazene molecule (N_2H_2) is that pyridazine presents a *cis* diazene moiety, while diazene is present in the *trans* form.

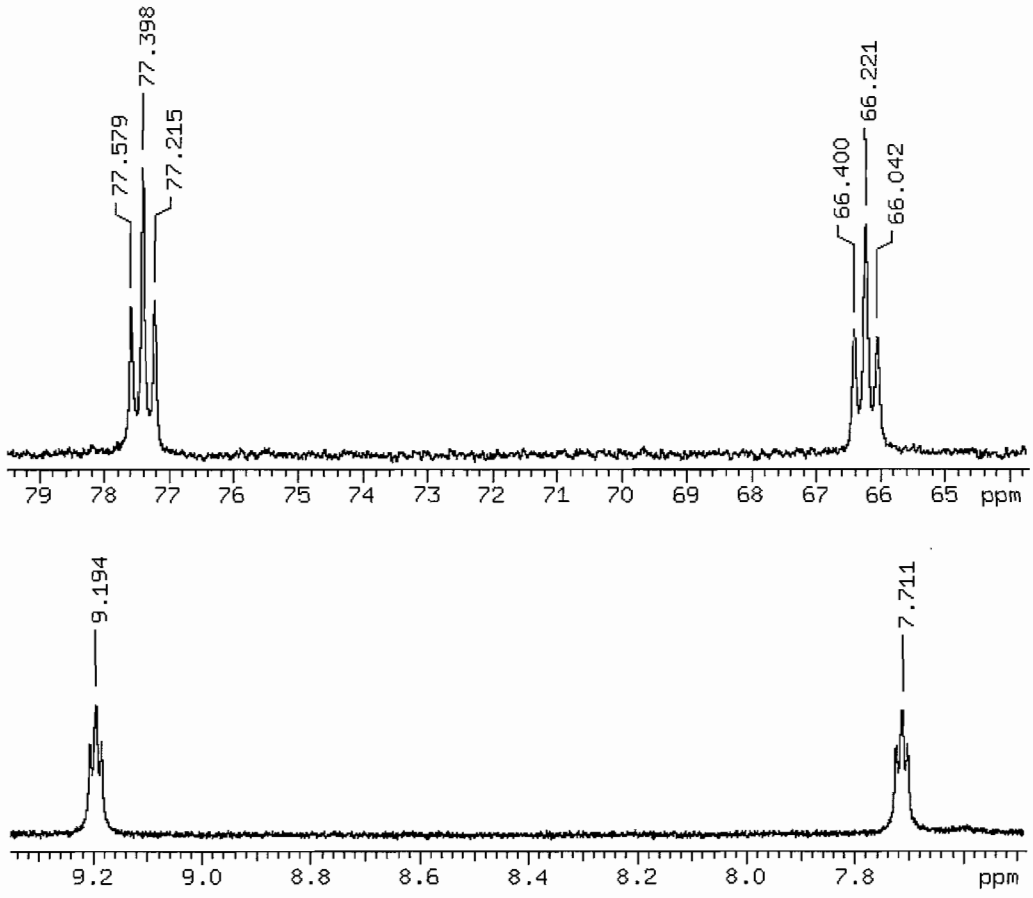

Figure 8. $^{31}P\{^{1}H\}$ (top) and ^{1}H (bottom) NMR spectra of *cis*-$[Fe(DMeOPrPE)_2(C_4H_4N_2)]^{2+}$ in acetone-d_6.

4.4 Conclusion

This chapter has described the synthesis and characterization of a series of iron complexes of hydrazine, hydrazido(1-), and diazene, as well as the attempted synthesis of an iron(II) diazene complex. The *cis* hydrazine complex was the first complex of iron displaying the η^2 coordination mode of hydrazine. Protonation of this complex resulted in the disproportionation of hydrazine to ammonia and N_2. The hydrazine, hydrazido(1-), and diazene complexes based on the $Fe(DMeOPrPE)_2$ scaffold were shown to interconvert in a series of protonation/deprotonation reactions.

From this data the mechanism shown in Scheme 2 (pg. 99) was proposed. Most of the complexes in the proposed scheme have been synthesized and characterized with the key exception being the iron(II) diazene complex (upper right complex, Scheme 2). Although this key intermediate has not yet been synthesized, the remaining synthetic routes have yielded promising preliminary results. DFT calculations of the proposed mechanism have been performed in collaboration with Dr. Robert Yelle and are presented in Appendix B.[55] These calculations show that the proposed mechanism shown in Scheme 4 is the most thermodynamically favorable of the three mechanisms tested thus far. This proposed mechanism is much different that the mechanism proposed for Mo and W systems[56,57] but agrees nicely with biochemical data for nitrogenase showing that the enzyme proceeds through diazene and hydrazine intermediates on the way to ammonia.[58]

4.5 Bridge

This chapter described the synthesis of several potential intermediates in the mechanism of dinitrogen reduction to ammonia using an iron phosphine scaffold. Based on these synthesized intermediates a mechanism was proposed for the reduction of N_2 to NH_3 for iron phosphine systems that is compatible with the proposed mechanism of biological N_2 reduction. Chapter V summarizes this dissertation and provides an outlook for the future of this project as well as the future of dinitrogen reduction using iron.

CHAPTER V

SUMMARY

The discovery of a process that converts atmospheric dinitrogen to ammonia has been one of the most important discoveries of the past century. The Haber-Bosch process, the industrial process responsible for this conversion, supplies a fixed source of nitrogen to roughly 50% of the world's crops. Unfortunately, the process requires high temperatures and extreme pressures and thus requires huge amounts of energy; as energy prices rise so to does the cost of producing ammonia.

Coordination chemists have long sought a low energy alternative to the Haber-Bosch process utilizing homogeneous transition metal catalysts. Recently, chemists have begun to focus on iron as a potential candidate to catalyze the reduction of dinitrogen to ammonia. This focus has been driven by biochemical studies on nitrogenase enzymes. Nitrogenase enzymes, nature's solution to nitrogen fixation, catalyze the reduction of dinitrogen and are capable of producing ammonia at biological temperatures and atmospheric pressures. Increasing biochemical evidence suggests that iron is responsible for dinitrogen coordination and reduction in these nitrogenase enzymes. Understanding the coordination chemistry of dinitrogen with iron should provide insights into how nitrogenase is able to convert atmospheric dinitrogen into ammonia at ambient temperature and pressure and could lead to the discovery of homogenous iron complexes that catalyze N_2 reduction.

This dissertation has focused on one particular system that is capable of producing ammonia directly from dinitrogen in the presence of a strong acid. This reduction occurs at room temperature and pressure; currently however the process is not catalytic and the yields of ammonia are low. In order to improve these yields, and ultimately achieve a catalytic cycle, knowledge of the mechanism is crucial. This dissertation described fundamental chemistry concerning the coordination of dinitrogen to iron and the reactivity of reduced dinitrogen intermediates. From this work a mechanism has been proposed that proceeds through diazene and hydrazine intermediates. This proposed mechanism shares many similarities with the proposed mechanism of nitrogenase and provides insights into how to further improve the yields of ammonia. Hopefully, continued work on this project will shed light on the mechanism of biological nitrogen fixation and eventually lead to an iron catalyst that can produce ammonia from atmospheric dinitrogen at room temperature and atmospheric pressure.

APPENDIX A

SYNTHESIS OF COMPLEXES FOR STUDY BY NUCLEAR RESONANCE VIBRATIONAL SPECTROSCOPY (NRVS)

A.1 Introduction

The active site of nitrogenase has been determined using x-ray crystallography;[1] however, even with such structural information the identity of the central atom of the FeMo cofactor as well as the mechanism of N_2 reduction remain a mystery. Preliminary spectroscopic evidence for the identity of the central atom of the FeMo cofactor has been acquired using ENDOR and ESEEM spectroscopy;[2] however, these data alone are not enough to confirm the identity of the mystery atom. New experimental techniques are needed for determining not only the identity of this central atom, but also for characterizing intermediates in the reduction of N_2 to ammonia.

Vibrational spectroscopy (i.e. infrared, Raman, etc.) is a powerful spectroscopic technique and can provide important structural information. The problem facing vibrational spectroscopy of biological systems is that these systems are so complex it is very difficult to obtain data solely for the active site. Another limiting factor for vibrational techniques is the selection rules that limit the observation of many important vibrations. A vibrational technique that is site-selective and not limited by selection rules would be a very powerful tool in the characterization of biological systems.

Nuclear resonance vibrational spectroscopy (NRVS) provides a solution to both of these problems.[3] NRVS is selective for all vibrations of Mössbauer-active nuclei, including ^{83}Kr, ^{119}Sn, ^{157}Eu, and ^{57}Fe. The ^{57}Fe isotope is the most commonly used nuclei as iron is present in numerous enzymes. In a NRVS experiment a synchrotron source provides an intense monochromatic x-ray beam. These x-rays excite the ^{57}Fe nuclei and a typical Mössbauer resonance is observed due to recoil-free absorption. On either side of the major Mössbauer peak are smaller peaks corresponding to nuclear transitions combined with vibrational modes. From these small peaks all vibrations associated with the iron nuclei can be observed.

NRVS has already been used to study nitrogenase;[4] however, because NRVS is in its infancy, data for comparison is limited. Therefore, the next step is to acquire the NRVS spectra of known molecules with similar properties to nitrogenase. This process has already begun with iron-sulfur model complexes.[5] Currently our complexes (*trans*-$[Fe(DMeOPrPE)_2(H_2)H]^+$, *trans*-$[Fe(DMeOPrPE)_2(N_2)H]^+$, and *cis*-$[Fe(DMeOPrPE)_2(N_2H_4)]^{2+}$) are being studied by NRVS. This data will hopefully provide insights into the mechanism of nitrogenase function. Specifically, determining the vibrational modes of iron coordinated to hydride, H_2, N_2, and N_2H_4 ligands would provide useful data to compare with trapped intermediates of N_2 reduction in nitrogenase.[6-8]

A.2 Experimental

Materials. All manipulations were carried out in a Vacuum Atmospheres Co. glove box (N_2 or Ar filled). HPLC grade THF, hexane, and diethyl ether (Burdick and

Jackson) were dried and deoxygenated by passing them through commercial columns of CuO, followed by alumina under an argon atmosphere. Toluene (Aldrich) was distilled under N_2 from CaH_2 and degassed via three freeze-pump-thaw cycles. Commercially available reagents were used as received. DMeOPrPE was synthesized as previously reported.[9] Elemental ^{57}Fe was supplied by Dr. Stephen Cramer. Deuterated toluene, D_2, $^{15}N_2$, and $^{15}N_2H_4(SO_4)$ were purchased from Cambridge Isotope Laboratories. Anhydrous $^{15}N_2H_4$ was prepared by extraction of $^{15}N_2H_4 \cdot SO_4$ with $NH_{3(l)}$ followed by removal of the ammonia.

Synthesis of $^{57}FeCl_2 \cdot 4H_2O$. ^{57}Fe (220 mg, 3.86 mmol) was stirred with concentrated HCl (20 mL) under argon for one week at room temperature and then filtered through Celite. The excess water and HCl were removed under reduced pressure until a pale blue-green solid remained. The resulting product was taken directly to the next step.

Synthesis of $^{57}Fe(DMeOPrPE)_2Cl_2$. DMeOPrPE (2.95 g, 7.72 mmol) and $^{57}FeCl_2 \cdot 4H_2O$ (0.772 g, 3.86 mmol) were dissolved in 20 mL of anhydrous toluene with stirring under an argon atmosphere at ambient temperature. The resulting green solution was allowed to rest and then carefully decanted into a clean flask, leaving a small amount of oily, red impurity in the original vessel. Approximately 15 mL of the toluene was removed under vacuum followed by addition of anhydrous *n*-hexane (50 mL). Vacuum was applied to remove some of the hexane and chill the mixture. A green crystalline product was obtained by filtration followed by hexane rinse and drying in vacuo. Yield 1.96 g, 57%. $^{31}P\{^1H\}$ NMR (toluene-d_8) at 213K: δ 57.3 (s). ^{31}P NMR (toluene-d_8) at 213K: δ 57.3 (s).

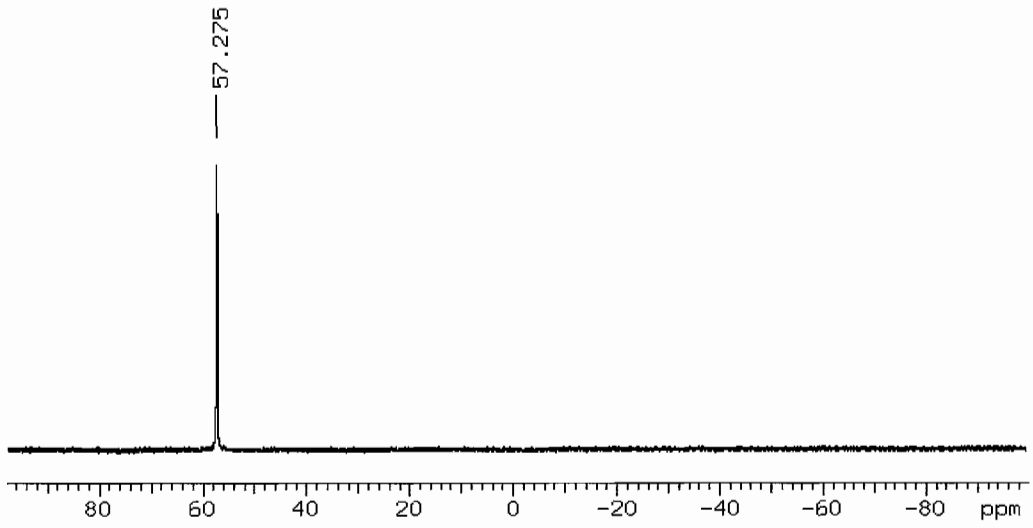

Figure A1. $^{31}P\{^{1}H\}$ NMR spectrum of $^{57}Fe(DMeOPrPE)_2Cl_2$ at -60°C.

Synthesis of *trans*-[^{57}Fe(DMeOPrPE)$_2$(H$_2$)H][BPh$_4$]. *trans*-$^{57}Fe(DMeOPrPE)_2Cl_2$ (0.146 g, 0.1635 mmol), $NaBPh_4$ (0.112 g, 0.327 mmol), and Proton Sponge (0.035 g, 0.1635 mmol) were combined as solids in a Fischer-Porter tube. THF (5 mL) and Et_2O (5 mL) were then added, and the resulting solution was immediately charged with 1 atm of H_2. The solution turned from green to orange to a faint yellow with the production of a white precipitate (NaCl) over the course of several hours. The reaction was allowed to stir for 48 hrs to ensure completion. The solution was then filtered through Celite under an argon atmosphere. The complex was precipitated as an oil by addition of hexane. The oil was redissolved in toluene, filtered through Celite, and again precipitated with hexane. The remaining oil was triturated with hexane to yield 0.18 g (96% yield) of a tan colored powder. $^{31}P\{^{1}H\}$ NMR (toluene-d_8): δ 88.1 (d, $^{1}J_{P\text{-}Fe}$ = 35 Hz). ^{1}H NMR (toluene-d_8) of the hydride region at 253K: δ -11.0 (s, br) and δ -15.1 (quintet, $^{2}J_{H\text{-}P}$ = 49 Hz).

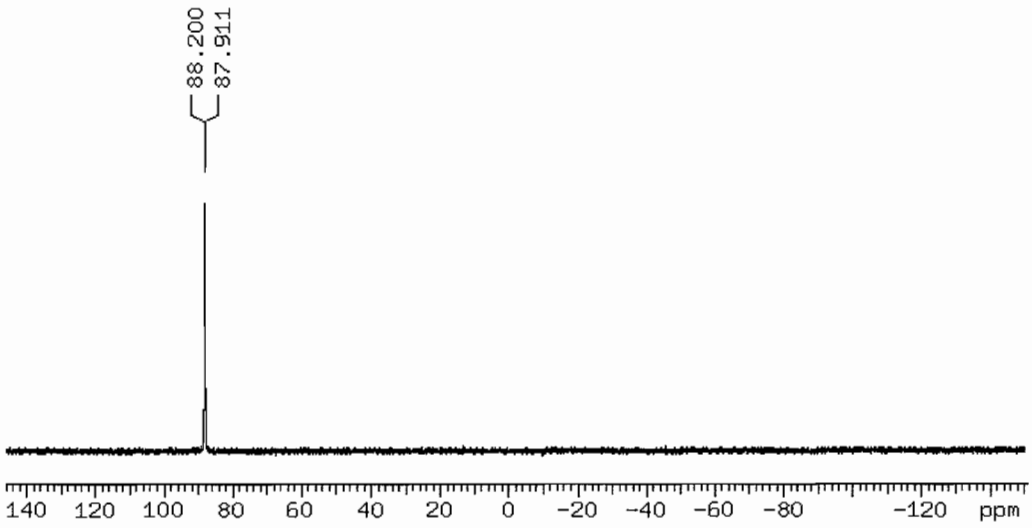

Figure A2. $^{31}P\{^{1}H\}$ NMR spectrum of *trans*-[^{57}Fe(DMeOPrPE)$_2$(H_2)H][BPh_4].

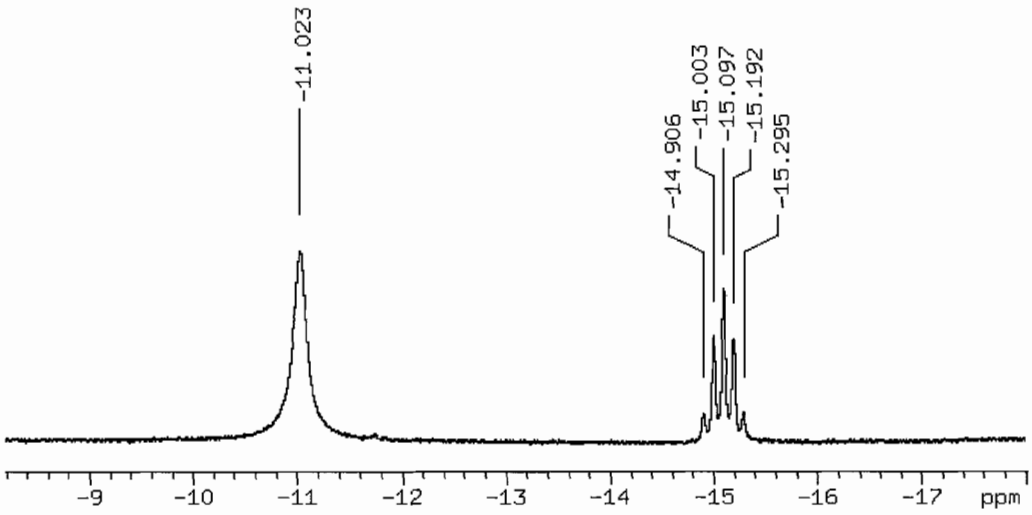

Figure A3. ^{1}H NMR spectrum of *trans*-[^{57}Fe(DMeOPrPE)$_2$(H_2)H][BPh_4].

Synthesis of *trans*-[^{57}Fe(DMeOPrPE)$_2$($^2H_2$)^{2}H][BPh_4]. The synthesis of this complex was identical to that described above except that D_2 was used in place of H_2. $^{31}P\{^{1}H\}$ NMR (toluene-d_8): δ 88.1 (d, $^{1}J_{P\text{-}Fe}$ = 35 Hz). ^{2}H NMR (THF) of the hydride region: δ -10.8 (s) and δ -15.1 (s, br).

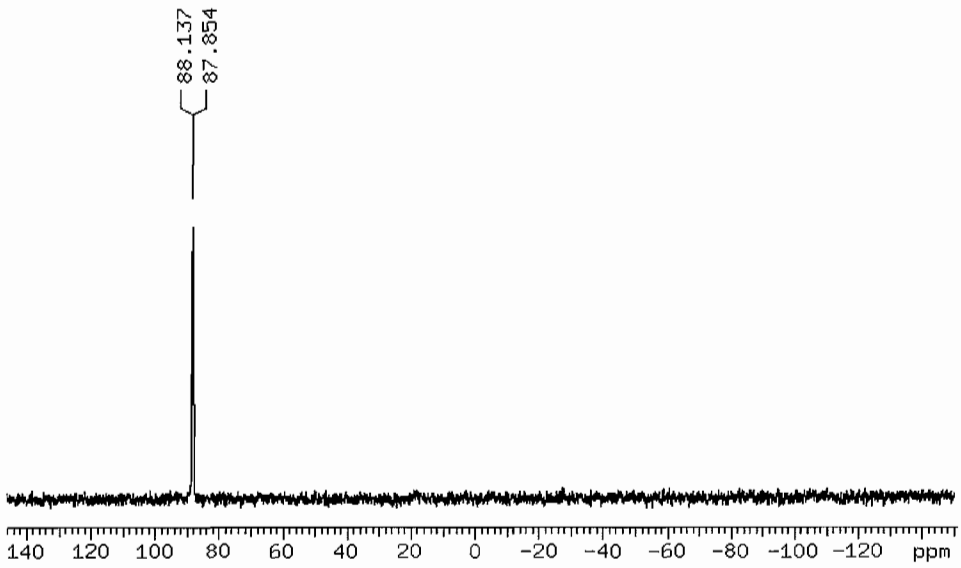

Figure A4. $^{31}P\{^{1}H\}$ NMR spectrum of *trans*-[^{57}Fe(DMeOPrPE)$_2$(D$_2$)D][BPh$_4$].

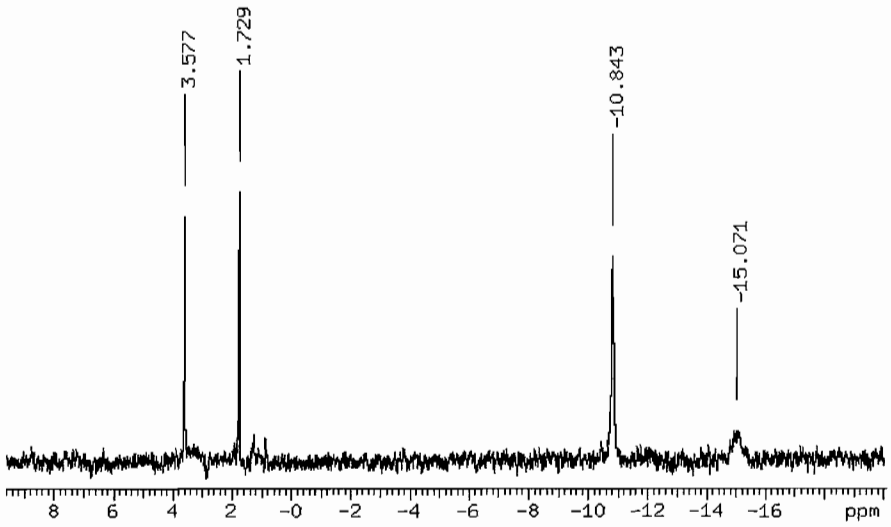

Figure A5. ^{2}H NMR spectrum of *trans*-[^{57}Fe(DMeOPrPE)$_2$(D$_2$)D][BPh$_4$] in THF-d_8.

Synthesis of *trans*-[^{57}Fe(DMeOPrPE)$_2$(N$_2$)H][BPh$_4$]. *trans*-[^{57}Fe(DMeOPrPE)$_2$(H$_2$)H][BPh$_4$] (250 mg, 0.219 mmol) was dissolved in 20 mL of THF/Et$_2$O (1:1), charged with 2 atm of N$_2$ in a Fischer-Porter tube, and stirred for 48 hrs. The Fischer-Porter tube was vented and refilled with N$_2$ several times over the course of

the reaction to remove the free H_2. The solution turns from light yellow to light brown over the course of the reaction. The solvent was evaporated under an N_2 atmosphere. The resulting brown oil was triturated with hexanes to yield 0.247 g of a tan solid (96% yield). $^{31}P\{^1H\}$ NMR (toluene-d_8): δ 76.05 (d, $^1J_{P\text{-}Fe}$ = 36 Hz). ^1H NMR (toluene-d_8) of the hydride region: δ -18.6 (quintet, $^2J_{H\text{-}P}$ = 49 Hz).

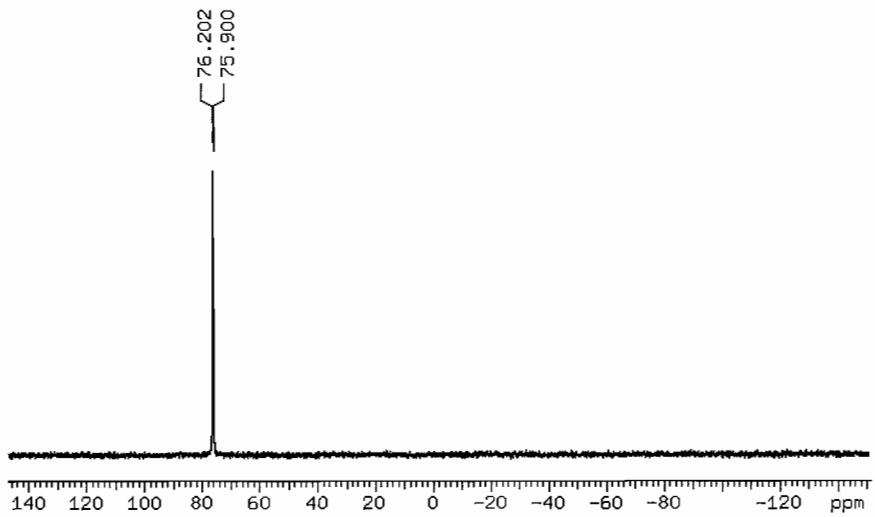

Figure A6. $^{31}P\{^1H\}$ NMR spectrum of *trans*-[^{57}Fe(DMeOPrPE)$_2$(N_2)H][BPh_4].

Synthesis of *trans*-[^{57}Fe(DMeOPrPE)$_2$($^{15}N_2$)H][BPh_4]. The synthesis of this complex was identical to that described above except that $^{15}N_2$ was used in place of N_2. $^{31}P\{^1H\}$ NMR (toluene-d_8): δ 76.05 (d, $^1J_{P\text{-}Fe}$ = 36 Hz). ^1H NMR (toluene-d_8) of the hydride region: δ -18.6 (quintet, $^2J_{H\text{-}P}$ = 49 Hz).

Synthesis of *cis*-[^{57}Fe(DMeOPrPE)$_2$(N_2H_4)][2BPh_4]. To a stirring solution of *trans*-^{57}Fe(DMeOPrPE)$_2Cl_2$ (0.95 g, 1.07 mmol) in THF, solid $NaBPh_4$ (0.073 g, 0.213 mmol) was added. Immediately a solution of N_2H_4 in THF (0.049 M, 2.17 mL) was

added. The mixture was stirred overnight and then filtered through Celite. The product was precipitated as a red-orange oil by addition of hexanes. The resulting oil was triturated with hexane to yield a pale orange powder (0.27 g, 96%). $^{31}P\{^{1}H\}$ NMR (CD_2Cl_2): δ 75.4 (dt, $^{1}J_{P\text{-}Fe}$ = 53 Hz, $^{2}J_{P\text{-}P}$ = 36 Hz), δ 62.4 (dt, $^{1}J_{P\text{-}Fe}$ = 53 Hz, $^{2}J_{P\text{-}P}$ = 36 Hz). ^{1}H NMR (CD_2Cl_2): δ 4.85 (s, br), δ 3.82 (s, br).

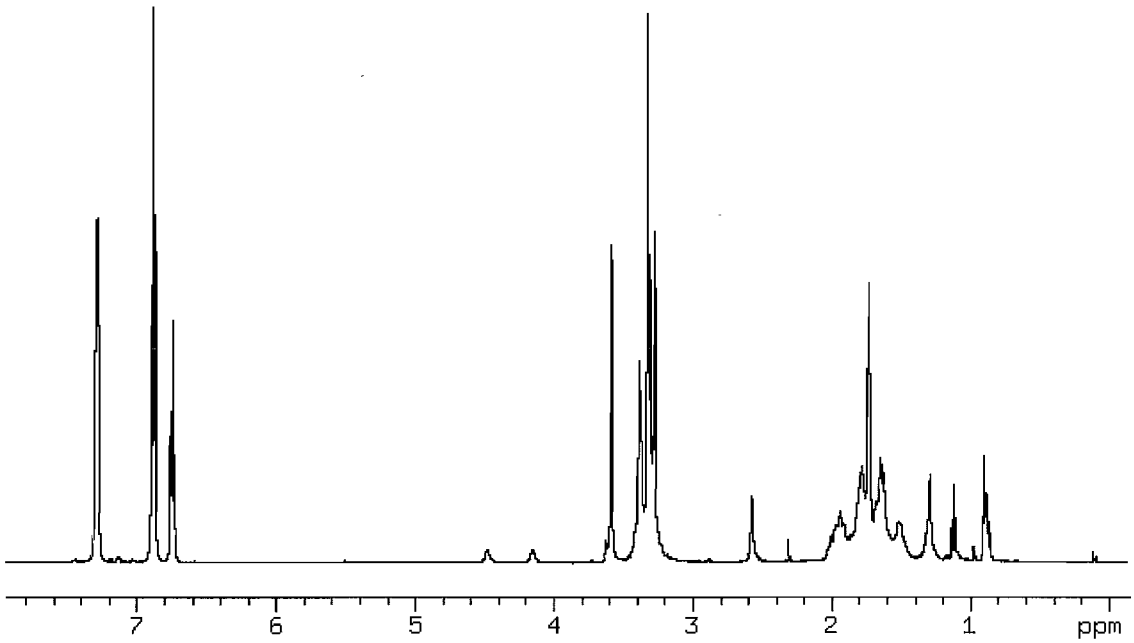

Figure A7. ^{1}H NMR spectrum of *cis*-[^{57}Fe(DMeOPrPE)$_2$(N_2H_4)][2BPh$_4$].

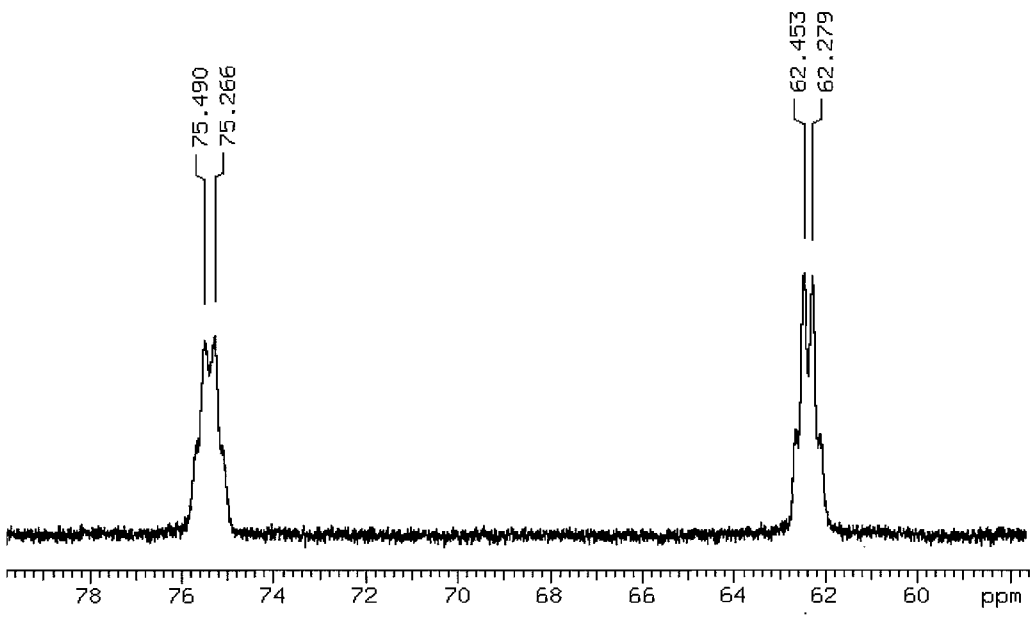

Figure A8. $^{31}P\{^{1}H\}$ NMR spectrum of *cis*-[^{57}Fe(DMeOPrPE)$_2$(N_2H_4)][2BPh_4].

Synthesis of *cis*-[^{57}Fe(DMeOPrPE)$_2$($^{15}N_2H_4$)][2BPh_4]. The synthesis of this complex was identical to that described above except that $^{15}N_2H_4$ was used in place of N_2H_4.

APPENDIX B

THEORETICAL STUDIES OF N_2 REDUCTION TO AMMONIA IN $FE(DMPE)_2N_2$

Reproduced with permission from Yelle, R. B.; Crossland, J. L.; Szymczak, N. K.; Tyler, D. R. *Inorg. Chem.* **2009**, *48*, 861-871.

B.1 Introduction

The conversion of N_2 to ammonia under mild conditions is a coveted goal for chemists,[1] and transition metal complexes have been actively investigated as catalysts for carrying out the transformation. Various group 4 and group 6 transition metal complexes have shown promise in this regard, with $[HIPTN_3N]Mo(N_2)$ ($HIPTN_3N$ = $[\{3,5\text{-}(2,4,6\text{-}{}^{i}Pr_3C_6H_2)_2C_6H_3NCH_2CH_2\}_3N]^{3-}$) being the only well-defined catalytic system to date.[2] Some intriguing reactivity has also been reported using iron complexes.[3,4] Leigh first demonstrated that $Fe(dmpe)_2N_2$ (dmpe = 1,2-bis(dimethylphosphino)ethane) can be protonated to yield ammonia.[5] Further work in our laboratory on a similar system using $Fe(DMeOPrPE)_2(N_2)$ (DMeOPrPE = 1,2-bis(bis(methoxypropyl)phosphino)ethane) demonstrated that, upon protonation, N_2 could be reduced to ammonia and hydrazine at atmospheric temperature and pressure (eq 1).[6] Noteworthy is that access to the $Fe^0P_4(N_2)$ precursor was gained through an $Fe^{II}P_4(H_2)H^+$ intermediate, formed by reaction of

$Fe^{II}P_4Cl_2$ with H_2. Thus, H_2 is the source of electrons for the reduction of N_2 to ammonia.

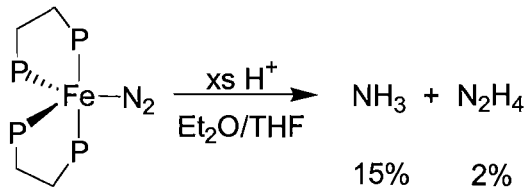

(1)

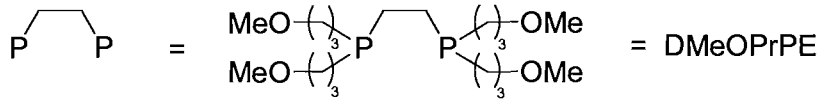

To achieve a catalytic N_2 fixation scheme based on eq 1, a better understanding of the mechanism of the N_2 reduction pathway is needed.[7,8] Understanding the mechanism of N_2 reduction in these complexes may also give insights into the mechanism of nitrogenase.[9] Increasing biochemical evidence has determined that iron is likely the site of N_2 binding and reduction in this enzyme.[10] Other recent work has shown that hydrazine and diazene are likely intermediates along the N_2 reduction pathway.[11] This evidence points to a different mechanism than the Chatt mechanism (three stepwise additions of a proton and an electron to the terminal N atom),[12] and suggests instead a mechanism in which protonation alternates between the proximal and distal nitrogen atoms of a bound N_2 ligand.[13]

Current hypotheses about the intermediates involved in the mechanism of N_2 reduction for $FeP_4(N_2)$ systems are speculative, and to our knowledge, a detailed theoretical study of the mechanism has not been reported. In order to perform the calculations at a high level of theory, the dmpe ligand was used instead of the DMeOPrPE ligand. We find this simplification to be acceptable because the $Fe(dmpe)_2N_2$ complex has

also been shown to produce ammonia in the presence of acid.[5]

Six electrons are required to fully reduce N_2 to two NH_3 molecules. Previous experiments suggest that protonation of $Fe^0(dmpe)_2N_2$ results in an Fe^{II} product,[6] suggesting that the complex provides only two electrons toward the reduction. Although the mechanism may involve two separate one-electron reductions, in this study mechanisms involving a two-electron reduction from a sacrificial $Fe(dmpe)_2N_2$ complex were considered. Using density functional theory (DFT) we investigated three possible pathways of N_2 reduction: an asymmetric monomer mechanism (Chatt-like) that involves successive protonation at the terminal nitrogen, a symmetric monomer mechanism that proceeds through diazene and hydrazine intermediates, and a dimer mechanism in which reduction takes place through a bridged N_2 species.

B.2 Computational Methods

All calculations were performed using NWChem versions 4.7 and 5.0.[14-16] Transition states were not examined in this study. Rather, as a first approximation, calculations were performed only on hypothetical intermediates of each mechanism, shown in Schemes 1-4. Building and modeling of $Fe(dmpe)_2N_2$ and all related intermediates was performed using the program Ecce v3.2.4.[17,18] Calculations were performed on singlet states of each intermediate, although for some monomer intermediates the triplet or quintet states were considered. Calculations involving open-shell (triplet or quintet) systems were performed using the unrestricted (spin-polarized) framework. In some cases, the triplet state is much higher in energy than the singlet, but

in other cases (**2a**, **6a**, **6b**) the triplet states were found to be slightly lower. However, in those cases where they are lower, they are sufficiently close to the singlet in energy that they would not affect the mechanisms described here. Thus, the analysis and discussion of these intermediates will focus on the singlet states, except where the higher spin states are clearly more important (such as complexes **15** and **16** in the Supporting Information). Protonation reactions were modeled using triflic acid (TfOH) as the proton source.[6] No external reductant was used by Gilbertson et al.;[6] therefore, the $Fe(dmpe)_2N_2$ reactant (**1**) was also modeled as the reductant ($Fe^0 \rightarrow Fe^{II}$) for steps involving outer-sphere electron transfer. Upon oxidation, the dinitrogen dissociates from the resulting high-spin $Fe^{II}(dmpe)_2$ (complex **16**, see Supporting Information).

All calculations employed the B3LYP hybrid functional.[19-22] The geometries of each structure **1**-**16** were optimized using the 6-31G* basis set.[23,24] While some of the molecules have C_2 or higher symmetry, symmetry was not enforced in the optimizations because the symmetric structures were not always the lowest energy structures. For complexes **3** and **4**, the use of a fine grid and tighter convergence criteria were needed to obtain a minimum energy structure. Single-point energy calculations were performed on each optimized structure. These employed the "Wachters+f" basis set for Fe,[25] which is a (14s11p6d3f)/[8s6p4d1f] contraction, and the 6-311G** basis set[26] for all other atoms. Solvation effects were incorporated into the single-point energy calculations using the COSMO reaction field[27] with a dielectric constant of 7.52 corresponding to tetrahydrofuran (THF).

The evaluation of solvation energies has an important bearing on the reaction energies. Solvation energies are highly dependent on the atomic radii used. The default radii in NWChem are close to the traditional van der Waal radii, which are generally quite small and can lead to an overestimate of the solvation energies. With the exception of iron, where the default NWChem value of 1.8 Å was used, the remaining atomic radii used were those developed by Stefanovich and Truong[28], which were optimized to give the best fit to experimental hydration energies for a representative group of molecules. Radii corresponding to "hydrogen-bonding" nitrogen atoms were used for all nitrogen atoms because binding to the iron results in polarizing the nitrogen atoms, making them susceptible to hydrogen bonding. In our studies, we found that the Stefanovich-Truong (S-T) radii gave solvation energies for NH_3 that were much closer to experimental hydration energies (-3 kcal/mol) than the default NWChem values (-6 for the S-T radii versus –12 kcal/mol for the default values). In general, the S-T radii are larger than the default values, and they result in a more conservative contribution of solvation energies to the total reaction energies.

Vibrational frequency calculations were performed on the optimized structures **1-9** in the singlet states, the triplet state of **15**, and the quintet state of **16**, using the 6-31G* basis set. Complex **16** had one imaginary frequency, but no other structures had any imaginary frequencies. Thermal and entropic corrections were obtained for monomer complexes **1-9**, **15**, **16**. Reaction energies are given with these corrections (free energies) and without these corrections (electronic energies) for Schemes 1 through 3. Frequency calculations were not performed on the dimeric structures **10-14** (Scheme 4) due to the

considerable computational expense, thus thermal and entropic corrections could not be obtained for these intermediates, so only electronic reaction energies are given there. Most of the differences in reaction energy due to these thermal and entropic corrections presented here were negligible, except for reactions involving the release of N_2 or NH_3 where entropy played a large role. However, due to the electronic energies obtained for the dimer, the neglect of entropy is not likely to change any conclusions drawn from this work (see Discussion). To compare all schemes on equal ground, the discussion of reaction energies will involve mainly the electronic energies, except where stated otherwise.

Mulliken population analysis was used to determine atomic populations from the single-point energy calculations, and N-N, Fe-N, and Fe-P bond orders were computed for each complex. When describing the electronic structure, the z-axis is taken to be parallel to the axial Fe-P bonds, with the equatorial Fe-P bonds on the xy-plane. For most structures, the x-axis is taken to be the Fe-N bond, except for structures with side-on binding (e.g. complexes **7-9**), in which case the x-axis bisects the N_α-Fe-N_β angle (Figure 1). Most of the molecular orbitals computed for these complexes contain significant contributions from several atomic orbitals, so the descriptions will focus only on the primary components of a given molecular orbital.

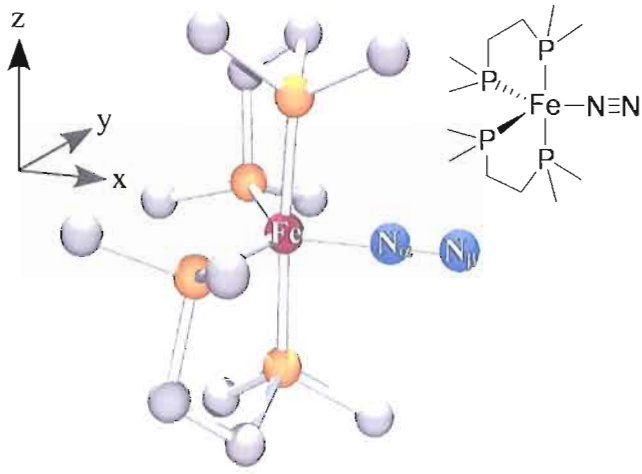

Figure 1. Optimized structure of $Fe(dmpe)_2N_2$ (**1**). Hydrogen atoms have been omitted for clarity. The axes chosen for describing the electronic structure are also shown.

B.3 Results and Analysis

Calculated data has been summarized in Tables 1-4 so as not to congest the discussion below. Table I contains Fe-P and Fe-N bond lengths and Fe-N-N bond angles from the geometry optimization of each intermediate. Calculated Fe-N and N-N vibrational frequencies of the monomer intermediates are given in Table II. Tables III and IV contain bond orders and atomic charges, respectively, derived from Mulliken population analysis. An energy level correlation diagram for complex **1** is shown in Figure 2. Energy level diagrams for the other monomeric intermediates are provided in the supporting information, as well as figures showing bonding molecular orbitals. The energy profiles for all three mechanisms are shown in Figure 3. In the text that follows, N_α and N_β refer to the coordinated (proximal) and non-coordinated (distal) nitrogen atoms in a linearly bonded M-N≡N unit, respectively.

B.3.1 Dinitrogen Complexes

$Fe(dmpe)_2N_2$ (**1**). The ground state of **1** is a singlet. The optimized singlet structure is trigonal bipyramidal (C_2 symmetry) with N_2 in an equatorial position (Figure 1), and the bond lengths and bond angles are in excellent agreement with those in the crystal structure of the closely related $Fe(depe)_2N_2$ complex[29] (Table I). The Fe-N-N linkage is linear, and end-on binding of N_2 is preferred over side-on binding by 11 kcal/mol. The N-N bond length is slightly elongated (by 0.035 Å) upon binding to the metal center, compared to free N_2. The $\nu_{N\text{-}N}$ is significantly reduced upon binding (Table II), and according to the Mulliken bond order analysis, most of the N-N triple-bond character is lost. Dissociation of N_2 from $Fe(dmpe)_2$ (**15**) costs 23 kcal/mol when calculated in vacuo. The $Fe(dmpe)_2N_2$ complex is stabilized in a THF solvent field by an additional 3 kcal/mol.

A molecular orbital diagram of complex **1** is given in Figure 2. Three orbitals are involved in Fe-N_2 binding. The HOMO (labeled $d_{xy}\_\pi_y^*$) can be described as an Fe d_{xy} orbital that is involved in the bonding of the equatorial phosphine ligands, as well as in bonding the dinitrogen via the π_y^* orbital. The $d_x2\text{-}_y2$ orbital is mostly nonbonding, but also forms a bonding combination with the N_2 σ_g orbital. (The σ_g orbital is the orbital formed by overlap of the two sp hybridized orbitals on each N atom.) The Fe d_{xz} orbital mixes with the π_z^* orbital (the $d_{xz}\_\pi_z^*$ orbital). The Fe d_z2 and d_{yz} orbitals are nonbonding with respect to the dinitrogen ligand, but one admixture of these orbitals is involved in bonding the phosphine ligands.

Mulliken population analysis (MPA) indicates that significant negative charge (-0.31e) is transferred to the N_2 upon binding (Table IV). Much of this charge is transferred

via π back-donation from the Fe d_{xy} and d_{xz} orbitals to the dinitrogen π_y^* and π_z^* orbitals, respectively. Most of the negative charge is transferred to the terminal nitrogen atom, N_β, suggesting that N_β is more susceptible to protonation than N_α.

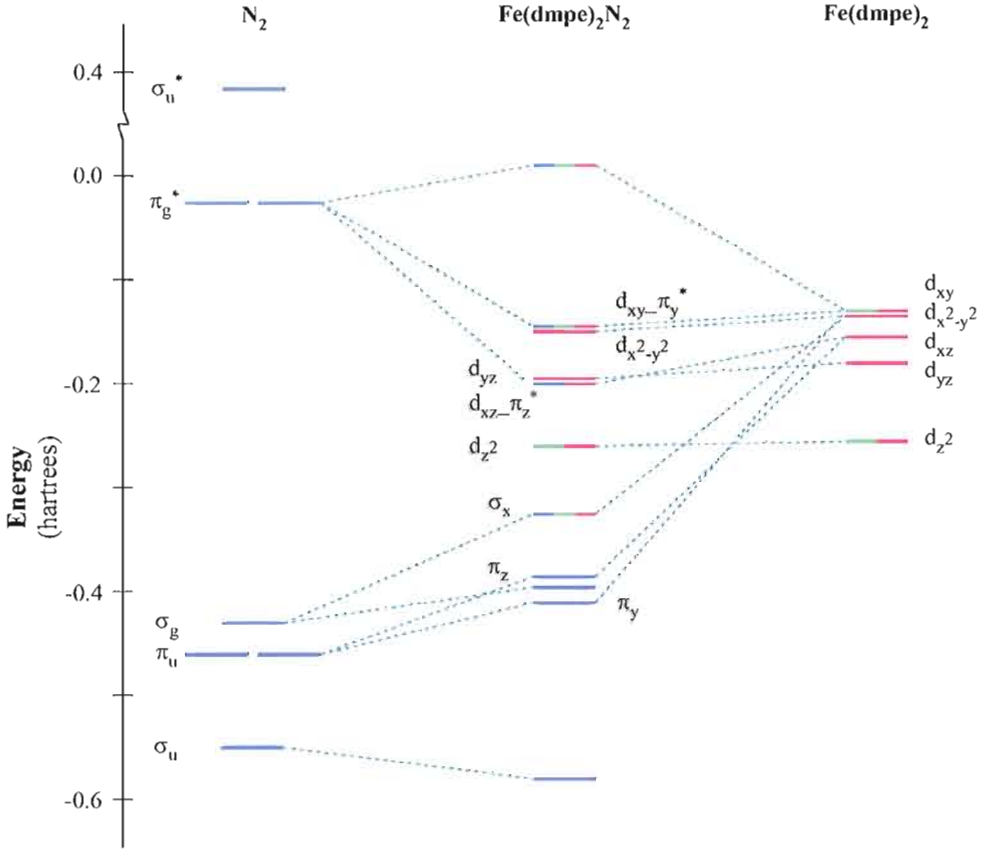

Figure 2. Energy level scheme for the bonding between N_2 and $Fe(dmpe)_2$ (**15**). The blue color indicates contributions from dinitrogen, red from iron, and green from phosphine. Other contributions are ignored, for clarity.

$[FeH(dmpe)_2N_2]^+$ (**2b**). This complex is not an intermediate for any of the mechanisms examined, but it is the thermodynamic product of the protonation of complex **1**. Indeed, protonation at the metal center is calculated to be favorable by 58 kcal/mol, about 40 kcal/mol more favorable than protonation at the terminal nitrogen (**2a**) (Scheme 1). Complex **2b** has octahedral coordination about the Fe, with the hydride trans to the N_2,

in good agreement with the crystal structure of Hills et al.[31] The N-N bond length is close to that of free N_2, which also agrees well with the published structure. In the protonation reaction to form complex **2b**, the proton bonds to the Fe $d_x2_{-y}2$ orbital, substantially lowering the energy of this orbital. There are two Fe-N π-bonding orbitals, which are mixtures of the Fe d_{xy} and d_{xz} orbitals and the dinitrogen π_y^* and π_z^* orbitals. Negative charge is transferred back to the iron-phosphine unit, making dinitrogen less activated for further protonation. Indeed, this complex is not a viable species in N_2 reduction as the subsequent protonation of N_2 in this complex is highly unfavorable (33 kcal/mol), which agrees with experimental results obtained by Henderson in which further reaction of this complex to yield ammonia was not observed. [30] Despite the fact that the dinitrogen is poorly activated, the calculations predict an Fe-N_2 dissociation energy of about 23 kcal/mol in THF, only 3 kcal/mol less than for complex **1**. The lowest energy triplet state is calculated to be about 30 kcal/mol higher in energy than that of the singlet.

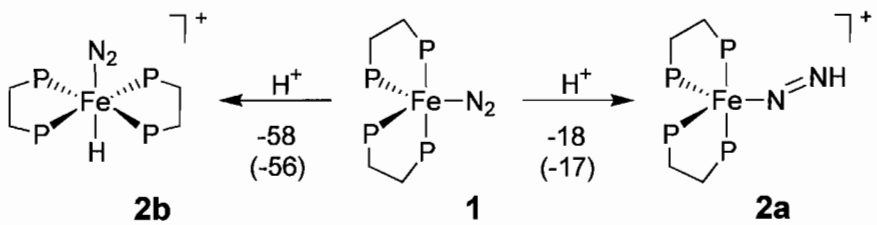

Scheme 1. Comparison of two initial protonation reactions of $Fe(dmpe)_2N_2$ (**1**). Reaction energies are in kcal/mol, and free energies are given in parentheses.

B.3.2 Asymmetric Monomer Mechanism

The asymmetric monomer mechanism and reaction energies are shown in Scheme 2. In this mechanism, the complex undergoes two successive protonations to the terminal

nitrogen (N_β) followed by a two-electron reduction by complex **1**. Subsequent protonation of N_β in complex **4** results in the formation of NH_3.

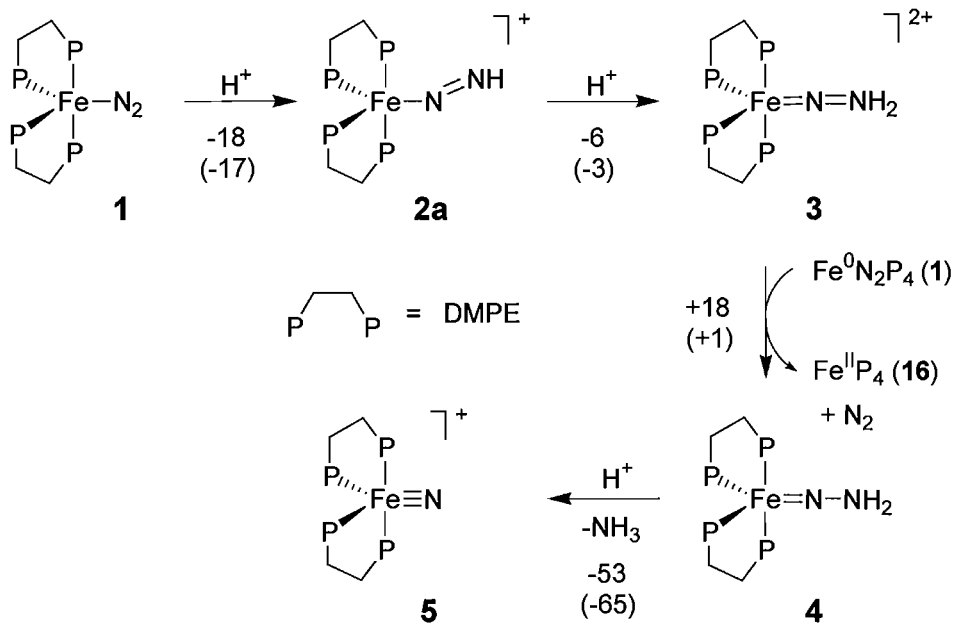

Scheme 2. Calculated intermediate structures for the asymmetric protonation of $Fe(dmpe)_2N_2$. Reaction energies are in kcal/mol, and free energies are given in parentheses.

*$[Fe(dmpe)_2NNH]^+$ (**2a**).* Formation of this complex via protonation of the terminal nitrogen of **1** is favorable by 18 kcal/mol. The five-coordinate complex displays trigonal bipyramidal geometry. The N-N bond is elongated upon protonation, and the Fe-N-N angle is slightly distorted from linear. End-on binding is preferred over side-on binding by about 8 kcal/mol. Protonation results in further weakening of the N-N bond, as shown by the reduced N-N stretching frequency and further reduction in the N-N bond order. Protonation also results in strengthening of the Fe-N bond, as shown by the 0.1 Å decrease in the Fe-N bond length and substantial increase in bond order. The terminal nitrogen, Nβ

has a trigonal planar geometry, suggesting some sp^2 character. The protonated N_2 is bound very tightly to the complex, having a dissociation energy of 109 kcal/mol. The complex becomes more polarized, in the sense that more positive charge is transferred to the iron and more negative charge (–0.5e) to the dinitrogen, with the terminal nitrogen slightly retaining the majority of that negative charge. The greater negative charge on the terminal nitrogen suggests that N_β is more primed than the coordinating nitrogen for addition of a second proton. The bonding of the newly added proton involves the $d_{xy}\_\pi_y^*$ orbital and the dinitrogen π_y orbital, effectively eliminating the triple bond. The lowest energy triplet state is calculated to be about 2 kcal/mol lower in energy than the singlet. The calculations indicate that the triplet state is stabilized by the solvent field by 14 kcal/mol over the singlet, which may be due to the larger dipole moment for the triplet (4.6 Debye) compared to the singlet (3.9 Debye). Calculations were also performed on an isomer in which the proton was added to the proximal nitrogen, N_α, of complex **1**. However, all attempts to optimize this structure resulted in metal hydride formation (**2b**) vide supra.

$[Fe(dmpe)_2NNH_2]^{2+}$ (3). Further protonation of **2a** at the terminal nitrogen results in the formation of the *iso*-diazene complex, **3**. This protonation is exothermic by 6.0 kcal/mol, and exergonic by 3 kcal/mol. The triplet form of this structure is calculated to be only 3 kcal/mol higher in energy. There is an additional increase in the N-N bond length and a corresponding decrease in the Fe-N bond length. The Fe-N-N angle is linear. The N-N stretch is computed to be 1515 cm^{-1}. The Fe-N and N-N bond orders are nearly equal at about 1.4, suggesting that both bonds have significant double-bond character. The

iso-diazene molecule is bound to the $[Fe(dmpe)]^{2+}$ unit with a dissociation energy of 32 kcal/mol. Despite the addition of another positive charge via protonation, there is still substantial negative charge present on the nitrogen atoms, although the MPA assigns slightly more negative charge to Nα. The net charge of the diazene is slightly positive (0.17e), suggesting a formal oxidation state of +2 for iron in this complex. Binding of the Fe to the dinitrogen involves primarily the $d_{xy}\_\pi_y^*$ and $d_{xz}\_\pi_z^*$ orbitals. Protonation of N_β or N_α to form $[Fe(dmpe)_2N_2H_3]^{3+}$ is very unfavorable (by 41 and 24 kcal/mol, respectively). The two-electron reduction of **3** by **1** to form the iso-hydrazido complex **4** is less endothermic than either protonation. Thus, this pathway to form the iso-hydrazido complex (**4**) is considered as the next step.

$Fe(dmpe)_2NNH_2$ (4). The two-electron reduction of **3** is endothermic by 18 kcal/mol, but endergonic by only 1 kcal/mol. This is due to the large increase in entropy resulting from the dissociation of N_2 from the oxidized $Fe(dmpe)^{2+}$ complex **16**. The Fe-N-N angle of complex **4** is about 131°, suggesting an sp^2-hybridized N_α. The Fe-N bond increases by over 0.10 Å in length, but the Fe-N bond order indicates slightly more double-bond character. The N-N bond loses most of its double-bond character, elongates by 0.08 Å, and is intermediate between that calculated for free *trans*-diazene and hydrazine. The N-N-H angles are in the range suggesting an sp^2 N_β. Both nitrogen atoms carry significant negative charge and are ready for further protonation.

$[Fe(dmpe)_2N]^+$ (5). Protonation of complex **4** at N_β forms an unstable $[Fe(dmpe)_2NNH_3]^+$ complex, which leads to the spontaneous dissociation of ammonia. This process is calculated to be extremely exothermic (-53 kcal/mol) and exergonic (-65

kcal/mol). The remaining Fe-N bond shows mostly triple-bond character. Protonation of this complex is favorable (-8 kcal/mol), but the addition of two more protons to form $[Fe(dmpe)_2NH_3]^{4+}$ becomes highly unfavorable (over 60 kcal/mol). Therefore, another two-electron reduction by 1 would likely be required before a second equivalent of ammonia could be released.

B.3.3 Symmetric Monomer Mechanism

The symmetric monomer mechanism and reaction energies are shown in Scheme 3. This mechanism involves protonation steps which alternate between the two nitrogen atoms. Electron transfer occurs after the second protonation step and is followed by two additional protonations, resulting in an η^2-hydrazine complex.

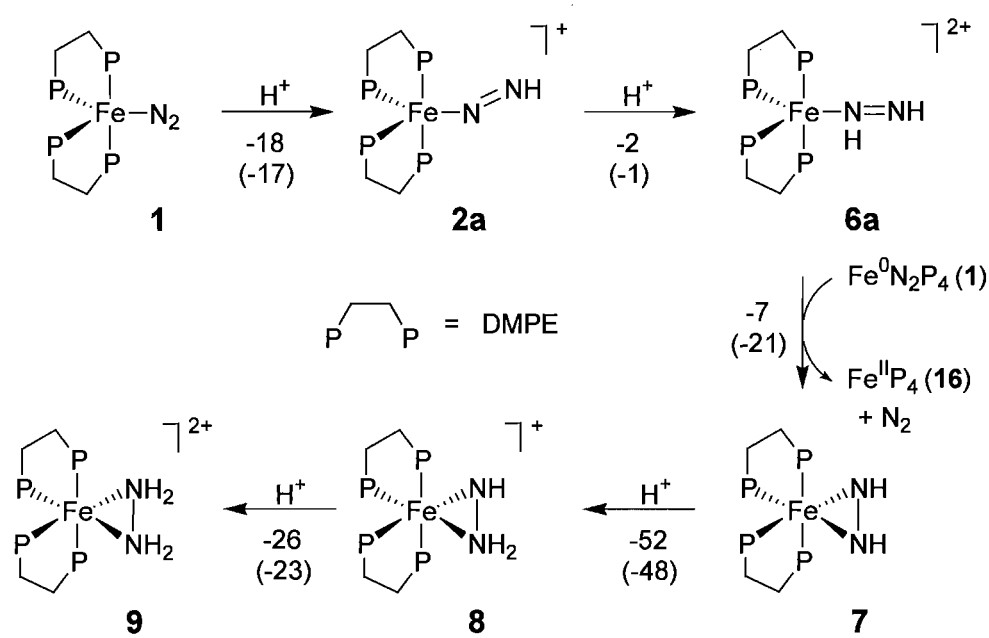

Scheme 3. Proposed intermediate structures for the symmetric protonation of $Fe(dmpe)_2N_2$. Reaction energies are in kcal/mol, and free energies are given in parentheses.

*$[Fe(dmpe)_2(trans\text{-}NHNH)]^{2+}$ (**6a**) and $[Fe(dmpe)_2(cis\text{-}NHNH)]^{2+}$ (**6b**).* Symmetric protonation of **2a** to yield either *trans*- or *cis*-diazene structures is nearly thermoneutral (-2 to 0 kcal/mol, -1 to 1 with thermal and entropic corrections), with the trans form (**6a**) being about 2 kcal/mol more stable the cis form (**6b**). This is very close to the calculated energy difference (2.6 kcal/mol) between the free forms of *trans*- and *cis*-diazene. The triplet forms of **6a** and **6b** are calculated to be about 3 kcal/mol more stable than their corresponding singlet forms. Both **6a** and **6b** exhibit a square-pyramidal structure about the iron, which implies that the iron may take on octahedral coordination in this state. Yet, the calculations showed only a bent, end-on coordination for the diazene, with an Fe-N-N angle of 131° for the trans and 114° for the cis forms. (Optimizations of side-on configurations were attempted, but most of them resulted in structures in which the dinitrogen bonded end-on to the iron, except when symmetry was enforced.) The N-N bond lengths are very similar to each other and to the *iso*-diazene form (**3**); they are roughly 0.01 Å more elongated than the free form of *trans*-diazene obtained from DFT optimizations. The N-N bond orders of the trans and cis forms indicate more double-bonded character than the iso form, but are slightly less than that of free *trans*-diazene. However, the Fe-N bond of the trans and cis forms are over 0.2 Å longer than the iso form, and the Fe-N bond order of about 0.5 suggests that the diazene is only weakly bound to the iron-phosphine complex. Indeed, the dissociation energy of the diazene from the complex in either form is only about 15 kcal/mol. The charge distributions of the trans and cis forms are also similar to that of the iso form except that there is more positive charge on the iron in **6a** and **6b**, suggesting more ionic character in the bonding between the complex

and the diazene. This is consistent with the calculated binding energies being significantly weaker for these ligands with the complex. The bonding between the iron and diazene involves a σ bond between the Fe $d_x2_{-y}2$ orbital and diazene sp^2-like orbital. Subsequent protonation of N_β in **6a** is endothermic by 20 kcal/mol. If the protonated species is formed, the release of $N_2H_3^+$ from $[Fe(dmpe)_2]^{2+}$ (**16**) is calculated to be slightly endothermic (4 kcal/mol) but exergonic by 10 kcal/mol. However, the outer-sphere two-electron reduction of complex **6a** by **1** resulting in **7** is calculated to be exothermic by about 7 kcal/mol and exergonic by 21 kcal/mol and will be considered in more detail.

cis-Fe(dmpe)$_2$NHNH (7). The trans-diazene binds side-on to the iron in this oxidation state, yielding pseudo-octahedral coordination about the iron. Side-on binding is preferred over the end-on binding form (**4**) by about 25 kcal/mol. This is in good agreement with a recent crystal structure of the $Fe(dmpe)_2(N_2H_2)$ complex which shows that the diazene is bound side-on to the iron.[32] The Fe-P bonds are overestimated by about 0.04-0.06 Å compared to the crystal structure values, and the Fe-N and N-N bond are underestimated by 0.05 and 0.03 Å, respectively. Overall, the nature of the Fe-N and N-N bonding is well described by DFT. Field et al. describe this as an Fe^0-diazene complex. However, based on the evidence presented below the complex is perhaps better described as a Fe^{II}-hydrazido(2-) complex. The length of the N-N bond is over 0.15 Å longer than that computed for free trans-diazene and is much closer to that of free hydrazine. In addition, when **6a** is reduced to form **7**, the N-N bond length increases by about 0.14 Å and the bond order decreases to 1.0. Thus, all double-bonded character is lost. There is also a substantial decrease in $\nu_{N\text{-}N}$ (from 1557 to 1062 cm^{-1}). The Fe-N bond length

increases by about 0.09 Å over complex **6a**, while the Fe-N bond order also increases. The dissociation energy of *trans*-diazene from $[Fe(dmpe)_2]^0$ is computed to be about 47 kcal/mol. The HOMO is mostly antibonding between the iron and diazene, with some overlap between the Fe $d_x2_{-y}2$ orbital and the diazene sp^2-like π_z^* orbital. The greatest contributions to the Fe-hydrazido bonding come from σ bonds formed by the Fe 4s and d_z2 orbitals with the dinitrogen π_x orbital, and π bonds between Fe $d_{xz/xy}$ and π_x^*, and between Fe d_{yz} and π_z^*. The back-donations from the Fe substantially increase the charge distribution on each nitrogen, resulting in a net negative charge (-0.54e) on the hydrazido, making it a likely site for further protonation.

*cis-$[Fe(dmpe)_2NHNH_2]^+$ **(8)***. This complex can be formed by protonation of **7** at N_β (-52 kcal/mol). The protonated hydrazido(1-) molecule remains side-on bound to the iron center, maintaining octahedral coordination of the iron. There is a 0.036 Å increase in the N-N bond and slight reduction in N-N bond order. Interestingly, there is substantial decrease in Fe-N bond order, yet a slight (0.017 Å) decrease in the Fe-N_α bond length. The Fe-N_β bond length is unchanged at 1.983 Å. These small structural changes upon protonation suggest a low energy barrier for this step. There is still a net negative charge on the hydrazido (over –0.20e), and the charge distribution suggests that the singly protonated N_α (-0.50e) would be more susceptible to additional protonation than the doubly protonated N_β (-0.43e).

*cis-$[Fe(dmpe)_2(N_2H_4)]^{2+}$ **(9)***. Formation of this complex via protonation of **8** is also thermodynamically downhill (26 kcal/mol). The N-N bond length, bond order, and $\nu_{N\text{-}N}$ are mostly unchanged, but the Fe-N bond length increases to 2.036 Å, and the Fe-N

bond orders decrease to 0.25. The predicted side-on binding of hydrazine to the iron is in very good agreement with the reported structure of *cis*-$[Fe(dmpe)_2(N_2H_4)]^{2+}$.[33] The Fe-P and Fe-N bonds are overestimated (by 0.08 Å and 0.04 Å, respectively), but the N-N bond is very close (0.01 Å) to that reported in the crystal structure. The dissociation energy of N_2H_4 from complex **9** is calculated to be +24 kcal/mol in THF. The main Fe-N bonding MO is a strong π bond between the Fe d_{xy} and the dinitrogen π_x^* orbital (the $d_{xy}\_\pi_x^*$ orbital). The HOMO is mostly antibonding between the iron and hydrazine, although there is some overlap between the nitrogen sp^3 hybrid orbitals and the Fe $d_{x^2-y^2}$ orbital. There is a net positive charge (~0.30e) on the hydrazine. Further protonation of this complex results in the dissociation of $N_2H_5^+$ from $[Fe(dmpe)_2(N_2H_5)]^{3+}$, with the net process being slightly endothermic (6 kcal/mol) but exergonic (-8 kcal/mol). Protonation and subsequent dissociation of NH_3 from $[Fe(dmpe)_2(N_2H_5)]^{3+}$ was also considered, and found to be endothermic by 48 kcal/mol.

B.3.4 Symmetric Dimer Mechanism

The intermediates and reaction energies for the symmetric dimer mechanism are shown in Scheme 4. The first step involves the formation of dinitrogen bridged dimer, followed by four successive protonation steps, resulting in the formation of a hydrazine intermediate.

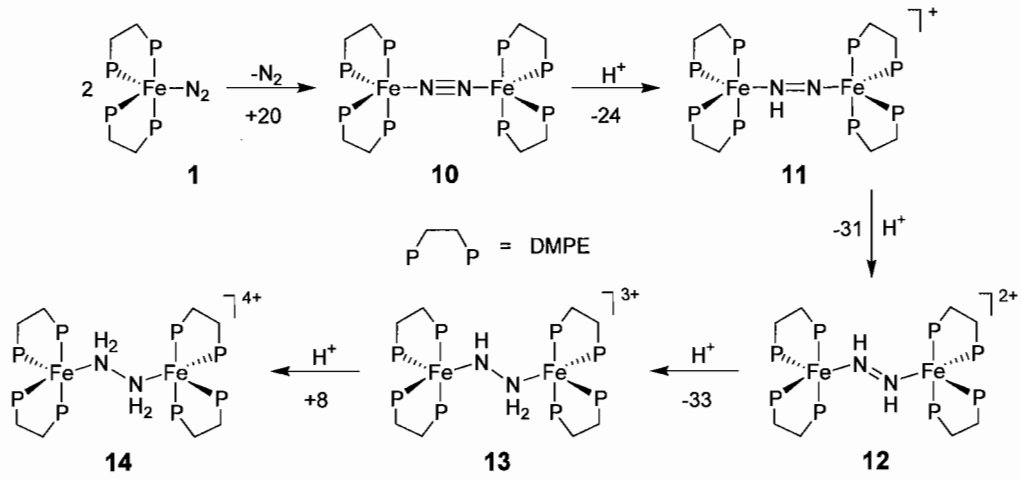

Scheme 4. Proposed intermediate structures for the symmetric protonation of $Fe_2(dmpe)_4N_2$. Reaction energies are in kcal/mol.

*$Fe_2(dmpe)_4N_2$ (**10**).* The formation of this complex via dimerization of complex **1**, resulting in the liberation of N_2, is calculated to be unfavorable by 20 kcal/mol. The geometry optimization yielded a structure in which the second $Fe(dmpe)_2$ is rotated almost 90° with respect to the first $Fe(dmpe)_2$. Both Fe atoms bind to the dinitrogen in linear (180°) fashion. The N-N bond length in the dimer is slightly (0.015 Å) longer than in **1**, but the Fe-N bond lengths are nearly 0.08 Å longer. This is consistent with the bond order analysis, which indicates that the N-N and Fe-N bonds are weaker for the dimer than for **1**. In fact, formation of the dimer results in fully eliminating the triple-bond character of the N-N bond. The MPA indicates that both nitrogen atoms in **10** have the same charge as the terminal nitrogen (N_β) of **1**, and the dinitrogen overall has a more negative charge in the dimer than in **1**. The slight elongation of the N-N bond length over the monomer complex and the transfer of more negative charge to the N_2 suggest that formation of a dimer would further activate N_2 for reduction. Once formed, the complex itself has limited stability; the

dissociation of complex **10** into $Fe(dmpe)_2$ and **1** is unfavorable by only 6 kcal/mol. The two HOMOs of **10** are interesting. They can be described as linear combinations of the $d_{xy}\_\pi_y$ and $d_{xz}\_\pi_z$ orbitals. The HOMOs are significantly higher in energy than those of the monomer complex, and the HOMO-LUMO gap is much smaller, suggesting this complex should be much more reactive. Each Fe is able to participate in the $d_{xy}\_\pi_y^*$ and $d_{xz}\_\pi_z^*$ backbonding, and these modes are stabilized by the extra Fe atom with respect to complex **1**.

$[Fe_2(dmpe)_4N_2H]^+$ (11). Formation of this complex via protonation of **10** is favorable by 24 kcal/mol, about 6 kcal/mol more favorable than the protonation of **1** to yield **2a**. Formation of this complex from the dimerization of **1** and **2a** (resulting in the loss of N_2) was also considered, but found to be unfavorable by 15 kcal/mol. The proton bonds to the $d_{xy}\_\pi_y^*$ orbital on N_β. The N-N bond is elongated by 0.07 Å, and the double-bonded character of the N-N bond is greatly reduced, having less double-bonded character than that of the monomer complex **2a**. Despite the fact that the two nitrogen atoms are not equivalent, both nitrogen atoms have nearly the same charge. Both nitrogen atoms are more negatively charged than those in **2a**, with the unprotonated N_α having twice the negative charge compared to the corresponding N_α in **2a** (Table IV). The increased negative charge and N-N bond length suggest this complex is more activated than **2a**. If formed, **11** could dissociate into $[Fe(dmpe)_2N_2H]^{0+}$ and $[Fe(dmpe)_2]^+$ (-5 kcal/mol).

$[Fe_2(dmpe)_4N_2H_2]^{2+}$ (12). Formation of this complex via protonation of **11** is favorable by 31 kcal/mol. This dimer can also be formed by the dimerization of **1** and **6a**, which is favorable by 14 kcal/mol. The N-N bond length is similar to but slightly longer

(by 0.02 Å) than that of the hydrazido complex **7**, but the Fe-N bond lengths are more representative of the monomer diazene complexes (**6a** and **6b**). The N-N bond has no double-bond character, in contrast to **6a** and **6b**, which both contain significant double-bond character. The charge distributions of the nitrogen atoms are similar to, but slightly greater than, that of the hydrazido complex **7**. If formed, **12** could dissociate into $[Fe(dmpe)_2N_2H_2]^+$ and $[Fe(dmpe)_2]^+$ (-16 kcal/mol).

$[Fe_2(dmpe)_4N_2H_3]^{3+}$ (13). Protonation of **12** is favorable by 33 kcal/mol. The N-N bond length is comparable to that of free hydrazine, and is longer than any of the intermediates in the symmetric monomer mechanism. More negative charge is transferred to the singly protonated nitrogen, similar to that of **8**. If formed, **13** would energetically prefer to dissociate into **8** and **16** (-15 kcal/mol), although dissociation into $[Fe(dmpe)_2N_2H_3]^{2+}$ and $[Fe(dmpe)_2]^+$ would also be possible (-8 kcal/mol).

$[Fe_2(dmpe)_4N_2H_4]^{4+}$ (14). Protonation of **13** is unfavorable (+8 kcal/mol). The N-N bond length shortens slightly. The structure becomes asymmetric, as there are two different Fe-N bond lengths (2.154 and 2.434 Å). The charge distribution also reflects this asymmetry. The asymmetry suggests that the complex is beginning to dissociate into complexes **9** and **16**. Indeed, the complete dissociation into **9** and **16** is computed to be favorable by 45 kcal/mol.

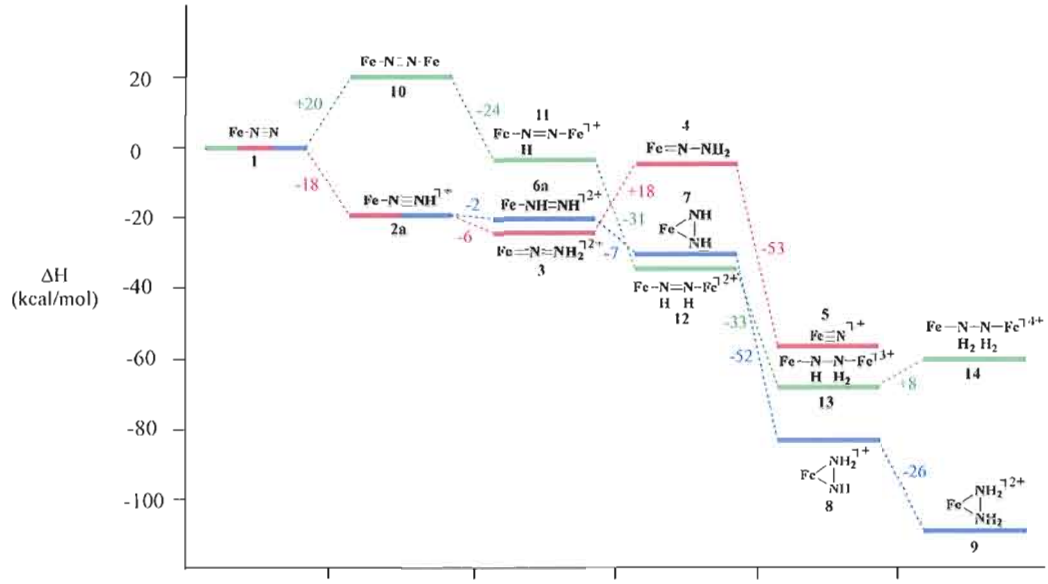

Figure 3. Calculated energy profile for the three schemes: asymmetric monomer mechanism (red), symmetric monomer mechanism (blue), and symmetric dimer mechanism (green). These energies do not include thermal and entropy corrections.

B.4 Discussion

B.4.1 Fe-N_2 Binding Modes

The results of the DFT calculations show that dinitrogen compounds with double or triple-bond character (N_2, N_2H, and all isomers of N_2H_2) prefer to coordinate end-on (η^1) rather than side-on (η^2). In the case of N_2, N_2H, and *iso*-diazene, end-on bonding involves a σ bond between the Fe $d_x2_{-y}2$ orbital and the sp_x orbital of N_α, as well as two π bonds between the Fe d_{xy} and d_{xz} orbitals and the dinitrogen π_y^* and π_z^* orbitals, respectively. Dimer formation (complexes **10** and **11**) provides additional π back-bonding. For the *trans*- and *cis*-diazene complexes (**6a** and **6b**), end-on bonding involves a σ bond between the Fe $d_x2_{-y}2$ orbital and a filled diazene sp^2-like orbital (see Figure S7). Dinitrogen compounds with mostly single-bond character (hydrazido, hydrazine) prefer to

bind in a side-on geometry (η^2). In addition to π back-bonding, this mode may also include σ and π bonding with the dinitrogen π orbitals (e.g. complex **7**).

B.4.2 Initial Site of Protonation

The calculations show that the terminal nitrogen in **1** has significant negative charge, suggesting that this is the site of initial protonation. Indeed, the first protonation of the terminal nitrogen to form **2a** is significantly downhill, with an energy of -19 kcal/mol. However, formation of the iron-hydride complex (**2b**) is nearly 40 kcal/mol more favorable than **2a** (Scheme 1). Much of this energy difference appears to come from the stabilization of the $d_x2_{-y}2$ orbital in **2b** upon binding the proton when compared to **2a**. There is also much less back-bonding from the iron to the dinitrogen antibonding orbitals in complex **2b** compared to **2a**, which lowers the energies of the dinitrogen π-bonding orbitals, as well as the Fe d_{xy} and d_{xz} orbitals, contributing further to the energy difference between **2a** and **2b**. It is suggested that N_β is the kinetic protonation site and the Fe center is the thermodynamic protonation site. The terminal nitrogen is more exposed than the iron, so there is a higher probability that the proton will attack the terminal nitrogen. In addition, the complex has a dipole with the negative end on the terminal nitrogen and the positive end on the iron. The proton would thus be more attracted to the terminal nitrogen and repelled by the iron, further increasing the probability of attacking the nitrogen. Therefore, if the concentration of acid is low, formation of **2a** is more likely to occur, but there may be sufficient time for it to isomerize to **2b** before another proton could be added. On the other hand, a high acid concentration would increase the probability of forming **3** (or **6a** or **6b**) from **2a**. At this point, further protonation of the iron center or isomerization

to an iron-hydride is very unfavorable. The fact that protonation of the iron center is so thermodynamically favorable likely contributes to the small observed yields of ammonia and/or hydrazine in these systems. Experimental work and transition state calculations are underway to explore the kinetic barriers for these two protonation sites.

B.4.3 Protonation of Phosphine Arm

The basicity of the phosphine ligand makes it another potential protonation site. To get an idea of whether or not this could be a side reaction, additional calculations were performed where the iron-phosphine bond was broken, and the free phosphine protonated. This was done for complexes **1**, **2a**, and **3**. Results of the newly optimized complexes indicated that protonation of the phosphine arm with triflic acid was unfavorable by 9 kcal/mol for complex **1**, 21 kcal/mol for complex **2a**, and 27 kcal/mol for complex **3**. In comparison, the first and second protonation of free dmpe by triflic acid was calculated to be -14 and -1 kcal/mol, respectively. Compared to the energetics for protonating the Fe atom or dinitrogen ligand, the protonation of the phosphine arm is not likely to interfere with the reduction of N_2, although such protonation may happen after the release of the nitrogen ligand.

B.4.4 Asymmetric Protonation of $Fe(dmpe)_2N_2$

Studies by Yandulov and Schrock[34] showed that the catalytic reduction of dinitrogen by molybdenum triamidoamine complexes occurs via one-electron reductions and addition of protons to the terminal nitrogen, resulting in the formation of ammonia and a molybdenum nitride complex. This nitride complex is then further reduced and protonated to yield a second equivalent of ammonia. Several intermediates (diazenido,

hydrazido, imido, and amino) for this mechanism have been crystallized.[34] For the iron-dinitrogen system, the addition of the first two protons to the same nitrogen is the most favorable pathway. This is particularly interesting because the calculations indicate that free *iso*-diazene is 17 kcal/mol less stable than free *trans*-diazene, suggesting a 21 kcal/mol net stabilization of *iso*-diazene by the iron-phosphine complex. (This number was obtained by recalling that complex **3** is 4 kcal/mol more stable than complex **6a**.) Most of this stabilization comes from the significant π back-bonding from the iron that is not present in the trans or cis isomers. Addition of a third proton to complex **3** followed by loss of ammonia and formation of an iron-nitride complex is significantly uphill (E=41, G=32 kcal/mol). While the two-electron reduction of **3** by complex **1** to yield an *iso*-hydrazido(2-) complex is only slightly endergonic (G=1 kcal/mol), the E value of 18 suggests a substantial enthalpic barrier. It is concluded that the asymmetric protonation of the coordinated dinitrogen is an unlikely pathway on the route to ammonia in this system.

B.4.5 Symmetric Protonation of $Fe(dmpe)_2N_2$

The symmetric protonation mechanism involves formation of an iron-diazene complex followed by the outer-sphere reduction via a sacrificial $Fe(dmpe)_2N_2$ complex (Scheme 3). While the *iso*-diazene structure **3** has the lowest energy of all diazene isomers considered, the *trans*-diazene isomer is only 4 kcal/mol higher in energy, making it reasonably accessible by direct protonation of **2a** or isomerization of **3**. Whereas two-electron reduction of **3** is endergonic, reduction of **6a** to **7** is exergonic (-21 kcal/mol). Once **7** is formed, two successive protonations of **7** to form complex **9** are highly favorable

(E=-78, G=-71 kcal/mol total). Further protonation of complex **9** to give $N_2H_5^+$ and $[Fe(dmpe)_2]^{2+}$ is slightly favorable (E=+6, G=-8 kcal/mol), but protonation of **9** followed by dissociation of NH_3 from $[Fe(dmpe)_2NH_2]^{3+}$ was found to be highly unfavorable (by nearly 50 kcal/mol). Thus, the mechanism of ammonia formation from this complex is not clear at this time. However, it was shown experimentally that treatment of *cis*-$[Fe(DMeOPrPE)_2(N_2H_4)]^{2+}$ with 1M TfOH produces a mixture of $N_2H_5^+$ (64%) and NH_4^+ (21%) via a disproportionation reaction.[33] Therefore, this pathway produces both hydrazine and ammonia and is energetically favorable (-100 kcal/mol overall).

B.4.6 Outer-Sphere Electron Transfer

A major concern of the outer-sphere electron transfer reactions described above is the amount of reductant (complex **1**) remaining after the initial protonation reactions. Because the initial protonation of complex **1** is about 20 kcal/mol downhill, by the time appreciable amounts of **3** or **6** begin to form, only a minute concentration of **1** would be expected to remain. Thus, it is perhaps unlikely that there would ever be enough of **1** available to drive the production of NH_3 toward the 12-18% yields observed by Leigh et al.[5] and Gilbertson et al.[6] One possibility is that other complexes downstream from **1**, such as **2a** or **7** may participate in either one- or two-electron reductions. Experimental and theoretical studies involving these intermediates as potential reductants are currently underway.

B.4.7 Dimer Mechanism

Dimer formation is another means by which electron transfer may occur. The dimer mechanism involves initial dimerization of two $Fe(dmpe)_2N_2$ complexes followed by four successive protonations leading to a bridged hydrazine species (Scheme 4). At first this appears to be an attractive mechanism because the first three protonations of the bridged dinitrogen are exothermic (-88 kcal/mol overall). However, the calculations show that the initial dimer-formation step leading to the formation of complex **10** is unlikely to occur (+20 kcal/mol). This result is consistent with the spectroscopic characterization of $Fe(DMeOPrPE)_2N_2$, which did not show any evidence for a bridged dinitrogen species.[6] The initial dimerization is a critical step for this mechanism because the protonation of the monomer is sufficiently favorable to prevent the formation of complex **10**.

It is possible that dimer formation occurs at other steps during the progress of the reaction. According to the calculations, dimer formation between complex **1** and complex **6a** to give complex **12** is possible (-14 kcal/mol). Once the diazene bridged iron(0)/iron(II) complex is formed, further protonation to give the hydrazine dimer **14** is downhill. Complex **14** is unstable and prefers to dissociate into an $Fe^{II}(dmpe)_2$ fragment and the *cis*-hydrazine complex **9**. In fact, complexes **11**-**14** all prefer to dissociate back to their monomeric constituents. The inclusion of entropic corrections would further encourage this. Thus, while dimer formation may be possible (e.g. complex **12**), and protonation of these dimers is favorable, it is unlikely that the dimeric/bridged structure itself would be maintained during the course of the reaction. Unfortunately, the formation of dimer **12** from **1** and **6a** suffers from the same problem as the outer-sphere electron

transfer mechanism described above. That is, there would be minimal amounts of **1** available to dimerize with **6a**. Alternative mechanisms in which electron transfer is not required are described next.

B.4.8 Disproportionation Mechanisms

It is possible that no electron transfer is required and that the first two protonation steps to form diazene are sufficient. Free diazene readily disproportionates in solution to N_2 and N_2H_4 (eq 2), and N_2H_4 could further disproportionate into N_2, H_2 and NH_3 (eq 3).

$$2N_2H_2 \longrightarrow N_2H_4 + N_2 \qquad (2)$$

$$3N_2H_4 \longrightarrow 4NH_3 + N_2 \qquad (3)$$

The dissociation energies of diazene in complexes **3**, **6a**, and **6b** range between 15 kcal/mol (*trans*-diazene) to 35 kcal/mol (*iso*-diazene). These results suggest that the iron-phosphine complex would stabilize the diazene, rather than promote disproportionation. Nevertheless, two disproportionation pathways were considered. One possibility is that another molecule, such as solvent (THF) or counterion (triflate), could displace the diazene molecule, releasing it into solution (eqs 4 and 5).

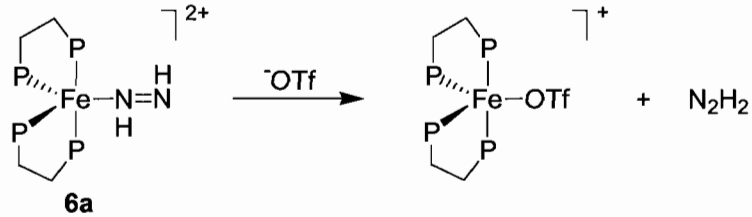

6a (4)

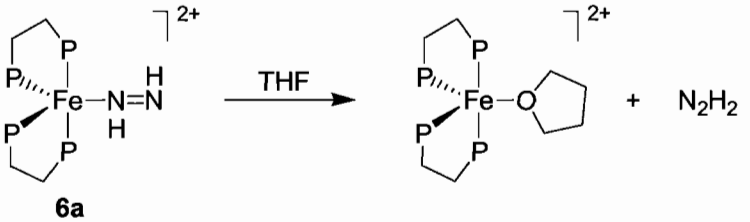

6a (5)

Binding of THF to the Fe^{II} form was found to be unfavorable, so THF is unlikely to displace diazene. However, binding of triflate to the Fe^{II} form was found to be favorable by about 11 kcal/mol, which is comparable to the dissociation energy of *trans*-diazene. Because the difference in energy between the *trans*-diazene complex and the lower energy *iso*-diazene complex is 4 kcal/mol, it is possible that, as *trans*-diazene is formed, it may be displaced by triflate. Because *trans*-diazene readily decomposes in solution, this would tend to drive the reaction towards the dissociation and disproportionation of diazene, leaving an iron-phosphine-triflate adduct. However, this mechanism leads to the formation of N_2H_4, and does not account for the observed yields of NH_3.

Another disproportionation pathway involves a bis-diazene complex. Optimizations of **6a** and **6b** yielded a square-pyramidal structure, suggesting that the complex might accommodate another ligand to form an octahedral complex. It is possible that another diazene can bind at the vacant position, possibly involving dimer formation with another **6a** or **6b** complex. If two diazene molecules were to bind to the complex, the newly formed six-coordinate complex might facilitate the disproportionation of diazene into N_2 and N_2H_4 by keeping the two diazene ligands in close proximity (Scheme 5). The resulting N_2 could then be displaced by another diazene, with subsequent mediated disproportionation of the diazene and hydrazine to generate ammonia.

B.5 Conclusions

Density functional calculations were performed on several potential intermediates

(but no transition states) for the reduction of N_2 to NH_3 by $Fe(dmpe)_2$. Three mechanisms were compared: an asymmetric monomer mechanism that involves successive protonation at the terminal nitrogen (Scheme 2), a symmetric monomer mechanism that proceeds through diazene and hydrazine intermediates (Scheme 3), and a dimer mechanism in which reduction takes place through a bridged dinitrogen species (Scheme 4).

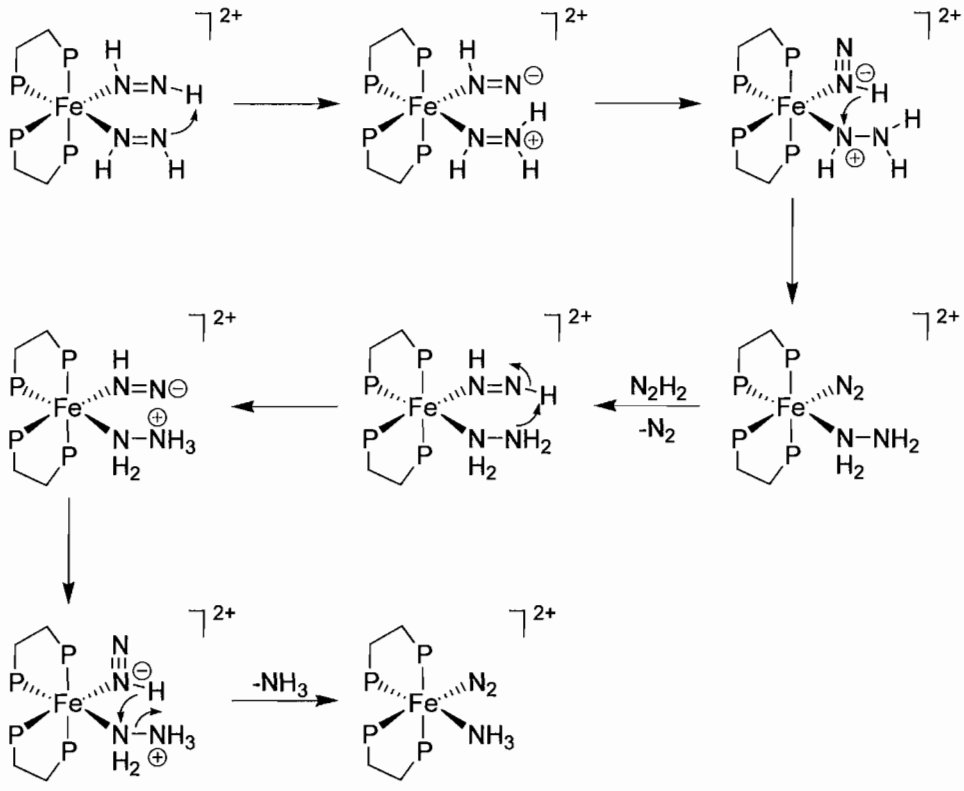

Scheme 5. Mechanism involving iron mediated disproportionation of diazene.

The dimer mechanism involving a bridged dinitrogen has several exothermic protonation steps, but the calculations indicate that the critical step of forming a bridged dinitrogen intermediate is highly unfavorable. Formation of a bridging diazene intermediate is favorable, but it relies on the presence of a sacrificial $Fe(dmpe)_2N_2$, whose

concentration may quickly vanish with an excess of strong acid. In addition, maintaining a dimer through each protonation step would be problematic, as each intermediate would prefer to dissociate into different monomeric intermediates.

Both monomer mechanisms begin with N_2 bonded in an end-on fashion to the $Fe(dmpe)_2$ moiety. Initial protonation at the terminal nitrogen forms **2a**, which is necessary in order to achieve NH_3 production and to avoid the formation of the inert thermodynamic product **2b**. The asymmetric addition of the second proton to form the *iso*-diazene complex **3** is slightly more favored than the symmetric addition to form **6a** or **6b**. However, additional protonation or two-electron reduction of this intermediate (complex 3) is highly unfavorable.

The most favorable of the three mechanisms tested is the symmetric monomer mechanism. This pathway involves alternating protonation steps, first at the distal nitrogen followed by the proximal nitrogen to form **6a**. (Alternatively, the formation of **6a** could proceed through isomerization of **3**.) At this point, a two-electron reduction occurs by an outer-sphere mechanism from complex **1**, resulting in complex **7**. Successive protonations of **7** are sufficient to drive the production of $N_2H_5^+$, but the exact mechanism leading to ammonia formation remains unclear (although experimentally we have shown disproportionation of N_2H_4 to NH_3 to be possible). Like the dimer mechanism, the symmetric monomer mechanism also relies on remaining amounts of $Fe(dmpe)_2N_2$, which in the presence of a strong acid may not be available in sufficient concentration at this point in the reaction. Should this be the case, the electron transfer step may involve other reductants such as **2a** or **7**.

APPENDIX C

SUPPORTING INFORMATION FOR CHAPTER II

C.1 Spectra

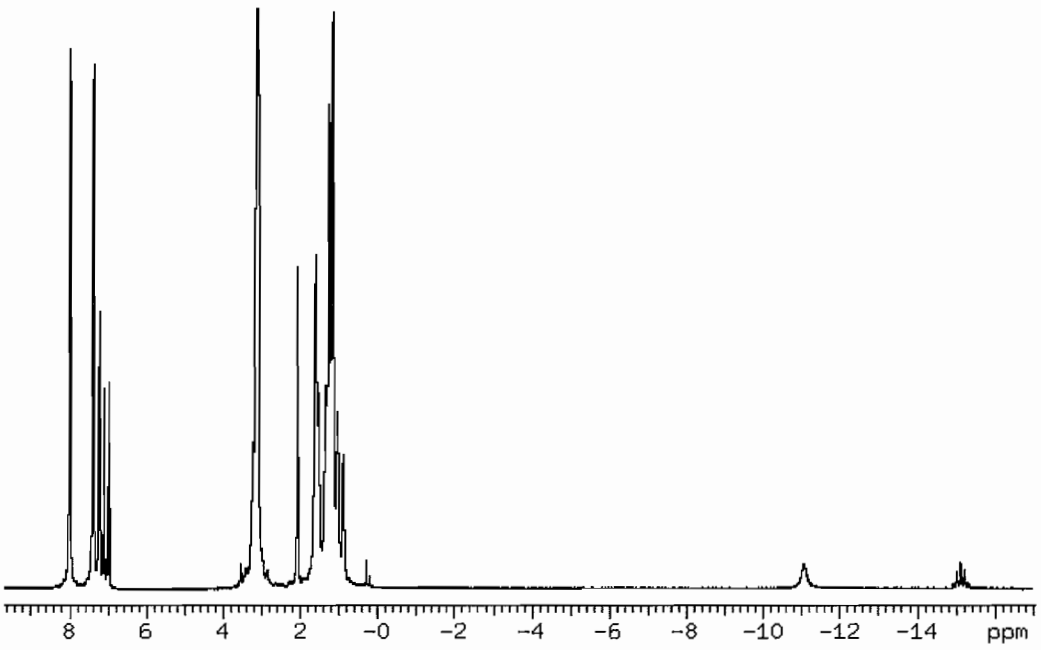

Figure C.1.1. ^{1}H NMR spectrum (toluene-d_8) at 233K of *trans*-[Fe(DMeOPrPE)$_2$(H_2)H][BPh_4].

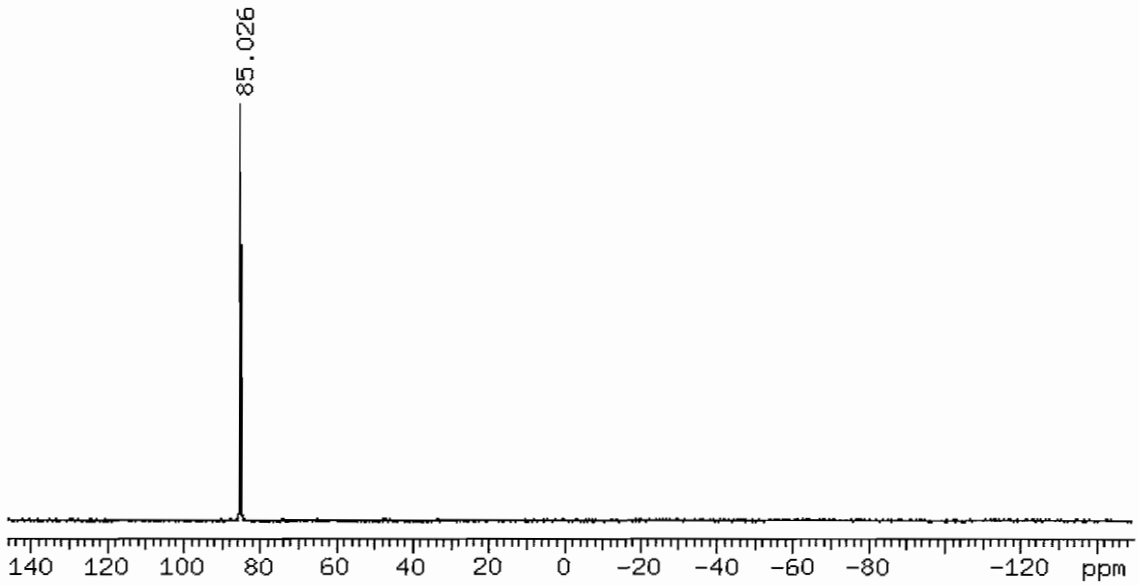

Figure C.1.2. $^{31}P\{^{1}H\}$ NMR spectrum (toluene-d_8) of *trans*-[Fe(DMeOPrPE)$_2$(H_2)H][BPh_4].

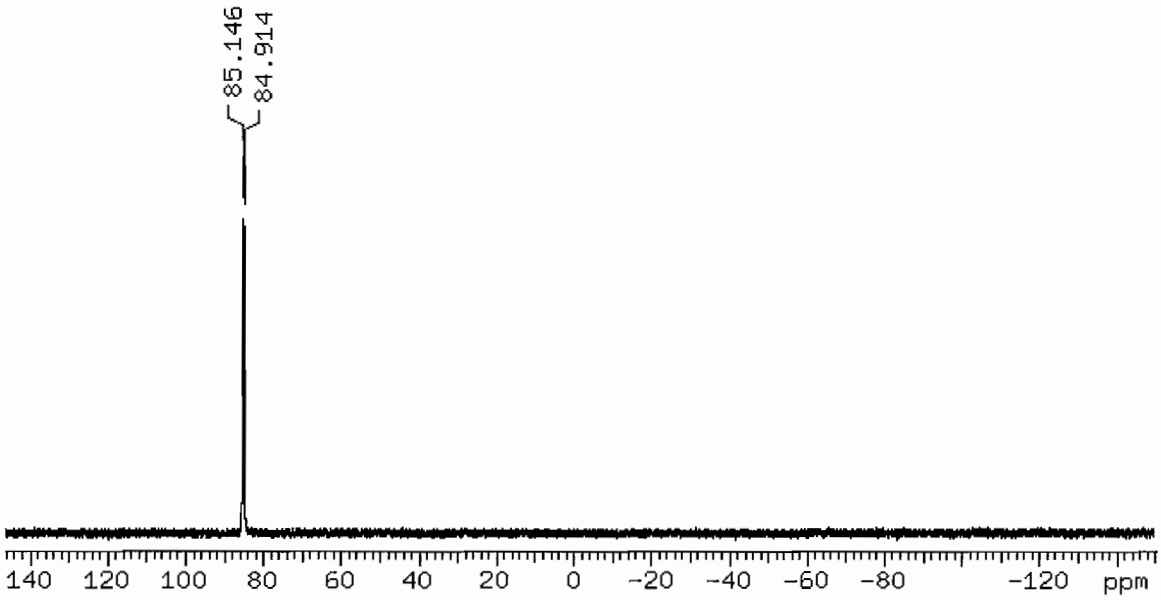

Figure C.1.3. ^{31}P NMR spectrum (toluene-d_8) at 233K of *trans*-[Fe(DMeOPrPE)$_2$(H_2)H][BPh_4].

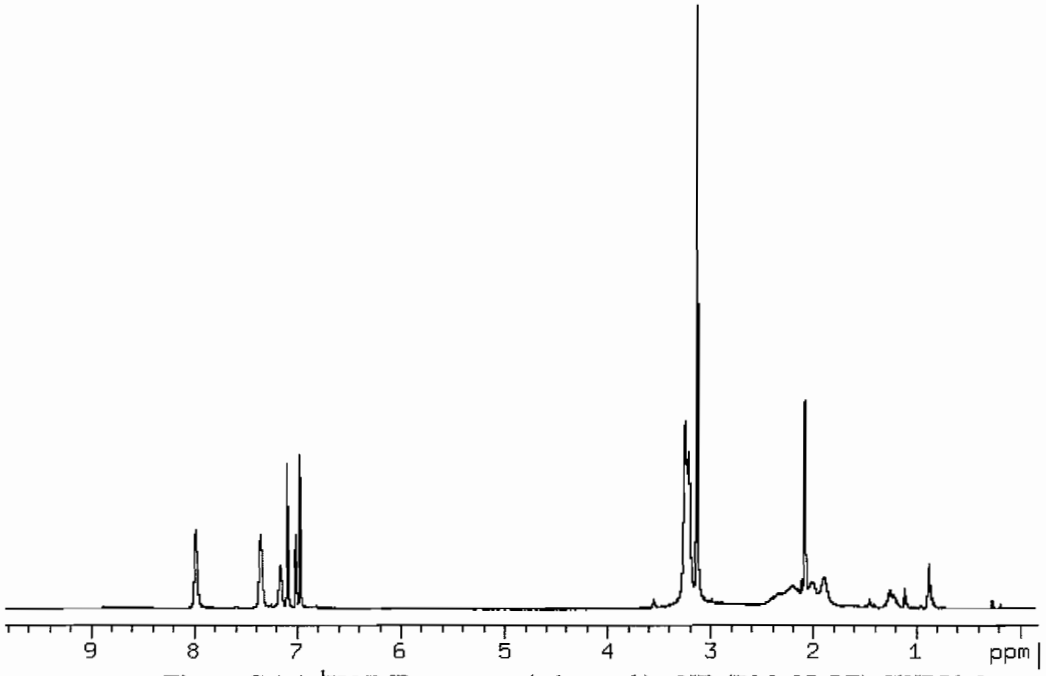

Figure C.1.4. ^{1}H NMR spectrum (toluene-d_8) of $[Fe(DMeOPrPE)_2Cl][BPh_4]$.

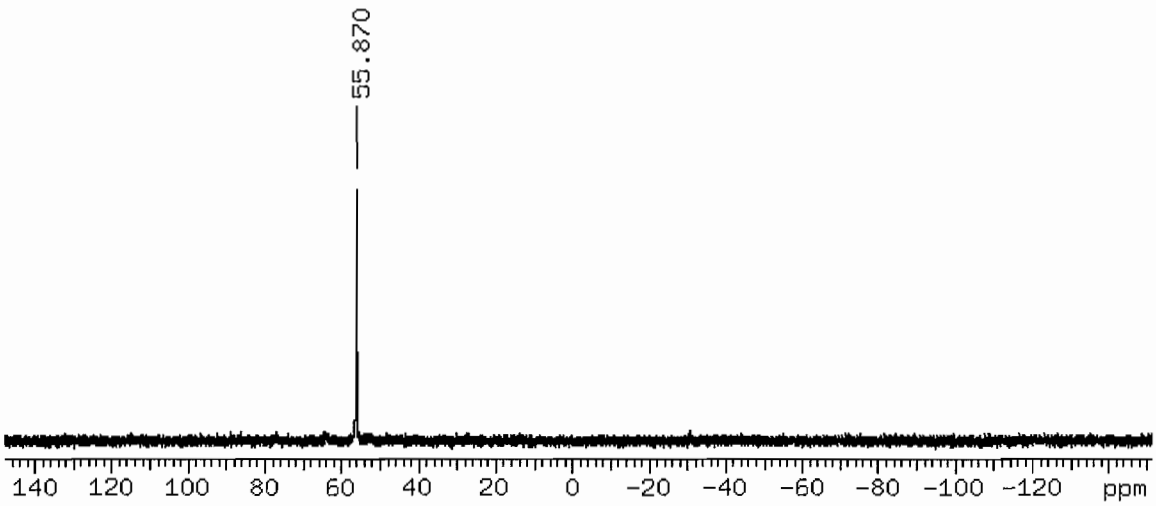

Figure C.1.5. $^{31}P\{^{1}H\}$ NMR spectrum (toluene-d_8) at 193K of $[Fe(DMeOPrPE)_2Cl][BPh_4]$.

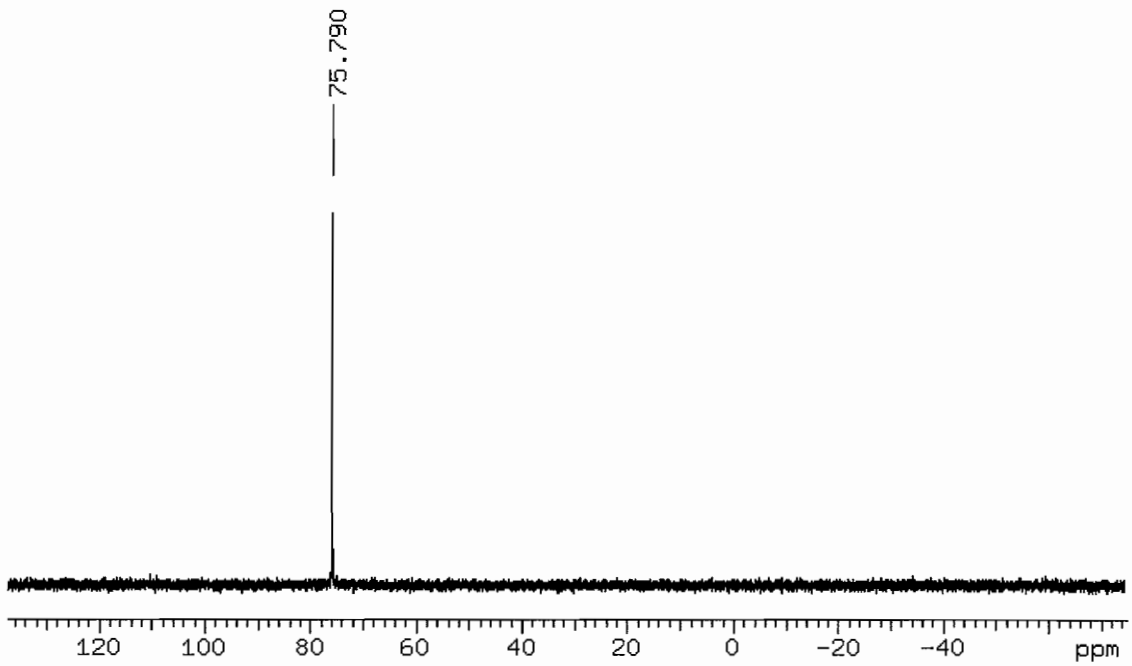

Figure C.1.6. $^{31}P\{^{1}H\}$ NMR spectrum of *trans*-[Fe(DMeOPrPE)$_2$H(N$_2$)][BPh$_4$].

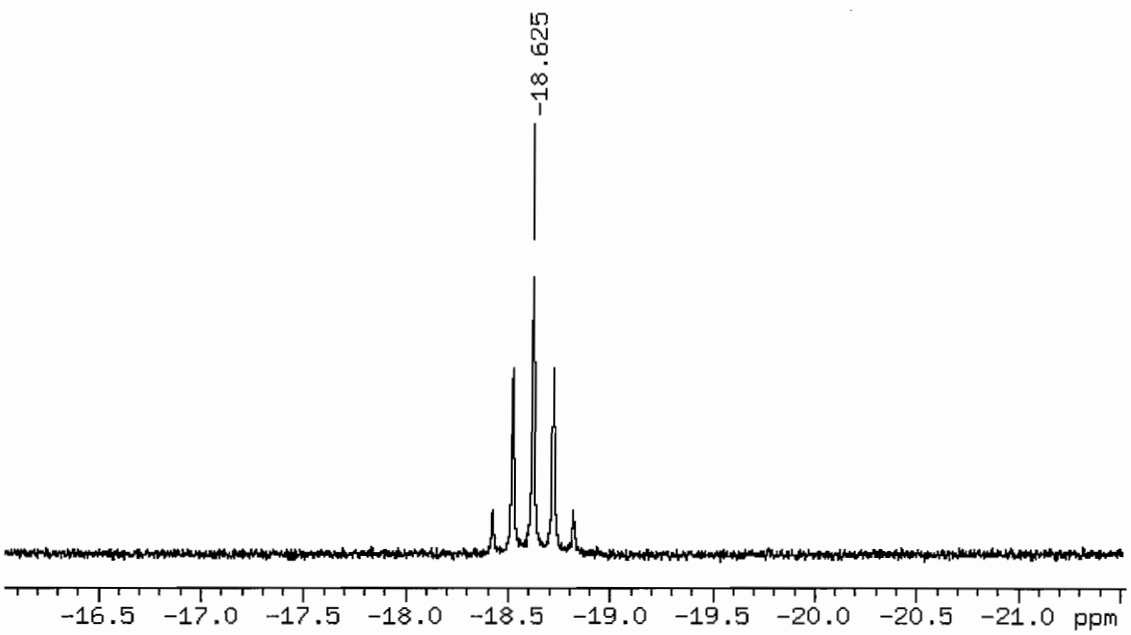

Figure C.1.7. ^{1}H NMR spectrum of the hydride region of *trans*-[Fe(DMeOPrPE)$_2$H(N$_2$)][BPh$_4$].

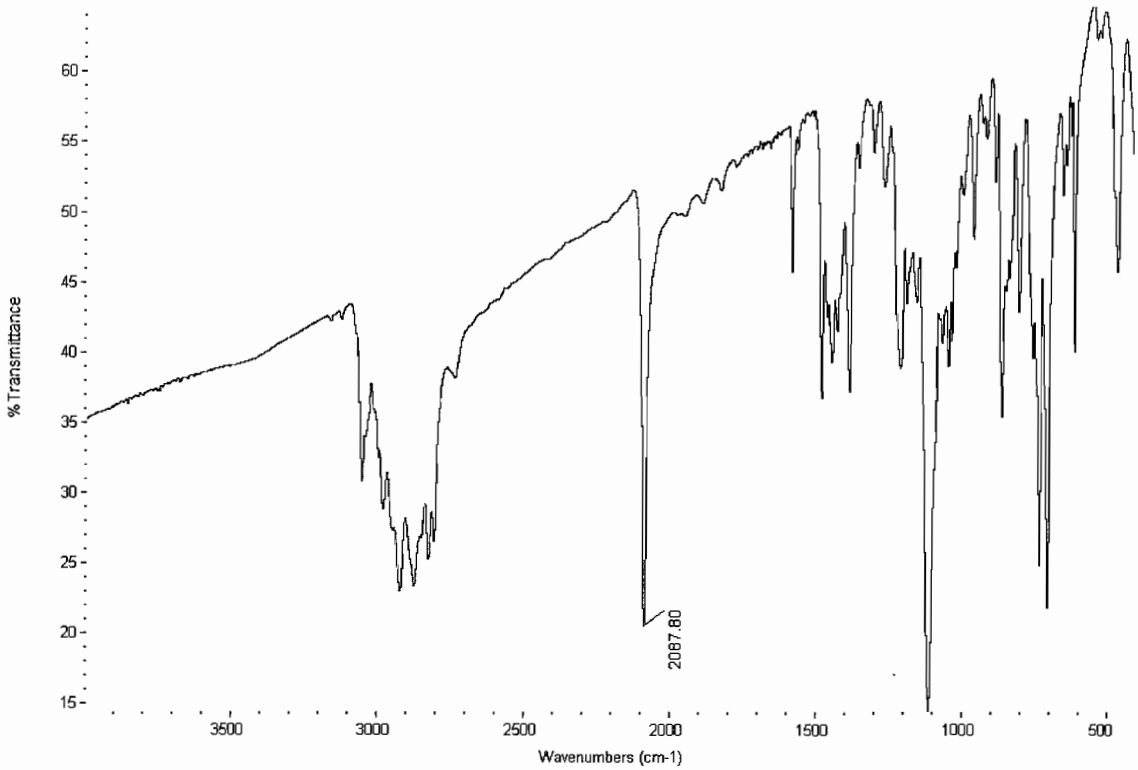

Figure C.1.8. IR spectrum (KBr pellet) of *trans*-[Fe(DMeOPrPE)$_2$H(N$_2$)][BPh$_4$].

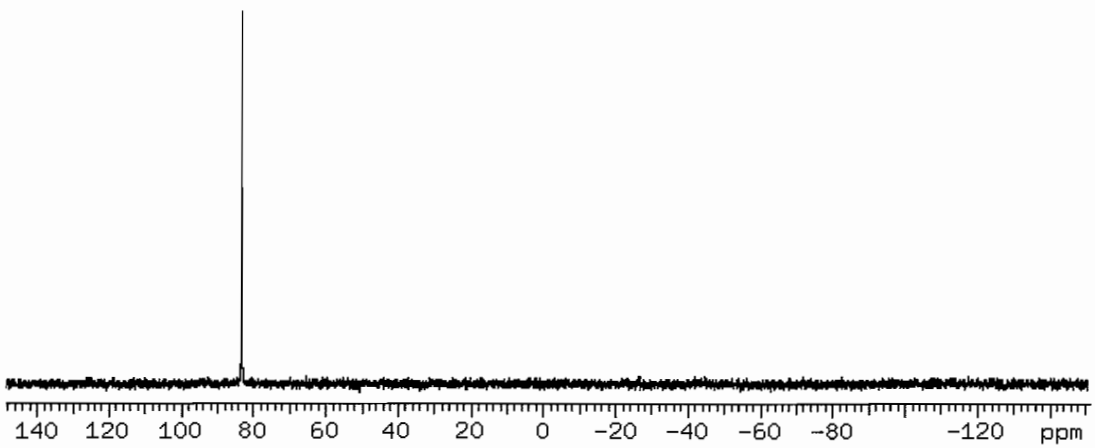

Figure C.1.9. $^{31}P\{^1H\}$ NMR spectrum of *trans*-Fe(DMeOPrPE)$_2$HCl.

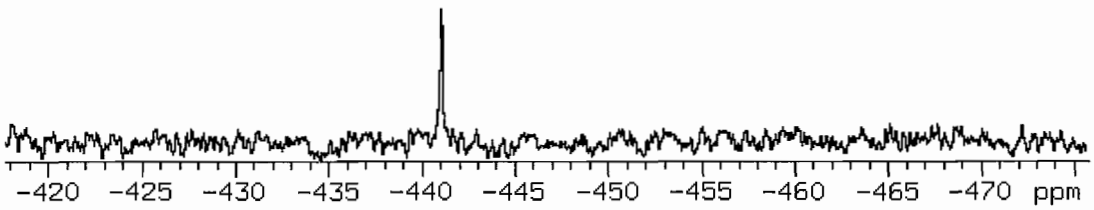

Figure C.1.10. $^{15}N\{^{1}H\}$ NMR spectrum of *trans*-[Fe(DMeOPrPE)$_2$H($^{15}NH_3$)][BPh$_4$].

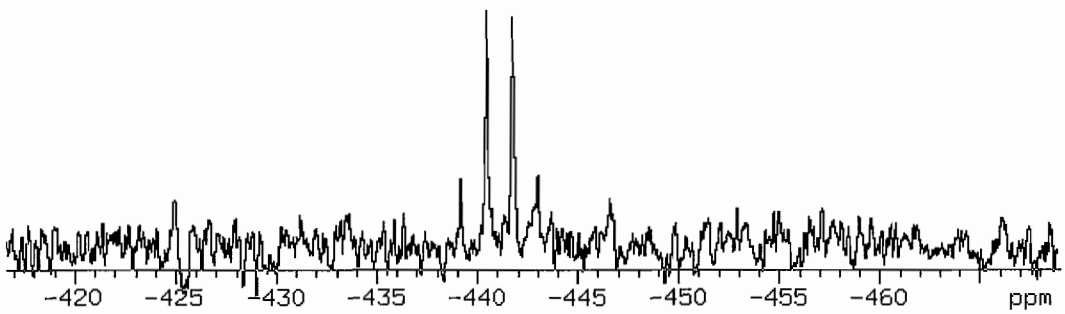

Figure C.1.11. ^{15}N NMR spectrum of *trans*-[Fe(DMeOPrPE)$_2$H($^{15}NH_3$)][BPh$_4$].

C.2 Crystal data for *trans*-Fe(DMeOEtPE)$_2$Cl$_2$

Table C.2.1. Crystal data and structure refinement for *trans*-Fe(DMeOEtPE)$_2$Cl$_2$.

Identification code	just7	
Empirical formula	C28 H64 Cl2 Fe O8 P4	
Formula weight	779.42	
Temperature	173(2) K	
Wavelength	0.71073 Å	
Crystal system	Monoclinic	
Space group	P2(1)/c	
Unit cell dimensions	a = 12.3417(7) Å	α = 90°.
	b = 12.1825(7) Å	β = 100.1240(10)°.
	c = 25.3621(15) Å	γ = 90°.
Volume	3753.9(4) Å^3	
Z	4	
Density (calculated)	1.379 Mg/m^3	
Absorption coefficient	0.757 mm^{-1}	
F(000)	1664	
Crystal size	0.32 x 0.19 x 0.09 mm^3	
Theta range for data collection	1.63 to 27.00°.	
Index ranges	-15<=h<=15, -15<=k<=15, -32<=l<=32	
Reflections collected	41489	
Independent reflections	8193 [R(int) = 0.0327]	
Completeness to theta = 27.00°	99.9 %	
Absorption correction	Semi-empirical from equivalents	
Max. and min. transmission	0.9350 and 0.7936	
Refinement method	Full-matrix least-squares on F^2	
Data / restraints / parameters	8193 / 0 / 388	
Goodness-of-fit on F^2	1.028	
Final R indices [I>2sigma(I)]	R1 = 0.0340, wR2 = 0.0876	
R indices (all data)	R1 = 0.0416, wR2 = 0.0941	
Largest diff. peak and hole	1.699 and -0.524 e.Å^{-3}	

Table C.2.2. Atomic coordinates (x 10^4) and equivalent isotropic displacement parameters ($Å^2$x 10^3) for *trans*-Fe(DMeOEtPE)$_2$Cl$_2$. U(eq) is defined as one third of the trace of the orthogonalized U^{ij} tensor.

	x	y	z	U(eq)
Fe(1)	2225(1)	9748(1)	1944(1)	15(1)
Cl(1)	864(1)	8377(1)	1879(1)	22(1)
Cl(2)	3562(1)	11136(1)	2003(1)	22(1)
P(1)	3013(1)	8752(1)	1362(1)	17(1)
P(2)	3309(1)	8723(1)	2579(1)	18(1)
P(3)	1337(1)	10647(1)	2531(1)	17(1)
P(4)	1120(1)	10742(1)	1300(1)	17(1)
O(1)	1924(2)	7164(1)	-46(1)	40(1)
O(2)	5412(1)	10302(1)	720(1)	34(1)
O(3)	2690(1)	6027(1)	2650(1)	35(1)
O(4)	5702(2)	9513(2)	3832(1)	64(1)
O(5)	2794(1)	11284(1)	3712(1)	34(1)
O(6)	-386(2)	9674(1)	3682(1)	38(1)
O(7)	-1827(1)	9805(1)	354(1)	32(1)
O(8)	1537(1)	12963(1)	149(1)	30(1)
C(1)	3520(2)	7470(2)	1706(1)	22(1)
C(2)	4166(2)	7793(2)	2252(1)	21(1)
C(3)	60(2)	11204(2)	2136(1)	22(1)
C(4)	348(2)	11745(2)	1635(1)	22(1)
C(5)	2196(2)	8279(2)	728(1)	21(1)
C(6)	2668(2)	7357(2)	436(1)	25(1)
C(7)	2245(3)	6320(2)	-361(1)	46(1)
C(8)	4314(2)	9209(2)	1171(1)	24(1)
C(9)	4309(2)	10196(2)	811(1)	27(1)
C(10)	5572(2)	11256(2)	427(1)	40(1)
C(11)	2635(2)	7818(2)	3014(1)	27(1)
C(12)	3051(2)	6653(2)	3119(1)	31(1)
C(13)	3024(3)	4922(2)	2711(1)	59(1)
C(14)	4312(2)	9458(2)	3069(1)	28(1)
C(15)	5095(2)	8796(2)	3467(1)	43(1)
C(16)	6081(3)	9017(3)	4329(1)	71(1)
C(17)	1872(2)	11948(2)	2857(1)	25(1)
C(18)	2925(2)	11940(2)	3265(1)	26(1)
C(19)	3712(2)	11381(2)	4134(1)	41(1)
C(20)	821(2)	9875(2)	3057(1)	23(1)
C(21)	-96(2)	10407(2)	3294(1)	26(1)
C(22)	-1338(2)	10037(2)	3872(1)	39(1)
C(23)	49(2)	9987(2)	835(1)	23(1)
C(24)	-1101(2)	10477(2)	717(1)	26(1)
C(25)	-2284(2)	8934(2)	616(1)	38(1)
C(26)	1731(2)	11614(2)	840(1)	23(1)
C(27)	924(2)	12292(2)	452(1)	26(1)
C(28)	831(2)	13495(2)	-276(1)	39(1)

Table C.2.3. Bond lengths [Å] and angles [°] for *trans*-Fe(DMeOEtPE)$_2$Cl$_2$.

Fe(1)-P(1)	2.2581(6)
Fe(1)-P(2)	2.2770(5)
Fe(1)-P(3)	2.2792(6)
Fe(1)-P(4)	2.2814(5)
Fe(1)-Cl(2)	2.3491(5)
Fe(1)-Cl(1)	2.3529(5)
P(1)-C(5)	1.835(2)
P(1)-C(8)	1.843(2)
P(1)-C(1)	1.843(2)
P(2)-C(14)	1.827(2)
P(2)-C(2)	1.843(2)
P(2)-C(11)	1.857(2)
P(3)-C(20)	1.836(2)
P(3)-C(3)	1.842(2)
P(3)-C(17)	1.854(2)
P(4)-C(26)	1.836(2)
P(4)-C(4)	1.845(2)
P(4)-C(23)	1.853(2)
O(1)-C(7)	1.401(3)
O(1)-C(6)	1.414(2)
O(2)-C(10)	1.411(3)
O(2)-C(9)	1.426(3)
O(3)-C(13)	1.409(3)
O(3)-C(12)	1.417(3)
O(4)-C(15)	1.391(3)
O(4)-C(16)	1.402(4)
O(5)-C(18)	1.418(3)
O(5)-C(19)	1.421(3)
O(6)-C(22)	1.417(3)
O(6)-C(21)	1.420(3)
O(7)-C(25)	1.421(3)
O(7)-C(24)	1.425(3)
O(8)-C(28)	1.417(3)
O(8)-C(27)	1.427(2)
C(1)-C(2)	1.523(3)
C(1)-H(1A)	0.9900
C(1)-H(1B)	0.9900
C(2)-H(2A)	0.9900
C(2)-H(2B)	0.9900
C(3)-C(4)	1.529(3)
C(3)-H(3A)	0.9900
C(3)-H(3B)	0.9900
C(4)-H(4A)	0.9900
C(4)-H(4B)	0.9900
C(5)-C(6)	1.517(3)
C(5)-H(5A)	0.9900
C(5)-H(5B)	0.9900
C(6)-H(6A)	0.9900
C(6)-H(6B)	0.9900
C(7)-H(7A)	0.9800
C(7)-H(7B)	0.9800

C(7)-H(7C)	0.9800
C(8)-C(9)	1.508(3)
C(8)-H(8A)	0.9900
C(8)-H(8B)	0.9900
C(9)-H(9A)	0.9900
C(9)-H(9B)	0.9900
C(10)-H(10A)	0.9800
C(10)-H(10B)	0.9800
C(10)-H(10C)	0.9800
C(11)-C(12)	1.517(3)
C(11)-H(11A)	0.9900
C(11)-H(11B)	0.9900
C(12)-H(12A)	0.9900
C(12)-H(12B)	0.9900
C(13)-H(13A)	0.9800
C(13)-H(13B)	0.9800
C(13)-H(13C)	0.9800
C(14)-C(15)	1.505(3)
C(14)-H(14A)	0.9900
C(14)-H(14B)	0.9900
C(15)-H(15A)	0.9900
C(15)-H(15B)	0.9900
C(16)-H(16A)	0.9800
C(16)-H(16B)	0.9800
C(16)-H(16C)	0.9800
C(17)-C(18)	1.513(3)
C(17)-H(17A)	0.9900
C(17)-H(17B)	0.9900
C(18)-H(18A)	0.9900
C(18)-H(18B)	0.9900
C(19)-H(19A)	0.9800
C(19)-H(19B)	0.9800
C(19)-H(19C)	0.9800
C(20)-C(21)	1.517(3)
C(20)-H(20A)	0.9900
C(20)-H(20B)	0.9900
C(21)-H(21A)	0.9900
C(21)-H(21B)	0.9900
C(22)-H(22A)	0.9800
C(22)-H(22B)	0.9800
C(22)-H(22C)	0.9800
C(23)-C(24)	1.521(3)
C(23)-H(23A)	0.9900
C(23)-H(23B)	0.9900
C(24)-H(24A)	0.9900
C(24)-H(24B)	0.9900
C(25)-H(25A)	0.9800
C(25)-H(25B)	0.9800
C(25)-H(25C)	0.9800
C(26)-C(27)	1.515(3)
C(26)-H(26A)	0.9900
C(26)-H(26B)	0.9900
C(27)-H(27A)	0.9900

C(27)-H(27B)	0.9900
C(28)-H(28A)	0.9800
C(28)-H(28B)	0.9800
C(28)-H(28C)	0.9800
P(1)-Fe(1)-P(2)	84.29(2)
P(1)-Fe(1)-P(3)	175.71(2)
P(2)-Fe(1)-P(3)	95.23(2)
P(1)-Fe(1)-P(4)	95.17(2)
P(2)-Fe(1)-P(4)	178.82(2)
P(3)-Fe(1)-P(4)	85.23(2)
P(1)-Fe(1)-Cl(2)	92.85(2)
P(2)-Fe(1)-Cl(2)	91.75(2)
P(3)-Fe(1)-Cl(2)	91.43(2)
P(4)-Fe(1)-Cl(2)	89.33(2)
P(1)-Fe(1)-Cl(1)	87.59(2)
P(2)-Fe(1)-Cl(1)	89.07(2)
P(3)-Fe(1)-Cl(1)	88.14(2)
P(4)-Fe(1)-Cl(1)	89.85(2)
Cl(2)-Fe(1)-Cl(1)	179.11(2)
C(5)-P(1)-C(8)	103.52(10)
C(5)-P(1)-C(1)	103.72(9)
C(8)-P(1)-C(1)	98.16(10)
C(5)-P(1)-Fe(1)	120.51(7)
C(8)-P(1)-Fe(1)	120.35(7)
C(1)-P(1)-Fe(1)	107.17(7)
C(14)-P(2)-C(2)	103.50(10)
C(14)-P(2)-C(11)	102.01(11)
C(2)-P(2)-C(11)	104.70(10)
C(14)-P(2)-Fe(1)	117.16(7)
C(2)-P(2)-Fe(1)	109.34(6)
C(11)-P(2)-Fe(1)	118.47(7)
C(20)-P(3)-C(3)	102.18(10)
C(20)-P(3)-C(17)	104.79(10)
C(3)-P(3)-C(17)	97.55(10)
C(20)-P(3)-Fe(1)	119.80(7)
C(3)-P(3)-Fe(1)	106.55(7)
C(17)-P(3)-Fe(1)	121.90(7)
C(26)-P(4)-C(4)	102.21(9)
C(26)-P(4)-C(23)	102.07(10)
C(4)-P(4)-C(23)	104.67(9)
C(26)-P(4)-Fe(1)	120.08(7)
C(4)-P(4)-Fe(1)	108.37(6)
C(23)-P(4)-Fe(1)	117.48(7)
C(7)-O(1)-C(6)	114.15(19)
C(10)-O(2)-C(9)	112.74(18)
C(13)-O(3)-C(12)	112.2(2)
C(15)-O(4)-C(16)	112.6(2)
C(18)-O(5)-C(19)	111.58(18)
C(22)-O(6)-C(21)	111.39(17)
C(25)-O(7)-C(24)	112.52(17)
C(28)-O(8)-C(27)	111.06(17)
C(2)-C(1)-P(1)	106.94(14)

C(2)-C(1)-H(1A)	110.3
P(1)-C(1)-H(1A)	110.3
C(2)-C(1)-H(1B)	110.3
P(1)-C(1)-H(1B)	110.3
H(1A)-C(1)-H(1B)	108.6
C(1)-C(2)-P(2)	108.53(13)
C(1)-C(2)-H(2A)	110.0
P(2)-C(2)-H(2A)	110.0
C(1)-C(2)-H(2B)	110.0
P(2)-C(2)-H(2B)	110.0
H(2A)-C(2)-H(2B)	108.4
C(4)-C(3)-P(3)	108.03(14)
C(4)-C(3)-H(3A)	110.1
P(3)-C(3)-H(3A)	110.1
C(4)-C(3)-H(3B)	110.1
P(3)-C(3)-H(3B)	110.1
H(3A)-C(3)-H(3B)	108.4
C(3)-C(4)-P(4)	108.11(13)
C(3)-C(4)-H(4A)	110.1
P(4)-C(4)-H(4A)	110.1
C(3)-C(4)-H(4B)	110.1
P(4)-C(4)-H(4B)	110.1
H(4A)-C(4)-H(4B)	108.4
C(6)-C(5)-P(1)	117.48(14)
C(6)-C(5)-H(5A)	107.9
P(1)-C(5)-H(5A)	107.9
C(6)-C(5)-H(5B)	107.9
P(1)-C(5)-H(5B)	107.9
H(5A)-C(5)-H(5B)	107.2
O(1)-C(6)-C(5)	107.35(16)
O(1)-C(6)-H(6A)	110.2
C(5)-C(6)-H(6A)	110.2
O(1)-C(6)-H(6B)	110.2
C(5)-C(6)-H(6B)	110.2
H(6A)-C(6)-H(6B)	108.5
O(1)-C(7)-H(7A)	109.5
O(1)-C(7)-H(7B)	109.5
H(7A)-C(7)-H(7B)	109.5
O(1)-C(7)-H(7C)	109.5
H(7A)-C(7)-H(7C)	109.5
H(7B)-C(7)-H(7C)	109.5
C(9)-C(8)-P(1)	119.28(15)
C(9)-C(8)-H(8A)	107.5
P(1)-C(8)-H(8A)	107.5
C(9)-C(8)-H(8B)	107.5
P(1)-C(8)-H(8B)	107.5
H(8A)-C(8)-H(8B)	107.0
O(2)-C(9)-C(8)	105.55(17)
O(2)-C(9)-H(9A)	110.6
C(8)-C(9)-H(9A)	110.6
O(2)-C(9)-H(9B)	110.6
C(8)-C(9)-H(9B)	110.6
H(9A)-C(9)-H(9B)	108.8

O(2)-C(10)-H(10A)	109.5
O(2)-C(10)-H(10B)	109.5
H(10A)-C(10)-H(10B)	109.5
O(2)-C(10)-H(10C)	109.5
H(10A)-C(10)-H(10C)	109.5
H(10B)-C(10)-H(10C)	109.5
C(12)-C(11)-P(2)	119.17(15)
C(12)-C(11)-H(11A)	107.5
P(2)-C(11)-H(11A)	107.5
C(12)-C(11)-H(11B)	107.5
P(2)-C(11)-H(11B)	107.5
H(11A)-C(11)-H(11B)	107.0
O(3)-C(12)-C(11)	107.94(18)
O(3)-C(12)-H(12A)	110.1
C(11)-C(12)-H(12A)	110.1
O(3)-C(12)-H(12B)	110.1
C(11)-C(12)-H(12B)	110.1
H(12A)-C(12)-H(12B)	108.4
O(3)-C(13)-H(13A)	109.5
O(3)-C(13)-H(13B)	109.5
H(13A)-C(13)-H(13B)	109.5
O(3)-C(13)-H(13C)	109.5
H(13A)-C(13)-H(13C)	109.5
H(13B)-C(13)-H(13C)	109.5
C(15)-C(14)-P(2)	118.23(16)
C(15)-C(14)-H(14A)	107.8
P(2)-C(14)-H(14A)	107.8
C(15)-C(14)-H(14B)	107.8
P(2)-C(14)-H(14B)	107.8
H(14A)-C(14)-H(14B)	107.1
O(4)-C(15)-C(14)	108.5(2)
O(4)-C(15)-H(15A)	110.0
C(14)-C(15)-H(15A)	110.0
O(4)-C(15)-H(15B)	110.0
C(14)-C(15)-H(15B)	110.0
H(15A)-C(15)-H(15B)	108.4
O(4)-C(16)-H(16A)	109.5
O(4)-C(16)-H(16B)	109.5
H(16A)-C(16)-H(16B)	109.5
O(4)-C(16)-H(16C)	109.5
H(16A)-C(16)-H(16C)	109.5
H(16B)-C(16)-H(16C)	109.5
C(18)-C(17)-P(3)	119.71(15)
C(18)-C(17)-H(17A)	107.4
P(3)-C(17)-H(17A)	107.4
C(18)-C(17)-H(17B)	107.4
P(3)-C(17)-H(17B)	107.4
H(17A)-C(17)-H(17B)	106.9
O(5)-C(18)-C(17)	110.17(18)
O(5)-C(18)-H(18A)	109.6
C(17)-C(18)-H(18A)	109.6
O(5)-C(18)-H(18B)	109.6
C(17)-C(18)-H(18B)	109.6

H(18A)-C(18)-H(18B)	108.1
O(5)-C(19)-H(19A)	109.5
O(5)-C(19)-H(19B)	109.5
H(19A)-C(19)-H(19B)	109.5
O(5)-C(19)-H(19C)	109.5
H(19A)-C(19)-H(19C)	109.5
H(19B)-C(19)-H(19C)	109.5
C(21)-C(20)-P(3)	116.59(14)
C(21)-C(20)-H(20A)	108.1
P(3)-C(20)-H(20A)	108.1
C(21)-C(20)-H(20B)	108.1
P(3)-C(20)-H(20B)	108.1
H(20A)-C(20)-H(20B)	107.3
O(6)-C(21)-C(20)	107.60(17)
O(6)-C(21)-H(21A)	110.2
C(20)-C(21)-H(21A)	110.2
O(6)-C(21)-H(21B)	110.2
C(20)-C(21)-H(21B)	110.2
H(21A)-C(21)-H(21B)	108.5
O(6)-C(22)-H(22A)	109.5
O(6)-C(22)-H(22B)	109.5
H(22A)-C(22)-H(22B)	109.5
O(6)-C(22)-H(22C)	109.5
H(22A)-C(22)-H(22C)	109.5
H(22B)-C(22)-H(22C)	109.5
C(24)-C(23)-P(4)	117.85(15)
C(24)-C(23)-H(23A)	107.8
P(4)-C(23)-H(23A)	107.8
C(24)-C(23)-H(23B)	107.8
P(4)-C(23)-H(23B)	107.8
H(23A)-C(23)-H(23B)	107.2
O(7)-C(24)-C(23)	111.16(18)
O(7)-C(24)-H(24A)	109.4
C(23)-C(24)-H(24A)	109.4
O(7)-C(24)-H(24B)	109.4
C(23)-C(24)-H(24B)	109.4
H(24A)-C(24)-H(24B)	108.0
O(7)-C(25)-H(25A)	109.5
O(7)-C(25)-H(25B)	109.5
H(25A)-C(25)-H(25B)	109.5
O(7)-C(25)-H(25C)	109.5
H(25A)-C(25)-H(25C)	109.5
H(25B)-C(25)-H(25C)	109.5
C(27)-C(26)-P(4)	115.60(14)
C(27)-C(26)-H(26A)	108.4
P(4)-C(26)-H(26A)	108.4
C(27)-C(26)-H(26B)	108.4
P(4)-C(26)-H(26B)	108.4
H(26A)-C(26)-H(26B)	107.4
O(8)-C(27)-C(26)	108.24(16)
O(8)-C(27)-H(27A)	110.1
C(26)-C(27)-H(27A)	110.1
O(8)-C(27)-H(27B)	110.1

C(26)-C(27)-H(27B)	110.1
H(27A)-C(27)-H(27B)	108.4
O(8)-C(28)-H(28A)	109.5
O(8)-C(28)-H(28B)	109.5
H(28A)-C(28)-H(28B)	109.5
O(8)-C(28)-H(28C)	109.5
H(28A)-C(28)-H(28C)	109.5
H(28B)-C(28)-H(28C)	109.5

Symmetry transformations used to generate equivalent atoms:

C.3 Crystal data for *trans*-[Fe(DMeOEtP(O)E)$_2$][2BPh$_4$]

Table C.3.1. Crystal data and structure refinement for *trans*-[Fe(DMeOEtP(O)E)$_2$][2BPh$_4$].

Identification code	just10	
Empirical formula	C80 H112 B2 Fe O13 P4	
Formula weight	1483.05	
Temperature	173(2) K	
Wavelength	0.71073 Å	
Crystal system	Monoclinic	
Space group	C2/c	
Unit cell dimensions	a = 24.3085(11) Å	α = 90°.
	b = 13.4538(6) Å	β = 107.1030(10)°.
	c = 25.1734(11) Å	γ = 90°.
Volume	7868.7(6) Å^3	
Z	4	
Density (calculated)	1.252 Mg/m^3	
Absorption coefficient	0.333 mm^{-1}	
F(000)	3168	
Crystal size	0.14 x 0.12 x 0.08 mm^3	
Theta range for data collection	1.69 to 27.49°.	
Index ranges	-31<=h<=31, -17<=k<=17, -32<=l<=32	
Reflections collected	44261	
Independent reflections	8992 [R(int) = 0.0800]	
Completeness to theta = 27.49°	99.5 %	
Absorption correction	Semi-empirical from equivalents	
Max. and min. transmission	0.9738 and 0.9548	
Refinement method	Full-matrix least-squares on F^2	
Data / restraints / parameters	8992 / 0 / 434	
Goodness-of-fit on F^2	1.034	
Final R indices [I>2sigma(I)]	R1 = 0.0757, wR2 = 0.1515	
R indices (all data)	R1 = 0.1304, wR2 = 0.1749	
Largest diff. peak and hole	0.391 and -0.340 e.Å^{-3}	

Table C.3.2. Atomic coordinates (x 10^4) and equivalent isotropic displacement parameters ($Å^2$x 10^3) for *trans*-[Fe(DMeOEtP(O)E)$_2$][2BPh$_4$]. U(eq) is defined as one third of the trace of the orthogonalized U^{ij} tensor.

	x	y	z	U(eq)
Fe(1)	2500	2500	0	38(1)
P(1)	3526(1)	2882(1)	-569(1)	52(1)
P(2)	3725(1)	3244(1)	892(1)	40(1)
O(1)	3016(1)	3212(2)	-416(1)	53(1)
O(2)	3152(1)	2724(2)	728(1)	43(1)
O(4)	2921(2)	2482(3)	-1829(1)	91(1)
O(5)	4277(1)	1374(2)	1515(1)	52(1)
O(6)	3669(1)	5276(2)	1631(1)	71(1)
C(1)	4178(2)	3183(3)	-44(2)	50(1)
C(2)	4229(2)	2806(3)	544(2)	44(1)
O(3)	2907(1)	1088(2)	-140(1)	56(1)
C(3)	3537(3)	1555(4)	-677(2)	95(2)
C(4)	3056(3)	969(5)	-682(3)	48(1)
O(3A)	2907(1)	1088(2)	-140(1)	56(1)
C(3A)	3537(3)	1555(4)	-677(2)	95(2)
C(4A)	3385(5)	909(8)	-332(4)	48(1)
C(5)	3029(2)	329(3)	269(2)	85(2)
C(6)	3560(2)	3528(4)	-1187(2)	74(1)
C(7)	3009(2)	3468(4)	-1654(2)	72(1)
C(8)	2410(2)	2353(4)	-2255(2)	96(2)
C(9)	4072(2)	3066(3)	1627(1)	52(1)
C(10)	4029(2)	2010(3)	1818(2)	56(1)
C(11)	4224(2)	368(3)	1653(2)	68(1)
C(12)	3646(2)	4560(3)	761(2)	55(1)
C(13)	3314(2)	5117(3)	1090(2)	67(1)
C(14)	3367(2)	5754(4)	1967(2)	85(2)
B(1)	3811(2)	2567(3)	4071(2)	33(1)
C(15)	4140(1)	2267(2)	4720(1)	34(1)
C(16)	4505(2)	1456(3)	4879(2)	46(1)
C(17)	4796(2)	1242(3)	5428(2)	58(1)
C(18)	4733(2)	1842(3)	5851(2)	60(1)
C(19)	4370(2)	2648(3)	5714(2)	51(1)
C(20)	4083(2)	2848(3)	5165(1)	41(1)
C(21)	3154(1)	2960(2)	4009(1)	36(1)
C(22)	2815(2)	2524(3)	4307(2)	45(1)
C(23)	2243(2)	2764(3)	4228(2)	53(1)
C(24)	1981(2)	3458(3)	3841(2)	55(1)
C(25)	2296(2)	3929(3)	3539(2)	53(1)
C(26)	2872(2)	3682(3)	3629(1)	43(1)
C(27)	4174(1)	3464(2)	3874(1)	33(1)
C(28)	4484(1)	4188(2)	4236(1)	36(1)
C(29)	4775(1)	4955(2)	4069(2)	41(1)
C(30)	4766(2)	5037(3)	3522(2)	47(1)
C(31)	4459(2)	4351(3)	3146(2)	50(1)
C(32)	4170(2)	3583(3)	3319(1)	43(1)
C(33)	3772(1)	1592(2)	3671(1)	34(1)

C(34)	4247(2)	1216(3)	3527(1)	43(1)
C(35)	4223(2)	366(3)	3211(2)	51(1)
C(36)	3719(2)	-151(3)	3013(2)	53(1)
C(37)	3243(2)	184(3)	3140(2)	61(1)
C(38)	3271(2)	1033(3)	3459(2)	47(1)

Table C.3.3. Bond lengths [Å] and angles [°] for *trans*-[Fe(DMeOEtP(O)E)$_2$][2BPh$_4$].

Fe(1)-O(2)#1	2.062(2)
Fe(1)-O(2)	2.062(2)
Fe(1)-O(1)	2.088(2)
Fe(1)-O(1)#1	2.088(2)
Fe(1)-O(3)	2.217(2)
Fe(1)-O(3A)#1	2.217(2)
Fe(1)-O(3)#1	2.217(2)
P(1)-O(1)	1.470(3)
P(1)-C(1)	1.786(4)
P(1)-C(6)	1.804(4)
P(1)-C(3)	1.807(5)
P(2)-O(2)	1.505(2)
P(2)-C(12)	1.800(4)
P(2)-C(2)	1.803(4)
P(2)-C(9)	1.809(4)
O(4)-C(7)	1.394(5)
O(4)-C(8)	1.393(5)
O(5)-C(10)	1.397(4)
O(5)-C(11)	1.412(5)
O(6)-C(13)	1.398(5)
O(6)-C(14)	1.426(5)
C(1)-C(2)	1.535(5)
O(3)-C(4)	1.518(6)
C(3)-C(4)	1.408(7)
C(6)-C(7)	1.503(6)
C(9)-C(10)	1.513(5)
C(12)-C(13)	1.512(6)
B(1)-C(33)	1.640(5)
B(1)-C(15)	1.645(5)
B(1)-C(21)	1.648(5)
B(1)-C(27)	1.653(5)
C(15)-C(16)	1.388(5)
C(15)-C(20)	1.406(4)
C(16)-C(17)	1.385(5)
C(17)-C(18)	1.379(5)
C(18)-C(19)	1.375(5)
C(19)-C(20)	1.380(5)
C(21)-C(26)	1.393(5)
C(21)-C(22)	1.396(5)
C(22)-C(23)	1.384(5)
C(23)-C(24)	1.365(6)
C(24)-C(25)	1.381(6)
C(25)-C(26)	1.393(5)
C(27)-C(28)	1.395(4)
C(27)-C(32)	1.405(4)
C(28)-C(29)	1.385(5)
C(29)-C(30)	1.376(5)
C(30)-C(31)	1.373(5)
C(31)-C(32)	1.389(5)
C(33)-C(38)	1.396(4)
C(33)-C(34)	1.402(4)

C(34)-C(35)	1.385(5)
C(35)-C(36)	1.370(5)
C(36)-C(37)	1.362(5)
C(37)-C(38)	1.386(5)

O(2)#1-Fe(1)-O(2)	180.00(17)
O(2)#1-Fe(1)-O(1)	92.25(9)
O(2)-Fe(1)-O(1)	87.75(9)
O(2)#1-Fe(1)-O(1)#1	87.75(9)
O(2)-Fe(1)-O(1)#1	92.25(9)
O(1)-Fe(1)-O(1)#1	180.00(15)
O(2)#1-Fe(1)-O(3)	89.73(10)
O(2)-Fe(1)-O(3)	90.27(10)
O(1)-Fe(1)-O(3)	87.20(10)
O(1)#1-Fe(1)-O(3)	92.80(10)
O(2)#1-Fe(1)-O(3A)#1	90.27(10)
O(2)-Fe(1)-O(3A)#1	89.73(10)
O(1)-Fe(1)-O(3A)#1	92.81(10)
O(1)#1-Fe(1)-O(3A)#1	87.19(10)
O(3)-Fe(1)-O(3A)#1	180.00(15)
O(2)#1-Fe(1)-O(3)#1	90.27(10)
O(2)-Fe(1)-O(3)#1	89.73(10)
O(1)-Fe(1)-O(3)#1	92.81(10)
O(1)#1-Fe(1)-O(3)#1	87.19(10)
O(3)-Fe(1)-O(3)#1	180.00(15)
O(3A)#1-Fe(1)-O(3)#1	0.00(15)
O(1)-P(1)-C(1)	111.75(17)
O(1)-P(1)-C(6)	109.7(2)
C(1)-P(1)-C(6)	105.79(18)
O(1)-P(1)-C(3)	112.8(2)
C(1)-P(1)-C(3)	106.6(3)
C(6)-P(1)-C(3)	109.9(2)
O(2)-P(2)-C(12)	111.50(17)
O(2)-P(2)-C(2)	114.92(15)
C(12)-P(2)-C(2)	106.54(18)
O(2)-P(2)-C(9)	109.55(16)
C(12)-P(2)-C(9)	108.06(18)
C(2)-P(2)-C(9)	105.92(18)
P(1)-O(1)-Fe(1)	132.08(16)
P(2)-O(2)-Fe(1)	135.98(14)
C(7)-O(4)-C(8)	112.4(4)
C(10)-O(5)-C(11)	111.5(3)
C(13)-O(6)-C(14)	111.7(3)
C(2)-C(1)-P(1)	116.2(2)
C(1)-C(2)-P(2)	119.1(3)
C(4)-O(3)-Fe(1)	118.0(3)
C(4)-C(3)-P(1)	120.4(4)
C(3)-C(4)-O(3)	110.5(4)
C(7)-C(6)-P(1)	113.1(3)
O(4)-C(7)-C(6)	108.5(4)
C(10)-C(9)-P(2)	113.3(3)
O(5)-C(10)-C(9)	108.6(3)
C(13)-C(12)-P(2)	115.7(3)

O(6)-C(13)-C(12)	109.5(3)
C(33)-B(1)-C(15)	109.7(3)
C(33)-B(1)-C(21)	108.6(3)
C(15)-B(1)-C(21)	110.3(3)
C(33)-B(1)-C(27)	109.9(3)
C(15)-B(1)-C(27)	109.3(3)
C(21)-B(1)-C(27)	109.0(3)
C(16)-C(15)-C(20)	114.3(3)
C(16)-C(15)-B(1)	124.2(3)
C(20)-C(15)-B(1)	121.4(3)
C(17)-C(16)-C(15)	123.1(3)
C(18)-C(17)-C(16)	120.5(4)
C(19)-C(18)-C(17)	118.5(4)
C(18)-C(19)-C(20)	120.2(4)
C(19)-C(20)-C(15)	123.3(3)
C(26)-C(21)-C(22)	114.5(3)
C(26)-C(21)-B(1)	123.7(3)
C(22)-C(21)-B(1)	121.6(3)
C(23)-C(22)-C(21)	123.4(4)
C(24)-C(23)-C(22)	120.0(4)
C(23)-C(24)-C(25)	119.4(4)
C(24)-C(25)-C(26)	119.6(4)
C(25)-C(26)-C(21)	123.0(4)
C(28)-C(27)-C(32)	114.5(3)
C(28)-C(27)-B(1)	123.2(3)
C(32)-C(27)-B(1)	122.2(3)
C(29)-C(28)-C(27)	123.3(3)
C(30)-C(29)-C(28)	120.3(3)
C(31)-C(30)-C(29)	118.8(3)
C(30)-C(31)-C(32)	120.5(3)
C(31)-C(32)-C(27)	122.7(3)
C(38)-C(33)-C(34)	113.6(3)
C(38)-C(33)-B(1)	123.5(3)
C(34)-C(33)-B(1)	122.9(3)
C(35)-C(34)-C(33)	123.1(3)
C(36)-C(35)-C(34)	120.7(4)
C(37)-C(36)-C(35)	118.5(3)
C(36)-C(37)-C(38)	120.6(4)
C(37)-C(38)-C(33)	123.5(3)

Symmetry transformations used to generate equivalent atoms:
#1 -x+1/2,-y+1/2,-z

APPENDIX D

SUPPORTING INFORMATION FOR CHAPTER III

D.1 Figures

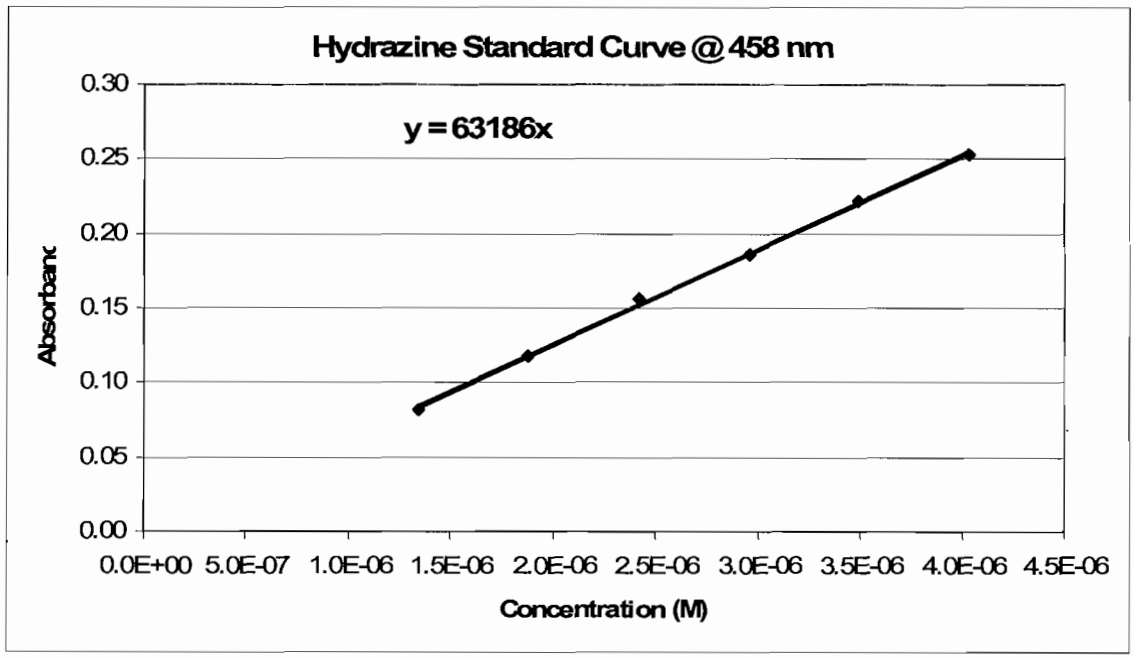

Figure D.1.1. Hydrazine standard curve used for hydrazine concentration determinations.

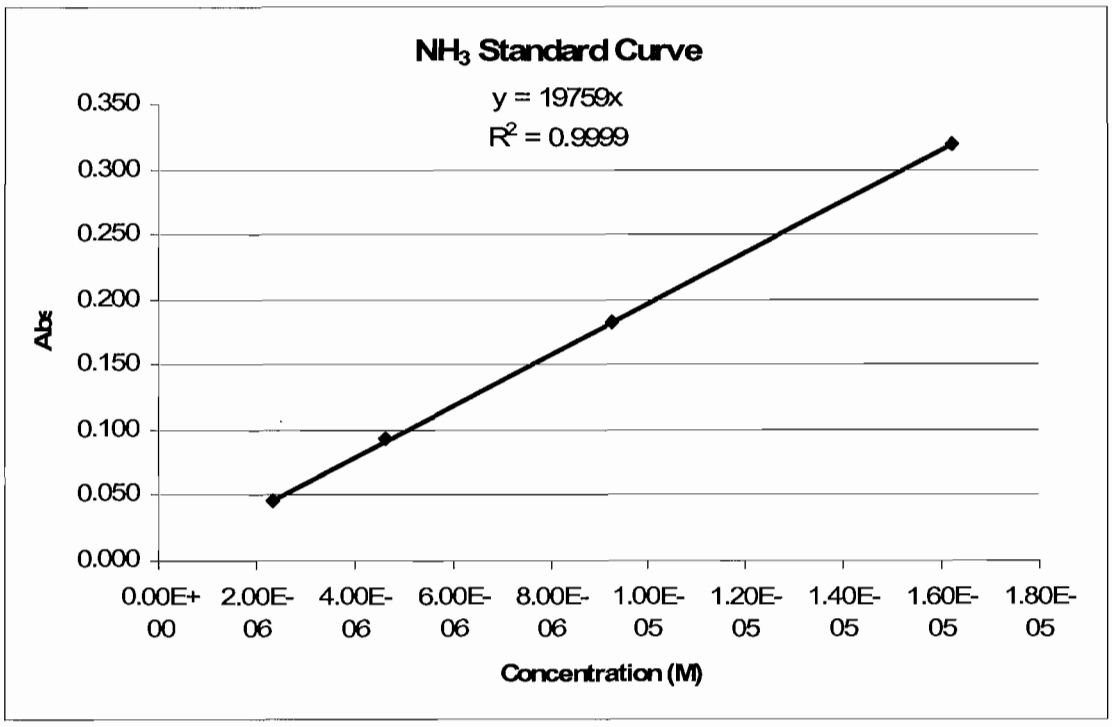

Figure D.1.2. Ammonia standard curve used for ammonia concentration determinations.

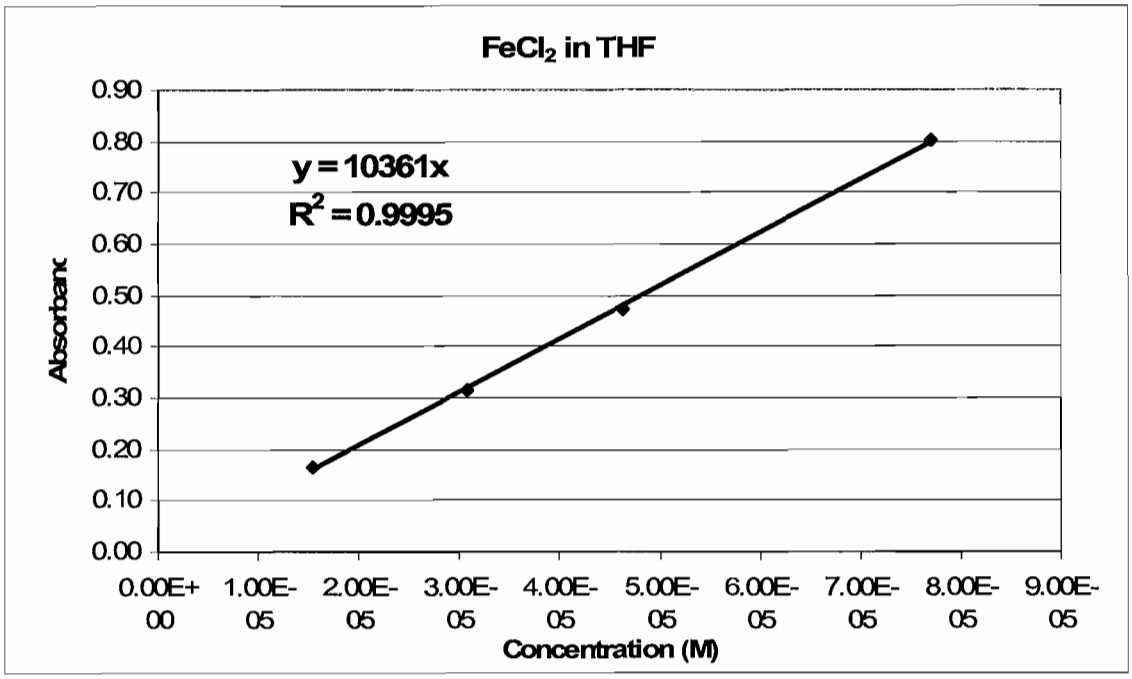

Figure D.1.3. Iron(II) standard curve used for iron(II) determinations.

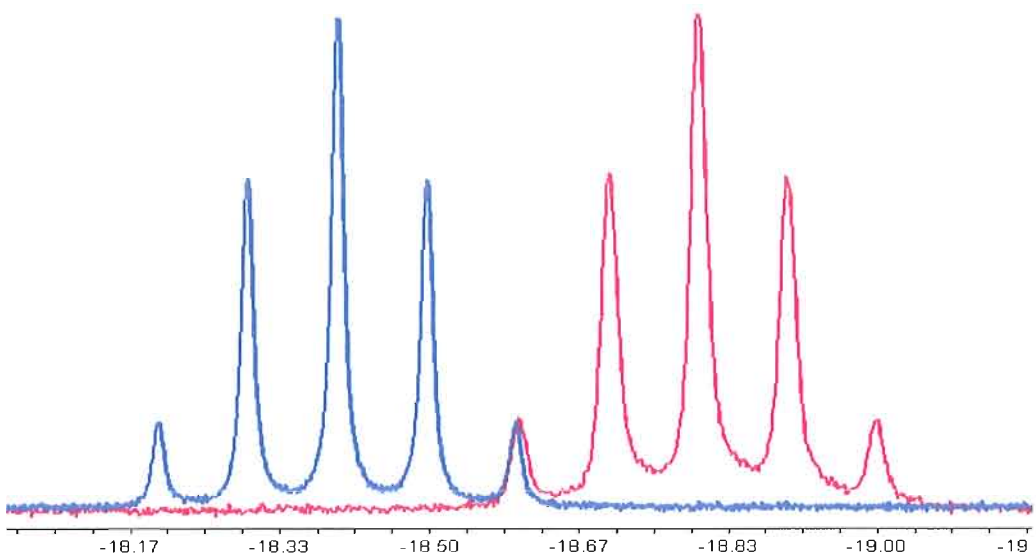

Figure D.1.4. Hydride region of ^{1}H NMR spectra of *trans*-[Fe(DMeOPrPE)$_2$(N$_2$)H][X] in toluene-d_8. Blue spectrum X = PF_6, red spectrum X = BAr_F.

APPENDIX E

SUPPORTING INFORMATION FOR CHAPTER IV

E.1 Spectra

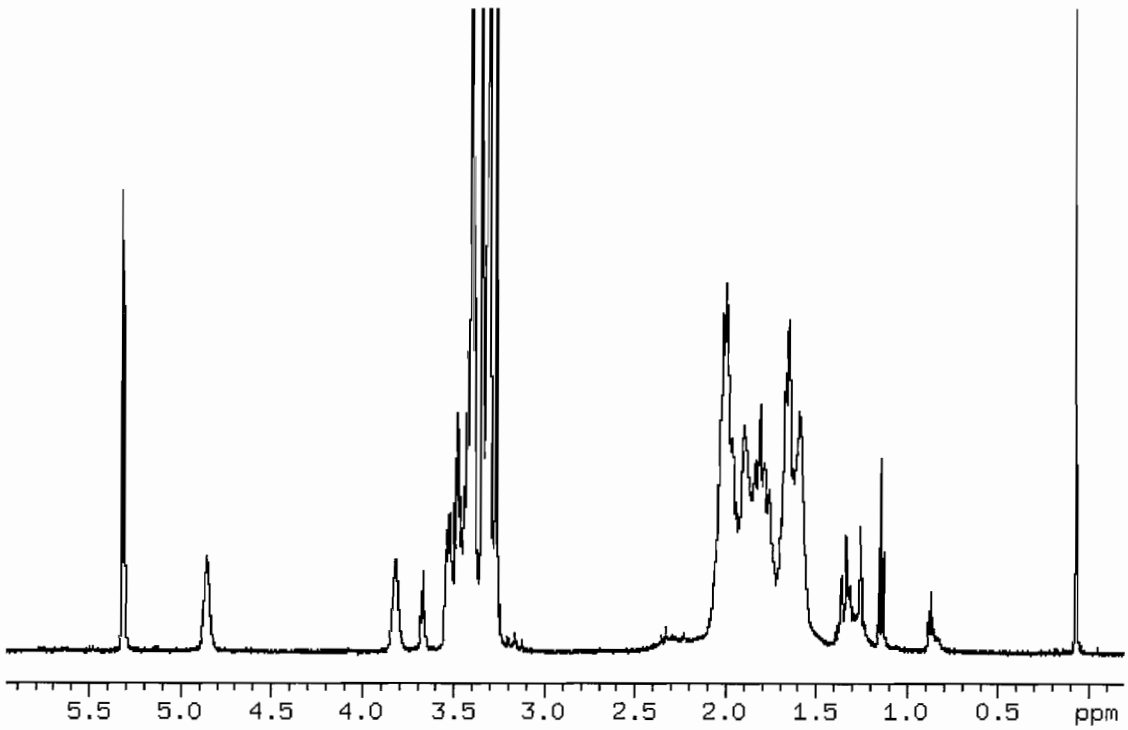

Figure E.1.1. ^{1}H NMR spectrum (CD_2Cl_2) of *cis*-[Fe(DMeOPrPE)$_2$(η^2-N_2H_4)][BPh_4]$_2$ (**I**).

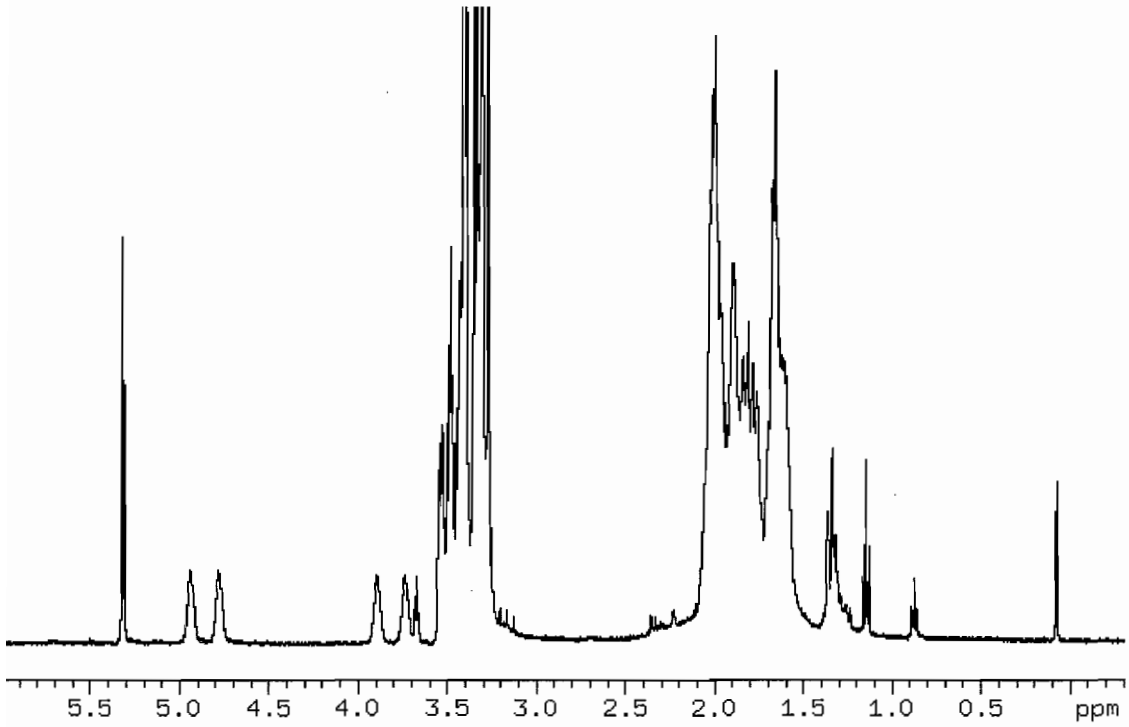

Figure E.1.2. ^{1}H NMR spectrum (CD_2Cl_2) of *cis*-[Fe(DMeOPrPE)$_2$(η^2-$^{15}N_2H_4$)][PF_6]$_2$.

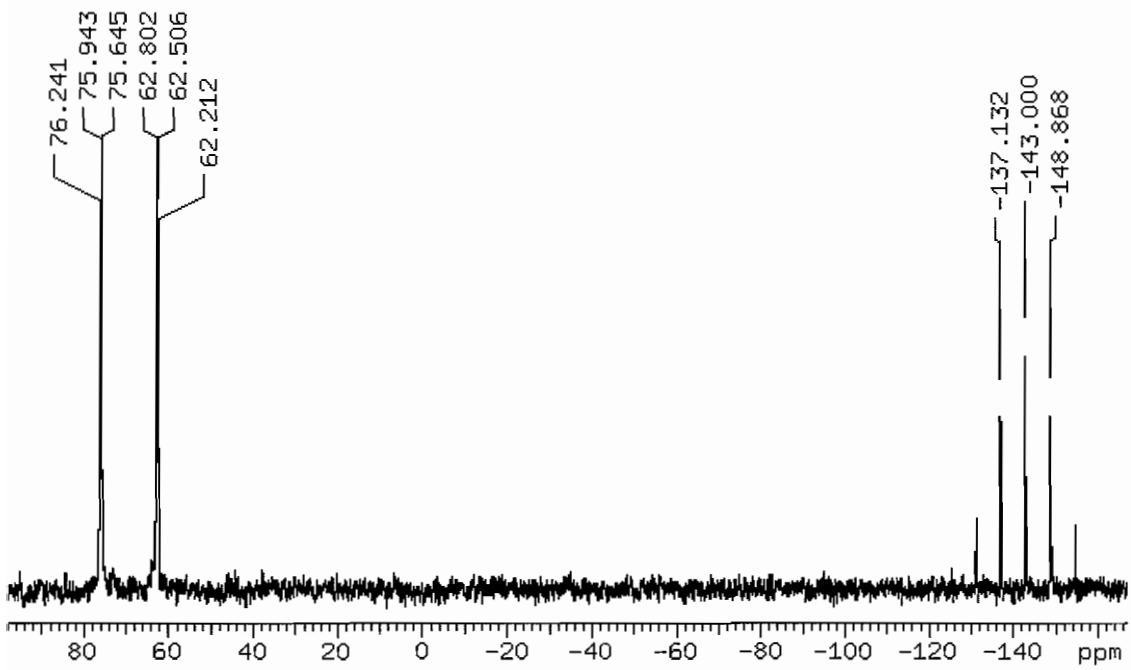

Figure E.1.3. ^{31}P NMR spectrum (CD_2Cl_2) of *cis*-[Fe(DMeOPrPE)$_2$(η^2-$^{15}N_2H_4$)][PF_6]$_2$.

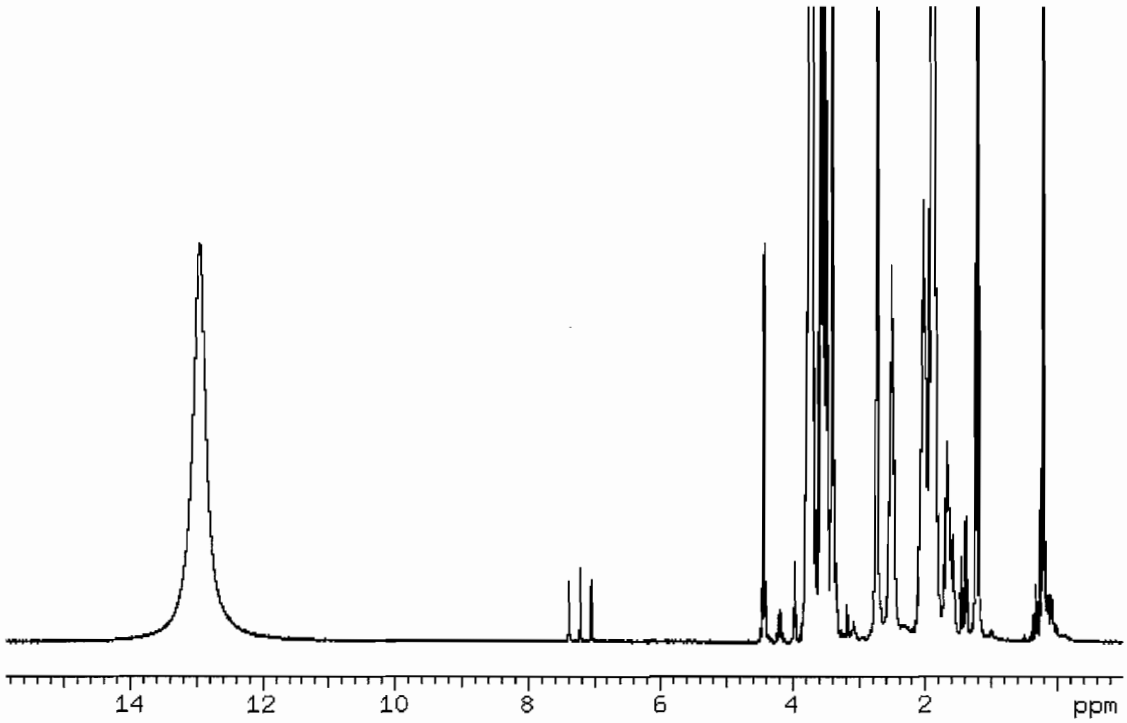

Figure E.1.4. ^{1}H NMR spectrum (DMSO-d_6) of *cis*-[Fe(DMeOPrPE)$_2$(η^2-^{15}N$_2$H$_4$)][PF$_6$]$_2$ after addition of excess 1M TfOH.

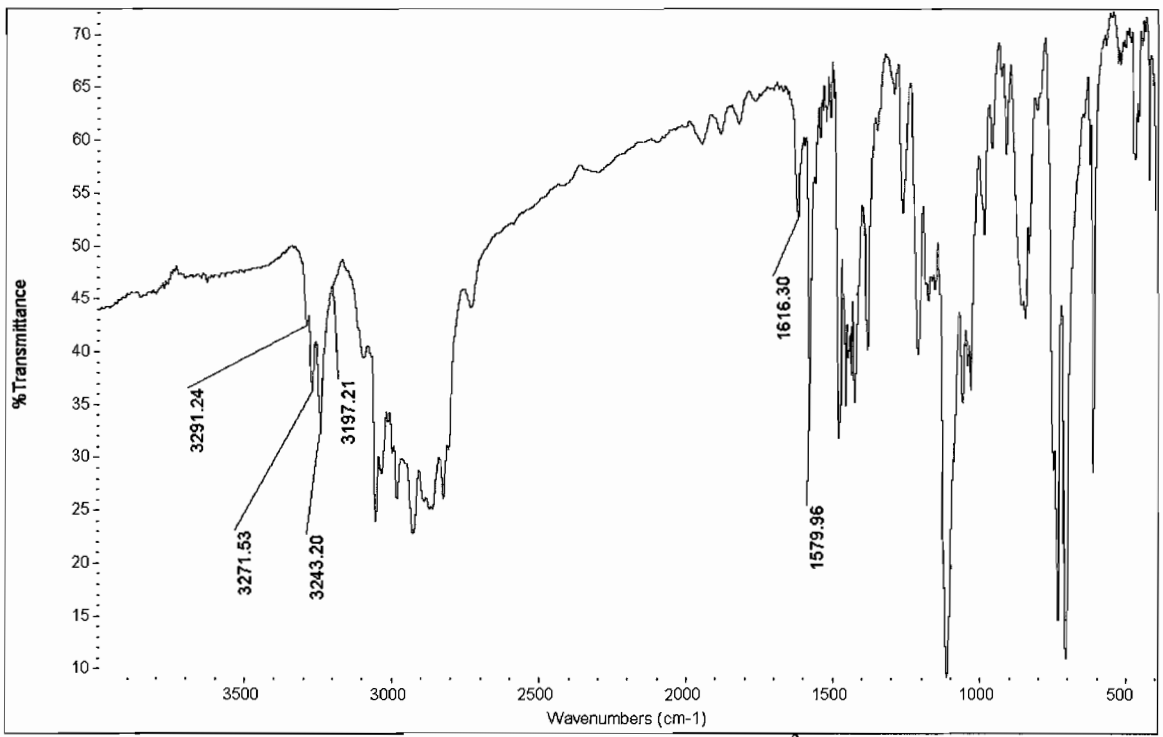

Figure E.1.5. IR spectrum (KBr) of *cis*-[Fe(DMeOPrPE)$_2$(η^2-N$_2$H$_4$)][BPh$_4$]$_2$ **(I)**.

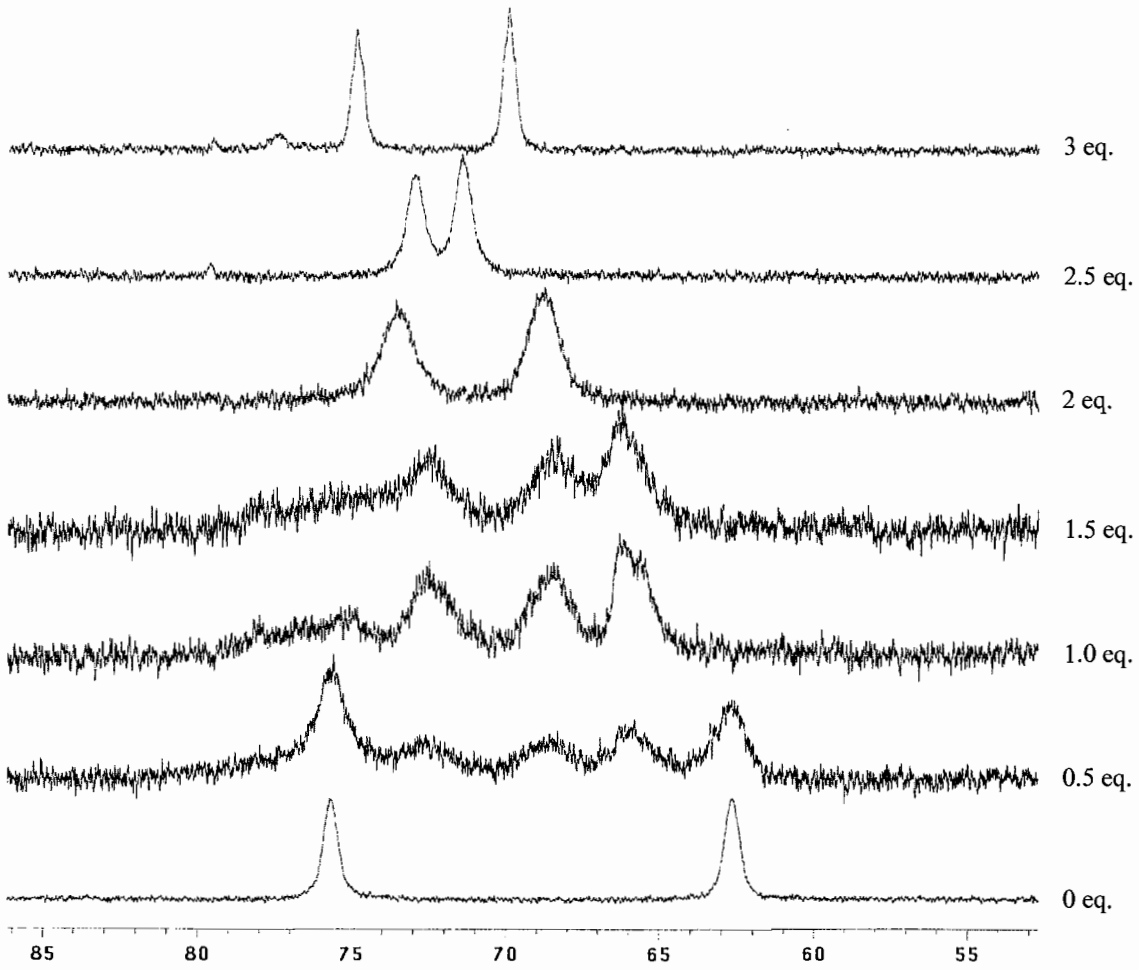

Figure E.1.6. $^{31}P\{^{1}H\}$ NMR spectra at 298K of titration of *cis*-$[Fe(DMeOPrPE)_2(N_2H_4)]^{2+}$ with varying equivalents of KO^{t}Bu.

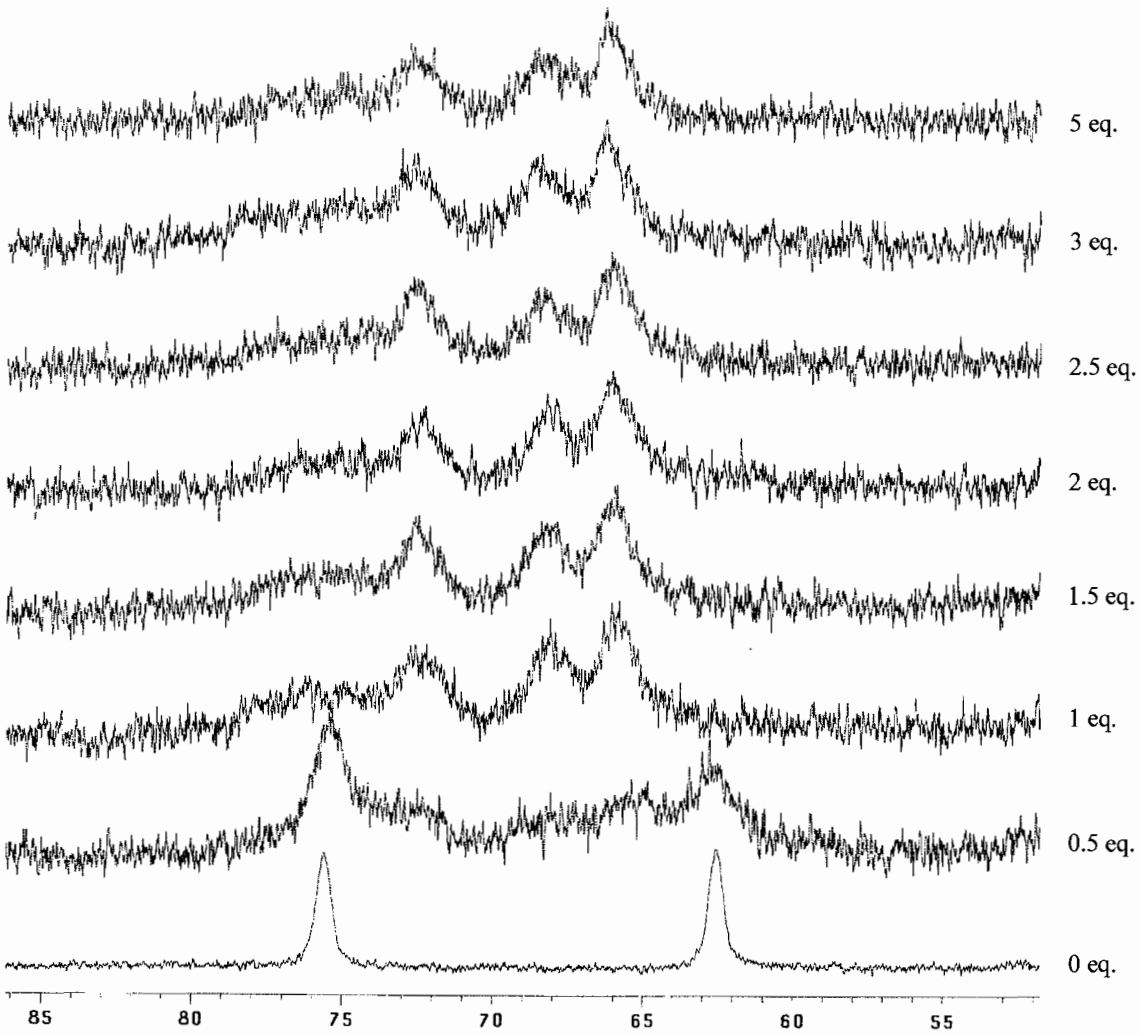

Figure E.1.7. $^{31}P\{^{1}H\}$ NMR spectra at 298K of titration of *cis*-$[Fe(DMeOPrPE)_2(N_2H_4)]^{2+}$ with varying equivalents of DBU.

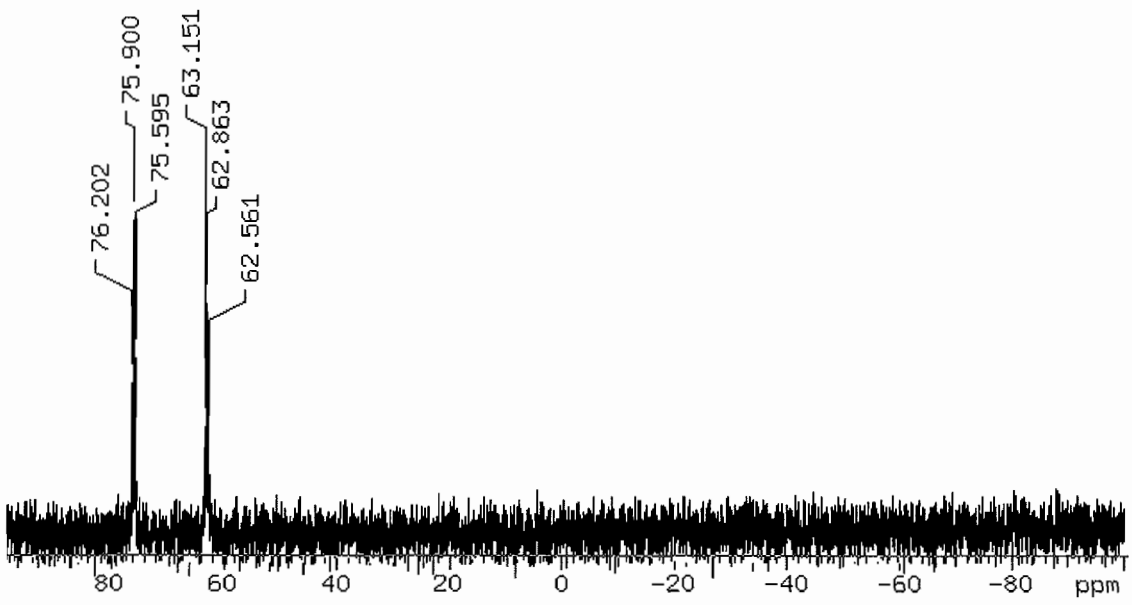

Figure E.1.8. $^{31}P\{^{1}H\}$ NMR spectrum of *cis*-[Fe(DMeOPrPE)$_2$(N_2H_4)][2BPh$_4$].

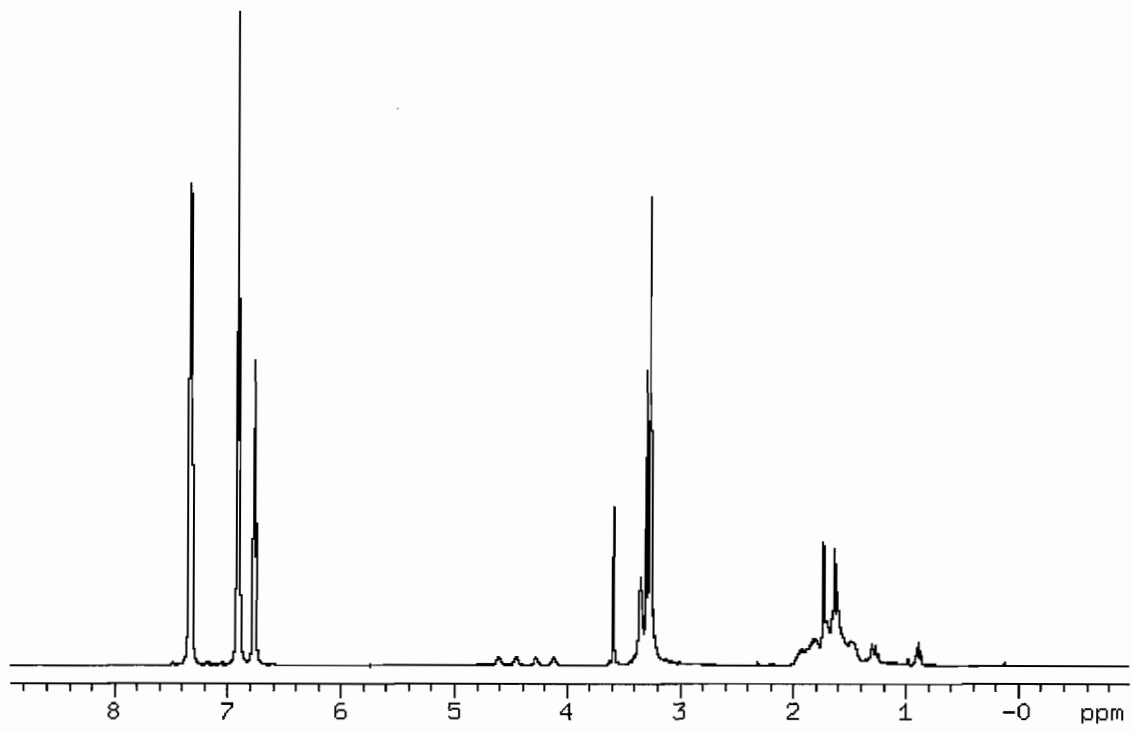

Figure E.1.9. ^{1}H NMR spectrum of *cis*-[Fe(DMeOPrPE)$_2$($^{15}N_2H_4$)][2BPh$_4$].

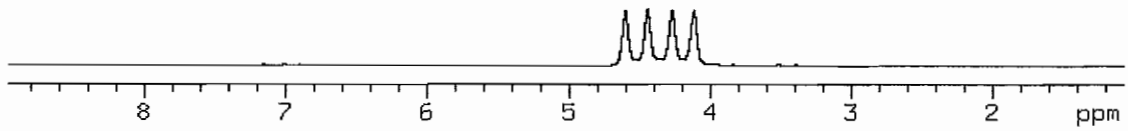

Figure E.1.10. ^{1}H HMQC NMR spectrum of *cis*-[Fe(DMeOPrPE)$_2$($^{15}N_2H_4$)][2BPh$_4$].

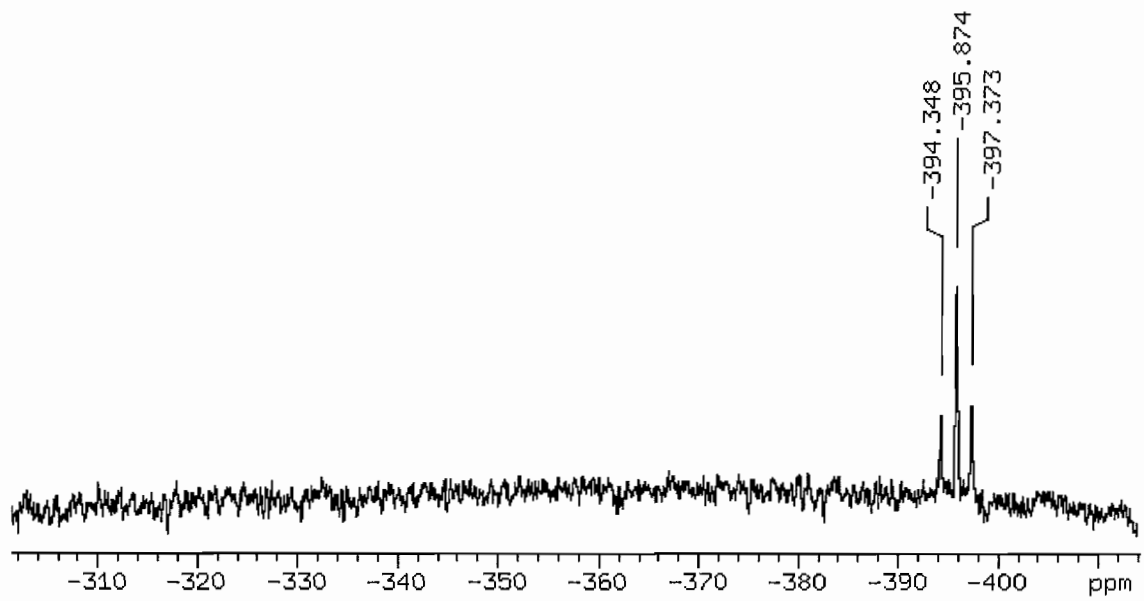

Figure E.1.11. ^{15}N NMR spectrum of *cis*-[Fe(DMeOPrPE)$_2$($^{15}N_2H_4$)]$^{2+}$.

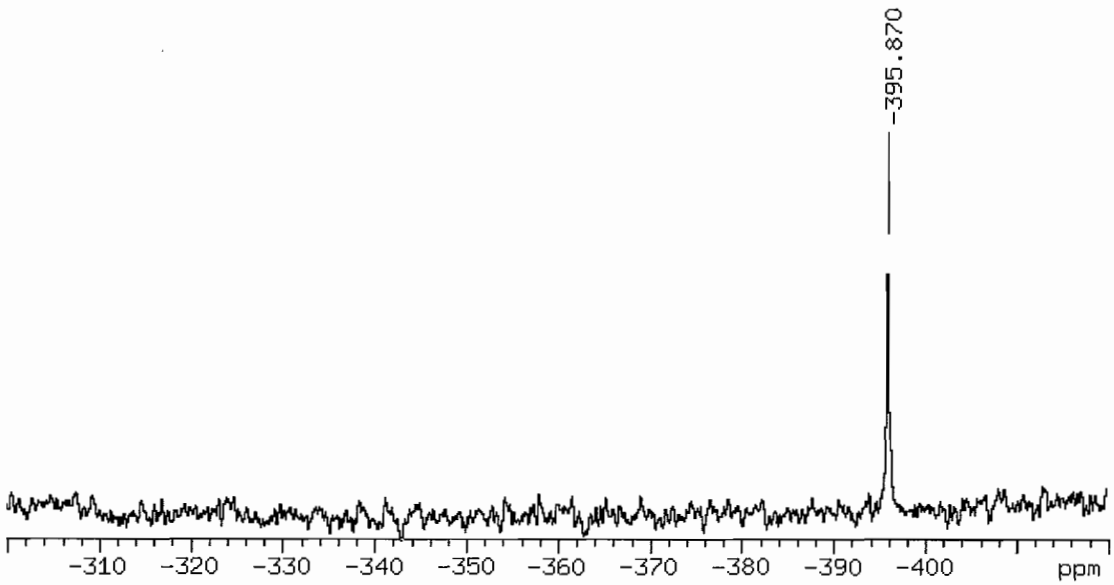

Figure E.1.12. $^{15}N\{^{1}H\}$ NMR spectrum of *cis*-$[Fe(DMeOPrPE)_2(^{15}N_2H_4)]^{2+}$.

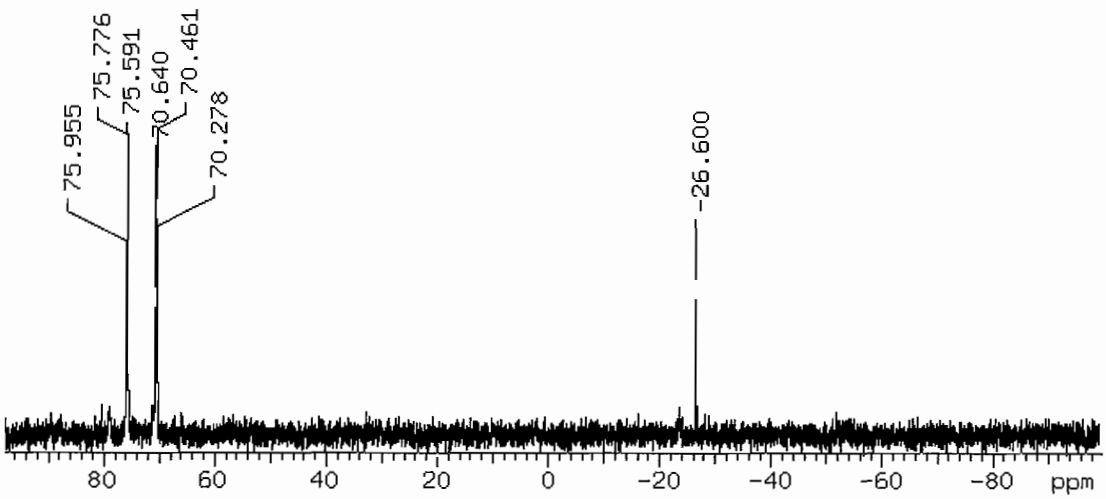

Figure E.1.13. $^{31}P\{^{1}H\}$ NMR spectrum of *cis*-$Fe(DMeOPrPE)_2(N_2H_2)$. The resonance at -26.6 ppm is uncoordinated DMeOPrPE.

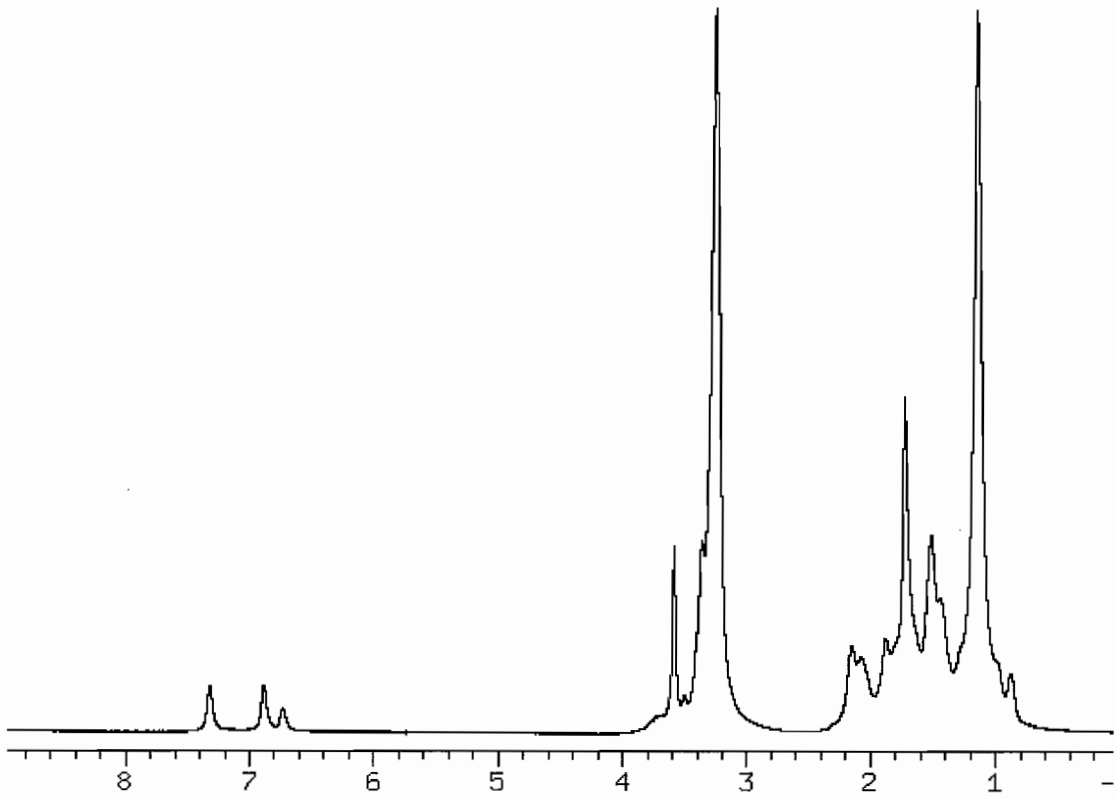

Figure E.1.14. ^{1}H NMR spectrum of *cis*-Fe(DMeOPrPE)$_2$($^{15}N_2H_2$).

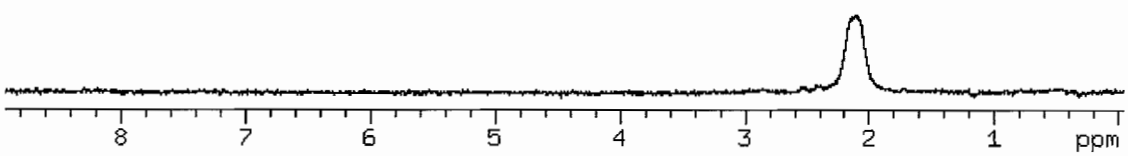

Figure E.1.15. ^{1}H HMQC (^{15}N coupled) NMR spectrum of *cis*-Fe(DMeOPrPE)$_2$($^{15}N_2H_2$).

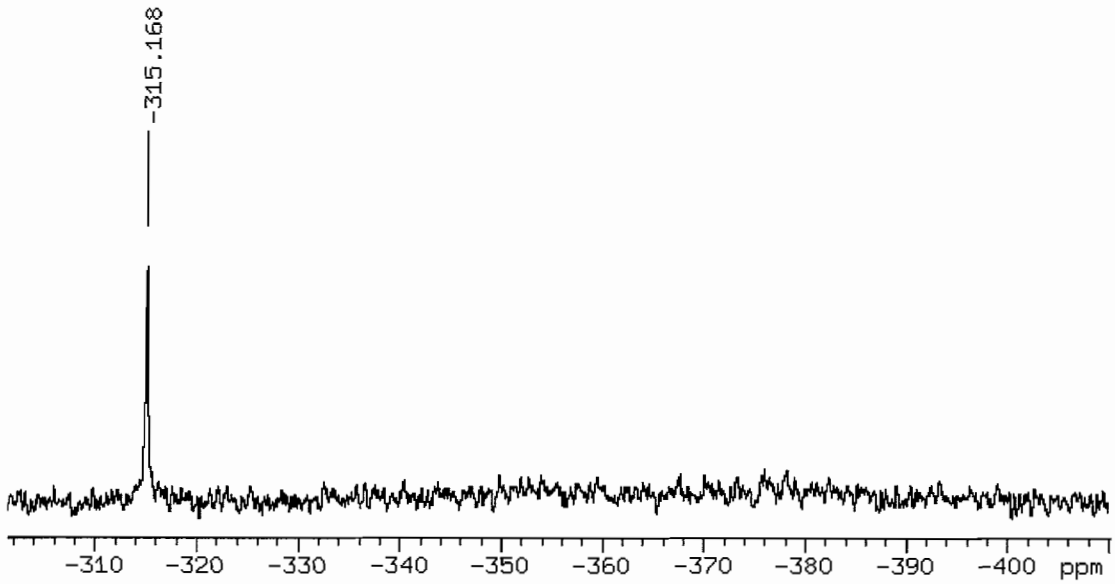

Figure E.1.16. $^{15}N\{^{1}H\}$ NMR spectrum of *cis*-Fe(DMeOPrPE)$_2$($^{15}N_2H_2$).

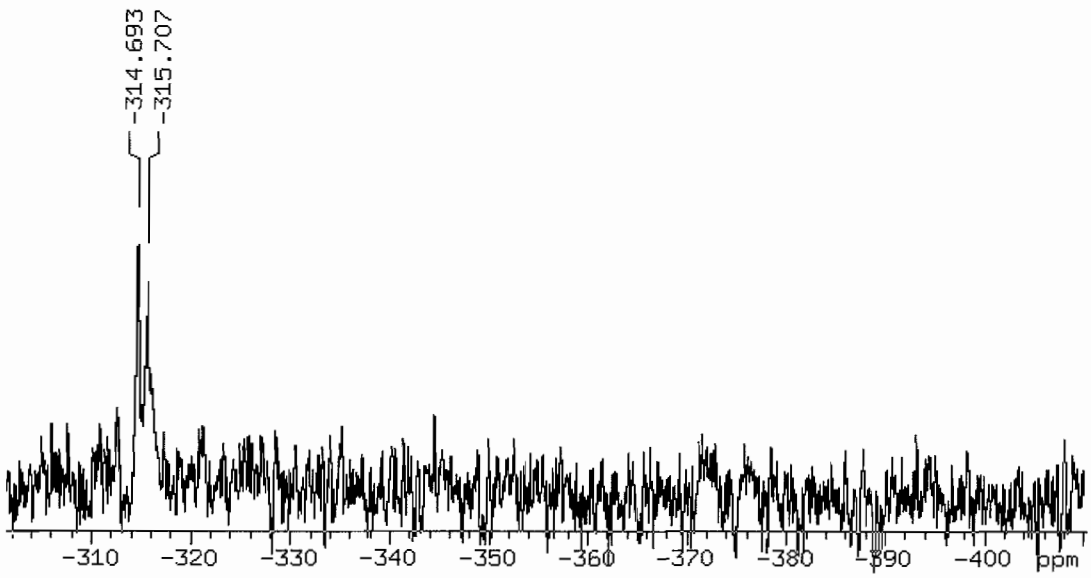

Figure E.1.17. ^{15}N NMR spectrum of *cis*-Fe(DMeOPrPE)$_2$($^{15}N_2H_2$).

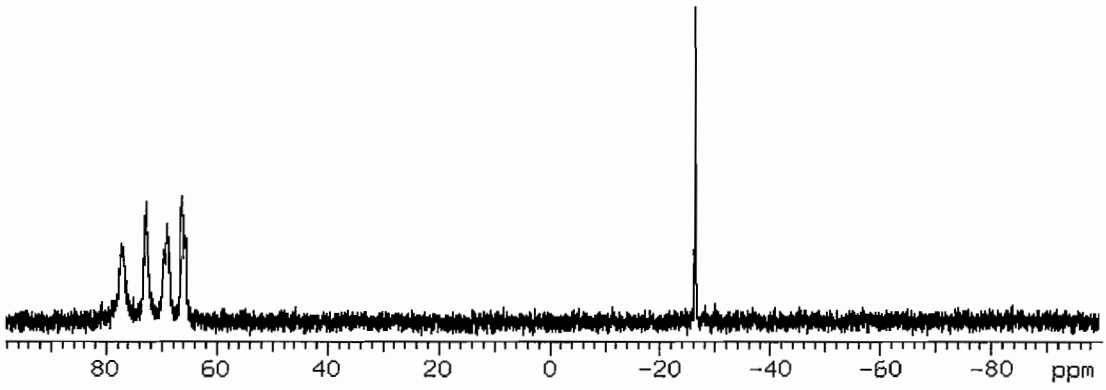

Figure E.1.18. $^{31}P\{^{1}H\}$ NMR spectrum of *cis*-$[Fe(DMeOPrPE)_2(N_2H_3)]^+$ at 298K. The resonance at -26.65 ppm is uncoordinated DMeOPrPE.

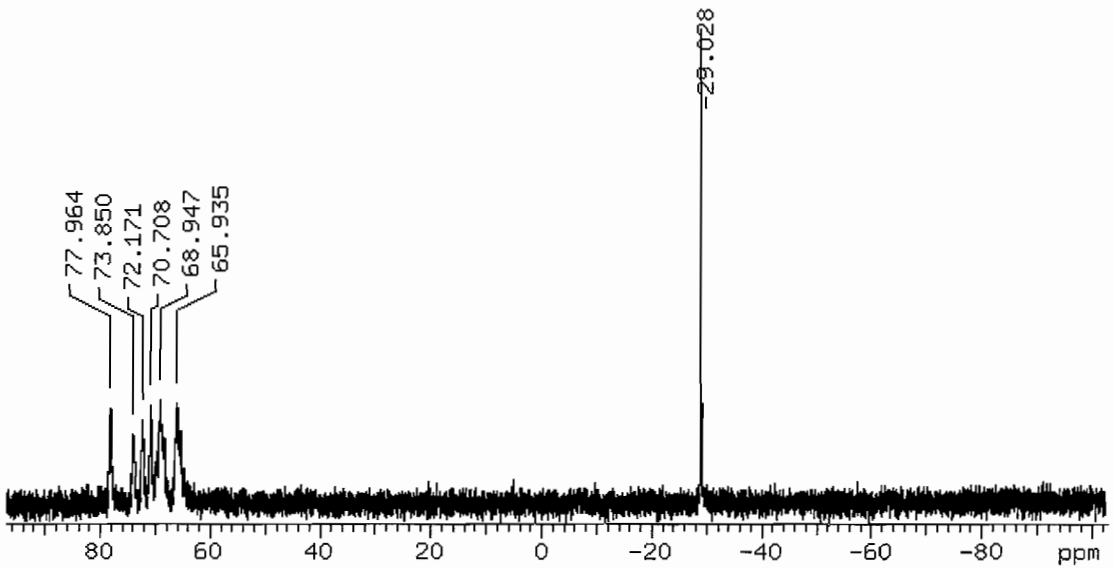

Figure E.1.19. $^{31}P\{^{1}H\}$ NMR spectrum of *cis*-$[Fe(DMeOPrPE)_2(N_2H_3)]^+$ at 193K. The resonance at -29.0 ppm is uncoordinated DMeOPrPE.

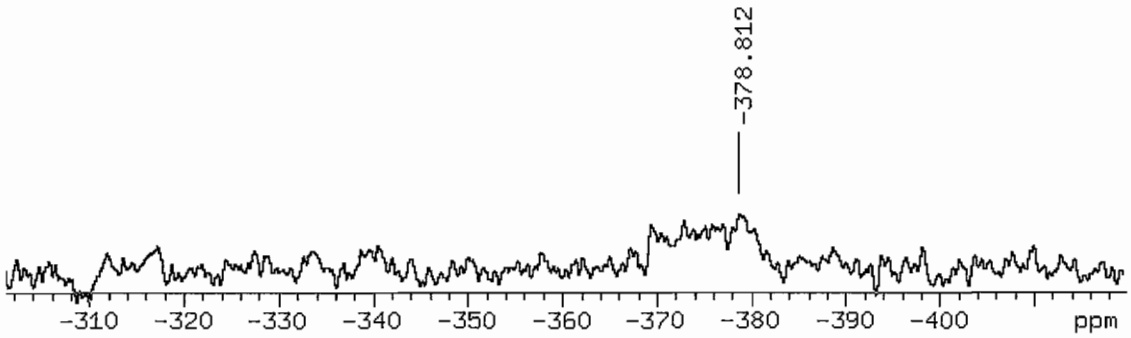

Figure E.1.20. $^{15}N\{^{1}H\}$ NMR spectrum of *cis*-[Fe(DMeOPrPE)$_2$($^{15}N_2H_3$)]$^+$ at 298K.

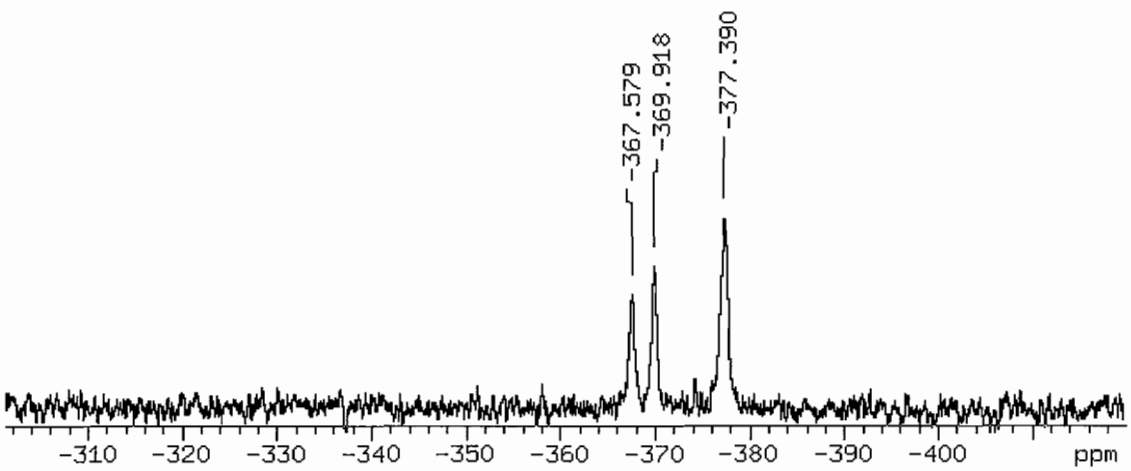

Figure E.1.21. $^{15}N\{^{1}H\}$ NMR spectrum of *cis*-[Fe(DMeOPrPE)$_2$($^{15}N_2H_3$)]$^+$ at 193K.

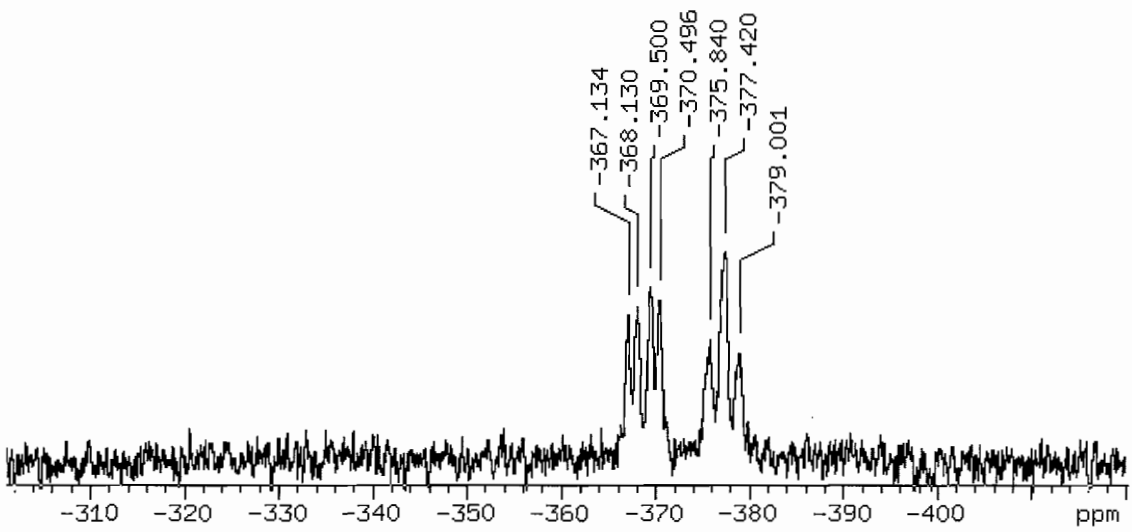

Figure E.1.22. ^{15}N NMR spectrum of *cis*-[Fe(DMeOPrPE)$_2$($^{15}N_2H_3$)]$^+$ at 193K.

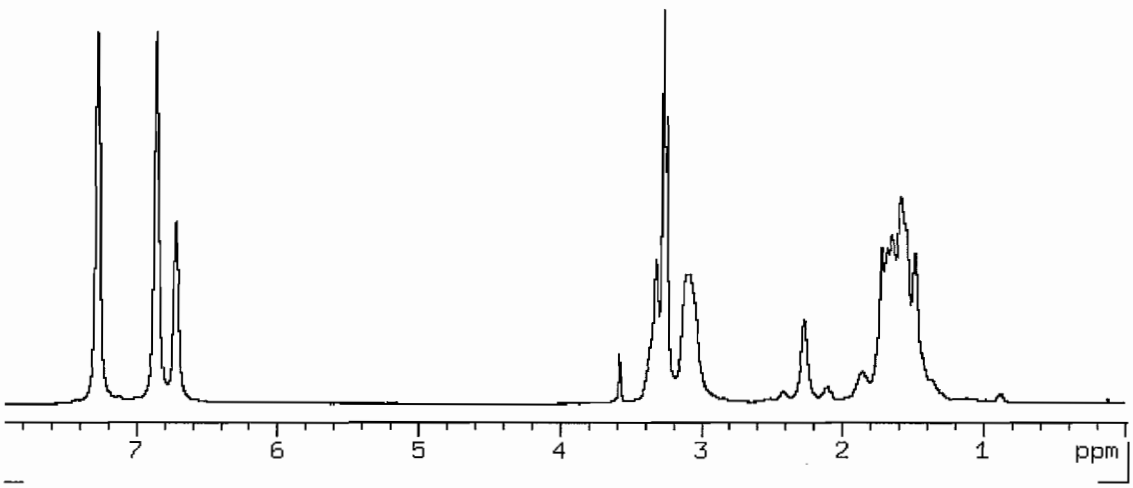

Figure E.1.22. ^1H NMR spectrum of *cis*-[Fe(DMeOPrPE)$_2$($^{15}N_2H_3$)]$^+$ at 298K.

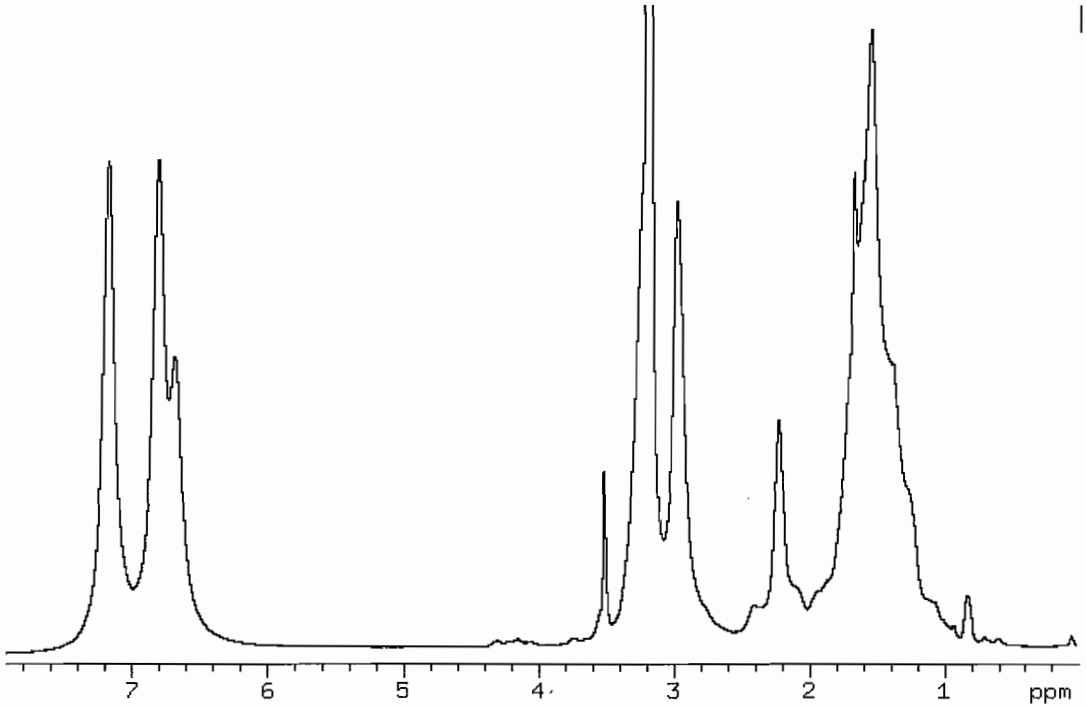

Figure E.1.23. ^{1}H NMR spectrum of *cis*-[Fe(DMeOPrPE)$_2$($^{15}N_2H_3$)]$^+$ at 193K. The hydrazido proton resonances are located at 4.2 and 0.7 ppm.

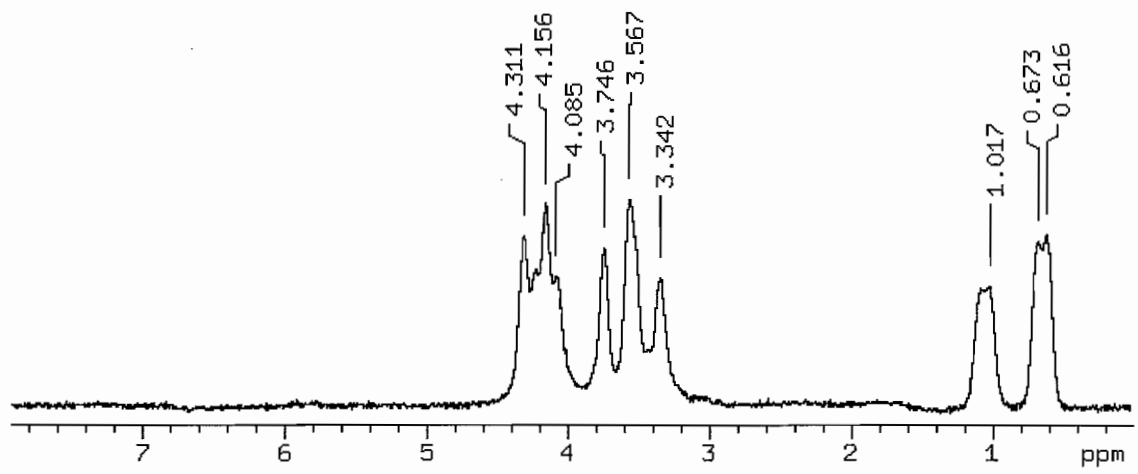

Figure E.1.24. ^{1}H HMQC (^{15}N coupled) of *cis*-[Fe(DMeOPrPE)$_2$($^{15}N_2H_3$)]$^+$ at 193K.

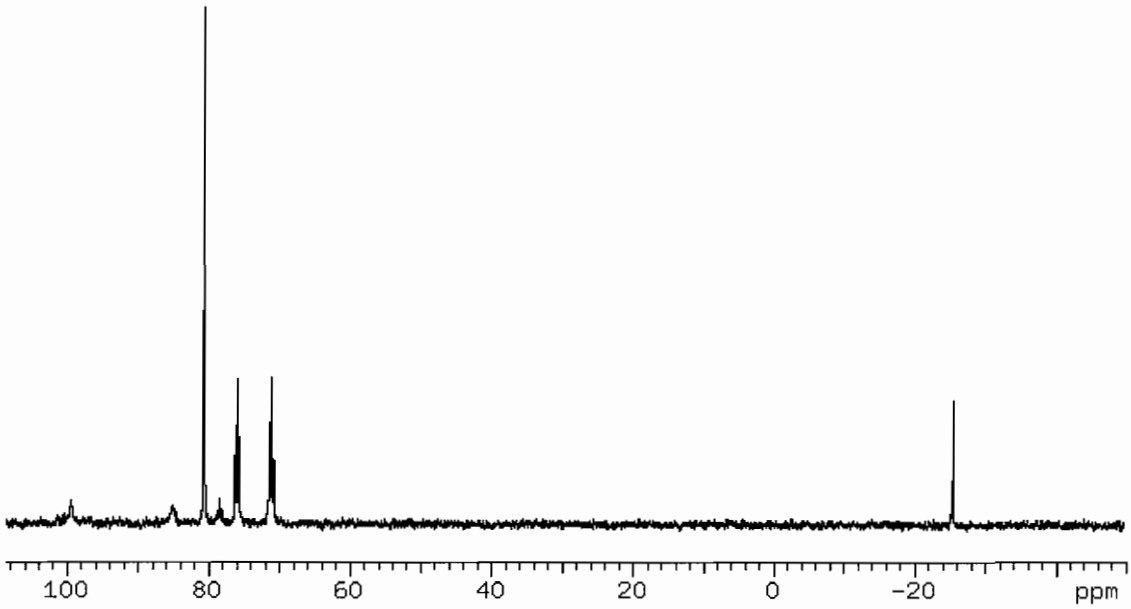

Figure E.1.25. ^{31}P NMR spectrum of addition of N_2H_4 to $Fe(DMeOPrPE)_2(N_2)$. Peak assignments: δ 99, 85 *cis*-$Fe(DMeOPrPE)_2(H)_2$; δ 81 $Fe(DMeOPrPE)_2(N_2)$; δ 78 unknown; δ 76, 71 *cis*-$Fe(DMeOPrPE)_2(N_2H_2)$; δ -26 DMeOPrPE.

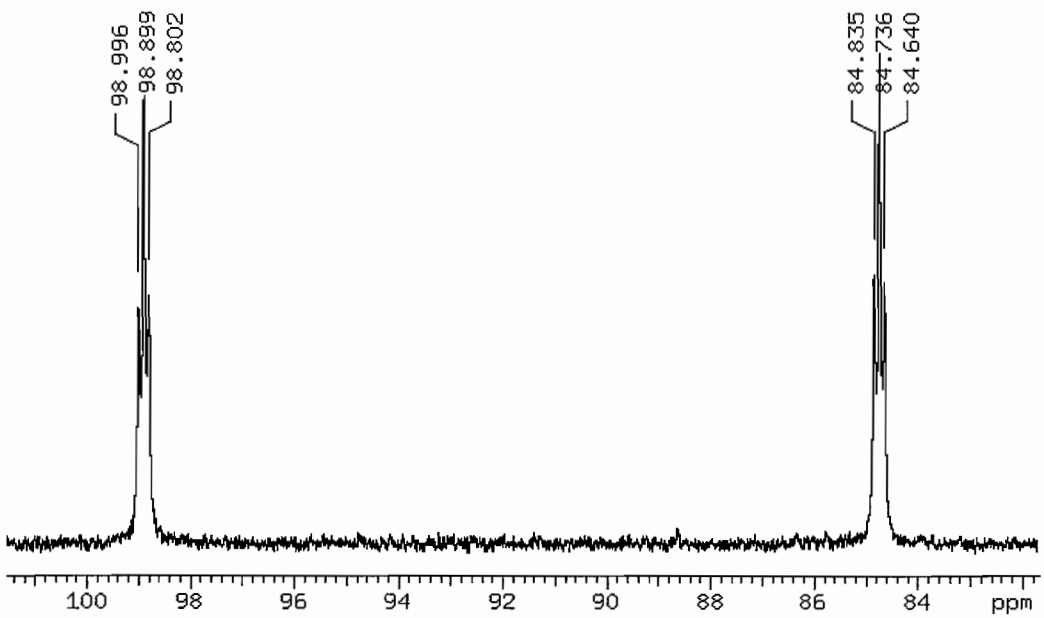

Figure E.1.26. $^{31}P\{^1H\}$ spectrum of *cis*-$Fe(DMeOPrPE)_2(H)_2$ at -20°C.

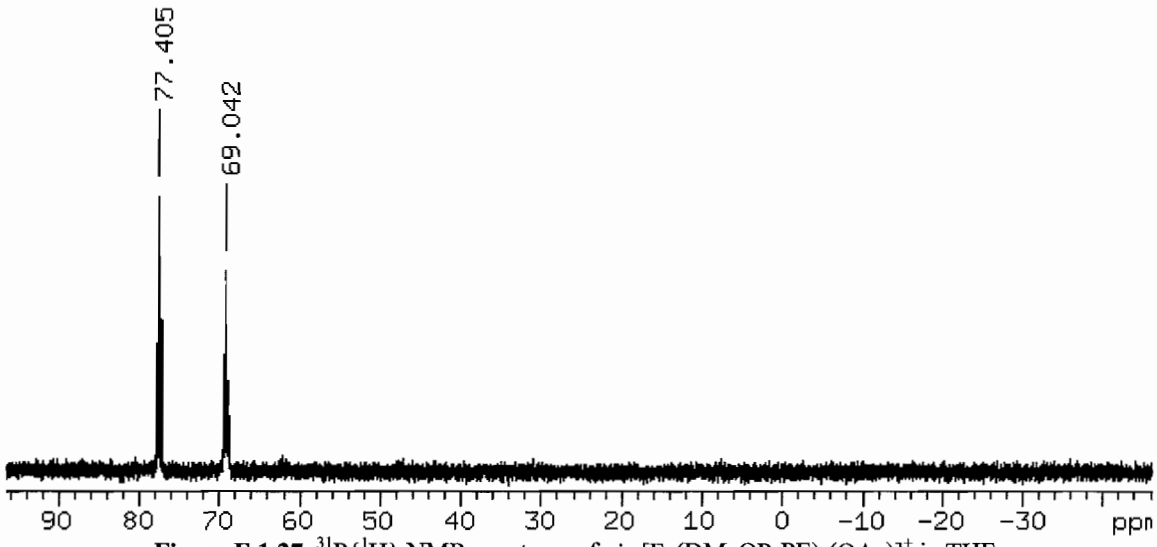

Figure E.1.27. $^{31}P\{^{1}H\}$ NMR spectrum of *cis*-$[Fe(DMeOPrPE)_2(OAc)]^+$ in THF.

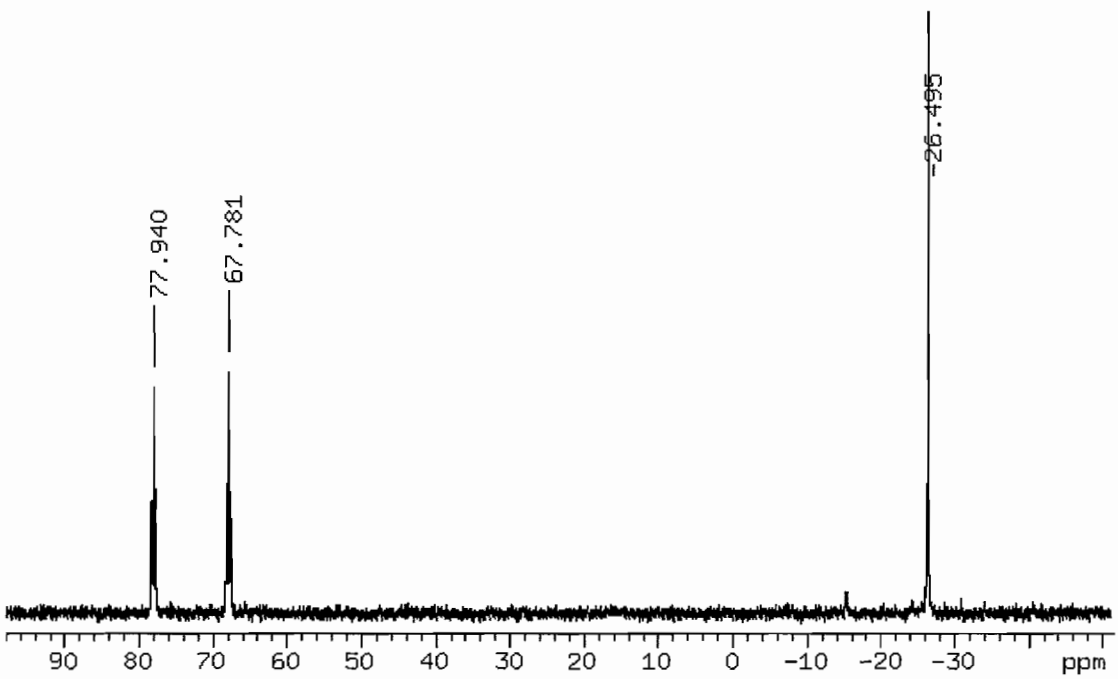

Figure E.1.28. $^{31}P\{^{1}H\}$ NMR spectrum of *cis*-$[Fe(DMeOPrPE)_2(CO_3)]^+$ in acetone-d_6.

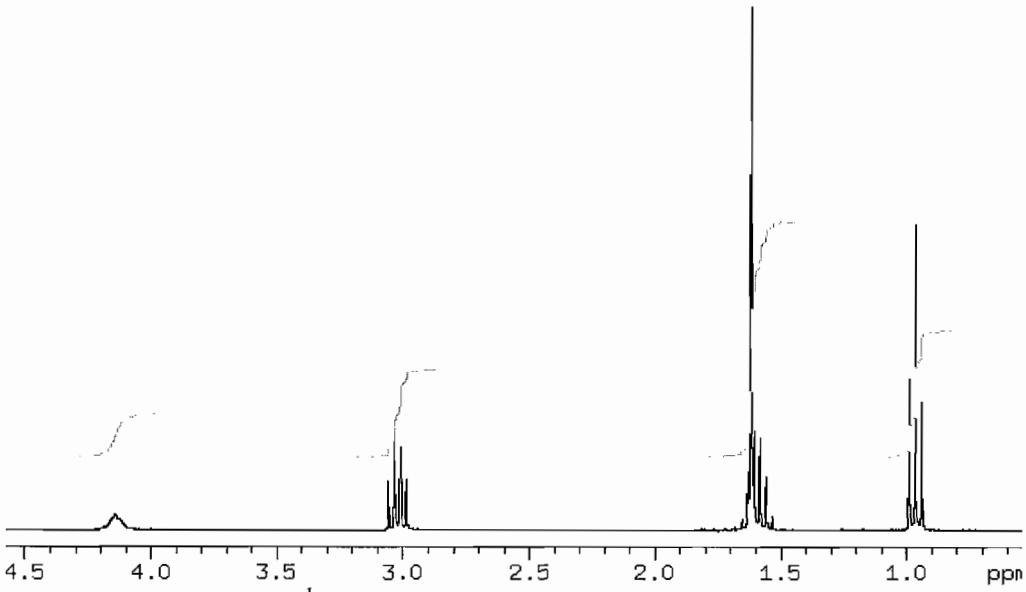

Figure E.1.29. ^{1}H NMR spectrum of *N*,*N*-dipropylsulfamide in $CDCl_3$.

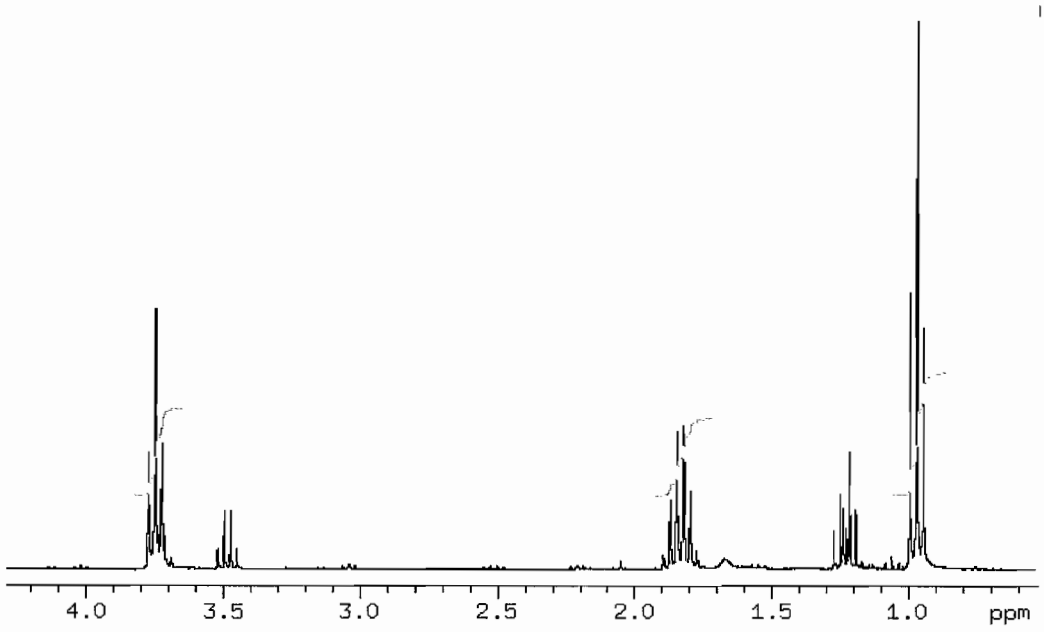

Figure E.1.30. ^{1}H NMR spectrum of azopropane in $CDCl_3$. The resonance marked by integrals represent the azopropane, the other resonances are due to impurities.

Table E.1.1. Crystal data and structure refinement for *cis*-[Fe(DMeOPrPE)$_2$(η^2-N_2H_4)][BPh_4]$_2$ (**I**)

Identification code	just1	
Empirical formula	C84 H124 B2 Fe N2 O8 P4	
Formula weight	1491.20	
Temperature	173(2) K	
Wavelength	0.71073 Å	
Crystal system	Monoclinic	
Space group	P2(1)/c	
Unit cell dimensions	a = 15.7238(13) Å	α = 90°.
	b = 13.7996(12) Å	β = 91.693(2)°.
	c = 37.097(3) Å	γ = 90°.
Volume	8045.8(12) Å^3	
Z	4	
Density (calculated)	1.231 Mg/m^3	
Absorption coefficient	0.322 mm^{-1}	
F(000)	3208	
Crystal size	0.33 x 0.14 x 0.10 mm^3	
Theta range for data collection	1.57 to 25.00°.	
Index ranges	-18<=h<=18, -16<=k<=16, -44<=l<=44	
Reflections collected	58835	
Independent reflections	14153 [R(int) = 0.0628]	
Completeness to theta = 25.00°	99.9 %	
Absorption correction	Semi-empirical from equivalents	
Max. and min. transmission	1.000 and 0.778	
Refinement method	Full-matrix least-squares on F^2	
Data / restraints / parameters	14153 / 6 / 948	
Goodness-of-fit on F^2	1.024	
Final R indices [I>2sigma(I)]	R1 = 0.0499, wR2 = 0.1099	
R indices (all data)	R1 = 0.0737, wR2 = 0.1238	
Largest diff. peak and hole	1.264 and -0.440 e Å^{-3}	

APPENDIX F

UNPUBLISHED CRYSTAL STRUCTURES

F.1 Crystal structure of *trans*-$Fe(DHPrPE)_2Cl_2$

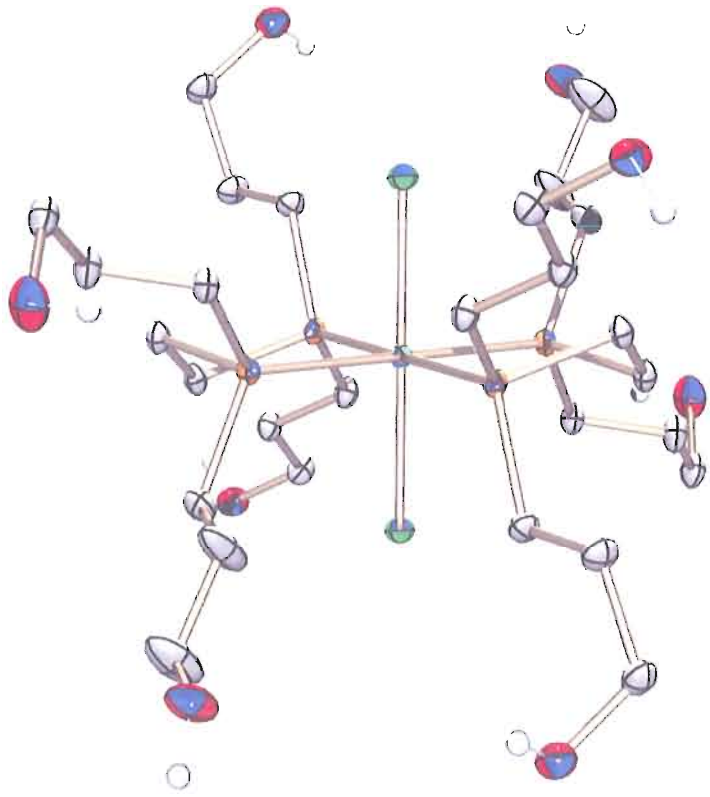

Figure F.1.1. ORTEP representation of *trans*-$Fe(DHPrPE)_2Cl_2$. Hydrogen atoms have been omitted for clarity.

Table F.1.1. Crystal data and structure refinement for *trans*-Fe(DHPrPE)$_2$Cl$_2$.

Identification code	just8	
Empirical formula	C28 H64 Cl2 Fe1 O8 P4	
Formula weight	779.42	
Temperature	173(2) K	
Wavelength	0.71073 Å	
Crystal system	Triclinic	
Space group	P-1	
Unit cell dimensions	a = 8.7120(4) Å	α = 96.0860(10)°.
	b = 10.4252(5) Å	β = 104.2150(10)°.
	c = 10.7441(5) Å	γ = 105.8600(10)°.
Volume	894.12(7) Å^3	
Z	1	
Density (calculated)	1.448 Mg/m^3	
Absorption coefficient	0.795 mm^{-1}	
F(000)	416	
Crystal size	0.29 x 0.26 x 0.18 mm^3	
Theta range for data collection	1.99 to 27.50°.	
Index ranges	-11<=h<=11, -13<=k<=13, -13<=l<=13	
Reflections collected	10287	
Independent reflections	4030 [R(int) = 0.0148]	
Completeness to theta = 27.50°	98.0 %	
Absorption correction	Semi-empirical from equivalents	
Max. and min. transmission	0.8701 and 0.8022	
Refinement method	Full-matrix least-squares on F^2	
Data / restraints / parameters	4030 / 0 / 324	
Goodness-of-fit on F^2	1.017	
Final R indices [I>2sigma(I)]	R1 = 0.0244, wR2 = 0.0642	
R indices (all data)	R1 = 0.0254, wR2 = 0.0651	
Largest diff. peak and hole	0.418 and -0.349 e.Å^{-3}	

Table F.1.2. Atomic coordinates (x 10^4) and equivalent isotropic displacement parameters ($Å^2$x 10^3) for *trans*-Fe(DHPrPE)$_2$Cl$_2$. U(eq) is defined as one third of the trace of the orthogonalized U^{ij} tensor.

	x	y	z	U(eq)
Fe(1)	5000	5000	0	10(1)
Cl(1)	3124(1)	5020(1)	1240(1)	17(1)
P(1)	6999(1)	6878(1)	1309(1)	12(1)
P(2)	4013(1)	6519(1)	-1103(1)	12(1)
O(1)	6890(1)	8722(1)	5626(1)	25(1)
O(2)	13434(1)	9555(1)	2270(1)	23(1)
O(3)	-736(2)	7472(1)	-3483(1)	31(1)
O(4)	1999(2)	5285(1)	-6234(1)	33(1)
C(1)	7019(2)	8268(1)	387(1)	15(1)
C(2)	5226(2)	8242(1)	-165(1)	16(1)
C(3)	6592(2)	7571(1)	2805(1)	17(1)
C(4)	7851(2)	8886(1)	3650(1)	20(1)
C(5)	7217(2)	9533(1)	4673(1)	21(1)
C(6)	9214(2)	6951(1)	1812(1)	16(1)
C(7)	10488(2)	8314(1)	1856(1)	17(1)
C(8)	12275(2)	8295(1)	2290(1)	19(1)
C(9)	1853(2)	6558(1)	-1378(1)	16(1)
C(10)	1643(2)	7952(1)	-1533(2)	20(1)
C(11)	-160(2)	7898(1)	-2089(2)	21(1)
C(12)	4346(2)	6728(2)	-2711(1)	20(1)
C(13)	3005(3)	5819(2)	-3901(2)	38(1)
C(14)	3315(3)	6101(2)	-5137(2)	43(1)

Table F.1.3. Bond lengths [Å] and angles [°] for *trans*-Fe(DHPrPE)$_2$Cl$_2$.

Fe(1)-P(1)#1	2.2791(3)
Fe(1)-P(1)	2.2791(3)
Fe(1)-P(2)	2.3008(3)
Fe(1)-P(2)#1	2.3008(3)
Fe(1)-Cl(1)#1	2.3506(3)
Fe(1)-Cl(1)	2.3506(3)
P(1)-C(1)	1.8385(13)
P(1)-C(3)	1.8448(13)
P(1)-C(6)	1.8496(13)
P(2)-C(9)	1.8442(13)
P(2)-C(12)	1.8456(14)
P(2)-C(2)	1.8475(13)
O(1)-C(5)	1.4279(18)
O(1)-H(1O)	0.75(2)
O(2)-C(8)	1.4272(17)
O(2)-H(2O)	0.74(2)
O(3)-C(11)	1.4350(19)
O(3)-H(3O)	0.80(2)
O(4)-C(14)	1.420(2)
O(4)-H(4O)	0.83(3)
C(1)-C(2)	1.5201(18)
C(1)-H(1A)	0.970(18)
C(1)-H(1B)	0.959(18)
C(2)-H(2A)	0.950(19)
C(2)-H(2B)	0.943(17)
C(3)-C(4)	1.5266(18)
C(3)-H(3A)	0.97(2)
C(3)-H(3B)	0.959(18)
C(4)-C(5)	1.5213(19)
C(4)-H(4A)	0.96(2)
C(4)-H(4B)	0.984(19)
C(5)-H(5A)	0.985(19)
C(5)-H(5B)	1.013(18)
C(6)-C(7)	1.5333(18)
C(6)-H(6A)	0.976(18)
C(6)-H(6B)	0.963(19)
C(7)-C(8)	1.5180(18)
C(7)-H(7A)	0.973(18)
C(7)-H(7B)	0.941(17)
C(8)-H(8A)	0.963(18)
C(8)-H(8B)	0.998(18)
C(9)-C(10)	1.5351(18)
C(9)-H(9A)	0.953(18)
C(9)-H(9B)	0.950(17)
C(10)-C(11)	1.5198(19)
C(10)-H(10A)	0.981(19)
C(10)-H(10B)	0.951(18)
C(11)-H(11A)	0.950(18)
C(11)-H(11B)	0.968(18)
C(12)-C(13)	1.518(2)
C(12)-H(12A)	0.88(2)

C(12)-H(12B)	0.97(2)
C(13)-C(14)	1.463(2)
C(13)-H(13A)	1.11(5)
C(13)-H(13B)	0.84(3)
C(14)-H(14A)	0.98(5)
C(14)-H(14B)	0.92(3)

P(1)#1-Fe(1)-P(1)	180.00(2)
P(1)#1-Fe(1)-P(2)	94.993(11)
P(1)-Fe(1)-P(2)	85.007(11)
P(1)#1-Fe(1)-P(2)#1	85.007(11)
P(1)-Fe(1)-P(2)#1	94.993(11)
P(2)-Fe(1)-P(2)#1	180.000(9)
P(1)#1-Fe(1)-Cl(1)#1	93.765(11)
P(1)-Fe(1)-Cl(1)#1	86.235(11)
P(2)-Fe(1)-Cl(1)#1	91.647(11)
P(2)#1-Fe(1)-Cl(1)#1	88.353(11)
P(1)#1-Fe(1)-Cl(1)	86.235(11)
P(1)-Fe(1)-Cl(1)	93.765(11)
P(2)-Fe(1)-Cl(1)	88.353(11)
P(2)#1-Fe(1)-Cl(1)	91.647(11)
Cl(1)#1-Fe(1)-Cl(1)	180.000(15)
C(1)-P(1)-C(3)	101.55(6)
C(1)-P(1)-C(6)	102.97(6)
C(3)-P(1)-C(6)	105.36(6)
C(1)-P(1)-Fe(1)	106.37(4)
C(3)-P(1)-Fe(1)	116.83(4)
C(6)-P(1)-Fe(1)	121.14(4)
C(9)-P(2)-C(12)	101.54(6)
C(9)-P(2)-C(2)	101.98(6)
C(12)-P(2)-C(2)	99.56(6)
C(9)-P(2)-Fe(1)	122.83(4)
C(12)-P(2)-Fe(1)	119.73(5)
C(2)-P(2)-Fe(1)	107.55(4)
C(5)-O(1)-H(1O)	110.2(18)
C(8)-O(2)-H(2O)	104.5(16)
C(11)-O(3)-H(3O)	106.8(17)
C(14)-O(4)-H(4O)	106.6(18)
C(2)-C(1)-P(1)	107.70(9)
C(2)-C(1)-H(1A)	109.5(10)
P(1)-C(1)-H(1A)	107.1(10)
C(2)-C(1)-H(1B)	112.8(10)
P(1)-C(1)-H(1B)	111.6(10)
H(1A)-C(1)-H(1B)	108.0(14)
C(1)-C(2)-P(2)	107.96(9)
C(1)-C(2)-H(2A)	110.3(11)
P(2)-C(2)-H(2A)	109.3(11)
C(1)-C(2)-H(2B)	111.5(10)
P(2)-C(2)-H(2B)	107.6(10)
H(2A)-C(2)-H(2B)	110.1(14)
C(4)-C(3)-P(1)	117.95(9)
C(4)-C(3)-H(3A)	108.7(12)
P(1)-C(3)-H(3A)	109.1(12)

C(4)-C(3)-H(3B)	109.4(10)
P(1)-C(3)-H(3B)	106.6(10)
H(3A)-C(3)-H(3B)	104.4(15)
C(5)-C(4)-C(3)	113.43(12)
C(5)-C(4)-H(4A)	111.0(12)
C(3)-C(4)-H(4A)	108.6(12)
C(5)-C(4)-H(4B)	106.8(11)
C(3)-C(4)-H(4B)	109.6(11)
H(4A)-C(4)-H(4B)	107.1(16)
O(1)-C(5)-C(4)	113.86(12)
O(1)-C(5)-H(5A)	108.7(10)
C(4)-C(5)-H(5A)	107.6(11)
O(1)-C(5)-H(5B)	111.4(10)
C(4)-C(5)-H(5B)	107.3(10)
H(5A)-C(5)-H(5B)	107.7(14)
C(7)-C(6)-P(1)	116.19(9)
C(7)-C(6)-H(6A)	111.3(10)
P(1)-C(6)-H(6A)	108.0(10)
C(7)-C(6)-H(6B)	109.8(11)
P(1)-C(6)-H(6B)	106.4(11)
H(6A)-C(6)-H(6B)	104.4(15)
C(8)-C(7)-C(6)	112.96(11)
C(8)-C(7)-H(7A)	107.6(10)
C(6)-C(7)-H(7A)	110.8(10)
C(8)-C(7)-H(7B)	108.1(10)
C(6)-C(7)-H(7B)	111.7(10)
H(7A)-C(7)-H(7B)	105.3(14)
O(2)-C(8)-C(7)	111.94(11)
O(2)-C(8)-H(8A)	110.4(10)
C(7)-C(8)-H(8A)	109.9(11)
O(2)-C(8)-H(8B)	106.4(10)
C(7)-C(8)-H(8B)	110.5(10)
H(8A)-C(8)-H(8B)	107.7(14)
C(10)-C(9)-P(2)	114.17(9)
C(10)-C(9)-H(9A)	111.2(10)
P(2)-C(9)-H(9A)	105.8(11)
C(10)-C(9)-H(9B)	109.9(10)
P(2)-C(9)-H(9B)	108.6(10)
H(9A)-C(9)-H(9B)	106.7(14)
C(11)-C(10)-C(9)	113.38(11)
C(11)-C(10)-H(10A)	107.7(11)
C(9)-C(10)-H(10A)	111.9(10)
C(11)-C(10)-H(10B)	109.4(11)
C(9)-C(10)-H(10B)	108.9(10)
H(10A)-C(10)-H(10B)	105.1(15)
O(3)-C(11)-C(10)	112.13(12)
O(3)-C(11)-H(11A)	106.5(11)
C(10)-C(11)-H(11A)	108.4(11)
O(3)-C(11)-H(11B)	110.2(10)
C(10)-C(11)-H(11B)	111.8(10)
H(11A)-C(11)-H(11B)	107.5(15)
C(13)-C(12)-P(2)	116.72(11)
C(13)-C(12)-H(12A)	110.9(14)

P(2)-C(12)-H(12A)	107.2(14)
C(13)-C(12)-H(12B)	108.4(12)
P(2)-C(12)-H(12B)	105.0(12)
H(12A)-C(12)-H(12B)	108.2(18)
C(14)-C(13)-C(12)	113.30(14)
C(14)-C(13)-H(13A)	98(2)
C(12)-C(13)-H(13A)	109(2)
C(14)-C(13)-H(13B)	115.4(19)
C(12)-C(13)-H(13B)	115.5(19)
H(13A)-C(13)-H(13B)	103(3)
O(4)-C(14)-C(13)	112.09(15)
O(4)-C(14)-H(14A)	106(3)
C(13)-C(14)-H(14A)	99(3)
O(4)-C(14)-H(14B)	117.7(18)
C(13)-C(14)-H(14B)	114.1(18)
H(14A)-C(14)-H(14B)	106(4)

Symmetry transformations used to generate equivalent atoms:
#1 -x+1,-y+1,-z

F.2 Crystal structure of *trans*-[Fe(DMeOPrP(O)E)$_2$(H$_2$O)$_2$][2BPh$_4$]

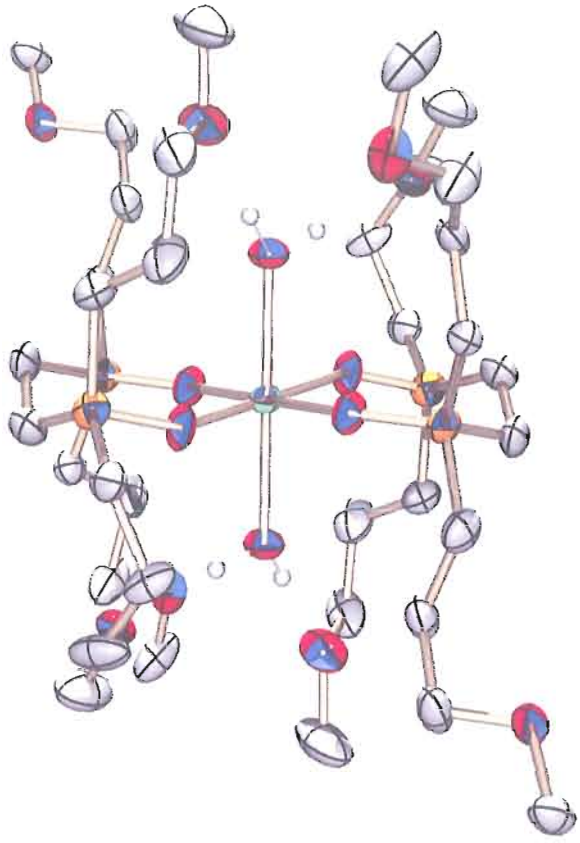

Figure F.2.1. ORTEP representation of *trans*-[Fe(DMeOPrP(O)E)$_2$(H$_2$O)$_2$][2BPh$_4$]. Hydrogen atoms and the tetraphenylborate counter-ions have been omitted for clarity.

Table F.2.1. Crystal data and structure refinement for *trans*-[Fe(DMeOPrP(O)E)$_2$(H_2O)$_2$][2BPh_4].

Identification code	justr6	
Empirical formula	C84 H124 B2 Fe O12.56 P4	
Formula weight	1536.06	
Temperature	110(2) K	
Wavelength	0.71073 Å	
Crystal system	Monoclinic	
Space group	P2(1)/n	
Unit cell dimensions	a = 14.2290(11) Å	α = 90°.
	b = 21.0298(17) Å	β = 101.3540(10)°.
	c = 14.2606(11) Å	γ = 90°.
Volume	4183.7(6) Å^3	
Z	2	
Density (calculated)	1.219 Mg/m^3	
Absorption coefficient	0.315 mm^{-1}	
F(000)	1649	
Crystal size	0.24 x 0.22 x 0.14 mm^3	
Theta range for data collection	1.75 to 28.28°.	
Index ranges	-18<=h<=18, -27<=k<=26, -18<=l<=18	
Reflections collected	48293	
Independent reflections	10031 [R(int) = 0.0329]	
Completeness to theta = 28.28°	96.8 %	
Absorption correction	Semi-empirical from equivalents	
Max. and min. transmission	0.9572 and 0.9282	
Refinement method	Full-matrix least-squares on F^2	
Data / restraints / parameters	10031 / 14 / 722	
Goodness-of-fit on F^2	1.068	
Final R indices [I>2sigma(I)]	R1 = 0.0534, wR2 = 0.1231	
R indices (all data)	R1 = 0.0676, wR2 = 0.1313	
Largest diff. peak and hole	0.428 and -0.424 e.Å^{-3}	

Table F.2.2. Atomic coordinates (x 10^4) and equivalent isotropic displacement parameters ($Å^2$x 10^3) for *trans*-[Fe(DMeOPrP(O)E)$_2$(H_2O)$_2$][2BPh_4]. U(eq) is defined as one third of the trace of the orthogonalized U^{ij} tensor.

	x	y	z	U(eq)
Fe(1)	0	0	0	29(1)
P(1)	154(1)	1293(1)	1446(1)	37(1)
P(2)	-1734(1)	278(1)	254(1)	30(1)
O(1)	451(1)	744(1)	892(1)	37(1)
O(2)	-182(1)	658(1)	-1208(1)	36(1)
O(3)	477(1)	3269(1)	250(1)	40(1)
O(4)	2669(2)	528(1)	4154(2)	69(1)
O(5)	-1755(2)	1131(1)	-2439(1)	69(1)
O(6)	-1241(1)	-577(1)	2278(1)	39(1)
P(2A)	-2061(4)	360(2)	394(4)	33(1)
O(1A)	-1217(5)	1(3)	244(5)	40(2)
C(1)	-1131(2)	1416(1)	1272(2)	46(1)
C(2)	-1746(2)	823(1)	1307(2)	46(1)
C(3)	637(2)	2031(1)	1104(2)	39(1)
C(4)	397(2)	2152(1)	25(2)	38(1)
C(5)	833(2)	2766(1)	-240(2)	46(1)
C(6)	803(2)	3871(1)	11(2)	42(1)
C(7)	465(3)	1165(2)	2707(2)	34(1)
C(8)	1498(3)	942(2)	2987(2)	45(1)
C(9)	1702(2)	702(2)	4045(2)	63(1)
C(7A)	1007(7)	1260(4)	2666(5)	26(2)
C(8A)	822(6)	655(4)	3185(5)	35(2)
C(9A)	1702(2)	702(2)	4045(2)	63(1)
C(10)	3052(2)	370(1)	5107(3)	62(1)
C(11)	-2438(2)	769(1)	-717(2)	48(1)
C(12)	-2612(2)	397(2)	-1653(2)	54(1)
C(13)	-2672(2)	823(2)	-2511(2)	63(1)
C(14)	-1732(4)	1619(3)	-3132(3)	96(2)
C(15)	-2661(3)	-315(2)	349(3)	38(1)
C(16)	-2350(4)	-939(3)	886(4)	43(1)
C(17)	-2134(2)	-892(2)	1977(2)	62(1)
C(15A)	-2952(9)	-167(6)	677(11)	51(3)
C(16A)	-2605(12)	-804(9)	1011(13)	78(7)
C(17A)	-2134(2)	-892(2)	1977(2)	62(1)
C(18)	-932(4)	-582(2)	3279(2)	72(1)
B(1)	-4980(1)	7870(1)	324(1)	20(1)
C(19)	-4724(1)	8141(1)	-680(1)	22(1)
C(20)	-5386(1)	8483(1)	-1350(1)	26(1)
C(21)	-5162(2)	8751(1)	-2171(1)	29(1)
C(22)	-4256(2)	8694(1)	-2354(2)	44(1)
C(23)	-3588(2)	8356(2)	-1716(2)	64(1)
C(24)	-3823(2)	8084(1)	-902(2)	42(1)
C(25)	-6098(1)	7610(1)	153(1)	21(1)
C(26)	-6645(1)	7622(1)	873(1)	25(1)
C(27)	-7569(2)	7375(1)	746(2)	30(1)
C(28)	-7996(1)	7103(1)	-115(2)	29(1)

C(29)	-7488(1)	7085(1)	-847(2)	28(1)
C(30)	-6561(1)	7332(1)	-713(1)	24(1)
C(31)	-4855(1)	8451(1)	1112(1)	22(1)
C(32)	-4930(2)	9095(1)	854(1)	30(1)
C(33)	-4876(2)	9588(1)	1515(2)	36(1)
C(34)	-4739(2)	9450(1)	2484(2)	32(1)
C(35)	-4659(1)	8822(1)	2777(1)	27(1)
C(36)	-4714(1)	8340(1)	2103(1)	23(1)
C(37)	-4252(1)	7273(1)	703(1)	21(1)
C(38)	-4446(2)	6655(1)	351(2)	28(1)
C(39)	-3820(2)	6148(1)	617(2)	34(1)
C(40)	-2971(2)	6238(1)	1262(2)	32(1)
C(41)	-2745(2)	6841(1)	1628(2)	29(1)
C(42)	-3376(1)	7343(1)	1347(1)	25(1)

Table F.2.3. Bond lengths [Å] and angles [°] for *trans*-[Fe(DMeOPrP(O)E)$_2$(H$_2$O)$_2$][2BPh$_4$].

Fe(1)-O(1A)	1.832(7)
Fe(1)-O(1A)#1	1.832(7)
Fe(1)-O(1)#1	2.0389(14)
Fe(1)-O(1)	2.0389(14)
Fe(1)-O(2)	2.1852(15)
Fe(1)-O(2)#1	2.1852(15)
Fe(1)-P(2)#1	2.629(2)
Fe(1)-P(2)	2.629(2)
P(1)-O(1)	1.5046(15)
P(1)-C(7)	1.786(3)
P(1)-C(3)	1.803(2)
P(1)-C(1)	1.815(3)
P(1)-C(7A)	1.917(8)
P(2)-C(15)	1.839(4)
P(2)-C(11)	1.855(3)
P(2)-C(2)	1.893(3)
O(2)-H(1O)	0.84(3)
O(2)-H(2O)	0.90(4)
O(3)-C(5)	1.414(3)
O(3)-C(6)	1.414(3)
O(4)-C(10)	1.401(4)
O(4)-C(9)	1.402(4)
O(5)-C(14)	1.430(4)
O(5)-C(13)	1.442(4)
O(6)-C(18)	1.410(3)
O(6)-C(17)	1.422(3)
P(2A)-O(1A)	1.469(11)
P(2A)-C(2)	1.617(5)
P(2A)-C(11)	1.789(5)
P(2A)-C(15A)	1.791(10)
C(1)-C(2)	1.530(4)
C(1)-H(1A)	0.96(3)
C(1)-H(1B)	1.00(3)
C(2)-H(2A)	0.96(3)
C(2)-H(2B)	0.96(3)
C(3)-C(4)	1.530(3)
C(3)-H(3A)	0.95(3)
C(3)-H(3B)	0.97(3)
C(4)-C(5)	1.512(3)
C(4)-H(4A)	1.04(3)
C(4)-H(4B)	0.95(3)
C(5)-H(5A)	1.05(3)
C(5)-H(5B)	0.99(3)
C(6)-H(6A)	0.99(3)
C(6)-H(6B)	0.98(3)
C(6)-H(6C)	1.02(3)
C(7)-C(8)	1.519(5)
C(7)-H(7A)	0.9900
C(7)-H(7B)	0.9900
C(8)-C(9)	1.562(4)
C(8)-H(8A)	0.9900

C(8)-H(8B)	0.9900
C(9)-H(9A)	0.9900
C(9)-H(9B)	0.9900
C(7A)-C(8A)	1.521(10)
C(7A)-H(7AA)	0.9900
C(7A)-H(7AB)	0.9900
C(8A)-H(8AA)	0.9900
C(8A)-H(8AB)	0.9900
C(10)-H(10A)	1.01(4)
C(10)-H(10B)	1.08(3)
C(10)-H(10C)	1.02(4)
C(11)-C(12)	1.524(4)
C(11)-H(11A)	0.94(2)
C(11)-H(11B)	0.93(3)
C(12)-C(13)	1.505(4)
C(12)-H(12A)	1.02(3)
C(12)-H(12B)	0.93(3)
C(13)-H(13A)	0.99(3)
C(13)-H(13B)	1.05(4)
C(14)-H(14A)	1.03(4)
C(14)-H(14B)	1.01(5)
C(14)-H(14C)	1.02(5)
C(15)-C(16)	1.541(6)
C(15)-H(15A)	0.9900
C(15)-H(15B)	0.9900
C(16)-C(17)	1.528(6)
C(16)-H(16A)	0.9900
C(16)-H(16B)	0.9900
C(17)-H(17A)	0.9900
C(17)-H(17B)	0.9900
C(15A)-C(16A)	1.473(15)
C(15A)-H(15C)	0.9900
C(15A)-H(15D)	0.9900
C(16A)-H(16C)	0.9900
C(16A)-H(16D)	0.9900
C(18)-H(18A)	0.98(3)
C(18)-H(18B)	0.91(4)
C(18)-H(18C)	1.05(5)
B(1)-C(31)	1.646(3)
B(1)-C(19)	1.649(3)
B(1)-C(37)	1.649(3)
B(1)-C(25)	1.654(3)
C(19)-C(24)	1.385(3)
C(19)-C(20)	1.402(3)
C(20)-C(21)	1.392(3)
C(20)-H(20)	0.94(2)
C(21)-C(22)	1.370(3)
C(21)-H(21)	0.93(2)
C(22)-C(23)	1.376(4)
C(22)-H(22)	0.86(3)
C(23)-C(24)	1.393(3)
C(23)-H(23)	0.91(3)
C(24)-H(24)	0.93(3)

C(25)-C(26)	1.406(3)
C(25)-C(30)	1.407(3)
C(26)-C(27)	1.393(3)
C(26)-H(26)	0.92(2)
C(27)-C(28)	1.383(3)
C(27)-H(27)	0.92(2)
C(28)-C(29)	1.381(3)
C(28)-H(28)	0.95(2)
C(29)-C(30)	1.395(3)
C(29)-H(29)	0.94(2)
C(30)-H(30)	0.94(2)
C(31)-C(32)	1.401(3)
C(31)-C(36)	1.407(3)
C(32)-C(33)	1.392(3)
C(32)-H(32)	0.90(3)
C(33)-C(34)	1.388(3)
C(33)-H(33)	0.95(3)
C(34)-C(35)	1.383(3)
C(34)-H(34)	0.94(3)
C(35)-C(36)	1.388(3)
C(35)-H(35)	0.92(2)
C(36)-H(36)	0.92(2)
C(37)-C(38)	1.401(3)
C(37)-C(42)	1.403(3)
C(38)-C(39)	1.393(3)
C(38)-H(38)	0.91(2)
C(39)-C(40)	1.381(3)
C(39)-H(39)	0.92(3)
C(40)-C(41)	1.385(3)
C(40)-H(40)	0.88(2)
C(41)-C(42)	1.392(3)
C(41)-H(41)	0.91(2)
C(42)-H(42)	0.90(2)

O(1A)-Fe(1)-O(1A)#1	180.0(4)
O(1A)-Fe(1)-O(1)#1	85.8(2)
O(1A)#1-Fe(1)-O(1)#1	94.2(2)
O(1A)-Fe(1)-O(1)	94.2(2)
O(1A)#1-Fe(1)-O(1)	85.8(2)
O(1)#1-Fe(1)-O(1)	180.00(8)
O(1A)-Fe(1)-O(2)	100.3(2)
O(1A)#1-Fe(1)-O(2)	79.7(2)
O(1)#1-Fe(1)-O(2)	91.21(6)
O(1)-Fe(1)-O(2)	88.79(6)
O(1A)-Fe(1)-O(2)#1	79.7(2)
O(1A)#1-Fe(1)-O(2)#1	100.3(2)
O(1)#1-Fe(1)-O(2)#1	88.79(6)
O(1)-Fe(1)-O(2)#1	91.21(6)
O(2)-Fe(1)-O(2)#1	180.00(8)
O(1A)-Fe(1)-P(2)#1	167.0(2)
O(1A)#1-Fe(1)-P(2)#1	13.0(2)
O(1)#1-Fe(1)-P(2)#1	86.11(5)
O(1)-Fe(1)-P(2)#1	93.89(5)

O(2)-Fe(1)-P(2)#1	90.04(5)
O(2)#1-Fe(1)-P(2)#1	89.96(5)
O(1A)-Fe(1)-P(2)	13.0(2)
O(1A)#1-Fe(1)-P(2)	167.0(2)
O(1)#1-Fe(1)-P(2)	93.89(5)
O(1)-Fe(1)-P(2)	86.11(5)
O(2)-Fe(1)-P(2)	89.96(5)
O(2)#1-Fe(1)-P(2)	90.04(5)
P(2)#1-Fe(1)-P(2)	180.00(9)
O(1)-P(1)-C(7)	111.94(12)
O(1)-P(1)-C(3)	110.91(11)
C(7)-P(1)-C(3)	111.72(15)
O(1)-P(1)-C(1)	114.63(11)
C(7)-P(1)-C(1)	101.68(17)
C(3)-P(1)-C(1)	105.51(12)
O(1)-P(1)-C(7A)	104.8(3)
C(7)-P(1)-C(7A)	24.9(2)
C(3)-P(1)-C(7A)	94.0(3)
C(1)-P(1)-C(7A)	124.8(3)
C(15)-P(2)-C(11)	98.17(17)
C(15)-P(2)-C(2)	103.53(16)
C(11)-P(2)-C(2)	99.59(15)
C(15)-P(2)-Fe(1)	124.48(13)
C(11)-P(2)-Fe(1)	113.87(12)
C(2)-P(2)-Fe(1)	113.50(12)
P(1)-O(1)-Fe(1)	146.08(10)
Fe(1)-O(2)-H(1O)	133(2)
Fe(1)-O(2)-H(2O)	113(2)
H(1O)-O(2)-H(2O)	107(3)
C(5)-O(3)-C(6)	112.64(18)
C(10)-O(4)-C(9)	110.9(2)
C(14)-O(5)-C(13)	114.6(3)
C(18)-O(6)-C(17)	112.6(3)
O(1A)-P(2A)-C(2)	108.8(4)
O(1A)-P(2A)-C(11)	103.3(4)
C(2)-P(2A)-C(11)	114.3(3)
O(1A)-P(2A)-C(15A)	110.5(5)
C(2)-P(2A)-C(15A)	106.7(5)
C(11)-P(2A)-C(15A)	113.2(5)
P(2A)-O(1A)-Fe(1)	149.1(5)
C(2)-C(1)-P(1)	116.52(18)
C(2)-C(1)-H(1A)	109(2)
P(1)-C(1)-H(1A)	102(2)
C(2)-C(1)-H(1B)	108.7(18)
P(1)-C(1)-H(1B)	107.9(18)
H(1A)-C(1)-H(1B)	113(3)
C(1)-C(2)-P(2A)	122.3(3)
C(1)-C(2)-P(2)	111.97(17)
P(2A)-C(2)-P(2)	16.32(19)
C(1)-C(2)-H(2A)	106(2)
P(2A)-C(2)-H(2A)	98(2)
P(2)-C(2)-H(2A)	114(2)
C(1)-C(2)-H(2B)	109.3(17)

P(2A)-C(2)-H(2B)	111.1(17)
P(2)-C(2)-H(2B)	106.7(17)
H(2A)-C(2)-H(2B)	108(3)
C(4)-C(3)-P(1)	113.16(16)
C(4)-C(3)-H(3A)	107.0(16)
P(1)-C(3)-H(3A)	111.5(16)
C(4)-C(3)-H(3B)	107.1(17)
P(1)-C(3)-H(3B)	111.3(17)
H(3A)-C(3)-H(3B)	106(2)
C(5)-C(4)-C(3)	111.8(2)
C(5)-C(4)-H(4A)	111.9(15)
C(3)-C(4)-H(4A)	107.6(15)
C(5)-C(4)-H(4B)	110.0(15)
C(3)-C(4)-H(4B)	110.3(16)
H(4A)-C(4)-H(4B)	105(2)
O(3)-C(5)-C(4)	108.11(18)
O(3)-C(5)-H(5A)	107.6(16)
C(4)-C(5)-H(5A)	111.4(16)
O(3)-C(5)-H(5B)	109.8(17)
C(4)-C(5)-H(5B)	108.1(17)
H(5A)-C(5)-H(5B)	112(2)
O(3)-C(6)-H(6A)	110.5(18)
O(3)-C(6)-H(6B)	110.6(19)
H(6A)-C(6)-H(6B)	109(3)
O(3)-C(6)-H(6C)	107.5(16)
H(6A)-C(6)-H(6C)	105(2)
H(6B)-C(6)-H(6C)	115(2)
C(8)-C(7)-P(1)	110.3(3)
C(8)-C(7)-H(7A)	109.6
P(1)-C(7)-H(7A)	109.6
C(8)-C(7)-H(7B)	109.6
P(1)-C(7)-H(7B)	109.6
H(7A)-C(7)-H(7B)	108.1
C(7)-C(8)-C(9)	109.9(3)
C(7)-C(8)-H(8A)	109.7
C(9)-C(8)-H(8A)	109.7
C(7)-C(8)-H(8B)	109.7
C(9)-C(8)-H(8B)	109.7
H(8A)-C(8)-H(8B)	108.2
O(4)-C(9)-C(8)	100.6(3)
O(4)-C(9)-H(9A)	111.7
C(8)-C(9)-H(9A)	111.7
O(4)-C(9)-H(9B)	111.7
C(8)-C(9)-H(9B)	111.7
H(9A)-C(9)-H(9B)	109.4
C(8A)-C(7A)-P(1)	109.5(6)
C(8A)-C(7A)-H(7AA)	109.8
P(1)-C(7A)-H(7AA)	109.8
C(8A)-C(7A)-H(7AB)	109.8
P(1)-C(7A)-H(7AB)	109.8
H(7AA)-C(7A)-H(7AB)	108.2
C(7A)-C(8A)-H(8AA)	112.2
C(7A)-C(8A)-H(8AB)	112.2

H(8AA)-C(8A)-H(8AB)	109.8
O(4)-C(10)-H(10A)	106(2)
O(4)-C(10)-H(10B)	109.4(15)
H(10A)-C(10)-H(10B)	116(3)
O(4)-C(10)-H(10C)	103(2)
H(10A)-C(10)-H(10C)	110(3)
H(10B)-C(10)-H(10C)	112(3)
C(12)-C(11)-P(2A)	119.9(3)
C(12)-C(11)-P(2)	109.80(19)
P(2A)-C(11)-P(2)	17.82(18)
C(12)-C(11)-H(11A)	115.8(15)
P(2A)-C(11)-H(11A)	105.6(15)
P(2)-C(11)-H(11A)	99.9(15)
C(12)-C(11)-H(11B)	112.1(17)
P(2A)-C(11)-H(11B)	95.4(17)
P(2)-C(11)-H(11B)	113.2(17)
H(11A)-C(11)-H(11B)	105(2)
C(13)-C(12)-C(11)	112.3(3)
C(13)-C(12)-H(12A)	109.2(18)
C(11)-C(12)-H(12A)	108.3(18)
C(13)-C(12)-H(12B)	107.8(18)
C(11)-C(12)-H(12B)	107.3(18)
H(12A)-C(12)-H(12B)	112(3)
O(5)-C(13)-C(12)	107.7(2)
O(5)-C(13)-H(13A)	105.1(18)
C(12)-C(13)-H(13A)	112.0(18)
O(5)-C(13)-H(13B)	106(2)
C(12)-C(13)-H(13B)	114(2)
H(13A)-C(13)-H(13B)	112(3)
O(5)-C(14)-H(14A)	106(2)
O(5)-C(14)-H(14B)	98(3)
H(14A)-C(14)-H(14B)	112(3)
O(5)-C(14)-H(14C)	107(2)
H(14A)-C(14)-H(14C)	122(3)
H(14B)-C(14)-H(14C)	110(4)
C(16)-C(15)-P(2)	118.3(3)
C(16)-C(15)-H(15A)	107.7
P(2)-C(15)-H(15A)	107.7
C(16)-C(15)-H(15B)	107.7
P(2)-C(15)-H(15B)	107.7
H(15A)-C(15)-H(15B)	107.1
C(15)-C(16)-C(17)	115.6(4)
C(15)-C(16)-H(16A)	108.4
C(17)-C(16)-H(16A)	108.4
C(15)-C(16)-H(16B)	108.4
C(17)-C(16)-H(16B)	108.4
H(16A)-C(16)-H(16B)	107.4
O(6)-C(17)-C(16)	109.0(3)
O(6)-C(17)-H(17A)	109.9
C(16)-C(17)-H(17A)	109.9
O(6)-C(17)-H(17B)	109.9
C(16)-C(17)-H(17B)	109.9
H(17A)-C(17)-H(17B)	108.3

C(16A)-C(15A)-P(2A)	115.4(11)
C(16A)-C(15A)-H(15C)	108.4
P(2A)-C(15A)-H(15C)	108.4
C(16A)-C(15A)-H(15D)	108.4
P(2A)-C(15A)-H(15D)	108.4
H(15C)-C(15A)-H(15D)	107.5
C(15A)-C(16A)-H(16C)	107.4
C(15A)-C(16A)-H(16D)	107.4
H(16C)-C(16A)-H(16D)	106.9
O(6)-C(18)-H(18A)	104.8(17)
O(6)-C(18)-H(18B)	108(2)
H(18A)-C(18)-H(18B)	109(3)
O(6)-C(18)-H(18C)	107(3)
H(18A)-C(18)-H(18C)	114(3)
H(18B)-C(18)-H(18C)	113(3)
C(31)-B(1)-C(19)	108.85(14)
C(31)-B(1)-C(37)	111.44(15)
C(19)-B(1)-C(37)	108.40(14)
C(31)-B(1)-C(25)	108.53(14)
C(19)-B(1)-C(25)	110.91(14)
C(37)-B(1)-C(25)	108.73(14)
C(24)-C(19)-C(20)	114.63(18)
C(24)-C(19)-B(1)	122.85(17)
C(20)-C(19)-B(1)	122.39(16)
C(21)-C(20)-C(19)	123.14(19)
C(21)-C(20)-H(20)	119.9(13)
C(19)-C(20)-H(20)	116.9(13)
C(22)-C(21)-C(20)	120.3(2)
C(22)-C(21)-H(21)	119.3(14)
C(20)-C(21)-H(21)	120.3(14)
C(21)-C(22)-C(23)	118.2(2)
C(21)-C(22)-H(22)	121.3(19)
C(23)-C(22)-H(22)	120.5(19)
C(22)-C(23)-C(24)	121.0(2)
C(22)-C(23)-H(23)	119(2)
C(24)-C(23)-H(23)	120(2)
C(19)-C(24)-C(23)	122.7(2)
C(19)-C(24)-H(24)	120.5(17)
C(23)-C(24)-H(24)	116.7(18)
C(26)-C(25)-C(30)	114.68(17)
C(26)-C(25)-B(1)	122.72(16)
C(30)-C(25)-B(1)	122.53(16)
C(27)-C(26)-C(25)	122.86(18)
C(27)-C(26)-H(26)	117.6(14)
C(25)-C(26)-H(26)	119.5(14)
C(28)-C(27)-C(26)	120.53(19)
C(28)-C(27)-H(27)	118.8(15)
C(26)-C(27)-H(27)	120.6(15)
C(29)-C(28)-C(27)	118.64(18)
C(29)-C(28)-H(28)	120.8(14)
C(27)-C(28)-H(28)	120.6(14)
C(28)-C(29)-C(30)	120.51(19)
C(28)-C(29)-H(29)	119.3(14)

C(30)-C(29)-H(29)	120.2(14)
C(29)-C(30)-C(25)	122.78(18)
C(29)-C(30)-H(30)	117.5(13)
C(25)-C(30)-H(30)	119.7(13)
C(32)-C(31)-C(36)	114.37(17)
C(32)-C(31)-B(1)	123.13(16)
C(36)-C(31)-B(1)	122.42(16)
C(33)-C(32)-C(31)	123.41(19)
C(33)-C(32)-H(32)	117.3(16)
C(31)-C(32)-H(32)	119.3(16)
C(34)-C(33)-C(32)	119.73(19)
C(34)-C(33)-H(33)	119.0(15)
C(32)-C(33)-H(33)	121.3(15)
C(35)-C(34)-C(33)	119.16(19)
C(35)-C(34)-H(34)	119.8(15)
C(33)-C(34)-H(34)	121.0(15)
C(34)-C(35)-C(36)	119.88(18)
C(34)-C(35)-H(35)	121.5(15)
C(36)-C(35)-H(35)	118.6(15)
C(35)-C(36)-C(31)	123.44(18)
C(35)-C(36)-H(36)	117.7(13)
C(31)-C(36)-H(36)	118.8(13)
C(38)-C(37)-C(42)	114.75(17)
C(38)-C(37)-B(1)	121.47(16)
C(42)-C(37)-B(1)	123.67(16)
C(39)-C(38)-C(37)	122.9(2)
C(39)-C(38)-H(38)	118.1(15)
C(37)-C(38)-H(38)	119.0(15)
C(40)-C(39)-C(38)	120.3(2)
C(40)-C(39)-H(39)	121.6(17)
C(38)-C(39)-H(39)	118.1(17)
C(39)-C(40)-C(41)	118.98(19)
C(39)-C(40)-H(40)	120.8(15)
C(41)-C(40)-H(40)	120.1(16)
C(40)-C(41)-C(42)	119.78(19)
C(40)-C(41)-H(41)	121.4(15)
C(42)-C(41)-H(41)	118.8(15)
C(41)-C(42)-C(37)	123.28(19)
C(41)-C(42)-H(42)	118.9(13)
C(37)-C(42)-H(42)	117.8(13)

Symmetry transformations used to generate equivalent atoms:
#1 -x,-y,-z

BIBLIOGRAPHY

Chapter I

(1) Bazhenova, T. A.; Shilov, A. E. *Coord. Chem. Rev.* **1995**, *144*, 69-145.

(2) Postgate, J. *Nitrogen Fixation*; 3rd Ed. ed.; Cambridge University Press: Cambridge, UK, 1998.

(3) Allen, A. D.; Senoff, C. W. *Chem. Commun.* **1965**, 621-622.

(4) Lee, S. C.; Holm, R. H. *Chem. Rev.* **2004**, *104*, 1135-1157.

(5) Holland, P. L. In *Comprehensive Coordination Chemistry II*; McCleverty, J., Meyer, T. J., Eds.; Elsevier: Oxford, 2004; Vol. 8, pp 569-599.

(6) Borodko, Y. G.; Broitman, M. O.; Kachapina, L. M.; Shilov, A. E.; Ukhin, L. Y. *J. Chem. Soc., Chem. Commun.* **1971**, 1185-1186.

(7) Broitman, M. O.; Vorontsova, T. A.; Shilov, A. E. *Kinet. Katal.* **1972**, *13*.

(8) Tchoubar, B.; Shilov, A. E.; Shilova, A. K. *Kinet. Katal.* **1975**, *16*, 179.

(9) Jezowska-Trzebiatowska, B.; Sobota, P. *J. Organometal. Chem.* **1972**, *46*, 339-343.

(10) Shilov, A. E. *New J. Chem.* **1992**, *16*, 213-218.

(11) Jennings, J. R. *Catalytic Ammonia Synthesis*; Plenum Press: New York, 1991.

(12) United Nations Industrial Development Organization (UNIDO), I. F. D. C. I. *Fertilizer Manual*; 3rd ed.; Kluwer Academic Publishers: The Netherlands, 1998.

(13) Seefeldt, L. C.; Hoffman, B. M.; Dean, D. R. *Annu. Rev. Biochem.* **2009**, *78*, 701–722.

(14) Burgess, B. K.; Lowe, D. J. *Chem. Rev.* **1996**, *96*, 2983-3011.

(15) Howard, J. B.; Rees, D. C. *Chem. Rev.* **1996**, *96*, 2965-2982.

(16) Smith, B. E.; Durrant, M. C.; Fairhurst, S. A.; Gormal, C. A.; Gronberg, K. L. C.; Henderson, R. A.; Ibrahim, S. K.; Le Gall, T.; Pickett, C. J. *Coord. Chem. Rev.* **1999**, *185–186*, 669–687.

(17) Eady, R. R. *Chem. Rev.* **1996**, *96*, 3013-3030.

(18) Rubio, L. M.; Ludden, P. W. *J. Bact.* **2005**, *187*, 405-414.

(19) Einsle, O.; Tezcan, A.; Andrade, S. L. A.; Schmid, B.; Yoshida, M.; Howard, J. B.; Rees, D. C. *Science* **2002**, *297*, 1696-1700.

(20) Vrajmasu, V.; Munck, E.; Bominaar, E. L. *Inorg. Chem.* **2003**, *42*, 5974–5988.

(21) Dance, I. *Chem. Commun.* **2003**, 324–325.

(22) Dance, I. *Inorg. Chem.* **2006**, *45*, 5084-5091.

(23) Hinnemann, B.; Nørskov, J. K. *J. Am. Chem. Soc.* **2003**, *125*, 1466-1467.

(24) Hinnemann, B.; Nørskov, J. K. *J. Am. Chem. Soc.* **2004**, *126*, 3920–3927.

(25) Pelmenschikov, V.; Case, D. A.; Noodleman, L. *Inorg. Chem.* **2008**, *47*, 6162-6172.

(26) Lovell, T.; Liu, T.; Case, D. A.; Noodleman, L. *J. Am. Chem. Soc.* **2003**, *125*, 8377-8383.

(27) Lee, H. I.; Benton, P. M. C.; Laryukhin, M.; Igarashi, R. Y.; Dean, D. R.; Seefeldt, L. C.; Hoffman, B. M. *J. Am. Chem. Soc.* **2003**, *125*, 5604-5605.

(28) Lee, H. I.; Sorlie, M.; Christiansen, J.; Yang, T. C.; Shao, J. L.; Dean, D. R.; Hales, B. J.; Hoffman, B. M. *J. Am. Chem. Soc.* **2005**, *127*, 15880-15890.

(29) Lukoyanov, D.; Pelmenschikov, V.; Maeser, N.; Laryukhin, M.; Yang, T.-C.; Noodleman, L.; Dean, D. R.; Case, D. A.; Seefeldt, L. C.; Hoffman, B. M. *Inorg. Chem.* **2007**, *46*, 11437–11449.

(30) Dos Santos, P. C.; Igarashi, R. Y.; Lee, H.-I.; Hoffman, B. M.; Seefeldt, L. C.; Dean, D. R. *Acc. Chem. Res.* **2005**, *38*, 208-214.

(31) Barney, B. M.; Igarashi, R. Y.; Dos Santos, P. C. D., D. R.; Seefeldt, L. C. *J. Biol. Chem.* **2004**, *279*, 53261-53624.

(32) Seefeldt, L. C.; Dance, I. G.; Dean, D. R. *Biochemistry* **2004**, *43*, 1401-1409.

(33) Benton, P. M. C.; Laryukhin, M.; Mayer, S. M.; Hoffman, B. M.; Dean, D. R.; Seefeldt, L. C. *Biochemistry* **2003**, *42*, 9102-9109.

(34) Hoffman, B. M.; Dean, D. R.; Seefeldt, L. C. *Acc. Chem. Res.* **2009**, *42*, 609-619.

(35) Barney, B. M.; Lee, H.-I.; Dos Santos, P. C.; Hoffman, B. M.; Dean, D. R.; Seefeldt, L. C. *Dalton Trans.* **2006**, 2277-2284.

(36) Barney, B. M.; Lukoyanov, D.; Yang, T.-C.; Dean, D. R.; Hoffman, B. M.; Seefeldt, L. C. *Proc. Natl. Acad. Sci. U. S. A.* **2006**, *103*, 17113-17118.

(37) Barney, B. M.; McClead, J.; Lukoyanov, D.; Laryukhin, M.; Yang, T.-C.; Dean, D. R.; Hoffman, B. M.; Seefeldt, L. C. *Biochemistry* **2007**, *46*, 6784–6794.

(38) Barney, B. M.; Yang, T.-C.; Igarashi, R. Y.; Dos Santos, P. C.; Laryukhin, M.; Lee, H.-I.; Hoffman, B. M.; Dean, D. R.; Seefeldt, L. C. *J. Am. Chem. Soc.* **2005**, *127*, 14960-14961.

(39) Chatt, J.; Pearman, A. J.; Richards, R. L. *J. Chem. Soc., Dalton Trans.* **1977**, 1852-1860.

(40) Schrock, R. R. *Angew. Chem., Int. Ed.* **2008**, *47*, 5512-5522.

(41) Shaver, M. P.; Fryzuk, M. D. *Adv. Synth. Catal.* **2003**, *345*, 1061-1076.

(42) Tuczek, F.; Lehnert, N. *Angew. Chem., Int. Ed.* **1998**, *37*, 2636-2638.

(43) Leigh, G. J. *Science* **1995**, *268*, 827-828.

(44) Fryzuk, M. D.; Johnson, S. A. *Coord. Chem. Rev.* **2000**, *200-202*, 379-409.

(45) Leal, A. D.; Jimenez-Tenorio, M.; Puerta, M. C.; Valerga, P. *Organometallics* **1995**, *14*, 3839-3847.

(46) Sacco, A.; Aresta, M. *Chem. Commun.* **1968**, 1223-1224.

(47) Gerlach, D. H.; Peet, W. G.; Muetterties, E. L. *J. Am. Chem. Soc.* **1972**, *94*, 4545.

(48) Borodko, Y. G.; Broitman, M. O.; Kachapina, L. M.; Shilova, A. K.; Shilov, A. E. *Zh. Struct. Khim.* **1971**, *12*, 545.

(49) Stoppioni, P.; Mani, F.; Sacconi, L. *Inorg. Chim. Acta* **1974**, *11*, 227-230.

(50) George, T. A.; Rose, D. J.; Chang, Y.; Chen, Q.; Zubieta, J. *Inorg. Chem.* **1995**, *34*, 1295-1298.

(51) Giannoccaro, P.; Rossi, M.; Sacco, A. *Coord. Chem. Rev.* **1972**, *8*, 77-79.

(52) Cable, R. A.; Green, M.; Mackenzie, R. E.; Timms, P. L.; Turney, T. W. *J. Chem. Soc., Chem. Commun.* **1976**, 270.

(53) Betley, T. A.; Peters, J. C. *J. Am. Chem. Soc.* **2003**, 10782-10783.

(54) MacBeth, C. E.; Harkins, S. B.; Peters, J. C. *Can. J. Chem.* **2005**, *83*, 332-340.

(55) Crossland, J. L.; Young, D. M.; Zakharov, L. N.; Tyler, D. R. *Dalton Trans.* **2009**, *manuscript submitted.*

(56) Miller, W. K.; Gilbertson, J. D.; Leiva-Paredes, C.; Bernatis, P. R.; Weakley, T. J. R.; Lyon, D. K.; Tyler, D. R. *Inorg. Chem.* **2002**, *41*, 5453-5465.

(57) Gilbertson, J. D.; Szymczak, N. K.; Tyler, D. R. *J. Am. Chem. Soc.* **2005**, *127*, 10184-10185.

(58) Hills, A.; Hughes, D. L.; Jimenez-Tenorio, M.; Leigh, G. J. *J. Organomet. Chem.* **1990**, *391*, C41-C44.

(59) Hills, A.; Hughes, D. L.; Jimenez-Tenorio, M.; Leigh, G. J.; Rowley, A. T. *J. Chem. Soc., Dalton Trans.* **1993**, 3041-3049.

(60) Buys, I. E.; Field, L. D.; Hambley, T. W.; McQueen, A. E. D. *Acta Crystallogr., Sect. C: Cryst. Struct. Commun.* **1993**, *49*, 1056-1059.

(61) Bancroft, G. M.; Mays, M. J.; Prater, B. E. *J. Chem. Soc., Chem. Commun.* **1969**, 585.

(62) Komiya, S.; Akita, M.; Yoza, A.; Kasuga, N.; Fukuoka, A.; Kai, Y. *J. Chem. Soc., Chem. Commun.* **1993**, 787-788.

(63) Wiesler, B. E.; Lehnert, N.; Tuczek, F.; Neuhausen, J.; Tremel, W. *Angew. Chem., Int. Ed.* **1998**, *37*, 815-817.

(64) Ghilardi, C. A.; Midollini, S.; Sacconi, L.; Stoppioni, P. *J. Organomet. Chem.* **1981**, *205*, 193-202.

(65) Field, L. D.; Messerle, B. A.; Smernik, R. J. *Inorg. Chem.* **1997**, *36*, 5984-5990.

(66) Field, L. D.; Guest, R. W.; Vuong, K. Q.; Dalgarno, S. J.; Jensen, P. *Inorg. Chem.* **2009**, *48*, 2246-2253.

(67) Mankad, N. P.; Whited, M. T.; Peters, J. C. *Angew. Chem., Int. Ed.* **2007**, *46*, 5768-5771.

(68) Whited, M. T.; Mankad, N. P.; Lee, Y.; Oblad, P. F.; Peters, J. C. *Inorg. Chem.* **2009**, *48*, 2507-2517.

(69) Bart, S. C.; Lobkovsky, E.; Chirik, P. J. *J. Am. Chem. Soc.* **2004**, *126*, 13794-13807.

(70) Archer, A. M.; Bouwkamp, M. W.; Cortez, M.-P.; Lobkovsky, E.; Chirik, P. J. *Organometallics* **2006**, *25*, 4269-4278.

(71) Trovitch, R. J.; Lobkovsky, E.; Chirik, P. J. *Inorg. Chem.* **2006**, *45*.

(72) Danopoulos, A. A.; Wright, J. A.; Motherwell, W. B. *Chem. Commun.* **2005**, 784-786.

(73) Kandler, H.; Gauss, C.; Bidell, W.; Rosenberger, S.; Bürgi, T.; Eremenko, I. L.; Veghini, D.; Orama, O.; Burger, P.; Berke, H. *Chem.-Eur. J.* **1995**, *1*, 541-548.

(74) Sellmann, D.; Kleinschmidt, E. *Angew. Chem., Int. Ed.* **1975**, *14*, 571.

(75) Silverthorn, W. E. *J. Chem. Soc., Chem. Commun.* **1971**, 1310-1311.

(76) Yamamoto, A.; Miura, Y.; Ito, T.; Chen, H. L.; Iri, K.; Ozawa, F.; Miki, K.; Sei, T.; Tanaka, N.; Kasai, N. *Organometallics* **1983**, *2*, 1429-1436.

(77) Betley, T. A.; Peters, J. C. *J. Am. Chem. Soc.* **2004**, *126*, 6252-6254.

(78) Bellerby, J. M.; Mays, M. J.; Sears, P. L. *J. Chem. Soc., Dalton Trans.* **1976**, 1232-1236.

(79) Berke, H.; Huttner, G.; Bankhardt, W.; von Seyerl, J.; Zsolnai, L. *Chem. Ber.* **1981**, *114*, 2754-2768.

(80) Smith, J. M.; Lachicotte, R. J.; Pittard, K. A.; Cundari, T. R.; Lukat-Rodgers, G.; Rodgers, K. R.; Holland, P. L. *J. Am. Chem. Soc.* **2001**, *123*, 9222-9223.

(81) Smith, J. M.; Sadique, A. R.; Cundari, T. R.; Rodgers, K. R.; Lukat-Rodgers, G.; Lachicotte, R. J.; Flaschenriem, C. J.; Vela, J.; Holland, P. L. *J. Am. Chem. Soc.* **2006**, *128*, 756-769.

(82) Gilbertson, J. D.; Szymczak, N. K.; Crossland, J. L.; Miller, W. K.; Lyon, D. K.; Foxman, B. M.; Davis, J.; Tyler, D. R. *Inorg. Chem.* **2007**, *46*, 1205-1214.

(83) Henderson, R. A. *J. Chem. Soc., Dalton Trans.* **1988**, 515-520.

(84) Hirano, M.; Akita, M.; Morikita, T.; Kubo, H.; Fukuoka, A.; Komiya, S. *J. Chem. Soc., Dalton Trans.* **1997**, 3453-3458.

(85) Hirano, M.; Akita, M.; Tani, K.; Kumagai, K.; Kasuga, N. C.; Fukuoka, A.; Komiya, S. *Organometallics* **1997**, *16*, 4206-4213.

(86) Morikita, T.; Hirano, M.; Sasaki, A.; Komiya, S. *Inorg. Chim. Acta* **1999**, *291*, 341-354.

(87) Leigh, G. J. *Acc. Chem. Res.* **1992**, *25*, 177-181.

(88) Leigh, G. J.; Jimenez-Tenorio, M. *J. Am. Chem. Soc.* **1991**, *113*, 5862-5863.

(89) Hall, D. A.; Leigh, G. J. *J. Chem. Soc., Dalton Trans.* **1996**, 3539-3541.

(90) Yelle, R. B.; Crossland, J. L.; Szymczak, N. K.; Tyler, D. R. *Inorg. Chem.* **2009**, *48*, 861-871.

(91) Crossland, J. L.; Zakharov, L. N.; Tyler, D. R. *Inorg. Chem.* **2007**, *46*, 10476-10478.

(92) Field, L. D.; Li, H. L.; Magill, A. M. *Inorg. Chem.* **2009**, *48*, 5-7.

(93) Zanotti-Gerosa, A.; Solari, E.; Giannini, L.; Floriani, C.; Chiesi-Villa, A.; Rizzoli, C. *J. Am. Chem. Soc.* **1998**, *120*, 437-438.

(94) Caselli, A.; Solari, E.; Scopelliti, R.; Floriani, C.; Re, N.; Rizzoli, C.; Chiesi-Villa, A. *J. Am. Chem. Soc.* **2000**, *122*, 3652-3670.

(95) Laplaza, C. E.; Cummins, C. C. *Science* **1995**, *268*, 861-863.

(96) Laplaza, C. E.; Johnson, M. J. A.; Peters, J.; Odom, A. L.; Kim, E.; Cummins, C. C.; George, G. N.; Pickering, I. J. *J. Am. Chem. Soc.* **1996**, *118*, 8623-8638.

(97) Hidai, M.; Mizobe, Y. *Chem. Rev.* **1995**, *95*, 1115-1133.

(98) Sutton, D. *Chem. Rev.* **1993**, *93*, 995.

(99) Mizobe, Y.; Ishii, Y.; Hidai, M. *Coord. Chem. Rev.* **1995**, *139*, 281-311.

(100) Miller, C. E. *J. Chem. Educ.* **1965**, *42*, 254-259.

(101) Hunig, S.; Muller, H. R.; Thier, W. *Angew. Chem., Int. Ed.* **1965**, *4*, 271-280.

(102) Sellmann, D.; Soglowek, W.; Knoch, F.; Moll, M. *Angew. Chem., Int. Ed.* **1989**, *28*, 1271.

(103) Sellmann, D.; Friedrich, H.; Knoch, F.; Moll, M. *Z. Naturforsch. B* **1994**, *48*, 76.

(104) Sellmann, D.; Hennige, A. *Angew. Chem., Int. Ed.* **1997**, *36*, 276-278.

(105) Sellmann, D.; Blum, D. C. F.; Heinemann, F. W. *Inorg. Chim. Acta* **2002**, *337*, 1-10.

(106) Sellmann, D. *Z. Naturforsch. B* **1993**, *48*, 76.

(107) Crossland, J. L.; Balesdent, C. G.; Tyler, D. R. *Dalton Trans.* **2009**, 4420-4422.

(108) Field, L. D.; Li, H. L.; Dalgarno, S. J.; Turner, P. *Chem. Commun.* **2008**, 1680-1682.

(109) Goedkin, V. L.; Peng, S.-M.; Norris, J. M.; Park, Y. *J. Am. Chem. Soc.* **1976**, *98*, 8391-8400.

(110) Sellmann, D.; Friedrich, H.; Knoch, F. *Z. Naturforsch. B* **1994**, *49*, 660-664.

(111) Sellmann, D.; Becker, T.; Hofmann, T.; Knoch, F.; Moll, M. *Inorg. Chim. Acta* **1994**, *219*, 75-84.

(112) Sellmann, D.; Soglowek, W.; Knoch, F.; Ritter, G.; Dengler, J. *Inorg. Chem.* **1992**, *31*, 3711-3717.

(113) Sellmann, D.; Kunstmann, H.; Knoch, F.; Moll, M. *Inorg. Chem.* **1988**, *27*, 4183-4190.

(114) Albertin, G.; Antoniutti, S.; Bordignon, E.; Chimisso, F. *Inorg. Chem. Commun.* **2001**, *4*, 402-404.

(115) Albertin, G.; Antoniutti, S.; Bordignon, E.; Pattaro, S. *J. Chem. Soc., Dalton Trans.* **1997**, 4445-4454.

(116) Zdilla, M. J.; Verma, A. K.; Lee, S. C. *Inorg. Chem.* **2008**, *47*, 11382-11390.

(117) Sellmann, D.; Shaban, S. Y.; Heinemann, F. W. *Eur. J. Inorg. Chem.* **2004**, 4591-4601.

(118) Sellmann, D.; Blum, N.; Heinemann, F. W. *Z. Naturforsch. B* **2001**, *56*, 581-588.

(119) Rath, S. P.; Olmstead, M. M.; Balch, A. L. *Inorg. Chem.* **2004**, *43*, 6357-6365.

(120) Yu, Y.; Brennessel, W. W.; Holland, P. L. *Organometallics* **2007**, *26*, 3217–3226.

(121) Sellmann, D.; Kreutzer, P.; Huttner, G.; Frank, A. *Z. Naturforsch. B* **1978**, *33*, 1341-1346.

(122) Vela, J.; Stoian, S.; Flaschenriem, C. J.; Munck, E.; Holland, P. L. *J. Am. Chem. Soc.* **2004**, *126*, 4522-4523.

(123) Bowman, A. C.; Bart, S. C.; Heinemann, F. W.; Meyer, K.; Chirik, P. J. *Inorg. Chem.* **2009**, *48*, 5587-5589.

(124) Fox, D. J.; Bergman, R. G. *Organometallics* **2004**, *23*, 1656-1670.

(125) Scepaniak, J. J.; Fulton, M. D.; Bontchev, R. P.; Duesler, E. N.; Kirk, M. L.; Smith, J. M. *J. Am. Chem. Soc.* **2008**, *130*, 10515-10517.

(126) Vogel, C.; Heinemann, F. W.; Sutter, J.; Anthon, C.; Meyer, K. *Angew. Chem., Int. Ed.* **2008**, *47*, 2681-2684.

(127) Berry, J. F.; Bill, E.; Bothe, E.; DeBeer George, S.; Mienert, B.; Neese, F.; Wieghardt, K. *Science* **2006**, *312*, 1937-1941.

(128) Aliaga-Alcalde, N.; DeBeer George, S.; Mienert, B.; Bill, E.; Wieghardt, K.; Neese, F. *Angew. Chem., Int. Ed.* **2005**, *44*, 2908-2912.

(129) Justel, T.; Muller, M.; Weyhermueller, T.; Kressl, C.; Bill, E.; Hildebrandt, P.; Lengen, M.; Grodzicki, M.; Trautwein, A. X.; Nuber, B.; Wieghardt, K. *Chem.-Eur. J.* **1999**, *5*, 793-797.

(130) Brown, S. D.; Peters, J. C. *J. Am. Chem. Soc.* **2005**, *127*, 1913-1923.

(131) Scepaniak, J. J.; Young, J. A.; Bontchev, R. P.; Smith, J. M. *Angew. Chem., Int. Ed.* **2009**, *48*, 3158-3160.

(132) Hendrich, M. P.; Gunderson, W.; Behan, R. K.; Green, M. T.; Mehn, M. P.; Betley, T. A.; Lu, C. C.; Peters, J. C. *Proc. Natl. Acad. Sci. U. S. A.* **2006**, *103*, 17107-17112.

Chapter II

(1) Allen, A. D.; Senoff, C. V. *J. Chem. Soc. Chem. Commun.* **1965,** 621-622.

(2) Chatt, J.; Dilworth, J. R.; Richards, R. L.; *Chem. Rev.* **1978,** *78,* 589-625.

(3) Hidai, M.; Mizobe, Y. *Chem. Rev.* **1995,** *95*, 1115-1133.

(4) MacKay, B. A.; Fryzuk, M. D. *Chem. Rev.* **2004,** *104*, 385-401.

(5) Fryzuk, M. D.; Love, J. B.; Rettig, S. J.; Young, V. G. *Science* **1997,** *275,* 1445-1447.

(6) Nishibayashi, Y.; Iwai, S.; Hidai, M. *Science* **1998,** *279,* 540-544.

(7) Pool, J. A.; Lobkovsky, E.; Chirik, P. J. *Nature,* **2004,** *427,* 527-529.

(8) Yandulov, D. V.; Schrock, R. R. *Science* **2003,** *301,* 76-78.

(9) Smith, J. M.; Sadique, A. R.; Cundari, T. R.; Rodgers, K. R.; Lukat-Rodgers, G.; Lachicotte, R. J.; Flaschenriem, C. J.; Vela, J.; Holland, P. L. *J. Am. Chem. Soc.* **2006**, *128*, 756-769.

(10) Betley, T. A.; Peters, J. C. *J. Am. Chem. Soc.* **2003**, *125*, 10782-10783.

(11) Dos Santos, P. C.; Igarashi, R. Y.; Lee, H.; Hoffman, B. M.; Dean, D. R.; Seefeldt, L. C. *Acc. Chem. Res.* **2005,** *38,* 208-214.

(12) Barney, B. M.; Igarashi, R. Y.; Dos Santos, P. C.; Dean, D. R.; Seefeldt, L. C. *J. Biol. Chem.* **2004,** *279,* 53261-53624.

(13) Dos Santos, P. C.; Igarashi, R. Y.; Lee, H.; Hoffman, B. M.; Dean, D. R.; Seefeldt, L. C. *Biochemistry* **2003,** *42,* 9102-9109.

(14) Hall, D.; Leigh, G. J. *J. Chem. Soc., Dalton Trans.* **1996**, 3539-3541.

(15) George, T. A.; Rose, D. J.; Chang, Y.; Chen, Q.; Zubieta, J. *Inorg. Chem.* **1995**, *34*, 1295-1298.

(16) Gilbertson, J. D.; Szymczak, N. K.; Tyler, D. R. *J. Am. Chem. Soc.* **2005,** *127,* 10184-10185.

(17) Mankad, N. P.; Whited, M. T.; Peters, J. C. *Angew. Chem. Int. Ed.* **2007**, *46*, 5768-5771.

(18) Hirano, M.; Akita, M.; Morikita, T.; Kubo, H.; Fukuoka, A.; Komiya, S. *J. Chem. Soc., Dalton Trans.*, **1997**, 3453-3458.

(19) Leigh, G. J. *J. Organomet. Chem.* **2004,** *689*, 3999-4005.

(20) Gilbertson, J. D.; Szymczak, N. K.; Tyler, D. R. *Inorg. Chem.* **2004,** *43,* 3341-3343.

(21) Gilbertson, J. D.; Szymczak, N. K.; Crossland, J. L.; Miller, W. K.; Lyon, D. K.; Foxman, B. M.; Davis, J.; Tyler, D. R. *Inorg. Chem.* **2007,** *46*, 1205-1214.

(22) Miller, W. K.; Gilbertson, J. D.; Leiva-Paredes, C.; Bernatis, P. R.; Weakley, T. J. R.; Lyon, D. K.; Tyler, D. R. *Inorg. Chem.* **2002**, *41*, 5453-5465.

(23) Sheldrick, G. M. *SADABS (2.01), Bruker/Siemens Area Detector Absorption Correction Program*; Bruker AXS: Madison, WI.

(24) Ricci, J. S.; Koetzle, T. F.; Bautista, M. T.; Hofstede, T. M.; Morris, R. H.; Sawyer, J. F. *J. Am. Chem. Soc.* **1989**, *111*, 8823-8827.

(25) Hills, A.; Hughes, D. L.; Jimenez-Tenorio, M.; Leigh, G. J.; Rowley, A. T. *J. Chem. Soc., Dalton Trans.* **1993**, 3041-3049.

(26) Franke, O.; Wiesler, B. E.; Lehnert, N.; Nather, C.; Ksenofontov, V.; Neuhausen, J.; Tuczek, F. *Inorg. Chem.* **2002**, *41*, 3491-3499.

(27) Hills, A.; Hughes, D. L.; Jimenez-Tenorio, M.; Leigh, G. J. *J. Organomet. Chem.* **1990,** *391*, C41-C44.

(28) Buys, I. E.; Field, L. D.; Hambley, T. W.; McQueen, A. E. D. *Acta Crystallogr., Sect. C: Cryst. Struct. Commun.* **1993,** *49,* 1056-1059.

(29) Szymczak, N. K.; Zakharov, L. N.; Tyler, D. R. *J. Am. Chem. Soc.* **2006**, *128*, 15830-15835.

(30) Helleren, C. A.; Henderson, R. A.; Leigh, G. J. *J. Chem. Soc., Dalton Trans.* **1999**, 1213-1220.

(31) Basallote, M. G.; Durán, J.; Fernández-Trujillo, M. J.; Máñez, M. A. *J. Organomet. Chem.* **2000**, *609*, 29-35.

(32) Basallote, M. G.; Durán, J.; Fernández-Trujillo, M. J.; González, G.; Máñez, M. A.; Martínez, M. *Inorg. Chem.* **1998**, *37*, 1623-1628.

(33) Marcus, Y. *Chem. Soc. Rev.* **1993**, 22, 409-416.

(34) Barney, B. M.; Lukoyanov, D.; Yang, T.; Dean, D. R.; Hoffman, B. M.; Seefeldt, L. C. *Proc. Natl. Acad. Sci. U. S. A.*, **2006**, *103*, 17113-17118.

(35) Barney, B. M.; Lee, H.; Dos Santos, P. C.; Hoffman, B. M.; Dean, D. R.; Seefeldt, L. C. *Dalton Trans.*, **2006**, 2277-2284.

(36) Hoffman, B. M.; Dean, D. R.; Seefeldt, L. C. *Acc. Chem. Res.*, **2009**, *42*, 609-619.

(37) Fox, D. J.; Bergman, R. G. *Organometallics* **2004**, *23*, 1656-1670.

(38) Block, E.; Ofori-Okai, G.; Kang, H.; Zubieta, J. *J. Am. Chem. Soc.* **1992**, *114*, 758-759.

(39) Takei, I.; Dohki, K.; Kobayashi, K.; Suzuki, T.; Hidai, M. *Inorg. Chem.* **2005**, *44*, 3768-3770.

(40) Hitchcock, P. B.; Hughes, D. L.; Maguire, M. J.; Marjani, K.; Richards, R. L. *J. Chem. Soc., Dalton Trans.* **1997**, 4747-4752.

(41) Crossland, J. L.; Zakharov, L. N.; Tyler, D. R. *Inorg. Chem.* **2007**, *46*, 10476-10478.

(42) Smith, M. R., III; Cheng, T. Y.; Hillhouse, G. L. *J. Am. Chem. Soc.* **1993**, *115*, 8638-8642.

(43) Albertin, G.; Antoniutti, S.; Bacchi, A.; Boato, M.; Pelizzi, G. *J. Chem. Soc., Dalton Trans.* **2002**, 3313-3320.

(44) Hunig, S.; Muller, H. R.; Thier, W. *Angew. Chem., Int. Ed.* **1965**, *4*, 271-280.

(45) Miller, C. E. *J. Chem. Educ.* **1965**, *42*, 254-259.

(46) Laing, D. R.; Robinson, S. D.; Uttley, M. F. *J. Chem. Soc., Chem. Comm.* **1973**, 176-177.

(47) Cheng, T-Y.; Peters, J. C.; Hillhouse, G. L. *J. Am. Chem. Soc.* **1994**, *116*, 204-207.

Chapter III

(1) Postgate, J. *Nitrogen Fixation,* 3rd ed.; Cambridge University Press: Cambridge, U.K., 1998; Chapters 1 & 2.

(2) Jennings, J. R. *Catalytic Ammonia Synthesis*; Plenum Press: New York, 1991.

(3) Smith, B. E. *Science* **2002**, *297,* 1654.

(4) Seefeldt, L. C.; Hoffman, B. M.; Dean, D. R. *Annu. Rev. Biochem.* **2009**, *78*, 701–722.

(5) Hoffman, B. M.; Dean, D. R.; Seefeldt, L. C. *Acc. Chem. Res.* **2009**, *42*, 609-619.

(6) Dos Santos, P. C.; Igarashi, R. Y.; Lee, H.-I.; Hoffman, B. M.; Seefeldt, L. C.; Dean, D. R. *Acc. Chem. Res.* **2005**, *38*, 208-214.

(7) Gilbertson, J. D.; Szymczak, N. K.; Tyler, D. R. *J. Am. Chem. Soc.* **2005**, *127*, 10184-10185.

(8) George, T. A.; Rose, D. J.; Chang, Y.; Chen, Q.; Zubieta, J. *Inorg. Chem.* **1995**, *34*, 1295-1298.

(9) Mankad, N. P.; Whited, M. T.; Peters, J. C. *Angew. Chem., Int. Ed.* **2007**, *46*, 5768-5771.

(10) Hall, D. A.; Leigh, G. J. *J. Chem. Soc., Dalton Trans.* **1996**, 3539-3541.

(11) R. P. Hughes, D. C. Lindner, A. L. Rheingold and G. P. A. Yap, *Inorg. Chem.* **1997**, *36*, 1726-1727.

(12) F. J. Arnáiz, *J. Chem. Ed.* **1997**, *74*, 1332-1333.

(13) Baker, M. V.; Field, L. D.; Young, D. J. *Appl. Organometal. Chem.* **1990,** *4,* 552.

(14) Chaney, A. L.; Marbach, E. P. *Clin. Chem.* **1962,** *8,* 130-132.

(15) Watt, G. W.; Chrisp, J. D. *Anal. Chem.* **1952,** *24,* 2006-2008.

(16) Darensbourg, M. Y.; Ludvig, M. M. *Inorg. Chem.* **1986**, *25*, 2894-2898.

(17) Hanckel, J. M.; Darensbourg, M. Y. *J. Am. Chem. Soc.* **1983**, *105*, 6979-6980.

(18) Epstein, L. M.; Shubina, E. S.; Krylov, A. N.; Kreindlin, A. Z.; Rybinskaya, M. I. *J. Organomet. Chem.* **1993**, *460*, 87-89.

Chapter IV

(1) Hidai, M.; Mizobe, Y. *Chem. Rev.,* **1995**, *95*, 1115.

(2) MacKay, B. A.; Fryzuk, M. D. *Chem. Rev.,* **2004**, *104*, 385.

(3) Smith, J. M.; Lachicotte, R. J.; Pittard, K. A.; Cundari, T. R.; Lukat-Rodgers, G.; Rodgers, K. R.; Holland, P. L. *J. Am. Chem. Soc.,* **2001**, *123*, 9222.

(4) Smith, J. M.; Sadique, A. R.; Cundari, T. R.; Rodgers, K. R.; Lukat-Rodgers, G.; Lachicotte, R. J.; Flaschenriem, C. J.; Vela, J.; Holland, P. L. *J. Am. Chem. Soc.,* **2006**, *128*, 756.

(5) Betley, T. A.; Peters, J. C. *J. Am. Chem. Soc.,* **2003**, *125*, 10782.

(6) Betley, T. A.; Peters, J. C. *J. Am. Chem. Soc.,* **2004**, *126*, 6252.

(7) Hendrich, M. P.; Gunderson, W.; Behan, R. K.; Green, M. T.; Mehn, M. P.; Betley, T. A.; Lu, C. C.; Peters, J. C. *Proc. Natl. Acad. Sci. U.S.A.,* **2006**, *103*, 17107.

(8) Sellmann, D.; Soglowek, W.; Knoch, F.; Ritter, G.; Dengled, J. *Inorg. Chem.,* **1992**, *31*, 3711.

(9) Sellmann, D.; Hennige, A. *Angew. Chem. Int. Ed.,* **1997**, *36*, 277.

(10) Gilbertson, J. D.; Szymczak, N. K.; Tyler, D. R. *J. Am. Chem. Soc.,* **2005**, *127*, 10184.

(11) George, T. A.; Rose, D. J.; Chang, Y.; Chen, Q.; Zubieta, J. *Inorg. Chem.,* **1995**, *34*, 1295.

(12) Leigh, G. J. *Acc. Chem. Res.,* **1992**, *25*, 177.

(13) Mankad, N. P.; Whited, M. T.; Peters, J. C. *Angew. Chem. Int. Ed.,* **2007**, *46*, 5768.

(14) Barney, B. M.; Lukoyanov, D.; Yang, T.; Dean, D. R.; Hoffman, B. M.; Seefeldt, L. C. *Proc. Natl. Acad. Sci. U.S.A.*, **2006**, *103*, 17113.

(15) Barney, B. M.; Lee, H.; Dos Santos, P. C.; Hoffman, B. M.; Dean, D. R.; Seefeldt, L. C. *Dalton Trans.,* **2006**, 2277.

(16) Miller, W. K.; Gilbertson, J. D.; Leiva-Paredes, C.; Bernatis, P. R.; Weakley, T. J. R.; Lyon, D. K.; Tyler, D. R. *Inorg. Chem.* **2002**, *41*, 5453-5465.

(17) Thiele, J. *Liebigs. Ann. Chem.* **1892**, *271*, 127.

(18) Connelly, N. G.; Geiger, W. E. *Chem. Rev.* **1996**, *96*, 877-910.

(19) Corey, E. J.; Mock, W. L. *J. Am. Chem. Soc.* **1962**, *84*, 685-686.

(20) Sheldrick, G. M. *SADABS* (2.01), Bruker/Siemens Area Detector Absorption Correction Program, Bruker AXS, Madison, Wisconsin, U.S.A.

(21) Chaney, A. L.; Marbach, E. P. *Clin. Chem.* **1962,** *8,* 130-132.

(22) Watt, G. W.; Chrisp, J. D. *Anal. Chem.* **1952,** *24,* 2006-2008.

(23) Heaton, B. T.; Jacob, C.; Page, P. *Coord. Chem. Rev.* **1996,** *154,* 193-229.

(24) Sellmann, D.; Becker, T.; Hofmann, T.; Knoch, F.; Moll, M. *Inorg. Chim. Acta*, **1994,** *219,* 75-84.

(25) Sellmann, D.; Soglowek, W.; Knoch, F.; Ritter, G.; Dengler, J. *Inorg. Chem.* **1992,** *31,* 3711-3717.

(26) Sellmann, D.; Kunstmann, H.; Knoch, F.; Moll, M. *Inorg. Chem.* **1988,** *27,* 4183-4190.

(27) Sellmann, D.; Kreutzer, P.; Huttner, G.; Frank, A. *Z. Naturforsch. B* **1978,** *33,* 1341-1346.

(28) Albertin, G.; Antoniutti, S.; Bordignon, E.; Chimisso, F. *Inorg. Chem. Commun.* **2001,** *4,* 402-404.

(29) Albertin, G.; Antoniutti, S.; Bordignon, E.; Pattaro, S. *J. Chem. Soc., Dalton Trans.* **1997,** 4445-4453.

(30) Antoniutti, S.; Albertin, G.; Bordignon, E. *Inorg. Chem.* **1987,** *26,* 2733-2736.

(31) Anagnostopoulos, A.; Nicholls, D.; Reed, J. *Inorg. Chim. Acta* **1979,** *32,* L17-L18.

(32) Glavic, P.; Slivnik, J.; Bole, A. *J. Inorg. Nucl. Chem.* **1980,** *42,* 1781-1782.

(33) Hirano, M.; Akita, M.; Morikita, T.; Kubo, H.; Fukuoka, A.; Komiya, S. *J. Chem. Soc. Dalton Trans.* **1997,** 3453-3458.

(34) Galindo, A.; Hills, A.; Hughes, D. L.; Richards, R. L.; Hughes, M.; Mason, J. *J. Chem. Soc. Dalton Trans.* **1990,** 283-288.

(35) Vogel, S.; Barth, A.; Huttner, G.; Klein, T.; Zsolnai, L.; Kremer, R. *Angew. Chem. Int. Ed. Engl.* **1991,** *30,* 303-304.

(36) Schrock, R. R.; Glassman, T. E.; Vale, M. G.; Kol, M. *J. Am. Chem. Soc.* **1993,** *115,* 1760-1775.

(37) Cai, S.; Schrock, R. R. *Inorg. Chem.* **1991,** *30,* 4105-4106.

(38) Allen, F. H.; Kennard, O.; Watson, D. G.; Brammer, L.; Orpen, A. G.; Taylor, R. *J. Chem. Soc. Perkin Trans. II* **1987,** S1-S9.

(39) Barney, B. M.; Laryukhin, M.; Igarashi, R. Y.; Lee, H.; Dos Santos, P. C.; Yang, T.; Hoffman, B. M.; Dean, D. R.; Seefeldt, L. C. *Biochemistry* **2005,** *44,* 8030-8037.

(40) Barney, B. M.; Yang, T.; Igarashi, R. Y.; Dos Santos, P. C.; Laryukhin, M.; Lee, H.; Hoffman, B. M.; Dean, D. R.; Seefeldt, L. C. *J. Am. Chem. Soc.* **2005,** *127,* 14960-14961.

(41) Block, E.; Ofori-Okai, G.; Kang, H.; Zubieta, J. *J. Am. Chem. Soc.* **1992,** *114,* 758-759.

(42) Takei, I.; Dohki, K.; Kobayashi, K.; Suzuki, T.; Hidai, M. *Inorg. Chem.* **2005,** *44,* 3768-3770.

(43) Hitchcock, P. B.; Hughes, D. L.; Maguire, M. J.; Marjani, K.; Richards, R. L. *J. Chem. Soc. Dalton Trans.* **1997,** 4747-4752.

(44) Field, L. D.; Li, H. L.; Magill, A. M. *Inorg. Chem.,* **2009**, *48*, 5.

(45) Hirano, M.; Akita, M.; Morikita, T.; Kubo, H.; Fukuoka, A.; Komiya, S. *J. Chem. Soc., Dalton Trans.* **1997**, 3453.

(46) Field, L. D.; Li, H. L.; Dalgarno, S. J.; Turner, P. *Chem. Commun.,* **2008**, 1680.

(47) Miller, C. E. *J. Chem. Educ.* **1965**, *42*, 254-259.

(48) Hunig, S.; Muller, H. R.; Thier, W. *Angew. Chem., Int. Ed.* **1965**, *4*, 271-280.

(49) Smith, M. R., III; Cheng, T. Y.; Hillhouse, G. L. *J. Am. Chem. Soc.* **1993**, *115*, 8638-8642.

(50) Albertin, G.; Antoniutti, S.; Bacchi, A.; Boata, M.; Pelizzi, G. *J. Chem. Soc., Dalton Trans.* **2002**, 3313-3320.

(51) Collman, J. P.; Hutchison, J. E.; Ennis, M. S.; Lopez, M. A.; Guilardt, R. *J. Am. Chem. Soc.* **1992**, *114,* 8074-8080.

(52) Sellmann, D.; Hennige, A. *Angew. Chem., Int. Ed.* **1997**, *36*, 276-278.

(53) Corey, E. J.; Mock, W. L. *J. Am. Chem. Soc.* **1962**, *84*, 685-686.

(54) Carpino, L. A.; Padykula, R. E.; Barr, D. E.; Hall, F. H.; Krause, J. G.; Dufresne, R. F.; Thoman, C. J. *J. Org. Chem.* **1988**, *53*, 2565-2572.

(55) Yelle, R. B.; Crossland, J. L.; Szymczak, N. K.; Tyler, D. R. *Inorg. Chem.* **2009**, *48*, 861-871.

(56) Chatt, J.; Pearman, A. J.; Richards, R. L. *J. Chem. Soc., Dalton Trans.*, **1977**, 1852.

(57) Schrock, R. R. *Angew. Chem. Int. Ed.*, **2008**, *47*, 5512.

(58) Hoffman, B. M.; Dean, D. R.; Seefeldt, L. C. *Acc. Chem. Res.* **2009**, *42*, 609-619.

Appendix A

(1) Einsle, O.; Tezcan, A.; Andrade, S. L. A.; Schmid, B.; Yoshida, M; Howard, J. B.; Rees, D. C. *Science* **2002,** *297,* 1696-1700.

(2) Lee, H.-I.; Benton, P. M. C.; Laryukhin, M.; Igarashi, R. Y.; Dean, D. R.; Seefeldt, L. C.; Hoffman, B. M. *J. Am. Chem. Soc.* **2003**, *125*, 5604-5605.

(3) Scheidt, W. R.; Durbin, S. M.; Sage, J. T. *J. Inorg. Biochem.* **2005**, *99*, 60-71.

(4) Xiao, Y.; Fisher, K.; Smith, M. C.; Newton, W. E.; Case, D. A.; George, S. J.; Wang, H.; Sturhahn, W.; Alp, E. E.; Zhao, J.; Yoda, Y.; Cramer, S. P. *J. Am. Chem. Soc.* **2006**, *128*, 7608-7612.

(5) Cramer, S. P.; Xiao, Y.; Wang, H.; Guo, Y.; Smith, M. C. *Hyperfine Interact.* **2006**, *170*, 47-54.

(6) Barney, B. M.; Yang, T-C.; Igarashi, R. Y.; Dos Santos, P. C.; Laryukhin, M.; Lee, H-I.; Hoffman, B. M.; Dean, D. R.; Seefeldt, L. C. *J. Am. Chem. Soc.* **2005**, *127*, 14960-14961.

(7) Barney, B. M.; Laryukhin, M.; Igarashi, R. Y.; Lee, H-I.; Dos Santos, P. C.; Yang, T-C.; Hoffman, B. M.; Dean, D. R.; Seefeldt, L. C. *Biochemistry* **2005**, *44*, 8030-8037.

(8) Barney, B. M.; McClead, J.; Lukoyanov, D.; Laryukhin, M.; Yang, T-C.; Dean, D. R.; Hoffman, B. M.; Seefeldt, L. C. *Biochemistry* **2007**, *46*, 6784-6794.

(9) Miller, W. K.; Gilbertson, J. D.; Leiva-Paredes, C.; Bernatis, P. R.; Weakley, T. J. R.; Lyon, D. K.; Tyler, D. R. *Inorg. Chem.* **2002**, *41*, 5453-5465.

Appendix B

(1) Postgate, J., *Nitrogen Fixation*. 3rd ed.; Cambridge University Press: Cambridge, U.K., 1998.

(2) Yandulov, D. V.; Schrock, R. R. *Science* **2003**, *301*, 76-78.

(3) Betley, T.; Peters, J. C. *J. Am. Chem. Soc.* **2004**, *126*, 6252-6254.

(4) Smith, J. M.; Lachicotte, R. J.; Pittard, K. A.; Cundari, T. R.; Lukat-Rodgers, G.; Rodgers, K. R.; Holland, P. L. *J. Am. Chem. Soc.* **2001**, *123*, 9222-9223.

(5) Leigh, G. J.; Jimenez-Tenorio, M. *J. Am. Chem. Soc.* **1991**, *113*, 5862-5863.

(6) Gilbertson, J. D.; Szymczak, N. K.; Tyler, D. R. *J. Am. Chem. Soc.* **2005**, *127*, 10184-10185.

(7) Hall, D. A.; Leigh, G. J. *Dalton Trans.* **1996**, 3539-3541.

(8) Hirano, M.; Akita, M.; Morikita, T.; Kubo, H.; Fukuoka, A.; Komiya, S. *Dalton Trans.* **1997**, 3453-3458.

(9) Igarashi, R. Y.; Seefeldt, L. C. *Crit. Rev. Biochem. Mol. Biol.* **2003**, *38*, 351-384.

(10) Dos Santos, P. C.; Igarashi, R. Y.; Lee, H; Hoffman, B. M. Seefeldt, L. C.; Dean, D. R. *Acc. Chem. Res.* **2005**, *38*, 208-214.

(11) Barney, B. M.; Lee, H.; Dos Santos, P. C.; Hoffman, B. M.; Dean, D. R.; Seefeldt, L. C. *Dalton Trans.* **2006**, 2277-2284.

(12) Chatt, J.; Dilworth, J. R.; Richards, R. L. *Chem. Rev.* **1978**, *78*, 589-625.

(13) Barney, B. M.; Lukoyanov, D.; Yang, T.; Dean, D. R.; Hoffman, B. M.; Seefeldt, L. C. *Proc. Natl. Acad. Sci. U.S.A.* **2006**, *103*, 17113-17118.

(14) Kendall, R. A.; Apra, E.; Bernholdt, D. E.; Bylaska, E. J.; Dupuis, M.; Fann, G. I.; Harrison, R. J.; Ju, J.; Nichols, J. A.; Nieplocha, J.; Straatsma, T. P.; Windus, T. L.; Wong, A. T. *Computer Phys. Comm.* **2000**, *128*, 260-283.

(15) Aprà, E.; Windus, T. L.; Straatsma, T. P.; Bylaska, E. J.; Jong, W. A. d.; Hirata, S.; Valiev, M.; Hackler, M.; Pollack, L.; Kowalski, K.; Harrison, R.; Dupuis, M.; Smith, D. M. A.; Nieplocha, J.; Tipparaju, V.; Krishnan, M.; Auer, A. A.; Brown, E.; Cisneros, G.; Fann, G. I.; Früchtl, H.; Garza, J.; Hirao, K.; Kendall, R.; Nichols, J. A.; Tsemekhman, K.; Wolinski, K.; Anchell, J.; Bernholdt, D.; Borowski, P.; Clark, T.; Clerc, D.; Dachsel, H.; Deegan, M.; Dyall, K.; Elwood, D.; Glendening, E.; Gutowski, M.; Hess, A.; Jafe, J.; Johnson, B.; Ju, J.; Kobayashi, R.; Kutteh, R.; Lin, Z.; Littlefield, R.; Long, X.; Meng, B.; Nakajima, T.; Niu, S.; Rosing, M.; Sandrone, G.; Stave, M.; Taylor, H.; Thomas, G.; Lenthe, J. v.; Wong, A.; Zhang, Z. NWChem, A *Computational Chemistry Package for Parallel Computers*, Version 4.7. 2005.

(16) Bylaska, E. J.; Jong, W. A. d.; Kowalski, K.; Straatsma, T. P.; Valiev, M.; Wang, D.; Aprà, E.; Windus, T. L.; Hirata, S.; Hackler, M. T.; Zhao, Y.; Fan, P.-D.; Harrison, R. J.; Dupuis, M.; Smith, D. M. A.; Nieplocha, J.; Tipparaju, V.; Krishnan, M.; Auer, A. A.; Nooijen, M.; Brown, E.; Cisneros, G.; Fann, G. I.; Früchtl, H.; Garza, J.; Hirao, K.; Kendall, R.; Nichols, J. A.; Tsemekhman, K.; Wolinski, K.; Anchell, J.; Bernholdt, D.; Hess, P. A.; Jaffe, J.; Johnson, B.; Ju, J.; Kobayashi, R.; Kutteh, R.; Lin, Z.; Littlefield, R.; Long, X.; Meng, B.; Wong, T. A.; Zhang, Z. NWChem, A *Computational Chemistry Package for Parallel Computers*, Version 5.0. 2006.

(17) Schuchardt, K. L.; Didier, B. T.; Black, G. D., *Ecce - A Problem-Solving Environment's Evolution Toward Grid Services and a Web Architecture.* Concurrency and Computation: Practice and Experience 2002, 14, 1221-1239.

(18) Black, G. D.; Didier, B. T.; Elsethagen, T.; Feller, D.; Gracio, D.; Hackler, M.; Havre, S.; Jones, D.; Jurrus, E.; Keller, T.; Lansing, C.; Matsumoto, S.; Palmer, B.; Peterson, M.; Schuchardt, K.; Stephan, E.; Taylor, H.; Thomas, G.; Vorpagel, E.; Windus, T., Ecce, *A Problem Solving Environment for Computational Chemistry*, Software Version 3.2. 2004.

(19) Becke, A. D. *Phys. Rev. A* **1988**, *38*, 3098-3100.

(20) Lee, C.; Yang, W.; Parr, R. G. *Phys. Rev. B* **1988**, *37*, 785-789.

(21) Becke, A. D. *J. Chem. Phys.* **1993**, *98*, 5648-5652.

(22) Becke, A. D. *J. Chem. Phys.* **1993**, *98*, 1372-1377.

(23) Hariharan, P. C.; Pople, J. A. Theoret. Chimica Acta 1973, 28, 213-222.

(24) Rassolov, V.; Pople, J. A.; Ratner, M.; Windus, T. L. *J. Chem. Phys.* **1998**, *109*, 1223.

(25) Wachters, A. J. H. *J. Chem. Phys.* **1970**, *52*, 1033-1036.

(26) Krishnan, R.; Binkley, J. S.; Seeger, R.; Pople, J. A. *J. Chem. Phys.* **1980**, *72*, 650-654.

(27) Klamt, A.; Schüürmann, G. *J. Chem. Soc., Perkin Trans. 2* **1993**, *5*, 799-805.

(28) Stefanovich, E. V.; Truong, T. N. *Chem. Phys. Lett.* **1995**, *244*, 65-74.

(29) Komiya, S.; Akita, M.; Yoza, A.; Kasuga, N.; Fukuoka, A.; Kai, Y. *J. Chem. Soc., Chem. Commun.* **1993**, 787-788.

(30) Field, L. D.; Li, H. L.; Dalgarno, S. J.; Turner, P. *Chem. Commun.* **2008**, 1680-1682.

(31) Crossland, J. L.; Zakharov, L. N.; Tyler, D. R. *Inorg. Chem.* **2007**, *46*, 10476-78.

(32) Hills, A.; Hughes, D. L.; Jimenez-Tenorio, M.; Leigh, G. J.; Rowley, A. T. *J. Chem. Soc., Dalton Trans.* **1993**, 3041-3049.

(33) Henderson, R. A. *J. Chem. Soc., Dalton Trans.* **1988**, 515-520.

(34) Yandulov, D. V.; Schrock, R. R. *Inorg. Chem.* **2005**, *44*, 1103-1117.